PhD THESIS

FIRE PERFORMANCE OF ARTIFICIAL TURF STRUCTURES: SMALL-SCALE TESTING AND DEVELOPMENT OF FIREPROOFING STRATEGIES

Submitted to and defended at

University of Lille

Doctoral School for Materials, Radiation and Environmental Sciences

Materials and Transformations Unit (UMET), UMR CNRS 8207, ENSCL

For the degree of

DOCTOR

In Materials chemistry

By

Angeline PATUREL

PhD thesis supervised by

Prof. Sophie DUQUESNE and Dr. Mathilde CASETTA

Defended on the 5th of November 2021 before an Examination Committee comprised of:

Prof. Christophe BALEY	Université de Bretagne Sud	Reviewer
Prof. Laurent FERRY	IMT Mines d'Alès	Reviewer
Prof. Yann ROGAUME	Université de Lorraine	President
Prof. Sophie DUQUESNE	ENSCL	Thesis supervisor
Dr. Mathilde CASETTA	Université de Lille	Co-supervisor

THESE DE DOCTORAT

ETUDE DU COMPORTEMENT AU FEU DE STRUCTURES DE GAZON ARTIFICIEL : ESSAIS A PETITE ECHELLE ET DEVELOPPEMENT DE STRATEGIES D'IGNIFUGATION

Présentée et soutenue publiquement à

L'Université de Lille

École Doctorale Sciences de la Matière, du Rayonnement et de l'Environnement

Unité Matériaux Et Transformation (UMET), UMR CNRS 8207, ENSCL

Pour le grade de

DOCTEUR

En Chimie des matériaux

Par

Angeline PATUREL

Thèse dirigée par

Prof. Sophie DUQUESNE et Dr. Mathilde CASETTA

Soutenue le 5 Novembre 2021 devant la Commission d'Examen composée de :

Prof. Christophe BALEY	Université de Bretagne Sud	Rapporteur
Prof. Laurent FERRY	IMT Mines d'Alès	Rapporteur
Prof. Yann ROGAUME	Université de Lorraine	Président
Prof. Sophie DUQUESNE	ENSCL	Directrice de thèse
Dr. Mathilde CASETTA	Université de Lille	Co-encadrante de thèse

*La folie, c'est de faire toujours la même chose
et de s'attendre à un résultat différent.*

A. Einstein

Acknowledgment

A l'issu de ces trois années de travail, je souhaite remercier Professeur Patrice Woisel, directeur du laboratoire Unité Matériaux Et Transformations (UMET), pour m'avoir donné l'opportunité de rejoindre le laboratoire pour y effectuer mes travaux de recherche.

Je tiens également à remercier mes encadrantes Professeur Sophie Duquesne et Docteur Mathilde Casetta. Pour votre encadrement, votre expertise, vos conseils précieux et pour le temps que vous m'avez accordé, je vous exprime toute ma reconnaissance. Ce fut un plaisir de travailler avec vous.

Je suis très reconnaissante envers Professeur Christophe Baley, Professeur Laurent Ferry et Professeur Yann Rogaume d'avoir accepté de prendre de leur temps pour étudier mon travail et de faire partie des membres du jury.

Je souhaite également remercier le « Fonds européen de développement régional » FEDER pour le financement du projet INTERREG GRASS dans le quel ma thèse s'inscrit ainsi qu'à tous les membres du projet pour leur contribution : Stijn Rambour et Geert De Clercq de l'Université de Gand (Belgique), Olivier Talon de MateriaNova (Belgique) et ces collègues et Nicolas Martin de EuraMaterials.

Par ailleurs, des collaborations essentielles au bon déroulement de la réalisation de ce travail de thèse ont eu lieu. Pour cela je tiens à remercier Séverine Bellayer de l'UMET pour avoir réalisé la partie microscopie (SEM et EPMA), Bertrand Revel pour la réalisation des analyses spectroscopiques par résonance magnétique nucléaire (NMR) et enfin, Catherine Candelier, Sandrine Caytan et Patrick Daubias de l'ENSCL pour avoir mis leur laboratoire à disposition pour me permettre de mener à bien mes expériences.

De plus, un grand merci à toute l'équipe du laboratoire, aux permanents (Maud, Fabienne, Séverine, Guillaume, …) et aux personnels techniques qui m'ont été d'une grande aide, notamment Pierre (mille mercis pour l'AngelFire), Ben et Johan. Un merci tout particulier aux doctorants, anciens et actuels, pour les moments partagés au quotidien, l'entraide, les repas du midi, les sorties et les bons moments : Elodie, Charlotte, Louis, Melvin, Tatenda, Fei, Matthieu, Marie Odile, Kevin, Greg (UCCS mais il mérite quand même sa place), …

Un merci particulier aux filles : Laura, Manon, Anne-Lise, Sophie et Mariette.

Un Big Up à Adi et Alex, mes amis du labo. Adi, mon bird sitter préféré, pour les moments au labo, pour ton aide précieuse, pour les jeux, les blagues pas drôles et les parties de palets endiablés. Alex, trop heureuse d'avoir passé ces trois ans avec toi, toujours dans le même

I

bureau, pour les longues pauses papotages et commérages (#Parurésie), pour s'être soutenu lors de la rédaction. A vous deux et à vos moitiés également, Marjo et Pauline, pour les soirées, pour avoir ri à vos côtés et aimé votre présence, merci.

A Mathilde et Corentin, mes ami(e)s de l'extérieur, ceux qui n'ont pas toujours compris ce que je faisais mais qui s'y sont sincèrement intéressés. Pour votre écoute et votre présence, pour tous ces moments de vie, heureux ou plus mélancoliques, pour nos amitiés en toute simplicité, merci.

Un spécial remerciement à mes cacahuètes enrobées : Blandine, Céline, Fanny, pour avoir pu discuter ensemble de nos quotidiens dans nos labos respectifs, pour les supers week-ends passés un peu partout, pour les rires, les sorties, les après-midi entiers de jeux, pour toutes ces parenthèses de fraicheur qui font du bien, merci.

Evidemment, à ma famille. Alexandrine, comme disait (presque) Shakespeare « Une sœur ressemble autant à sa sœur qu'une pomme sauvage à une rainette » parce qu'on est très différentes mais que sans toi je n'aurai pas été celle que je suis. Papa, maman, merci d'avoir essayé de comprendre ce que je faisais, merci de m'avoir toujours soutenu et de m'avoir apporté tout ce dont j'ai toujours eu besoin. Cet aboutissement, je vous le dois en partie.

Enfin, la cerise sur le gâteau, il ne Mangue plus que ceux qui partagent ma vie, mon quotidien. Corneille, merci pour ta présence, ton entièreté, les longues siestes dans mon dos, les pauses réconfort et les mignonitudes. Camille, merci d'avoir été là dans tous ces moments, merci pour ta patience (je ne le dirai pas souvent ça !), merci pour ton soutien sans failles, pour m'avoir écouté, pour m'avoir soutenu et être toujours à mes côtés, pour les surprises, pour les soirées d'excès (Mojjjito !), merci de me faire rire, et parce que « j'ai foie en notre nation », simplement : merci d'être toi. On verRA OU tout cela nous mène, tant que cela nous y mène ensemble.

Table of content

Abbreviations

A

ABS   Acrylonitrile Butadiene Styrene

B

BCA	Building Code of Australia
β_{ii}	Quadratic terms
β_{ij}	Interaction terms
BSE	Backscattered Electron

C

[C]	Central matrix
$CaCO_3$	Calcium Carbonate
CHF	Critical Heat Flux
CMR	Carcinogenic, Mutagenic and Reprotoxic
CP MAS	Cross-Polarisation with Magic Angle Spinning

D

d	Length of the magnetic stirrer
[D]	Dimensional matrix
dp	Diameter of cork particle
d-cork	Denser cork
DA	Dimensional analysis
DMF	Dimethylformamide
DTG	Derivative Curve
DVS	Dynamic Vapour Sorption

E

ECHA	European Chemicals Agency
EPDM	Ethylene Propylene Diene Monomer
EPMA	Electron Probe Micro Analysis
ERCAT	European Research Centre for Artificial Turf
ERDF	European Regional Development Fund
Et_3PO_4	Triethyl Phosphate
EtOH	Ethanol

F

Fr	Froude number
FR	Fire Retardant
FR EPDM	Flame Retardant Ethylene Propylene Diene Monomer
Fs	Flame spread

FTT   Fire Testing Technology

G
Ga   Galileo number
gow/gos   g of water per gram of sample

H
H   Hydrogen
H_3PO_4 Phosphoric acid
HDPP   N-hydroxymethyl-3-dimethylphosphonopropionamide
HPDEC   High Power Decoupling
HR   Relative Humidity
HRR   Heat Release Rate
HTT   Heat Treatments

I
[I]   Identity matrix
ICP   Inductively Coupled Plasma
IS   International System
IR   Infrared
IRB   International Rugby Board

L
L   Length
LbL   Layer-by-Layer technique
LiCl   Lithium Chloride
LiH_2PO_4 Monobasic lithium phosphate
LCA   Life Cycle Assessment
LLDPE   Low Density Polyethylene
LOI   Limiting Oxygen Index
LS P-cork   Large Scale Phosphorylated cork

M
M   Mass
MLC   Mass Loss Cone

N
N   Stirrer rotation speed
NBS   National Bureau of Standard
NaH_2PO_4 Monobasic sodium phosphate
Na_2HPO_4 Dibasic sodium phosphate
$NH_4H_2PO_4$ Monobasic ammonium phosphate
$(NH_4)_2HPO_4$ Dibasic ammonium phosphate

NMR   Nuclear Magnetic Resonance

O
OH   Hydroxyl group

P
P   Power number
P-cork   Phosphorylated cork
PA   Polyamide
PE   Polyethylene
PET   Polyester
P_2O_5 Phosphorus Pentoxide
PhF   Phenol Formaldehyde
pHRR   peak of Heat Release Rate
PN lignin   Phosphorus-Nitrogen lignin
$POCl_3$ Phosphorus Oxychloride
PP   Polypropylene
PU   Polyurethane

Q
Q^2 Prediction coefficient of design of experiments

R
[R]   Residual matrix
[Rm]   Linearized residual matrix
R^2 Determination coefficient of design of experiments
Re   Reynolds number
RF   Radio Frenquency
RCT   Room Corner Test
RSM   Response Surface Methodology

S
S - Cork   Cork – based structure
S – d-cork   Dense cork – based structure
S - EPDM   Ethylene Propylene Diene Monomer – based structure
S – P-cork   Phosphorylated cork – based structure
S - SBR   Styrene-Butadiene Rubber – based structure
S - TPE   Thermoplastic Elastomer – based structure
SBR   Styrene-Butadiene Rubber
SBI   Single Burning Item
SEM   Scanning Electron Microscope
SiO_2 Silicon dioxyde
SS NMR   Solid State Nuclear Magnetic Resonance

T

T	Temperature
$T_{2\%}$	Onset temperature of degradation leading to 2 % of mass loss
TFO	Time of Flame Out
TGA	Thermogravimetric Analyses
TC	Thermocouples
THF	Tetrahydrofuran
THR	Total Heat Release
T_{MAX}	Maximum temperature of degradation
TPE	Thermoplastic Elastomer
TTi	Time To ignition

U

UEFA	Union of European Football Association
Ui	Experimental conditions of design of experiments
UL	Flammability standard

V

VOF	Volume Of Fumes
VPA	Vinyl Phosphonic Acid

X

Xi	Coded values of design of experiments

Y

Y	Yield of reaction
Yi	Responses of design of experiments

Others

%.wt	Percentage by weight
ρ	Density of the medium
π	Dimensionless number

General introduction

Over the years, the search for performance has led to the development of new and more effective materials: they must offer a large range of functionalities, being lighter, having better physical and/or chemical properties, etc. This trend also includes the development of new synthetic materials comparable to natural ones in terms of properties and characteristics, but without their disadvantages (like maintenance, durability, etc.). Among them are floorings, a material intended to cover a part or all of a floor. Flooring serves as protection or decoration but is specifically adapted to withstand the passage of people, animals or gears. The floorings are various (such as carpets, linoleum, PVC floor tiles, etc.) and must be chosen according to the application. Representing a very large flooring range, textile floorings include artificial turf structures. As shown in Figure 1: Artificial turf for sport applications with (a) the backing, (b) the sand, (c) the infill and (d) the pile., artificial turf is a complex material composed of synthetic fibres (usually made of polyethylene (PE) or polypropylene (PP)) inserted into a backing, usually in PP through a tufting process. A backcoating is spread and then cured to bind the fibres to the backing. For sports applications, sand and a damping infill material are added respectively to stabilize the structure and to act as a shock absorption system and avoid player injuries.
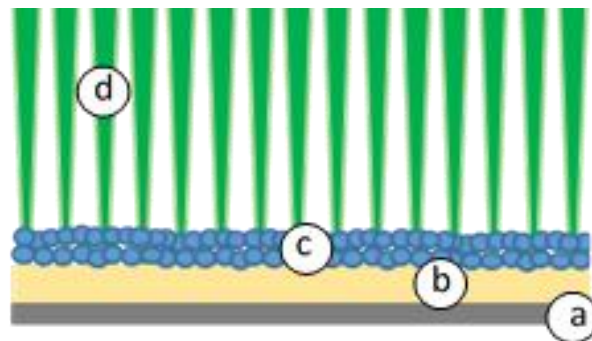
Figure 1: Artificial turf for sport applications with (a) the backing, (b) the sand, (c) the infill and (d) the pile.

Initially, artificial turf, developed in the early 1960s, was only used for outdoor sports stadiums. Over the years, artificial turf market increased significantly due to constant improvements in terms of composition(fibres, infills, back coating) [1], [2], design of structures [3], mechanical properties [4] or technical aspects of manufacturing processes [5]. Nowadays, artificial turf is very popular in many sports and could be considered as a crucial element as it has allowed considerable progress in the sport field. As an example, regarding hockey, nowadays more than

1

90 % of clubs practice on synthetic field. With the introduction of artificial turf, the play has become much faster, the rules have been amended and techniques refined taking into account the fact that synthetic sports surface has modified the way of playing. On the other hand, from the late 1990s, landscaping applications were considered and actually, artificial turf is increasingly used in the private sector (gardens, balconies, etc.). At the same time, indoor use also developed, whether in private structures (covered event halls, enclosed children's playgrounds, etc.) or for indoor sports competitions. Moreover, the architecture of sports stadiums is becoming more and more complex, leading to hybrid structures that can be both closed and open (removable roof). Thus, stadiums are increasingly used for some events other than sports competitions, like concerts. The applications of artificial turf are thus becoming more and more diverse.

Considering its high organic content, artificial turf could represent a significant fire risk [6]. Indeed, the materials composing the structure that have been previously described are mainly polymeric and thus easily flammable. This aspect represents a drawback when compared to the self-extinguishing character of natural turf. Spectacular fires have already occurred in public places, such as a children's playground in Alaska (USA) in April 2017 [7], some storage warehouses, like the dramatic fire in an artificial turf warehouse in Marseille (France) in 2020 [8], or several fires in sports stadiums, as the spectacular fire in Westfield (USA) in March 2011 [9]. These fires can have catastrophic consequences on human beings (death, injury, asphyxiation...), particularly when used in closed areas.

Regarding the classification of artificial turf in terms of fire behaviour, it is a flooring and the European EN ISO 13501-1 fire regulation for building products [10] applies. In this so-called Euroclass system, floor coverings are considered separately and the classification of the reaction to fire performance is based on four test methods: the EN ISO 1182 non-combustibility test and EN ISO 1716 gross calorific potential test if a A_{FL} classification is required (artificial turfs are not concerned) ; the EN ISO 9239-1 radiant panel test [11] and EN ISO 11925-2 Single-flame source test [12] for a B_{FL} to F_{FL} classification (Table 1).

The EN ISO 11925-2 Single-flame source test [12] aims at determining the ignitability of vertically oriented specimens by direct small flame impingement under zero impressed irradiance. The classification criteria are based on observations whether the flame spread (Fs) reaches 150 mm within a given time and whether the filter paper below the specimen ignites due to flaming debris. In addition, the occurrence and duration of flaming and glowing are observed.

The EN ISO 9239-1 radiant panel test [11] allows determining the critical radiant flux of horizontally-mounted floor covering systems exposed to a flaming ignition source within a test chamber. The specimen is exposed to a defined field of heat flux: 11 kW/m² at the hotter end close to the radiant panel, and decreasing to 1 kW/m² at the other end, farther away from the radiant panel. The progress of the flame front along the specimen length is recorded in terms of time taken to reach various distances. The smoke development during the test is measured on the basis of light obscuration by smoke in the exhaust duct: s1 classification if the smoke rate is lower than 750 %.min and s2 classification otherwise. The maximum duration of the test is 30 minutes and the classification criterion is the critical heat flux (CHF) corresponding to the furthest extent of flame spread. It is defined as the radiant flux (in kW/m^2): (a) at the point where the flame stops advancing in the case of a self-extinguishing specimen or; (b) at the position of the flame front after 30 minutes of test.

Table 1 gathers the classes of reaction to fire performance for flooring products and the corresponding classification criteria required by the two previously described fire tests.

Table 1: Classes of reaction to fire performance for floorings according to EN ISO 13501-1 (Euroclass).

Class	EN ISO 9239-1 (test time = 30 min)	EN ISO 11925-2 (ignition time = 15 s)
B_{FL}	CHF ≥ 8.0 kW/m²	Fs ≤ 150 mm within 20 s
C_{FL}	CHF ≥ 4.5 kW/m²	Fs ≤ 150 mm within 20 s
D_{FL}	CHF ≥ 3.0 kW/m²	Fs ≤ 150 mm within 20 s
E_{FL}	No requirements	Fs ≤ 150 mm within 20 s
F_{FL}	No requirements	No requirements

Due to the presence of different layers (sand and infill) above the backing, the single-flame source test cannot be performed on artificial turf structures for sports applications as the specimens must be vertically oriented. Thus, the fire performance of artificial turf structures is based on the EN ISO 9239-1 radiant panel test. However, the behaviour of this type of materials in such large-scale test has been seldom reported in the literature. Thus, information on the fire behaviour of turf structures in the standardized conditions is poor.

Several approaches have been developed to improve the fire properties of artificial turf. Indeed, some authors worked on the development of fire retardant (FR) solutions for infills [2], [13] or for turf fibres [14]. Occasionally a fire retarded infill material or back-coating containing halogenated compounds are used. However some of these derivatives are suspected to be

harmful to health and thus represent a risk for users if used in artificial turf structures [15], [16]. Commercial solutions [17], [18] also exist but at the moment the protection against fire of such structure is mainly obtained by the incorporation of the sand layer providing a physical barrier to protect the backing and sand is rarely added for private applications. On the other hand, the hazard associated with the use of artificial turf also arises from users not being aware of the fire risks associated with artificial turf. Dangerous behaviours are therefore common (thrown cigarette butts, barbecues, etc) leading to an increase in the risk of fire starting in private households in particular. Thus, the current solutions for the fireproofing of artificial turf are not satisfactory and need to be optimized.

Finally, the life cycle of artificial turf is currently problematic for a number of factors: the base of the structure cannot be recycled without separating each element (pile + backing) and the presence of sand, embedded in the spaces of the backing, prevents the reuse of materials. Moreover, the use of petroleum based infill materials increases the environmental impact of the structure.

For all these reasons, the prevention and the development of new innovative fire retarded systems, more environmentally friendly, are therefore essential to ensure better protection for users of artificial turf fields against fire.

In this context, the **Interreg GRASS project on safe and durable fire-resistant artificial turf (2018-2022)**, funded by the **European Regional Development Fund (ERDF)**, was proposed. It is a cross-border project carried out in collaboration with four main partners:

- The University of Lille provides its expertise in the field of fire retardancy of materials.
- The **University of Ghent** (Belgium) provides the combined expertise in artificial turf and fire testing and has the objective to develop new FR solutions for artificial turf.
- **Materia Nova** (Belgium) is a company active in the evaluation of the environmental impacts and is therefore in charge of the life cycle assessment (LCA) of the turf.
- **EuraMaterials** (France) has expertise in European projects and acts as a coordinator and booster of innovations. In the GRASS project, EuraMaterials' general objective is to act as a link between the project partners, the producers, the suppliers and the users of artificial turf.

On the other hand, **four associated partners**, namely Sport Vlaanderen, InfraSports, UNION Sport & Cycle and Fedustria, are also participating in this project with the general aim of improving information and collective awareness of the fire risks of artificial turf and providing their expertise in their field.

The GRASS project is divided into two main axes. The first axis aims at raise public awareness on the difference in fire behaviour between natural and artificial turf. The second one, led by the University of Lille, concerns the development of flame retarded artificial turf structures that could be used for indoor applications. To achieve this, two main issues have to be removed: (1) the understanding of the fire behaviour of artificial turf, as a whole and element by element, as well as (2) the fireproofing processes applicable to such systems and their mechanisms. In addition, the aim is to adopt an eco-friendly fireproofing strategy in order to reduce the environmental impact of the structure. **As a part of this project, the aim of this PhD work is to develop a new artificial turf structure used for sports applications, flame retarded by an innovative, environmentally and health friendly approach and that could be applicable in industry. The proposed solution should comply with the previously described standard (rate C$_{FL}$, s1).**

This manuscript presents the work performed during this PhD and is divided into **four parts**.

PART I consists of a **general presentation** of artificial turf structures, focusing mainly on the different improvements since their development, on the manufacturing process and on their properties. Then, information on the fireproofing processes is given, detailing the main classes of fire retardants (FR) as well as on the current fireproofing solutions applied to flooring structures. **PART II** is dedicated to the presentation of the different materials and experimental methods used in this PhD work.

PART III presents the results obtained in this project. It is divided into **four chapters**. A 'literature review' section and a 'materials and methods' section are carried out at the beginning of **Chapter 2** and **Chapter 3**.

It is first necessary to clearly understand the fire behaviour of artificial turf and the literature is poor on that topic. It was thus the objective of **Chapter 1.** To implement a fireproofing strategy, study of the fire behaviour and thermal stability of each component of the artificial turf is carried out using Mass Loss Cone calorimetry test (MLC), in order to better understand the role of each and to determine what component is the most important. The results lead us to pay specific attention to the infill, and in particular to cork, a bio-sourced, bio-degradable and

environmentally friendly material. An in-depth study of the fire behaviour of a cork-based structures is thus carried out.

In addition, since the fire scenario and the characteristic data are different between MLC test and the EN ISO 9239-1 test, tests carried out at the radiant panel test are needed to validate the FR performance of new materials. However, an important issue concerns the size of the sample in the standard test (EN ISO 9239-1). As a consequence, to allow a fast screening of artificial turf structures, **Chapter 2** deals with the reproduction at laboratory scale of the radiant panel fire test device (European standard EN ISO 9239 – 1 [11] that classifies the fire behaviour of floorings according to the Euroclass standard EN ISO 13501 – 1 [10]).

Chapter 3 then focuses on the development of an innovative fireproof method of cork granules, one of the infill studied in Chapter 1. A significant literature review is firstly carried out on cork (composition, properties, etc.) and on the various existing ways of modifying cork. Then, the protocols developed for the bulk modification of cork, based on the literature, are evaluated. Various characterizations are performed in order to select the most promising protocol. Once the modification process of cork is optimized, dimensional analysis modelling is applied to upscale the method to larger amounts of cork. Detailed characterizations of the properties of modified cork are then carried out.

Finally, **Chapter 4** is dedicated to the fire properties of artificial turf structures containing the modified cork, using MLC and the bench-scale radiant panel tests. Characterizations are then performed to propose the mechanisms of action of modified cork.

PART IV, finally, concludes about the different results obtained during this PhD work as a comparison of the state of the art. The outlooks are also proposed.

PART I - Literature review and background

As previously discussed, the aim of this part is to present the context of the project that led to the scientific and experimental approach proposed in the PhD thesis work. This part is divided into **3 sections**. A general presentation of artificial turf structures is first carried out, mainly focusing on their development, process and properties. Then, the fire behaviour of polymeric materials and the current fireproofing solutions applied to flooring structures are detailed. Based on these, the strategies and the scientific approach considered in this work are presented and discussed.

I. Artificial turf

A. Evolution and composition of turf surfaces

Artificial turf was originally developed for sports fields to replace natural grass. These structures provide attractive, durable and safe playing surfaces that can withstand high levels of use and a wide range of weather conditions. In 2020, the European market for artificial turf is really significant with over 16,000 full-size sports fields in use in Europe, and approximately 4,000 new fields are being built each year, representing a 25% growth per year [19]. Currently, the use of artificial turf for sport fields is supported by Union of European Football Association (UEFA), International Rugby Board (IRB) and many national federations.

The history of synthetic turf begins in the 1960s when the first multisport stadium with synthetic turf is installed in Texas [20]. At that time, artificial turf products are a real technological advance but they present risks of injury for athletes, being too abrasive and uncomfortable. These so-called 'first generation turfs' are made up of short polyamide (PA) fibres, without comfort pads or infills. In the 1970s, the use of synthetic turf spreads, mainly in the United States for baseball and American football in particular. A few years later, in 1976, its use at the Montreal Olympic Games in Canada for hockey competitions allowed the general public to be aware of the existence of such structures. From the 1980s, artificial turf manufacturers work on its visual aspect and also on its playing properties. The second-generation turf arises, with longer polypropylene (PP) fibres, a less abrasive material, and also with a layer of sand, leading to more comfortable and more flexible surfaces. But turf structures predominantly used nowadays are the third-generation ones, developed in the 1990s, as shown in Figure 1: Artificial turf for sport applications with (a) the backing, (b) the sand, (c) the infill and (d) the pile.. With an even longer pile, turf is composed of polyethylene (PE) fibres, further reducing abrasion and injuries. Moreover, in addition to sand, a damping infill layer consisting generally of rubber crumb is added to the structure. Although the presence of these two layers complicates the recycling process, they both play an important role. Sand provides stability and protects the turf; it helps to filter water and to keep the pile straight [21]. It also allows the structure staying in place and helps to make it more fire-resistant. The damping infill layer is added in order to improve playing comfort, rebound and shock absorption to ensure the safety of players. When a shock is absorbed only at the point of impact, it is then partially returned to the player which can cause injuries in case of violent fall. Thus, the use of a damping infill, combined with sand, makes it possible to obtain a real comfort of playing as well as a better shock absorption and reduced injuries. The development of this performance layer has resulted in a revolution in the

use of artificial turf for contact sports: infills allow good flexibility and better hold of the turf pile.

Over the years, infills nature diversifies and the choice depends on expected properties. Infills are mainly derived from petrochemicals. SBR (Styrene-Butadiene Rubber) is the most commonly used as it is an economic infill derived from scrap vehicle tires. EPDM (Ethylene Propylene Diene Monomer) or TPE (Thermoplastic Elastomer) can also be used but natural materials such as cork, are developing as potential alternative. Nowadays, a shock pad can be added under the backing to further improve shock absorption, providing a more uniform ground, improving the lifespan of the field and reducing the amount of infill [20]. This is the development of the fourth generation of turf.

Artificial turf presents a number of advantages. It can be used in all weather conditions since it is designed to be used intensively throughout the year, while fields with natural grass can hardly be used when temperature is too low. In addition, although the installation of artificial turf requires a greater investment, in light of its longer life cycle and great savings from low maintenance costs (no pesticides, no watering, no mowing, no need for regular marking, leading to a better environmental impact [15]), a quick return on investment (less than 5 years [22]) is noted. Indeed, average maintenance cost for an artificial field is around 3000 € per year (considering the first 10 years of use), compared to 50000 € for a natural field. Moreover, synthetic turf can withstand up to 1500 hours of playing time per year against 300 hours for a natural grass [23]. Thus, artificial turf is nowadays considered as a cost efficient, environmentally and user friendly product that can replace natural grass on sports fields [15].

However, since the 2010's, the toxicity of some of the components of artificial turf, and in particular of infill materials, has been highlighted both for humans [24]–[26] and for the environment partly due to the leaching of heavy metals into the soil [15]. As an example, Massey et al [26] have addressed the issue of chemical contents in common artificial turf infills, including styrene-butadiene rubber (SBR), ethylene propylene diene monomer (EPDM), thermoplastic elastomer (TPE) and mineral or plant-based infills. They showed that toxic compounds, such as metals, phtalate esters, polychlorinated biphenyls or polyaromatic hydrocarbons, are present in significant amounts in SBR but also, in smaller amounts, in TPE and EPDM. Natural infills contain less or no toxic compounds, making them an interesting alternative. In order to ensure the safety of players, the environmental and toxicological characteristics of artificial turf are regulated at different international levels. The European Union complies with REACH regulation ("Registration, Evaluation, Authorization &

Restriction of Chemicals") that aimed in particular at ensuring a high level of protection of human health and of the environment against the use of chemical substances. Artificial turf infills shall in particular comply with regulation 28 of Annex XVII of REACH regulation [27]. In addition, the use of microplastics is currently under debate at the European Chemicals Agency (ECHA). Thus, the use of non-natural infills such as SBR, TPE or EPDM will be soon prohibited. Only materials of natural origin could be further used. For this reason, natural infills, such as cork, are used extensively in Belgium, for example. All those aspects have to be considered in the development of new artificial turf structures.

In order to establish what can be modified in the development of FR products, the next section will be dedicated to the description of the process required to obtain artificial turf.

B. Manufacturing process

Tufting technology [28] is the most common process for the manufacture of textile floorings and it is the only one used for artificial turf production. Developed on the basis of the stitching technique, it consists in pushing the fibres through a support, called primary supports, which are then bound together by a set of loops. This technique is performed with a tufting machine, similar to a sewing machine, composed of a tufting device, a presser foot device, a thread feeding device and a framework which allow, among other things, to control the length of the stitches, the density and the direction of tufting. Hundreds of needles, arranged in the width direction and connected to a pneumatic jack in order to properly control the tuft length, insert the yarns in parallel and continuously into the primary supports. The yarn feeder provides a tufting yarn of a certain length and tension. As shown in Figure 2 [29], the tufting machine's needles perforate the primary support from behind. When the hollow needle retracts, the tufted yarn is held in the support by friction and forms a loop. The tufting machine is configured to produce structures with pile cut at the same level or multi-level pile. Finally, a back coating is spread and cured to bind the fibres to the support. This method results in good quality and resistant floorings with low production costs and high production rates, an important advantage for industry.

Tufting Diagram

1. Needle
2. Pile Yarn
3. Primary Backing
4. Looper
5. Pile Cutting Knife
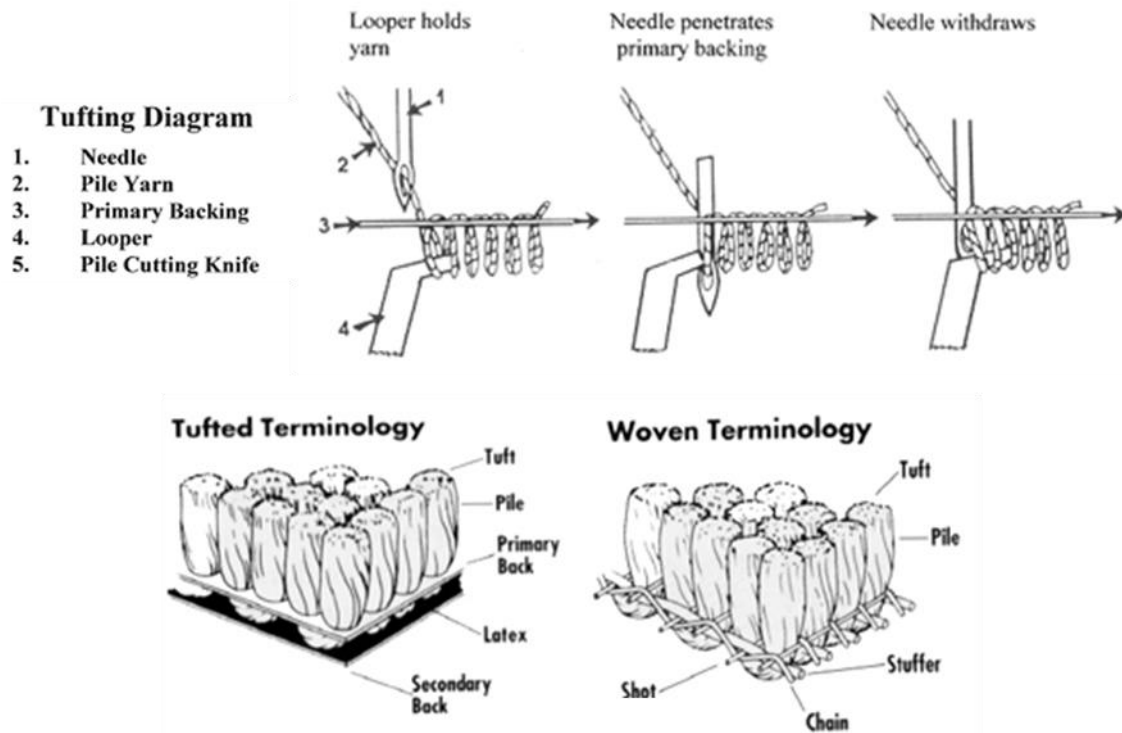
Figure 2: Tufting process.

When manufactured, the artificial turf is put in place. Its installation requires a lot of time and preparation. A clean, smooth and compact surface is essential for the correct laying of the artificial turf. The installation area must first be cleaned, weeded, levelled with sand and compacted, if it is an outdoor field. Next, a geotextile is used as a sub-layer. This is a non-woven, rot-proof textile placed between the artificial turf and the ground to prevent any weeds from penetrating and blocking the permeability holes in the turf. The turf sheets are then laid out in the direction of the grass fibres. Finally, they are held to the ground by nails. For indoor use, the floor must be clean and smooth. The strips are then glued directly to the floor. For outdoor and sport applications, sand and infill are added to the structure.

The processing of artificial turf is thus complex as well as its installation. Those aspects have to be considered in the present work. Moreover, not only fire retarded properties are required for artificial turf but specifications are needed. These properties are detailed in the following section.

C. Required functional properties

The properties required for artificial turf surfaces used for community, educational and recreational sport are gathered in the EN 15330-1 European standard [30]: it defines the tests to perform both at laboratory scale and on installed surfaces to ensure that the sports performance and player/surface interaction is suitable for the intended use. Many functional properties, such

as simulated resistance to the use of cleats to ensure a good durability of the ground, and mechanical properties (resilience, shock absorption, rebound, rolling, resistance to rotation, etc.), are evaluated to allow artificial turf to be used and marketed. Table 2 summarizes the performance requirements for football and rugby artificial turf fields according to EN 15330-1 standard [30]. The main aim is to prevent injuries ensuring good shock absorption and an optimal grip [20] as well as a long service life. Sanchez et al [31] studied the influence of structural components on the in situ mechanical behaviour of third-generation artificial turf football pitches. Each component of the turf was tested separately, showing a significant influence of the length and bulk density of the pile, of the tuft per square meter and of the sub-base material on the mechanical properties of the surface. Other authors, such as Hufenus et al [32], highlighted the high mechanical performance, namely stress relaxation, elastic recovery, and creep behaviour of a new developed bicomponent polyethylene (PE) and polyamide (PA) melt spun fibre used as pile.

Table 2: Performance requirements for football and rugby artificial turf fields according to EN 15330. Extracted from [30]

Specifications	Test methods	Performance requirements for:			
		Football		Rugby	
Vertical bounce	EN 12235	45 – 75 % (0.60 m – 1.0 m)		45 % – 75 % (0.60 m – 1.0 m)	
Ball rolling	EN 12234	Initial on-site testing	≥ 4 m $- \leq 10$ m	Initial on-site testing	≥ 1.3 m
		Periodic testing	≥ 4 m $- \leq 12$ m	Periodic testing	≥ 1.0 m
Shock absorption	EN 14808	$\geq 55\% - \leq 70\%$		$\geq 55\% - \leq 70\%$	
Vertical deformation	EN 14809	≥ 4 mm $- \leq 9$ mm		≥ 4 mm $- \leq 10$ mm	
Resistance to rotation	EN 15301-1	25 Nm – 50 Nm		30 Nm – 50 Nm	
Water permeability (if applicable)	EN 12616	≥ 180 mm/h		≥ 180 mm/h	
Surface smoothness	EN 13036-7	3 m rule	< 10 mm	3 m rule	≤ 10 mm

However, whereas mechanical properties are well regulated, there are few related fire safety requirements specific to the use of artificial turf especially as at the beginning it was mainly used for outdoor. Whereas, as previously stated, stadiums are increasingly used for some events other than sports competitions and can be both closed and opened. Thus, the fire risks associated with the use of synthetic turf are real and not negligible. Mainly composed of highly flammable polymers, artificial turf, considered as a flooring, must meet the EN ISO 9239 – 1 standard [11] according to the classification EN ISO 13501 – 1 [10] for indoor uses. Still rarely studied, the fire properties of artificial turf are nevertheless a key issue to improve the safety of its users and

thus is the objective of this project. The next part is thus dedicated to establish a state of the art on fireproofing methods.

II. Fireproofing methods

Fire is a chain reaction resulting from the thermal decomposition and combustion processes of flammable materials. For the combustion process to occur, the presence of three elements in proper combination is required: a combustible material, an oxidizing agent (such as oxygen from the air) and a source of energy (heat). If one element is missing, the fire declines until complete extinguishment. This called the fire triangle. Polymeric materials are commonly involved in fires [33]–[40] since they are highly combustible materials. They can release a huge amounts of energy when burn if specific conditions of temperature and air are met. The combustion is a highly exothermic chemical reaction involving many phenomena and depending mainly on the chemical composition of the material [41]. It takes place in four main phases:

- The first one is <u>the heating</u> of the material depending on the radiative properties, in particular heat transfers by conduction within the material and convective heat exchanges at the surface of the material. The activation energy must be sufficient enough to heat the material to a critical temperature when the weakest chemical bonds break.
- Then, <u>thermal degradation</u>, called thermo-oxidation (or pyrolysis in the absence of oxygen), occurs and the material is broken down into different compounds of lower molecular weight. During this step, various compounds are released, including combustible and volatile gases that may play the role of fuel.
- <u>Combustion of the degradation products</u> takes place when the concentration of fuel in the gas phase reaches a critical concentration, depending on the temperature.
- <u>Finally, the propagation phase</u> consists in the development and the propagation of the combustion. A large energy production (heat) takes place and is partly returned to the material by convective or radiative phenomena, contributing to maintain the combustion process [42] until the concentration in fuel is still high enough.

A. Fire-retardant approaches

As most of polymeric materials are inherently highly flammable, improving their fire behaviour is essential in order to ensure safety of people and buildings. The aim of fire retardant systems

is to delay polymer ignition or to decrease the amount of energy released in order to slow down the combustion and/or to decrease the amount of toxic compounds released.

To do so, three main strategies can be considered [43].

- The first one is the reactive approach, consisting in the chemical modification of the macromolecular chain during polymer synthesis or the grafting through chemical bounding of fire-retardant (FR) moieties on the polymeric chain. This technique is not widely used because it is expensive and hardly applicable to industry.

- The second one is the surface treatment method leading to a fire protection of the material. This fireproofing process does not alter the intrinsic properties of the polymer but problems related to adhesion and ageing of the coatings can occur, leading to a decrease of the FR properties. Moreover, it cannot be applied to all categories of materials, it is mainly considered for dense materials such as wood or steal. In that case, intumescent systems that swell under thermal irradiation to protect from heat flux the substrate by the formation of an expanded layer of low thermal conductivity was widely studied [42], [44]–[46].

- The last and more common approach is the physical method consisting in the incorporation of flame retardants additives (FR) into the polymer during its transformation processes. It is the less expensive method, easily applicable at industrial scale, leading to efficient fire retarded behaviour.

Following this last approach, various classes of FR additives are reported. In a non-exhaustive way, flame retardants can be halogenated [47]–[50], phosphorous-based [51]–[54], nitrogen-based [55]–[57] compounds, metal hydrates [58]–[60] or nanoparticles [61]–[64]. These flame retardant additives can be used alone or in combination to obtain synergistic effects [65]–[67]. Depending on their nature, flame retardants can act either chemically, physically or both; in the gas phase, in the condensed phase or in both, in at least one of the four main combustion steps [44] previously described. Table 3 reports the main types of flame retardants and their respective modes of action and mechanisms. The addition of flame retardants (FR) in the polymers is intended to increase the ignition time, to reduce the propagation of the flame, to modify the flame regime, to improve the self-extinguishing capacity of the fuel, or to inhibit the chain reactions of the combustion [68]–[70]. They are also intended to reduce the smokes and toxic gases released (CO, HCN, etc.) and to prevent the formation of flammable drops during combustion [44], [71]. However, some of these derivatives, especially some halogenated

FR, are suspected to be harmful to health and some of them have already been banned by the European Commission and forbidden by REACH regulation in 2007 [72].

Table 3: Main flame retardants used in polymers and their associated modes of action and mechanisms.

FR categories	Actions	Mechanisms	Refs
Halogenated	Chemical action in gas phase	Inhibition of radical reactions*	[47]–[50]
Phosphorus	Chemical action in gas phase Physical action in condensed phase	Inhibition of radical reactions* Dilution of combustible gases** Formation of a phospho-carbonaceous solid residue***	[51]–[54]
Nitrogen	Physical action in gas phase Physical action in condensed phase	Dilution of combustible gases** Promotion of the formation of a carbonaceous solid residue***	[55]–[57]
Metal hydrates	Chemical actions in gas phase Physical action in condensed phase	Dilution of combustible gases** Endothermic effect Formation of a ceramified barrier	[58]–[60]
Nanoparticles	Physical action in condensed phase	Formation of a diffusion barrier (labyrinth effect)***	[61]–[64]

Capture of energy of the radicals H° and OH° reacting with halogenated X° or phosphorus PO- and HPO2- of lower energy, causing the combustion reaction to slow down by cleaving the reaction chain.

**Release of non-combustible gases (H_2O, CO_2) leading to the dilution of combustible gases in the gas phase below the flame's ignition threshold leading to flame extinction.*

***Limiting oxygen and fuel transfer as well as heat transfer that slow down the rate of degradation of the polymer and the emission of a smaller amount of fuel gas also contributing to slow the development of fire.*

After considering the different possible approaches to fireproofing materials, the next section describes the fire behaviour and fireproofing methods applied specifically to floorings. The study was also carried out on carpets since literature regarding the fire retardancy of carpet is poor.

B. Fire behaviour and fireproofing methods of floorings

Synthetic floorings include a wide range of textile floorings, generally called 'carpets', such as rugs, needle punched floorings, floorings made of plant fibres (sisal, sea rush, coir, etc.), etc. The structure of 'carpets' is similar to that of artificial turf as they are also composed of synthetic fibres inserted into a polymeric backing and held together by a back coating. Since the middle of the XXth century, the fire behaviour of carpet floorings was extensively studied.

The influence of the carpet's constituents has been investigated by several authors [73], [74]. They highlighted that each component of the carpet contributes to the overall flammability performances but conventional latex back coatings, and the optional secondary backing, were the most influential factors in the fire behaviour of carpets, their presence leading to an ignition at lower radiant heat (0.78 W/cm² for the structure with a secondary backing against 1.25 W/cm² for the conventional structure). Other authors [75], [76] assessed the fire behaviour of carpets composed of different types of fibres or blend of fibres, especially using the radiant panel test. They demonstrated that wool and FR wool have shorter flame spread (only 8 cm within 10 min) than other synthetic fibres such as polyamide (PA), polyester (PET) or PP (up to 37 cm within 10 min). The density, the weight and the thickness of the pile also strongly influence heat dissipation. Nowadays, numerical simulations are even used to predict the fire behaviour and thermal properties of certain types of carpets, such as described in the study carried out by Diswat et al [77] who developed, and validated, a mathematical model to predict the thermal resistance of a cut pile hand tufted carpet.

Based on these observations, many patents proposing solutions to improve the fire behaviour of carpets have been published [78]–[81]. Most authors have focused on the flame retardancy of carpet pile [82], [83] such as Erdem et al [84] who produced slow burning PP for carpet pile by incorporating silicon dioxide (SiO_2) nanoparticles into the polymer at different rates. The Limiting Oxygen Index value (LOI) of the filaments increased progressively until 22 vol.% was achieved with 3 wt.% of SiO_2 nanoparticles. Fireproofing of cotton and polyester carpet pile was also performed [85] by modifying the pile with polycarboxylic acid crosslinking systems by a spray, dry and cure process to impart flame-retardant properties, leading to improvements in LOI values up to 24.4 vol.% instead of 19.1 vol.% for untreated pile. In addition, Benisek [75] highlighted that using a FR latex back coating permitted to limit the spread of flame (9 cm of flame spread within 10 min for the FR latex back coating structure against 26 cm for the conventional one).

In order to find out whether these types of fireproofing methods are also relevant for artificial turf, a thorough study of its fire behaviour is first necessary. However, unlike carpets, fire hazards associated to the use of artificial turf are rarely discussed while the flammable organic materials composing these structures can greatly contribute to the development and spread of fire. In 2018, Kukfisz B [86] studied the degree of flammability of turf systems used for landscaping in residential and public buildings. The horizontal radiant panel test, in accordance with EN ISO 9239-1 standard, was used to characterize the structures by measuring the flame

spread. The tested structures, mainly composed of polyethylene (PE) and polypropylene (PP), meet the requirements of class E_{FL}, meaning that they are suitable only for household use (like outdoor decoration), and entail a considerable risk in roofed buildings.

Regarding artificial turf, only very few structures currently meet the standards and articles or patents dealing with the development of flame retardant (FR) solutions to improve its fire behaviour are scarce. Reddick [2] patented a new infill composed of recycled waste glass or glass beads, giving the infill a non-flammable character. Rodgers [13] mentioned the use of inorganic salts encapsulated in a water-insoluble material as flame-retardant infill. Commercial FR solutions have also been developed. Recently, ethylene propylene diene monomer (EPDM) infill materials have been fire retarded with a high percentage of calcium carbonate ($CaCO_3$) (up to 80 wt.%) [17]. Moreover, styrene butadiene rubber (SBR) infill material can be flame retarded with halogenated compounds. Studies have also been carried out on the development of FR solutions for turf fibres. Lehner [14] et al. have developed the use of 6H-dibenz[c,e][1,2] oxaphosphorin,6-[(1-oxido-2,6,7-trioxa-1-phosphabicyclo[2.2.2]oct-4-yl)methoxy]-, 6-oxide (DOPO-PEPA), as flame retardant for low density polyethylene (LLDPE). Mixed with commercial thermal stabilizers, the thermal stability as well as the fire retardancy of LLDPE/DOPO-PEPA films have been tested and promising results were obtained with 10 wt.% DOPO-PEPA and 2.5 wt.% stabilizer (increase of 26 vol.% in LOI value). The small amounts of flame retardants used are compatible with the processing of fibres and can therefore be considered as a solution to improve the fire behaviour of artificial turf. Some masterbatch manufacturers, such as Avient [18], also provide commercial halogenated-based solutions to enhance the flame retardancy of turf fibres. In addition to infills (SBR) and fibres, the latex used as back coating can also be flame retarded with halogenated compounds. However, as previously discussed, this approach is not considered in this project for reasons of health and environmental protection [72].

III.   Goal and scope of the PhD thesis – scientific approaches and defined strategy

We have thus shown that the use of artificial turf for sports fields is becoming more and more popular and, that the uses of such materials are moving (not only sport but other activities such as concert…). This is explained because they have many advantages such as low maintenance and playability in all weather conditions. However, being mainly composed of highly

flammable polymers, in case of fire, these structures can ignite and spread flames quickly representing of risk.

Currently, there is very little information on the fire behaviour of such complex multi-layer materials, yet this information is essential to be able to define fire proofing strategies for artificial turf. Therefore, the first part of the study has been focused on a better understanding of the fire behaviour of artificial turf. These aspects are detailed in **Chapter 1**, **PART III** in which the impact on the artificial turf fire behaviour of each component, of the association of component and of the whole structure will be investigated. The results obtained in this chapter will permit to define the component with the highest impact and thus, a fireproofing method will be selected. Indeed, as explained in the previous section, the choice of fireproofing methods and of flame retardant additives will depend on the material to be fireproofed and of the expected properties. The selected method will be developed in **Chapter 3**, **PART III**. In this chapter, we will consider that the flame retardants used should not be toxic compounds (halogen-free, no nanoparticles …) to avoid being harmful to health and to the environment.

On the other hand, this literature review shows that artificial turf has to meet several specifications to be used either for indoor or outdoor applications. Regarding its fire properties, the EN ISO 9239-1 fire test has to be used. However, this test required large amount of materials and thus it could appear as a break considering development of new fireproofing methods and formulation. That is the reason why the design, optimization and validation of a laboratory scale test mimicking the EN ISO 9239-1 was considered. The results are presented in **Chapter 2**, **PART III**. This test as well as other technics will further be used in **Chapter 4**, **PART III** to validate the accuracy of the approach as well as to determine the main mechanisms of action of the fireproofing method that was selected.

However, before presenting all the results of the study in PART III of this manuscript, the description of 'materials and experimental methods' used in the whole study is considered in the following part.

PART II – Materials & experimental techniques

The aim of this part is to describe the materials as well as the methods used to assess the properties of artificial turf structures. This part is divided into two sections. **Section 1** details the composition of the different artificial turf structures and the properties of infill materials. **Section 2** focuses on the main experimental techniques used throughout the PhD work to characterize the materials and to evaluate their fire retardant properties.

In this part, only the materials and methods that will be used during the whole study are reported. However, a specific 'Materials and methods' section will be added at the beginning of **Chapter 2 and Chapter 3** in **PART III** to describe the experimental techniques used exclusively in these two Chapters.

Section 1 – Composition of artificial turf structures

Artificial turf structures (Figure 3) for sports applications are considered in this project. They are composed of: a polypropylene (PP) tufted backing (Figure 3, a); a layer of sand (10 mm) (Figure 3, b); a damping infill layer (Figure 3, c) and PE pile (40 mm long) (Figure 3, d).
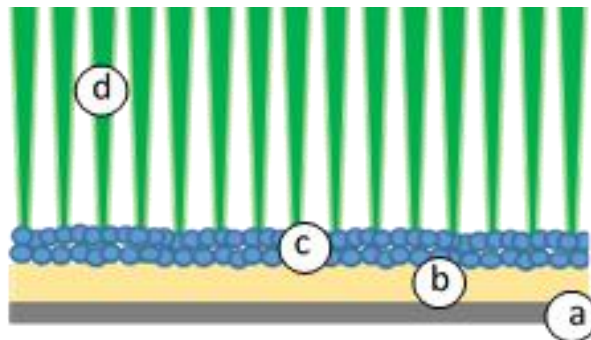
Figure 3: Artificial turf for sports applications with (a) the backing, (b) the sand, (c) the infill and (d) the pile

Several infill materials (Table 4) were used: styrene butadiene rubber (SBR) (15 mm thickness), ethylene propylene diene monomer (EPDM) filled with about 45 % of calcium carbonate ($CaCO_3$) (10mm thickness), a flame retarded (FR) EPDM (FR EPDM) (10 mm), thermoplastic elastomer (TPE) filled with about 35 % of $CaCO_3$ (5 mm) or cork (15 mm). Two types of corks were used, whose density was determined thanks to a pycnometer: a 'lighter' cork (referred as Cork) with an apparent density of 0.32 g/cm^3 and a 'denser' cork (referred as d-Cork) with a 0.72 g/cm^3 density. Considering the whole structures (backing, sand, infill and pile), **SBR-based, Cork-based, d-Cork-based, EPDM-based, FR EPDM-based and TPE-based artificial turf structures will be referred to as S - SBR, S - Cork, S - d-Cork, S - EPDM, S - FR EPDM and S - TPE respectively.** As specific damping properties are required, the thickness of the infill layer differs from one material to another. It corresponds to the thickness that has to be used to obtain good damping properties.

All components of artificial turf structures (backing, sand and infill materials) are provided by the European Research Centre for Artificial Turf (ERCAT) at the Centre for Textile Science and Engineering (Department of Materials, Textiles and Chemical Engineering) of Ghent University (Belgium) (GRASS project coordinator).

Table 4: Infills used in the study and their properties

	SBR	EPDM		TPE	Cork	
		EPDM	EPDM FR		Lighter	Denser
Density (g/cm^3)	1.06	1.33	1.49	1.45	0.32	0.72
Thickness (mm)	15	10	10	5	15	15
Colour	Black	Green	Lighter green	Green	Brown	
Cost (€ per full size field)	Around 350.000€	Around 60.000€ extra per field compared to SBR	Around 70.000€ extra per field compared to SBR	Around 70.000€ extra per field compared to SBR	Around 40.000€ extra per field compared to SBR	
Properties	Very good UV resistance Good wear properties Smell possible High heat generation	UV stabilisers needed Risk of hardening Smell possible Medium heat generation		UV stabilisers needed Good wear properties Less risk of smell Medium heat generation	Good UV resistance Good wear properties No risk of smell Low heat generation	
Possible fillers	Fire retardants	CaCO$_3$ Fire retardants		CaCO$_3$ Fire retardants	No fillers	

Section 2 – Methods

I. Fire testing: Mass Loss Cone calorimetry

The fire behaviour of materials has to be evaluated through fire tests. Mass Loss Calorimeter (MLC) is used because it is an efficient, fast and low material consumption way of determining the heat release rate of a material. This data is important because it can be a factor in the spread of a fire. In the case of flooring studies, it therefore provides additional information to that obtained from the standard radiant panel test (mainly providing information on the length burnt). MLC can be used to assess the burning behaviour of artificial turf structures or to investigate the fire behaviour of flame retarded solutions.

A. Artificial turf structures preparation

To perform the MLC tests, 'backing + pile' samples of 100 x 100 mm² size are cut with a cutter. Then, a metal grid (size of 110 x 110 mm²) is placed onto the backing, making sure that the pile remains straight. The grid prevents the sample from moving during the fire test. Sand is then distributed as evenly as possible over the backing and the grid, keeping the pile as straight as possible. Finally, the damping infill material is also uniformly spread above the sand layer. The specimens are weighed before and after fire testing in order to determine the weight loss.

This procedure is used when the complete artificial turf structures are tested. However, specimens can also be tested:

- Without any damping infill material ('backing + pile + sand' sample)
- Without sand and infill ('backing + pile' sample)
- Without sand, infill and pile ('backing' sample). In that case, fibres emerging from the backing are removed using a razor blade.

Infill materials can also be tested alone. In such case, no metal grid is used to perform the test. The next part is dedicated to the description of the MLC testing.

B. Mass Loss Calorimeter testing

To evaluate the fire behaviour of artificial turf structures, a MLC from Fire Testing Technology (FTT) (Figure 4 (a)) is used and tests are performed according to the EN ISO 13927 procedure [87], [88]. This bench-scale apparatus allows testing the reaction to fire of materials in a forced flaming combustion scenario. In MLC, the temperature of the degradation products during combustion is measured by a thermopile, consisting of four thermocouples located at the top of the chimney, and allows obtaining the heat release rate (HRR) according to a calibration curve obtained by burning methane at various flow. This is the main difference between the MLC and the cone calorimeter (ASTME-1354-90) [89], in which the oxygen consumption is measured during the test to determine the HRR.
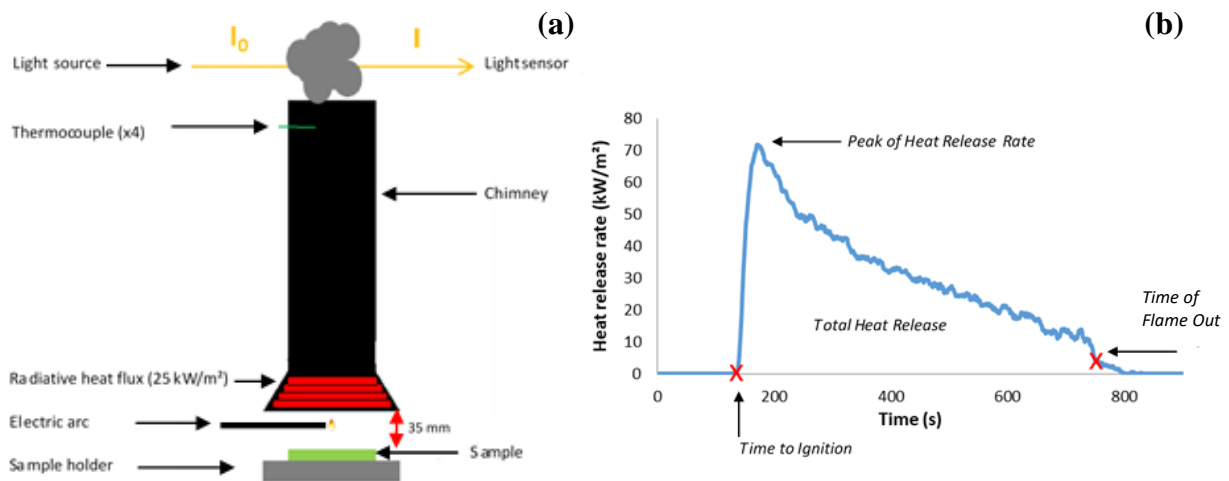
Figure 4: (a) Mass loss calorimeter fire testing and (b) an example of a recorded HRR vs time curve with the main determined parameters

To perform a test, the assembly previously described or the materials (infill, backing, …) are placed onto a ceramic board and held by a frame covering the edges of the samples. This assembly is exposed horizontally to an external heat flux of 25 kW/m² corresponding to a developing fire scenario [90]. The distance between the upper infill surface and the radiant source is fixed at 35 mm. At the beginning of the test, an electric arc is placed between the sample and the heating resistance. During testing, air velocity is measured by an anemometer (supplied by OMEGA) and was fixed at around $(1 \pm 0,1)$ m.s^{-1}.

MLC allows measuring the evolution of the HRR as a function of time (Figure 4 (b)). The main parameters considered for the comparison of the different results are: the peak of heat release rate (pHRR); the time to ignition (TTi); the total heat release (THR) corresponding to the area under the HRR vs time curve; and the time of flameout (TFO). All tests were performed at least

three times to ensure repeatability and results are reproducible within a relative standard deviation of ±15 % for the TTi and of ±10 % for the pHRR and the THR. For the THR determination, the shortest TOF of a series of measurements is taken as the last measurement point to allow comparison of the THR data.

To obtain additional information about the temperature evolution inside the samples during the fire tests, 6 thermocouples (0.5 mm diameter) are inserted from the bottom of the sample, bent and maintained at the backing surface, below the infill and sand layers as presented in Figure 5.
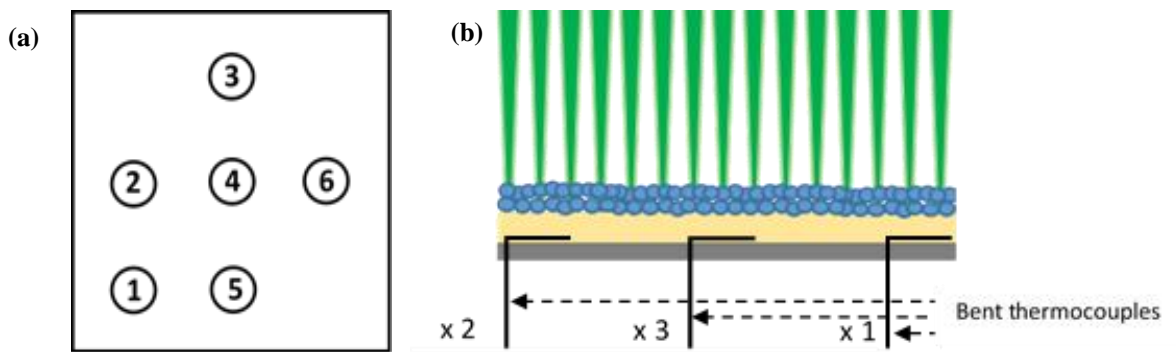
Figure 5: Position of the six thermocouples onto the backing: (a) top view and (b) side view

II.   Thermal stability

A. Thermogravimetric analyses

Thermogravimetric analyses (TGA) were carried out using a TGA Discovery 5500 supplied by TA Instruments. This technique allows studying the thermal decomposition of samples by determining the weight loss versus temperature. Because of their small size and in order to obtain representative results, the granules of infills were not grinded and about 10 mg of sample were directly deposited in an open alumina crucible equipped with a gold foil. The thermograms were recorded in the 40–800°C temperature range, with a heating rate of 10°C/min under a 50 mL/min nitrogen flow. Then, data were analysed using the TRIOS software. The main parameters considered to have information on the thermal stability of the samples are: the temperature at the onset and at the maximum of the degradation, the final residual mass at 800°C and the mass loss rate at specific temperatures, thanks to the derivative curve (DTG).

B. Heat treatments

The thermal stability of infill materials was also evaluated by heating it in a benchtop furnace (Nabertherm, Controller P320) from room temperature to 600°C, the temperature at which cork is usually fully degraded. The purpose of these tests is to assess the degradation of material at high temperature and also to determine the percentage of residual mass in order to evaluate in a simple and rapid way its thermal stability. To perform the test, samples of around 250 mg were exposed to a temperature rise of 10 °C/min from room temperature to 600°C by going through 4 intermediate degradation temperatures, i. e. 200, 300, 400 and 500°C (no step at intermediate temperatures). When the required temperature was reached, i.e. 200, 300, 400, 500 or 600°C, residues were immediately taken out from the furnace and were cooled down until room temperature. Samples were then weighed after calcination to determine the final residual mass.

III. Stability of materials towards water

As artificial turf can be used outdoors, external aggressions linked to the weather (rain, snow, etc.) must be taken into account. In order to limit any potential soil contamination due to leaching, as well as to study the ageing due to the impact of water on the components of the artificial turf (in particular the infill), it is essential to study the stability of the infill materials in water.

A. Evaluation of leaching in water

Leaching refers to the extraction of soluble products by a solvent, and in particular by water circulating into the soil. The behaviour of infill regarding leaching in water is important to assess if toxic elements could be released into the soil over time. A first approach was proposed in this project but further experiments will be required for commercial applications. The preliminary test established by the lab is the following: 2.5 g of infill were immersed into 400 mL of demineralised water (pH = 7.9), under magnetic stirring (300 rpm) and maintained at 25 °C. For five days, three times a day at regular intervals, the pH value of the solution containing the infill was measured (MeterLab PHM210), and then a final value was measured 30 days after the first measurement. Beforehand, the pH meter was calibrated with two buffer solutions (pH 4 and 7).

B. Dynamic Vapour Sorption

Dynamic Vapour Sorption (DVS) is a gravimetric technique used to determine the interactions of vapours with solids. Sorption of infill materials were collected on a gravimetric vapor sorption analyser (TA Instrument, Q5000 SA) equipped with a microbalance resolution of 0.1 μg. Without pre-drying, around 5 mg of sample were placed in a stainless-steel mesh pan suspended from the balance inside a separate chamber with controlled temperature and relative humidity. From the beginning of the test, sample mass was continuously recorded. The first step consists of exposing the sample to an isotherm at 60 °C, for a maximum of one hour, until the sample mass variation for a time interval of 5 minutes is lower than 0.001wt.%. Sample is then exposed to a relative humidity (HR) varying from 0 % HR to 95 % (each 5 %), followed by the same procedure but decreasing the HR from 95 % to 0 %. Relative humidity value is changed as soon as the sample mass variation for a time interval of 5 minutes is lower than 0.001 wt.%. This allows sorption-desorption cycles to be obtained, knowing that a complete sorption-desorption cycle requires approximately 48 hours.

IV. Spectroscopic analyses

A. Infrared Spectroscopy

The principle of infrared (IR) spectroscopy is based on the absorption of light by molecules in the infrared region of the electromagnetic spectrum. This absorption corresponds specifically to the molecular vibrations of the bonds of a molecule. This absorption is measured as a function of wavelength. Infrared spectra were obtained using a Thermo scientific spectrometer (Nicolet iS50 FT-IR) in ATR configuration. Infill materials, in granular form, were pressed on a diamond crystal and were scanned (64 scans) in the 4000-400cm^{-1} region. After being collected, spectra were treated with OMNIC software.

B. Solid state nuclear magnetic resonance (SS NMR)

Nuclear magnetic resonance (NMR) spectroscopy is one of the most advanced tools for determining the chemical structure of a material. NMR is based on the measurement of the absorption of radio frequency (RF) radiation by an atomic nucleus in a strong magnetic field. When subjected to electromagnetic radiation, usually applied in pulses, atomic nuclei can absorb the energy of the radiation and then release it during relaxation. The energy involved in

this resonance phenomenon corresponds to a very precise frequency, depending on the magnetic field and other molecular factors. This phenomenon therefore allows the observation of the magnetic quantum properties of nuclei, by obtaining an NMR spectrum, leading to the identification of the nature of the chemical species.

Solid state NMR was used in this PhD work to determine the changes of chemical environment of two nuclei (^{13}C and ^{31}P) after several thermal treatments. Experiments have been performed on infill materials at room temperature and after heat treatments (HTT) at different temperatures (200, 300, 400, 500 and 600 °C) in a furnace. A Bruker AVANCE III HD (9.4 tesla) spectrometer operating at 100 MHz was used for the ^{13}C solid-state experiments. These experiments were operating using cross-polarisation with magic angle spinning (CP MAS). A 4 mm CP-MAS probe was used with a spin rate of 12.5 kHz. The contact time was set at 1 ms and the number of accumulated scans was 1024 or 10240. Regarding the ^{31}P solid state NMR, a Bruker AVANCE III HD (9.4 tesla) spectrometer operating at 162 MHz was used. A 4 mm CP MAS probe was used with a spin rate of 12.5 kHz. High Power Decoupling (HPDEC) sequence was used for these experiments. The recycle delay was 30 s and the pulse angle was 2 µs. The accumulated number of scans was 256.

The next part is dedicated to the presentation of the experimental results obtained during this PhD work.

PART III – Experimental results

The aim of **PART III** of this manuscript is to present the results obtained during this project. It is divided into **four chapters**.

Firstly, as the literature data is poor on the fire behaviour of artificial turf, the objective of **Chapter 1** is intended to better understand the fire behaviour of artificial turf structures. As a consequence, the study of the fire behaviour and thermal stability of each component of the artificial turf is carried out using MLC test, in order to determine the role of each component of the artificial turf. After identifying the component being the most impacting factor, the work further focuses on it.

Secondly, the literature review and context presented in **PART I** also highlights that an important issue linked to the development of artificial turf is the size of the standard test that requires high amount of materials. As a consequence, **Chapter 2** deals with the development of a bench scale test. The design and test protocol are fully developed and described. An experimental design methodology is implemented to determine the optimal settings of the small-scale device. After validation of the radiant heat flux distribution map of the downscaled test, the artificial turf structures are evaluated using both scale tests to validate the bench scale test.

Based on the results obtained in Chapter 1 and Chapter 2, **Chapter 3** focuses on the development of an innovative fireproof method of the component that mainly contribute to the fire behaviour of the turf, i.e. the infill. Attention is focus on cork, a bio-sourced material. Its fire behaviour was improved through phosphorylation. Some protocols to bulk modify the cork are developed and their efficiency are evaluated through various characterizations. The selected cork modification protocol is then optimized and dimensional analysis modelling is applied to upscale the method to larger amounts of cork. Detailed characterizations of the efficiency of grafting as well as the evaluation of the functional properties of modified cork are then carried out.

Chapter 4 ends this part dealing with the investigation of the fire behaviour of modified cork using MLC test and the small-scale radiant panel test previously developed. This evaluation is required in order to assess if cork modifications have been efficient enough to meet the specification defined in the project (C_{FL} and s1 rating). Characterizations of the influence of

temperature on the modified cork are also performed to propose a flame retardant mechanism of action.

Chapter 1 - Comprehensive study of the fire behaviour of artificial turf

As mentioned previously, the widening of artificial turf market can be explained by the constant improvements in terms of designs, materials, manufacturing processes, properties. In the 1980's, patents and articles dealing with artificial turf mainly focused on the description of the composition, design and applications [1], [3]–[5]. In the following years, specific properties (such as mechanical properties) [4], technical aspects of manufacturing processes [5], design of the structures [3] or of their composition (fibres, infills, back coating) [1], [2] were further investigated. It allowed a better understanding of the role of the different components and thus the development of new structures with higher performance. More recently, the better environmental impact of artificial turf [15] was considered compared to natural turf. It was evidenced that artificial turf presents better performances due to water savings and low maintenance requirements, justifying the increase of its use. Fire hazards associated to the use of artificial turf are rarely discussed while the flammable organic materials composing these structures can greatly contribute to the development and spread of fire. In the case of a fire, especially in public places, the consequences could be dramatic. Determining the impact of each component of the artificial turf and their influence on the overall fire behaviour of the structure is therefore essential to enable the development of a suitable fireproofing method. Thus, this chapter is intended to have a better understanding of the fire behaviour of artificial turf structures so as to find the most efficient way to bring FR properties.

The fire behaviour of the complete artificial turf structures defined in the GRASS project and of each component of these structures is studied using Mass Loss Calorimetry (MLC). After determining the main components contributing to the fire behaviour, further MLC experiments are performed varying some characteristics of the turf structure in order to have an even better understanding of the fire behaviour.

I.   Fire behaviour of artificial turf

The aim of this part is to better understand the exact contribution of each component of the artificial turf structure on its fire behaviour. Thus, the fire properties of each element of the structure are investigated using MLC. The structure is divided into two main parts: on the one hand, the backing, pile and sand and on the other hand, the infill alone. Once the influence of each component is defined, the fire behaviour of the complete structure is evaluated.

A. Fire behaviour of the backing / pile / sand

In this part, the fire behaviour of the backing with and without pile as well as with and without sand was evaluated. To test the backing alone, the emerging turf fibres were removed using a razor blade. By comparing MLC data obtained for the 'backing + pile' sample and for the 'shaved' one, the contribution of the 40 mm long fibres is determined. MLC curves of the backing with and without pile and of the backing with sand are shown in Figure 6 and the corresponding data are given in Table 5.
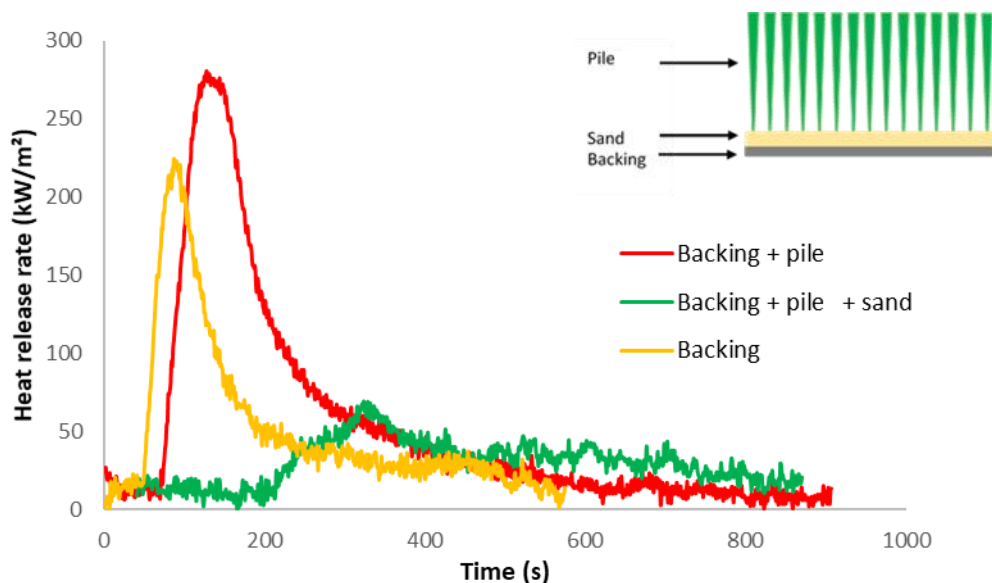
Figure 6: Heat release rate curves of the backing, of the backing without pile and of the backing with sand obtained at Mass Loss Calorimeter test

When the 'backing + pile' system is exposed to the MLC radiative heat flux, the fibres melt immediately and form a uniform layer of melted polymer at the backing surface. The amount of energy required to ignite this layer is significant, leading to an increase of around 40 s of the ignition time compared to the structure without pile. Moreover, a non-negligible increase of 25 % of the pHRR and of 92 % of the THR, compared to the backing without pile is observed. The

two previously mentioned structures burn completely. Thus, the combustion of the pile almost leads to a twofold increase of the THR value which is not surprising since pile is composed of a highly combustible polymer (PE). Considering the composition of the artificial turf structure, the backing and the pile respectively account for around 62 % and 38% of the total weight, showing the high contribution of the pile to the fire behaviour.

Table 5: Mass Loss Calorimeter results obtained for the backing, the backing without pile and the backing with sand

Structures	TTi (s)	pHRR (kW/m²)	THR (MJ/m²)	TFO (s)
Backing	44 ± 1	224 ± 13	25 ± 1	293 ± 26
Backing + pile	86 ± 6	281 ± 8	48 ± 2	752 ± 32
Backing + pile + sand	211 ± 11	69 ± 3	25 ± 1	746 ± 8

When sand is added into the structure, the fibres melt once exposed to the radiative heat source, and small clusters of melted polymer can be observed at the sand surface. A significant decrease in the heat release rate is noticeable, with 75 % and 48 % decrease for the pHRR and the THR respectively. Sand, being an inert mineral infill, thus forms a protective layer at the backing surface, limiting heat transfer from the radiant source to the tested structure. This considerable improvement in the fire behaviour brought by sand is consistent with artificial turf manufacturers recommendations in the case of landscaping applications, to incorporate a layer of sand to ensure fire safety and to comply with C_{FL} class of the EN 13501-1 European fire standard [10]. For sports applications, the sand layer is conventionally covered by an infill material to bring comfort and damping properties and to prevent player injuries. Therefore, the fire behaviour of infill materials must be evaluated.

B. Fire behaviour of infill materials

Fire performance of the different infill materials has been studied. As mentioned in the 'Materials' section (**PART II**), the layer thickness depends on the infill material (Table 4, page 21). MLC curves giving the HRR evolution versus time for the different infill materials are shown in Figure 7 and the corresponding data are given in Table 6.
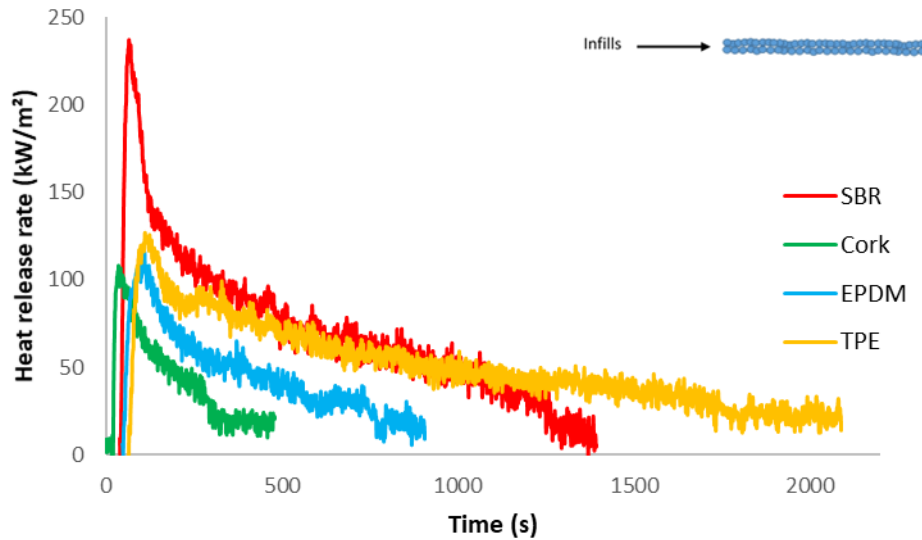
Figure 7: Heat release rate curves of the different infill materials

Table 6: Mass Loss Calorimeter results of the different infill materials

Infills	Thickness (mm)	TTi (s)	pHRR (kW/m²)	THR (MJ/m²)	TOF (s)
SBR	15	39 ± 2	237 ± 24	81 ± 8	1267 ± 204
Cork	15	19 ± 3	108 ± 1	20 ± 1	284 ± 4
EPDM	10	47 ± 3	115 ± 2	39 ± 2	782 ± 62
TPE	5	66 ± 4	127 ± 3	86 ± 7	1895 ± 236

Fire behaviour differs greatly from one infill to another. Firstly, in terms of pHRR, SBR presents the worst fire behaviour but, in terms of THR, SBR and TPE lead to similar values considering the standard deviation (81 MJ/m² and 86 MJ/m² respectively). Although TPE contains 35 wt.% of $CaCO_3$ as mineral filler, the small thickness of the TPE layer (5 mm) leads to a rapid flame propagation through the infill thickness. The presence of a mineral filler cannot prevent the combustion of TPE, leading to a significant total heat release. Then, EPDM and cork present close pHRR values but the THR value is much lower for cork, i.e. only 20 MJ/m² versus 39 MJ/m² for EPDM. The better performance of EPDM compared to other synthetic infill materials can be explained by the high amount of $CaCO_3$ as mineral filler (45 wt.%) included into EPDM granules, leading to a lower amount of organic material. Moreover, the EPDM layer thickness (10 mm) allows a different combustion behaviour. As for cork, its structural characteristics (gas enclosed in small cells) and its chemical composition make it naturally an excellent thermal insulator, showing a considerable fire resistance [91], [92]. These

properties are consistent with the low THR and the short burning time (low TFO) observed for cork infill.

C. Fire properties of the complete structures

The fire behaviour of the complete structures (backing with pile, sand and infill) has then been determined with MLC test. The infill thickness is the one mentioned in the experimental section. HRR curves are shown in Figure 8 and the corresponding data are given in Table 7.
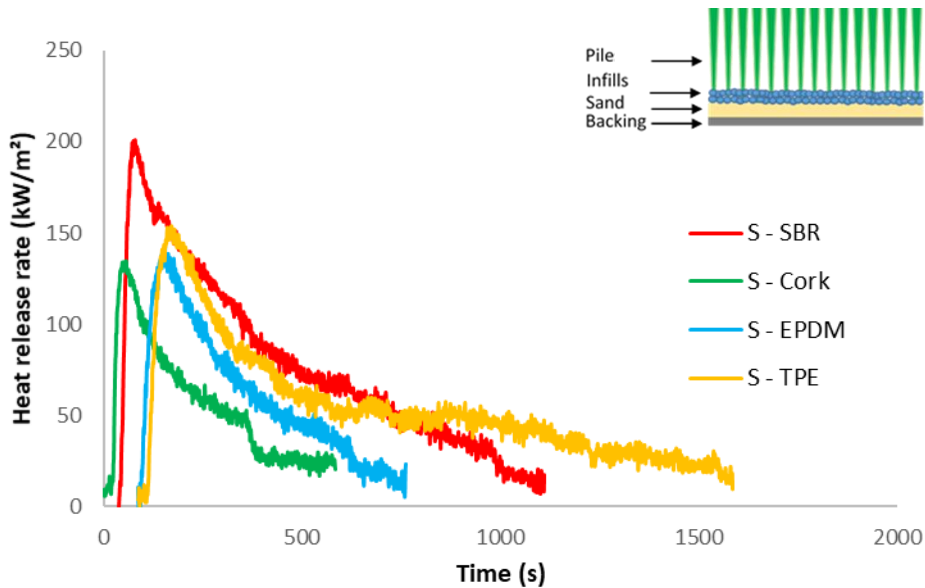
Figure 8: Heat release rate curves of the complete structures with the different infills obtained at Mass Loss Calorimeter test

Table 7: Mass Loss Calorimeter results obtained for the complete structures with the different infills

Structures	Infill thickness (mm)	TTI (s)	pHRR (kW/m²)	THR (MJ/m²)	TFO (s)
S – SBR	15	40 ± 4	201 ± 21	82 ± 2	981 ± 30
S – Cork	15	22 ± 1	143 ± 6	34 ± 1	272 ± 22
S – EPDM	10	86 ± 1	143 ± 4	41 ± 3	617 ± 75
S – TPE	5	86 ± 14	154 ± 1	82 ± 4	1739 ± 30

The fire behaviour differs from one structure to another. The worst result in terms of pHRR is obtained for the structure containing SBR with a value of 201 kW/m². The structures containing cork, EPDM and TPE have equivalent or similar pHRR, i.e. 143 kW/m², 143 kW/m² and 154 kW/m² respectively, but their THR values are much different. S – TPE and the S – SBR have the highest THR (82 MJ/m²) and also the longest combustion times (1739 s and 981 s

respectively). S – EPDM exhibits an intermediate behaviour, in terms of THR (41 MJ/m²) and combustion time (617 s). Finally, S – Cork presents the lowest THR (34 MJ/m²), more than twice lower than those of S – SBR and S – TPE. Moreover, even if S – Cork has the much shorter ignition time, its combustion time is also very short (272 s).

Observation of the residues after MLC testing can provide additional information on the behaviour of the samples during burning as shown by the pictures in Table 8.

Table 8:Top view and side view pictures of complete structures after MLC fire tests for the four different infills, i.e. SBR, cork, EPDM and TPE

	S-SBR	S-Cork	S-EPDM	S-TPE
Top view				
Side view				
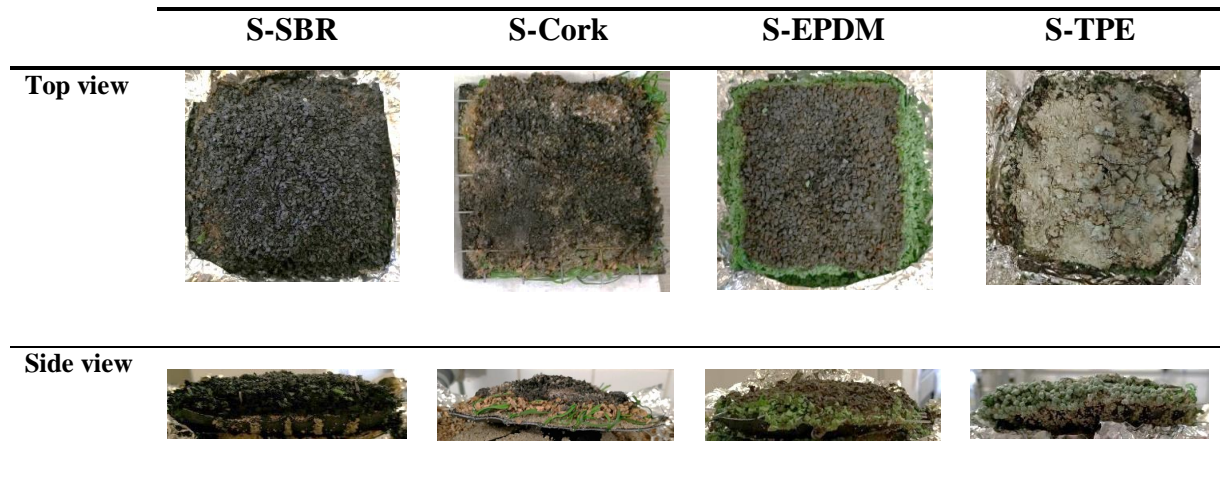
For S – SBR, S – EPDM and S – Cork structures, most of the infill burns but the lower part, in contact with sand, is only partially degraded. The remaining infill material is then mixed with the sand layer containing itself a certain amount of PE fibres in molten state. It is assumed that this compact layer (sand + melted fibres + remaining infill) allows limiting the access of heat to the backing thus providing effective protection. Despite this protective effect, the backing of S – SBR structure is slightly softened, probably because of the higher thermal conductivity of SBR (0.17 W/m K [93]), while the backing of S – EPDM and S – Cork structures is preserved. The thermal conductivity of an unfilled EPDM is around 0.18 W/m K [94] but EPDM used here as infill material contains 45 wt.% of $CaCO_3$. It is assumed that the presence of this high amount of mineral filler leads to a decrease of the heat release rate [95] and to a lower heat transfer to the backing. Regarding cork infill, its thermal conductivity is much lower (0.045 W/m K), providing very important insulating properties [96]. On the contrary, all the infill of the S – TPE structure burns (except the mineral part that remains after combustion, TPE being filled with 35 wt.% of $CaCO_3$) and the layer of sand is not effective enough to protect the backing that degrades in several points. The combustion of the backing occurs in the second part of the fire

test and corresponds to the plateau observed from 600 s up to 1000 s on the MLC curve (Figure 8). The lower TPE layer thickness (5 mm) can also explain the worse fire results of the S – TPE structure. Thus, both the nature of the infill material and the damping layer thickness have to be considered when studying the fire behaviour of artificial turf structures.

D. Discussion and conclusion

If the fire behaviour of the backing, of the backing + sand and of the complete structure is compared, the major contribution of both the sand and the infill is obvious. Now, comparing the results of the pure infill materials (Table 6) and of the complete structures (

), pHRR value of SBR is 18 % higher than the corresponding S – SBR structure. On the contrary, the other three complete structures (with cork, EPDM and TPE) have higher pHRR values (32 %, 24 % and 21 % respectively) than the infills tested alone. In terms of THR, pure infill materials and the complete turf structures lead to similar values for SBR, TPE and EPDM whereas the THR of the S – cork structure is 70 % higher than that of pure cork.

In order to better understand those differences, it is essential to discuss the fire behaviour of complete structures and of infill alone during MLC testing.

Firstly, considering SBR and EPDM, all the infill burns when tested alone (only the mineral part of EPDM (45 wt.% of $CaCO_3$) remains after combustion). In the case of the structures containing those infills, the PE pile height located above the infill layer is rather significant: 15 mm and 20 mm respectively. Thus, when samples are exposed to the radiant source, the pile melts, remains at the surface of the infill, leading to the formation of a uniform layer of melted polymer in which part of the infill is embedded. The PE pile and the infill both contribute to the combustion of the samples. In the case of EPDM, the pHRR is higher for the complete structure since both the melted PE and EPDM granules contribute to the increase in the amount of heat released. Whereas in the case of SBR, the pHRR values are equivalent considering the standard deviation. This is linked to the fact that SBR generates much higher amounts of heat than PE [97], [98].

The fire behaviour of the S – TPE structure is slightly different from that of the structures containing EPDM and SBR. When exposed to the radiant source, the pile of the S – TPE structure melts but the melted PE fibres do not remain at the surface of the infill layer: the fibres shrink and tend to go inside the TPE layer. However, as the infill layer thickness is very small (5 mm), the pile length above the infill layer is important (around 25 mm) and thus, a mixture

of melted PE and TPE can still be observed at the surface of the turf structure. The PE fibres burn immediately, leading to a 21% increase in the pHRR for the complete structure.

Finally, when cork is tested alone, only the upper part (about 5 mm thick) of the material burns. It is assumed that this behaviour is related to the very low thermal conductivity of cork (0.045 W/m K), leading to the extinction of the flame. On the contrary, considering the complete structure, almost all the cork burns, and a layer composed of melted polymer and sand is observed just above the backing, leading to a significant increase in THR (+ 70 %). A wicking effect can be assumed due to the presence of the PE pile: once exposed to the radiant source, the fibres shrink and move inside the infill, propagating heat through the cork layer thickness and thus maintaining the combustion of the sample. Moreover, PE fibres contribute to the heat release, leading to a higher pHRR for the complete structure.

The difference in the pile behaviour (melting or shrinking) can thus greatly affect the fire properties of the whole turf structure. To get a better understanding of this phenomenon, the surface tension properties of the materials can be considered. During the fire tests, the melted PE fibres shrink and tend to go inside the infill layer in the case of S – TPE and S – Cork structures. TPE surface energy can hardly be determined from the literature because TPE family is large and the surface energy can vary depending on the exact composition of the material (e.g. presence of fillers). However, the literature mentions a TPE surface energy close to 25 mN/m [99] whereas that of cork is reported to be equal to 18 mN/m [100]. On the contrary, S – SBR and the S – EPDM structures behave differently during the fire tests: PE pile also melts but remains above the infill layer. Data from the literature give similar surface energy values for SBR and EPDM (around 31 mN/m and 32 mN/m respectively) [101], [102], the exact value depending on the composition of the material (presence of fillers). As PE surface tension is around 32 mN/m [103], it can be assumed that if the surface tensions of melted PE and of infill are close, compatibility is better and thus the pile will preferably melt above the infill: the higher the infill surface tension, the better the compatibility and, the formation of a melted layer at the surface of the infill layer is favoured. On the contrary, if the surface tensions of the two materials are too different, the compatibility between the pile and the infill is poor and fibres rather shrink. In that case, the infill is totally exposed to the flame and if the material is highly combustible, the fire behaviour of artificial turf is strongly affected. These explanations are compatible with observations done during the MLC fire tests and with literature data. We can thus conclude that MLC characterizations allowed highlighting the importance of the combined choice of pile and infill regarding the fire behaviour of artificial turf structures. Moreover, considering MLC

results, the cork-based structure shows the most interesting behaviour: lowest pHRR, lowest THR and shortest combustion time. In addition, the use of microplastics is currently under debate at the European Chemicals Agency (ECHA): particles from 1 nm to 5 mm and fibres between 3 nm and 15 mm in length will probably be prohibited in the next few years. Thus, the use of non-natural infills such as SBR, TPE or EPDM should be avoided. Among the four infills tested, cork is the only material of natural origin and also the one showing the best fire behaviour. Consequently, cork was selected for further investigation in this PhD project. The following part thus focuses on the cork-based artificial turf structure. The aim is to better understand the influence of cork properties (two types of cork will be considered) and of the cork layer thickness on the fire performance of the complete structure.

II. Cork contribution in the fire properties of the cork-based turf structures

In this part, the role of cork on the fire behaviour of the complete structure is investigated, more precisely the influence of the cork layer thickness and of the cork density. Three thicknesses of cork (5, 10 and 15 mm) and two types of corks were used, i.e. the one already used in the previous part ('lighter' cork, referred to as cork) with an apparent density of 0.32 g/cm^3 and a 'denser' cork (referred to as d-Cork) with a 0.72 g/cm^3 density (properties given in Table 4, page 21). The objective is to determine a critical thickness for the protection of the backing, and whether or not this thickness depends on the cork properties.

A. Influence of the cork layer thickness on the fire properties

The complete structures, consisting of a backing with a 40 mm long pile, a 10 mm thickness of sand layer and a cork layer, have been tested with both types of corks, varying the infill thickness.

1. Lighter cork

MLC curves of the different structures with the lighter cork are shown in Figure 9 and the corresponding data are given in Table 9.

Figure 9: Heat release rate curves of the structures with different cork thicknesses obtained at Mass Loss Calorimeter test for the lighter cork (cork)

Table 9: Mass Loss Calorimeter results according to the cork layer thickness

Infill	Cork layer thickness (mm)	TTi (s)	pHRR (kW/m²)	THR (MJ/m²)	TFO (s)
Cork 0.32g/cm³	5	36 ± 1	142 ± 7	20 ± 1	222 ± 6
	10	27 ± 1	159 ± 5	30 ± 1	372 ± 82
	15	22 ± 1	143 ± 6	34 ± 1	402 ± 18
d-Cork 0.72g/cm³	5	59 ± 5	145 ± 5	25 ± 1	188 ± 25
	10	44 ± 3	158 ± 5	39 ± 1	382 ± 11
	15	40 ± 1	139 ± 1	31 ± 1	298 ± 16

When a 5 mm or 10 mm thickness of lighter cork is used as infill, all the damping material as well as a part of the backing are burnt at the end of MLC test. During this test, the PE pile melts and remains at the surface of the cork layer, contrary to what was observed previously with 15 mm of cork. This phenomenon can be explained by the higher length of PE pile located above the damping layer: 25 mm and 20 mm respectively when 5 mm and 10 mm thicknesses of cork are used. In this case, the amount of melted PE formed after exposure under the radiant source is too important to penetrate entirely inside the infill layer. For 15 mm of cork, as described previously, the cork is not totally burnt and a layer composed of melted polymer and sand is observed just above the backing, protected by the remaining cork and thus non-degraded. The pictures in Table 10 show the residues of lighter cork-based structures (S - Cork) after MLC testing. It is possible to assume that when a higher amount of cork is used, the temperature gradient inside the material is larger and thus cork acts as an insulating barrier. Further experiments will be carried out in the next part of this chapter (section B. Protective behaviour of the cork layer, page 43) to confirm this assumption.

As far as concern, the THR values increase as the cork layer thickness increases, which seems logical since this parameter reflects the total amount of heat released by a material during combustion: the higher the amount of combustible material, the higher the expected THR. A 50 % increase of THR can be observed when the sample with 10 mm of cork is compared to the one with 5 mm of cork. This difference can be explained by the higher amount of cork as the cork layer is totally burnt at the end of the test for both structures. On the contrary, for the sample with 15 mm of cork, the cork layer is not entirely burnt and the backing is not damaged. Consequently, the THR value for this structure is only 13% higher than that of the structure containing 10 mm of cork.

Table 10: Top view and side view pictures of complete lighter cork-based structures after MLC fire tests for the three different thicknesses, i.e. 5, 10 and 15 mm

	5 mm	10 mm	15 mm
Top view			
Side view			
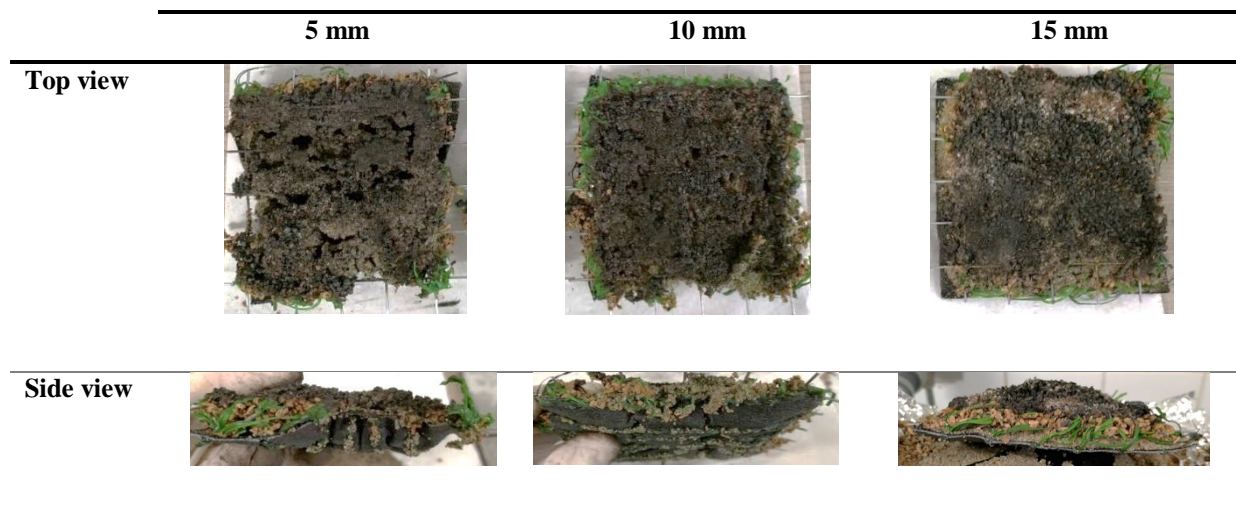
It is shown here that depending on the cork layer thickness, two different behaviours can be observed when the structures are exposed to a radiant source: formation of a melted polymer layer above the infill layer (with 5mm or 10mm of cork) or shrinking of PE fibres with formation of a mixture with the infill and/or the sand (with 15mm of cork). The same phenomenon was previously observed when the different turf structures were tested using MLC and the difference in the surface tensions between the infill and the PE fibres was considered to explain this behaviour (Section D.

Discussion and conclusion, page 36). Thus, the surface energy of the infill is not the only parameter governing the behaviour of the fibres when they melt but the infill layer thickness is also a key factor. In order to limit the impact of the pile on the pHRR, a 15 mm cork layer thickness is necessary. Then, the influence of the cork structure on the fire behaviour of the turf

structure has been studied: fire tests were performed with a denser cork and results are given in the following section.

2. Denser cork

MLC curves of the different structures with the denser cork (d-Cork) are shown in Figure 10 and the corresponding data are given in Table 9.
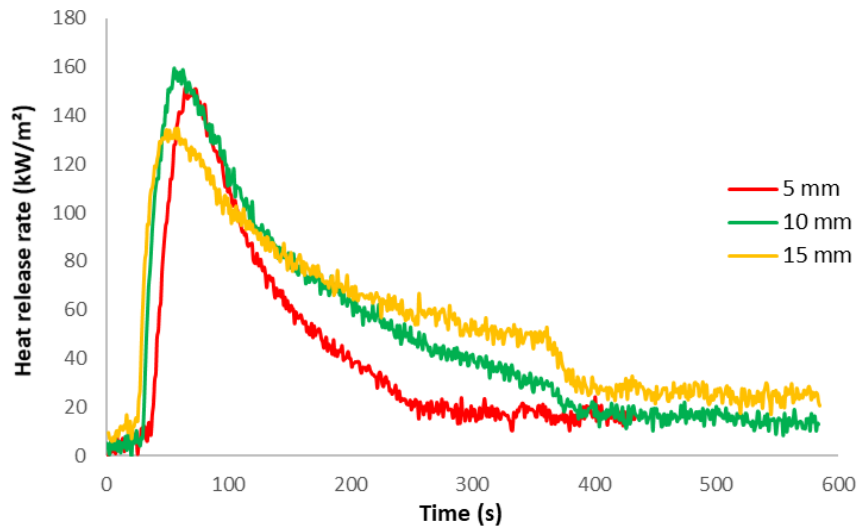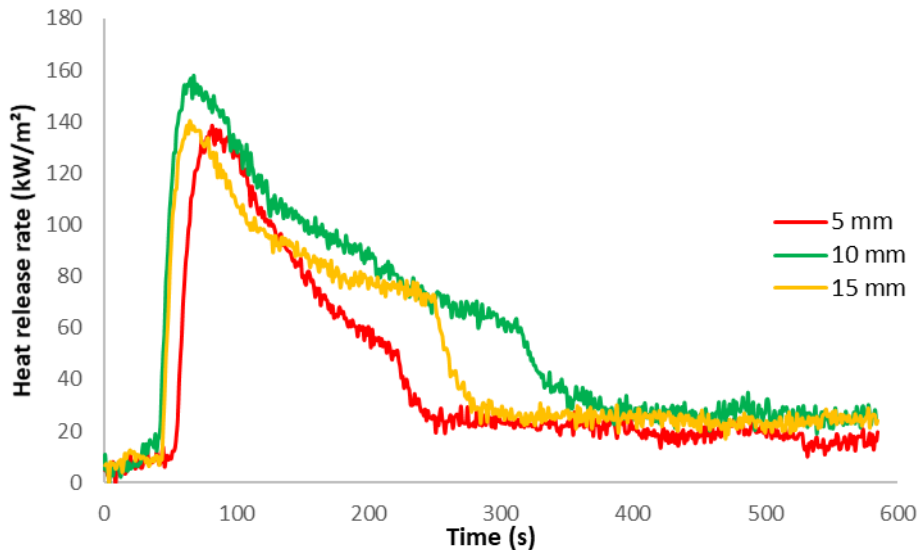

Figure 10: Heat release rate curves of the structures with different cork thicknesses obtained at Mass Loss Calorimeter test for the denser cork (d-Cork)

First, the samples at the end of MLC tests are in the same degradation state as the samples containing the lighter cork: for an infill layer thickness of 5 or 10 mm, cork is totally burnt as well as a part of the backing and for a 15 mm thickness, part of the infill is preserved and the backing is not damaged. Moreover, the behaviour of the PE pile when subjected to the radiant source is similar to the one previously described for the lighter cork and also depends on the cork layer thickness: fibres shrinking from a 15 mm cork thickness. The residues of denser cork-based structures (S – d-Cork) after MLC testing are shown by the pictures in Table 11.

The main differences between the two types of corks lie in the THR values. While, for the lighter cork, THR increases with increasing thickness, the highest THR value is obtained for a 10 mm cork layer thickness in the case of the denser cork. From 5 to 10 mm, THR increases significantly (+56 %) due to the increase in the amount of burned cork: 5 mm corresponds to an additional cork weight of 14 g, i.e. 26 wt.% of the sample weight (compared to 17 wt.% of the sample weight for the lighter cork). The percentage of combustible material being higher, the increase in the THR value is more important as the cork layer is completely burnt considering the two thicknesses (5 and 10 mm) and the two densities of cork.

Table 11: Top view and side view pictures of complete denser cork-based structures after MLC fire tests for the three different thicknesses, i.e. 5, 10 and 15 mm

	5 mm	10 mm	15 mm
Top view			
Side view			
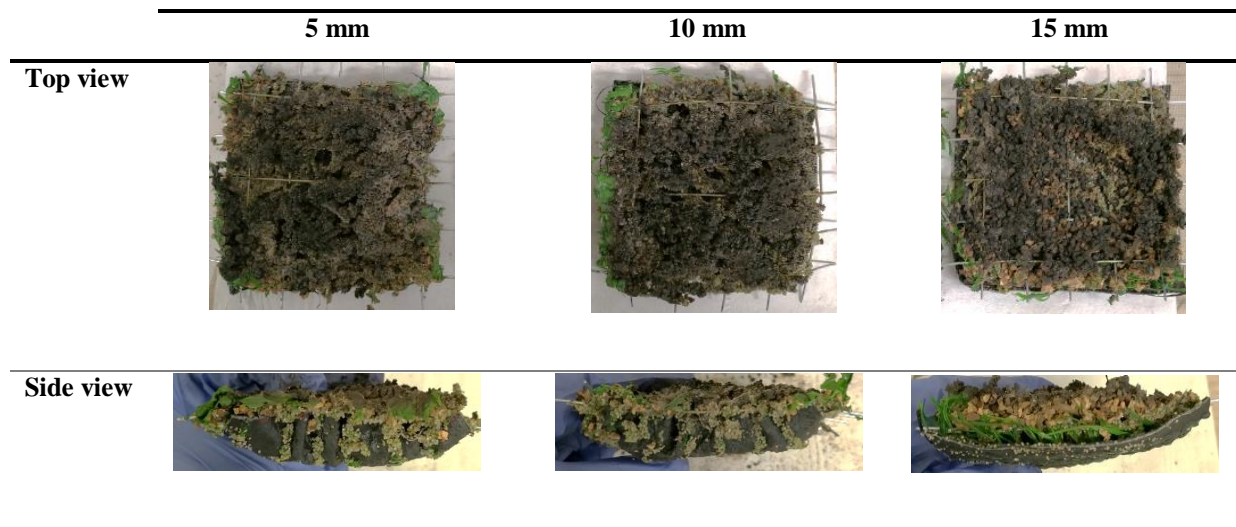
On the contrary, the THR value obtained for a 15 mm cork layer thickness is lower than when 10 mm of cork are used. This result can be explained by the protective effect brought by the high amount of dense cork: at the end of the test, only part of the infill and of the pile are burnt and the whole backing is preserved. A 15 mm thickness of dense cork thus permits to achieve a good compromise between the amount of combustible material and the protective role of cork during the fire test. However, the barrier effect is slightly more efficient when the denser cork is used: it allows limiting the access of oxygen to the combustible material and thus stopping the combustion cycle quicker. This assumption is confirmed by the shorter burning time compared with 10 mm of dense cork and with 15 mm of lightweight cork. Considering the density of both corks, it is assumed that it is necessary to use a greater thickness of lighter cork to obtain equivalent barrier effect than that of d-Cork. This will be further investigated in the following part.

3. Conclusion

Both the infill layer thickness and, to a lesser extent, the apparent cork density, have an influence on the fire properties of artificial turf structures. When 15 mm of cork are used, similar pHRR and THR values are obtained for both types of corks whereas the combustion time is much shorter with the denser cork. A minimum thickness of 15 mm is also required to prevent the backing degradation. It is assumed that due to insulative cork properties, the performance of the turf structure is improved when the cork layer thickness increases. In order to better

understand this phenomenon, the evolution of temperature within the materials has been studied during MLC tests.

B. Protective behaviour of the cork layer

To evaluate the protection brought by the cork layer to the turf structure, six thermocouples were placed between the backing and the sand layer (Figure 5, page 24) to measure the temperature gradient within the sample during MLC tests. The curves giving the temperature evolution for the six thermocouples are shown in Figure 11.

Whatever the type of cork, the temperatures measured with the six thermocouples for a given test time and a given cork thickness are different, meaning that the temperature distribution is not uniform over the backing surface. However, the temperature is more homogeneous when the cork layer thickness increases. With 5 or 10 mm of cork, an important increase of temperature is observed during MLC tests and temperatures measured with the different thermocouples vary significantly. It shows that heat diffuses into the structure randomly and cork does not protect the backing. It is confirmed by the appearance of the residues obtained after the tests as previously discussed. The backing of the sample is degraded over its entire surface using a 5 mm or 10 mm cork layer thickness. On the contrary, with 15 mm of cork, the temperatures measured with the different thermocouples are rather homogenous and the backing remains intact. This result confirms that 15 mm of cork is the minimum thickness to ensure an efficient protection of the backing.
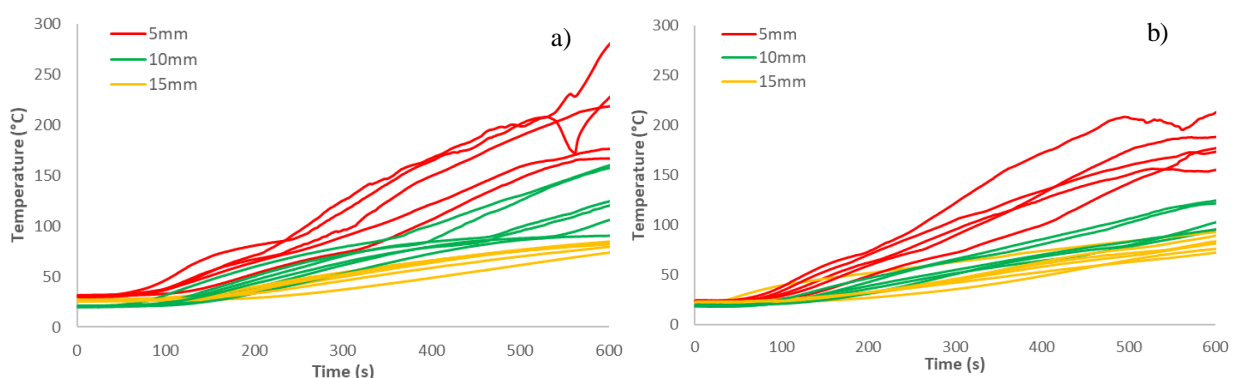
Figure 11: Temperature evolution of the six thermocouples considering different cork thicknesses for (a) the lighter cork and for (b) the denser cork

Moreover, two phenomena due to cork have to be considered: first, cork can act as a protective layer due to its good insulating performance and secondly, cork can degrade and burn due to its flammable properties, leading to an increase in the amount of heat released. Both phenomena are antagonist i.e. thermal insulation leads to a decrease in the temperature gradient and thus to

a protection of the underlying materials whereas the combustion of cork brings energy and thus leads to a temperature increase at the backing surface.

In order to go further in the understanding of the fire behaviour of artificial turf containing cork, a simple heat transfer model, Fourier's law (Equation 1), can be considered: a linear temperature decrease at the backing surface may be expected when the cork thickness increases. This relationship is verified only if cork does not degrade and if the heat flow through the sample is the same regardless of cork density and of cork layer thickness.

Equation 1:
$$\Delta T = \frac{\Delta x}{A \times k} \times q$$

where q is the rate of heat flow through an area A and thickness Δx, across which the temperature change is ΔT with $\Delta T = t1 - t2$: the temperature difference in the sample with t1 and t2 the temperatures recorded at top surface (upper part of the cork layer) and down surface (lower part of the cork layer on the surface of the sand) respectively. k is the thermal conductivity of the material.

In order to verify this model, the temperature values obtained after 70, 200 and 600 s of testing with thermocouples (TC) 1, 2 and 4 according to the cork layer thickness for both densities are given in Table 12. Those thermocouples have been selected since they are representative of the different locations over the whole backing surface: respectively corner, middle of the lateral side and centre as shown in Figure 5 (page 24).

Table 12: Maximum temperatures (°C) of thermocouples 1, 2 and 4 for both lighter and denser corks for three infill thicknesses at 70, 200 and 600 s

		Thermocouple 1 (TC1)			Thermocouple 2 (TC2)			Thermocouple 4 (TC4)		
	Time (s) / Thickness (mm)	70	200	600	70	200	600	70	200	600
Cork	5	26	62	155	44	104	148	24	49	177
	10	18	32	113	30	82	203	18	34	111
	15	23	31	82	33	52	93	23	27	76
d-Cork	5	32	53	167	33	67	218	37	81	227
	10	21	39	106	24	60	160	21	34	90
	15	25	33	79	25	36	84	24	27	76

First, considering a 5 mm cork thickness, the temperature increase from 70 to 600 s is really important for both corks (temperature difference ranging from 104 to 190°C), confirming that cork does not protect the backing efficiently. Moreover, if temperature values obtained with the

two types of corks are compared for 5 mm of infill at 600 s, it appears that the temperature is significantly higher for the denser cork, especially for TC 2 and 4. Thus, heat spreads quickly and not homogeneously inside the turf structure and this phenomenon is more pronounced with the denser cork. In that case and since the whole material burns, the organic weight content for a given cork thickness is higher for the denser cork and thus the potential energy release during combustion is more important, justifying the higher temperature measured at the backing surface.

Then, when 10 mm of infill are used, the increase in the cork thickness brings a slight barrier effect towards the backing as the temperature increase from 70 to 600 s is less pronounced than with 5 mm of cork. Moreover, the temperature at 600 s is lower for the denser cork, particularly for TC 2 and 4, demonstrating that the protective role played by the cork layer is more important for d-Cork. But for both thicknesses, the backing is not sufficiently protected and is partly degraded at the end of the test.

Finally, with 15 mm of cork, the temperature increase from 70 s to 600 s is even lower than for the other two thicknesses, confirming that an increase in the cork layer thickness allows a better protection of the turf structure. As the backing is not damaged at the end of the test, it proves that a 15 mm cork layer thickness is sufficient enough to protect the backing. This statement is consistent with temperature values similar for both types of corks, even at 600 s. It can be assumed that for such a thickness, the amount of cork involved in the combustion process is lower. The heat flow through the sample is thus lower, leading to a decrease in the temperature measured at the backing surface. For a 15 mm cork thickness, the temperature measured until the end of the test is always lower than the melting temperature of polypropylene (Tm around 160°C), which explains why the PP backing is not damaged. For this thickness, no significant difference is observed between both corks and it is not possible to confirm previous assumption of better protective effect for the d-Cork (section A. 2. Denser cork, page 41). The fact that the critical thickness allowing a good protection of the backing is reached (15 mm) can however explain the similar temperature values between both corks.

Those results thus prove that a compromise between both phenomena (thermal insulation and combustion of cork) has to be found to obtain the best fire properties. For both corks, a minimum thickness of 15 mm is required to ensure a uniform heat distribution into the sample and also a good protection of the backing. Those conclusions are in good agreement with previous studies dealing with the thermal insulation of cork. Novais et al [104] evaluated the thermal stability and thermal conductivity of ultra-light inorganic cork-based polymer composites. These composites, with a cork content ranging from 0 to 92 vol.%, were subjected

for 2 hours to a decreasing temperature gradient through the sample thickness. It was shown that an increase in the cork content led to a higher thermal inertia. These data are consistent with our results, showing that an increase of the cork layer thickness leads to an increase of the thermal insulation and thus to a better protection of the backing.

III.   Conclusion of Chapter 1

In this chapter, the fire behaviour of the different components of artificial turf (backing, pile and infill) was investigated through Mass Loss Calorimeter experiments. It was found that the infill layer has the greatest impact on the fire behaviour of the whole structure contributing not only to the amount of heat released but also modifying the behaviour of the pile (melting or shrinking) during the combustion process. Among the four most commonly used infills, namely SBR, TPE, EPDM and cork, the latter proved to be the most interesting in terms of fire behaviour and in terms of human and environmental impacts. Therefore, an in-depth study of cork was carried out using two corks with different densities and varying the cork layer thickness. For both types of corks, it was shown that a minimum thickness of 15 mm is necessary to ensure good protection of the backing and also to limit the heat release during combustion. In these conditions, similar temperatures are measured at the surface of the backing whatever the cork density and the fire behaviour is similar for both corks in terms of THR and pHRR values. Since the two corks have equivalent fire behaviour with a 15 mm layer thickness, the cork considered in the following studies will be the lighter one as it is the reference material used in the GRASS project.

Therefore, the MLC tests have provided a better understanding of the fire behaviour of artificial turf structures. However, the fire test used in the EN ISO 13501-1 standard is the EN ISO 9239-1 radiant panel test. One of the main issues with the use of this test is the size of the samples required ((1050 $\pm$ 5) mm $\times$ (230 $\pm$ 5) mm), especially as the test has to be repeated several times. Thus, in order to assess the fire behaviour of artificial turf structures with less material consumption, it appears necessary to develop a radiant panel test on a small scale. As a consequence, the next chapter is dedicated to the downscaling reproduction of the EN ISO 9239-1 radiant panel test allowing subsequently to assess the fire behaviour of artificial turf structures according to the standard.

Key points & strategies of Chapter 1

Key points:

- ✓ Infill: main component affecting the fire behaviour of the structure.
- ✓ Focus on the 15 mm cork-based turf structure to bring both good fire properties and adequate shock absorption.

Strategies and objectives for the next chapter:

- ✓ Assessment of the fire behaviour of artificial turf structures using the EN ISO 9239-1 radiant panel test [11] and determination of the classification of the different structures according to the European EN ISO 13501-1 classification [10].
- ✓ Based on the information gathered from MLC and radiant panel tests on the fire behaviour of artificial turf structures, development of an innovative fireproofing strategy allowing the use of artificial turf structures for both outdoor and indoor applications.

Chapter 2 – Development of the EN ISO 9239-1 radiant panel test on a lab scale

In **Chapter 1**, MLC tests highlighted the major impact of the infill layer on the overall fire behaviour of the turf structure. However, to assess the fire behaviour of floorings according to the EN ISO 13501-1 European classification [10], the EN ISO 9239-1 radiant panel test [11] has to be used. Samples have to meet the C_{FL} rating and s1 rate for smoke production for indoor applications. However, the size of the samples required to perform the radiant panel test is very large ((1 050 ± 5) mm × (230 ± 5) mm size) and it can obviously become a problem if several turf structures have to be tested or if new structures with better fire properties have to be developed as for the GRASS project. Thus, to use lower amounts of materials and to allow a faster screening of the different formulations, the downscaling of the radiant panel test was considered and the approach is presented in this chapter.

First, an overview of the main methods used to assess the fire behaviour is given. Then, a specific 'Materials and methods' section aims mainly at describing the samples preparation and the design of the downscaled radiant panel test. As the test is reproduced on a 1/3 scale, specific settings are needed to get the right calibration of the device and more particularly to obtain the heat flux distribution required by the standard. The experimental design methodology was thus implemented: after a brief description of the theoretical approach, the results are reported and analysed in order to determine the optimal settings. Finally, the fire behaviour of artificial turf structures is evaluated using both scale tests to assess the reliability of small-scale reproduction. As Chapter 1 evidenced the interest of cork as infill material, further experiments were also carried out on different cork-based turf structures, varying the infill layer thickness.

I.   Overview of the methods of fire behaviour assessment

In the field of science and particularly to determine the fire behaviour of materials, large-scale tests are usually time and materials consuming [105]. In order either to assess the fire properties faster using less materials, to perform rapid screening, or to optimize a material, three main methods exist. The first one is the <u>modelling</u> consisting of simulating real and complex physical phenomena by means of equations implemented on a specific software. Once the model has been found, this technique saves considerable time and money. It is often combined with experimental tests. Applicable to many fire tests, modelling can also be an efficient and fast way to assess the fire behaviour of structures [105]–[107]. Secondly, the determination of a discriminant parameter can be performed: the <u>discriminant analysis</u>, a statistical technique that aims to describe, explain and predict the membership of groups of observations from a set of predictor variables, can be carried out. Used in many fields, including machine learning, this technique has been recently used in the field of fire [108]. Identifying which parameter is mainly responsible for the fire behaviour of a structure (usually experimentally) allows to focus on the most important element, leading to significant time savings. However, extensive data are required. Finally, the <u>downscaling</u> of standardised tests is commonly used as it allows reducing the dimensionality of a complex system to a lower level [109]. In the field of fire, this approach has already been followed by a number of authors for various applications. As an example, Girardin et al [110] designed the EN ISO 50399 fire test at a reduced scale in order to evaluate the fire behaviour of cables. The assessment of the reaction to fire of cables by small-scale methods has also been documented by others authors [105], [111]. The reduction on a 1/8 scale of the Steiner tunnel (ASTM E84) allowed Bourbigot et al [112] assessing quickly the fire behaviour of composites protected by different intumescent paints, using much smaller samples. In addition, the furnace test (UL 1709) and the burner test (ISO 2685) have also been reproduced at small scale [113]. Initially, the full scale Room Corner Test (RCT), complying with the Euroclass system for building products, was considered as the standard for the classification of linings in many countries but as large amounts of material were needed, it was replaced by the SBI leading to a lower material consumption [107], [108], [114]. This decision is supported by the fact that in 87% of cases, the fire growth behaviour at full scale (RCT) is correctly represented by intermediate scale test (SBI). Downscaling of the single burning item (SBI) test, which simulates a fire in the corner of a room, has also been widely reported [113], [115], [116]. The main difficulty raised by these studies is to obtain a good correlation between

the developed small-scale test and the standardized one, as downscaling can modify the thermal phenomena involved during the fire test.

In the literature, no paper deals with the downscaling of the EN ISO 9239-1 radiant panel test. In several papers, the radiant panel test is rather considered as a small-scale test to assess the flame spread of flooring materials in comparison with other larger tests such as the Building Code of Australia (BCA) [117] or the National Bureau of Standards (NBS) tests for corridor fires [118]–[120]. In addition, after performing different fire tests on carpets, Quintiere and Huggett [121] recommended the use of a radiant panel test to assess the fire behaviour of floorings (smaller scale than conventional methods). However, considering the sample size required in the EN ISO 9239-1 radiant panel test, i.e. $(1\,050 \pm 5)$ mm $\times$ (230 ± 5) mm), and the fact that each experiment has to be done six times per structure (three in the production direction and three in the perpendicular one) to ensure repeatability and to assess the direction influence of the structure. Thus, an industrial equipment is usually required to produce the specimens and it clearly appears as a break for the development of new structure. The downscaling of the radiant panel test is therefore relevant as it allows the use of much lower amounts of materials and thus, allows the production of the specimens using laboratory scale equipment.

The following section presents the materials and methods used in this chapter. Since the aim of this chapter is to develop and validate the bench scale test, the design and test protocol of the radiant panel test at both scales are fully described. The theoretical approach of the experimental design methodology used to optimize the settings of the small-scale test is also detailed.

II.   Materials & Methods

In this section, the materials will be briefly presented. In a second part, the samples preparation, specific to the radiant panel fire test, is described. Then, the principle and procedure of the standardised test are detailed and also the development of the radiant panel test at reduced scale. In a last part, theoretical information dealing with the experimental design methodology used to determine the optimal settings of the small-scale device is given.

A. Materials

For the radiant panel fire tests, the structures correspond to those presented in the 'Materials' section of **PART II**. However, compared to **Chapter 1**, the FR EPDM-based structure is also studied and only the "lighter" cork (referred to as cork) is used. In the second part of this

chapter, additional experiments were performed on cork–based structures, varying the infill layer thickness.

B. Methods

1. Turf structures preparation before testing

For the small-scale tests, 'backing + pile' samples of (338 ± 2) mm x (120 ± 1) mm size are cut in the production direction with a cutter. The pile is removed over a width of 26 mm on both longitudinal sides of the specimens. These samples are then placed in a horizontal position and two flat metal bars $((340 \pm 1)$ mm x (26 ± 1) mm size) are maintained on the areas without pile, thus preventing the sample from moving or rising up during the fire test. Then, the inner part of the sample $((338 \pm 2)$ mm x (67 ± 1) mm size i.e. distance between both bars) is filled with sand, making sure that the distribution is uniform over the backing surface while keeping the fibres as straight as possible. Finally, the infill material is evenly spread above the sand layer. The large-scale tests were carried out by the European Research Centre for Artificial Turf (ERCAT) at the Centre for Textile Science and Engineering (Department of Materials, Textiles and Chemical Engineering) of Ghent University (Belgium). The specimens $((1\,050 \pm 5)$ mm $\times$ (230 ± 5) mm size and inner part of $(1\,015 \pm 5)$ mm $\times$ (200 ± 5) mm size) were prepared in a similar way as the method used for the small-scale tests.

2. Large-scale fire testing according to the EN ISO 9239-1 standard

2.a. Test description

As shown in Figure 12, the apparatus mainly consists of:

- A test chamber, made of stainless-steel plates, with an observation window at the front and with the lower part of the structure open to allow natural ventilation and airflow, including:
  - A radiant heat panel, $(300 \pm 10) \times (450 \pm 10)$ mm size, with its longer dimension oriented at $(30 \pm 1)°$ to the horizontal plane
  - A heat resistant sample holder, positioned horizontally under the radiative heat source whose point at the right end, located at 190 mm from the inside surface of the test chamber wall, corresponds to the zero point (Figure 12, b).
  - A pilot flame whose height varies from approximately 60 mm to approximately 120 mm across the width of the burner
- An exhaust duct (chimney) for the evacuation of smokes during the test.

- A <u>smoke density analyser</u>, consisting of a light source (lamp) and a sensor (detector), aligned with the centre of the chimney.

1   Lamp
2   Exhaust duct
3   Detector
4   Exhaust hood
5   Test chamber
6   Gas-fired radiant panel
7   Pilot flames from line burner
8   Scale
9   Observation window
10 Specimen holder with specimen together on sliding platform
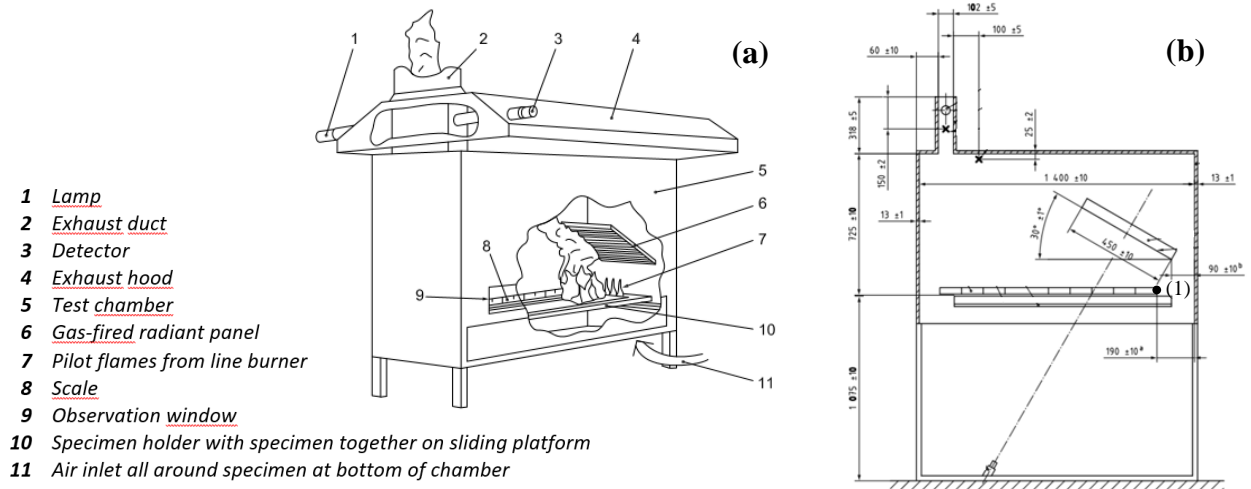11 Air inlet all around specimen at bottom of chamber

Figure 12: (a) Perspective view showing test principle and (b) view of the section showing the inside of the test and (1) the position of the zero point according to EN ISO 9239-1 standard - Adapted from [11]

2.b.   Test protocol

As described in the standard [11], the specimen is placed horizontally on the heat resistant sample holder, the end of the sample located just below the radiant source corresponding to the zero point (Figure 12, b). At the beginning of the test procedure, the height of the radiant heat source is adjusted so that the distance from the upper surface of the infill layer is always the same, whatever the tested artificial turf structure. After specimen positioning, the burner is ignited and kept at least 50 mm away from the intended zero point of the test specimen. The door of the test chamber is immediately closed and remains throughout the test, in order to maintain a stable temperature. After a preheating period of 2 minutes, the test can start: the pilot flame is brought into contact with the test specimen 10 mm from the edge of the holder and left for 10 min in this position. Then, the pilot burner is moved away from the test specimen and the pilot flame is extinguished. At 10 min intervals from the start of the test and until the flame-out, the distance between the flame front and the zero point is measured. If there is no self-extinguishment after 30 min of test, the maximum distance reached by the flame front is recorded. The position of the flame front at the end of the test, determined visually through the observation window, represents the maximum flame-spread distance and the corresponding critical heat flux (CHF) value can be determined. At least once a month, the apparatus must be calibrated, recording the heat flux value as a function of distance along the specimen plane. To carry out the calibration step, the heat flux meter has to be parallel to the sample holder. It is

moved horizontally, starting with the heat flux measurement at 110 mm from the zero point and ending with the measurement at 910 mm. The heat flux values are recorded over a 30 s period for each distance, leading to the heat flux profile curve as a function of the distance from the zero point. The heat flux distribution generated by the radiant source must be within the specifications given in Table 13. If the curve is within the tolerances, the test equipment is calibrated and the heat flux profile determination is completed.

Table 13: Required heat flux distribution along the sample for the large-scale test.

Distance to zero point of specimen on large scale (mm)	110	210	310	410	510	610	710	810	910
Heat flux (kW/m²)	10.9	9.2	7.1	5.1	3.5	2.5	1.8	1.4	1.1
Tolerances (kW/m²)	± 0.4	± 0.4	± 0.4	± 0.2	± 0.2	± 0.2	± 0.2	± 0.2	± 0.2

The classification relative to floorings is given in Table 1 (page 3). A minimum critical heat flux (CHF) value of 8 kW/m², 4.5 kW/m² or 3 kW/m² is required to achieve respectively a B_{FL}, C_{FL} or D_{FL} rating. Additionally, for B_{FL} to D_{FL} ratings, a smoke rate lower than 750%.min (s1 classification) is required. Thus, the radiant panel apparatus is instrumented with a smoke density analyser. The initial intensity light beam I_0 is generated by a lamp and the transmitted light after passing through the smokes going into the exhaust duct is received by the sensor with an intensity I. Light attenuation is determined thanks to Equation 2:

Equation 2: $$Light\ attenuation\ (\%) = (I_0 - I) \times 100$$

With I_0 the initial intensity light beam and I the intensity received by the sensor.

The curve representing light attenuation over time is recorded and the integrated smoke value is calculated, allowing determine the smoke rate.

3. Small – scale test development

3.a. Test design

The small-scale apparatus developed in this study is a direct 1/3 reduction of the standardized test as shown in Figure 13. The same components have been used but dimensions of the test chamber, of the radiant source and of the specimens were divided by three. The radiant source (supplied by AEM), of $(100 \pm 3) \times (150 \pm 3)$ mm size, is supported by a stainless-steel structure: the distance from the test specimen can be varied as well as the angle of inclination of the heat

source. A heat resistant sample holder with the pilot flame at the zero point is positioned under the radiant panel and a smoke density analyser is placed at the centre of the chimney. Finally, thermocouples (TC) are used in order to check the temperature of the chamber during the tests. The settings of the different parameters will be optimized thanks to the experimental design methodology (next section of this chapter).
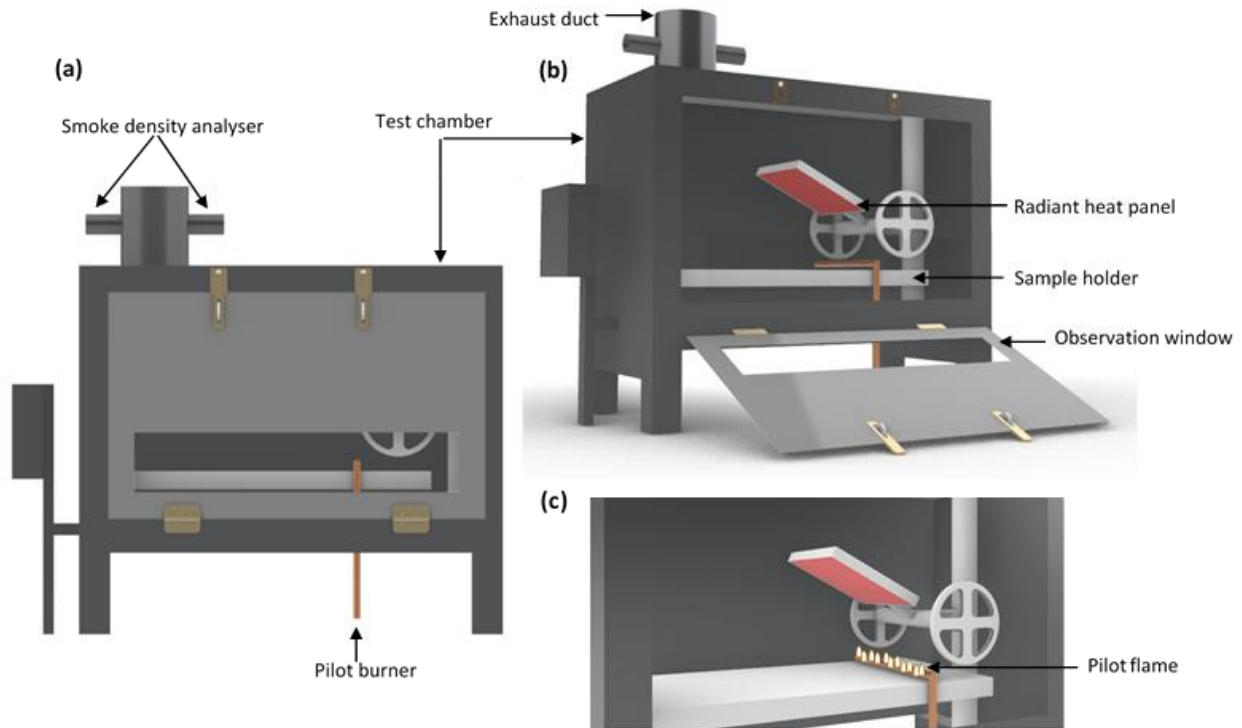

Figure 13: Design of the small-scale radiant panel test: (a) front view (b) perspective view showing the inside of the test and (c) focus on the pilot flame

3.b.   Test protocol

Firstly, a flow meter is used to measure the propane flow rate. The heat source is ignited and a preheating period of about one hour is necessary to ensure that the temperature of the chamber is stabilized. Then, the calibration is performed following the same procedure as in the large-scale test. The air velocity is measured through a hole in the chimney by a hot wire anemometer (supplied by Testo) and is fixed at (2.5 ± 0.2) m/s. The small-scale test is carried out under the same conditions as the large-scale test: the pilot flame is in contact for 10 minutes with the specimen (at the zero point) at the beginning of the test, with a maximum duration of 30 minutes for the test. The volume of fumes (VOF) is recorded using the smoke density analyser.

4. Design of experiments: theoretical part

Experimental design was used to optimize the heat flux distribution along the test specimen since it has to correspond to the one required by the ISO standard (Table 13), knowing that the

specimen size is three times smaller. The main difficulty is that the heat flux value must be within specific tolerances for 9 different distances from the zero point. Thus, to determine the settings of the small-scale radiant panel allowing to obtain the heat flux distribution defined by the ISO standard, experimental design was implemented using response surface methodology (RSM). Four parameters were considered (Figure 14) to adjust the heat flux distribution: (1) the angle of the radiative source from the horizontal plane; (2) the obstructed area of the radiative source (part of the radiant source is covered with an insulating material); (3) the distance between the lowest point of the radiative source and the upper surface of the tested sample; and finally, (4) the propane flow rate.

Thus, a central composite design, consisting of 27 experiments was performed and is composed as follows:

- the first 16 experiments correspond to a 2^k full factorial design, k being the number of studied variables (4 in this experimental design)

- the following 8 experiments ($2 \times k$) are axial points at a distance of $\alpha = 2$ (in coded values) from the design center

- and finally, 3 experiments being replicates of the center point
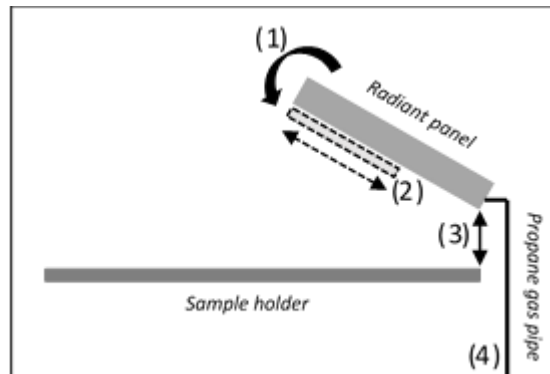
Figure 14: Illustration of the different parameters used for the design of experiments: (1) The angle of the radiative source, (2) the obstructed area, (3) the distance between the lowest point of the radiant source and the sample, and (4) the propane flow rate

Experiments were conducted randomly to provide protection against the extraneous factors, which could affect the measured response. For statistical calculations, the variables U_i were coded as X_i according to Equation 3:

Equation 3:
$$X_i = \frac{(U_i - U_0)}{\Delta U_i}$$

where X_i is the dimensionless coded value of the variable U_i; U_0 represents the value of U_i at the center point and ΔU_i is the step change.

The experimental values associated to the coded levels of the different variables are given in Table 14.

Table 14: Coded and real values of experimental parameters used in the experimental design.

Coded variables	Parameters	Levels				
		-2	-1	0	+1	+2
X_1	U_1: Radiant source angle (°)	10	20	30	40	50
X_2	U_2: Radiant source obstructed area (%)	0	15	30	45	60
X_3	U_3: Radiant source position* (mm)	75	100	125	150	175
X_4	U_4: Propane flow rate (L/h)	200	275	350	425	500

*U_3 corresponds to the distance between the lowest point of the radiant source and the upper surface of the tested sample

The quadratic model used to predict the optimal conditions is expressed according to Equation 4:

Equation 4:

$$Y = \beta_0 + \sum_{i=1}^{n} \beta_i X_i + \sum_{i<j}^{n} \beta_{ij} X_i X_j + \sum_{i=1}^{n} \beta_{ii} X_i^2$$

where Y is the considered response variable; β_0 is the value of the fitted response at the center point; β_i, β_{ii} and β_{ij} correspond to the linear, quadratic and interaction terms respectively.

For each experiment, the heat flux was measured at 9 different distances from the zero point and thus nine responses are considered in the experimental design. As the small-scale device aims at testing samples three times smaller than those of the large-scale test, the distances corresponding to heat flux measurements are divided by three compared to those of the ISO standard test (Table 13). The distances considered for the nine responses are given in Table 15.

Table 15: Distances corresponding to the heat flux measurement (kW/m²) for the nine responses on the small-scale radiant panel test.

	Y_1	Y_2	Y_3	Y_4	Y_5	Y_6	Y_7	Y_8	Y_9
Distance from the zero point (mm)	37	70	103	137	170	203	237	270	303

Modde7.0 software developed by Umetrics was used for regression and analysis of the obtained experimental data. The statistical significance of the main, quadratic and interaction effects of the variables was determined by analysis of variance (ANOVA) and a multiple regression analysis was performed to fit the experimental data to the second-order polynomial equation (Equation 4).

III. Results and discussion

A. Optimization of the small-scale device settings through experimental design methodology

The experimental conditions (U_i) associated to the coded values (X_i) applied for the 27 experiments are given in Table 16 and the measured heat fluxes (kW/m²) corresponding to the nine responses (Y_i) are given in Table 17.

Table 16: Experimental conditions (Ui) associated to the coded values (Xi) applied for the 27 experiments.

Exp	X1	X2	X3	X4	U1 (°)	U2 (%)	U3 (mm)	U4 (L/h)
1	-1	-1	-1	-1	20	15	100	275
2	1	-1	-1	-1	40	15	100	275
3	-1	1	-1	-1	20	45	100	275
4	1	1	-1	-1	40	45	100	275
5	-1	-1	1	-1	20	15	150	275
6	1	-1	1	-1	40	15	150	275
7	-1	1	1	-1	20	45	150	275
8	1	1	1	-1	40	45	150	275
9	-1	-1	-1	1	20	15	100	425
10	1	-1	-1	1	40	15	100	425
11	-1	1	-1	1	20	45	100	425
12	1	1	-1	1	40	45	100	425
13	-1	-1	1	1	20	15	150	425
14	1	-1	1	1	40	15	150	425
15	-1	1	1	1	20	45	150	425
16	1	1	1	1	40	45	150	425
17	-2	0	0	0	10	30	125	350
18	2	0	0	0	50	30	125	350
19	0	-2	0	0	30	0	125	350
20	0	2	0	0	30	60	125	350
21	0	0	-2	0	30	30	75	350
22	0	0	2	0	30	30	175	350
23	0	0	0	-2	30	30	125	200
24	0	0	0	2	30	30	125	500
25	0	0	0	0	30	30	125	350
26	0	0	0	0	30	30	125	350
27	0	0	0	0	30	30	125	350

Table 17: Measured heat fluxes (kW/m²) corresponding to the nine responses (Yi).

Exp	Y1	Y2	Y3	Y4	Y5	Y6	Y7	Y8	Y9
1	13.60	11.20	8.40	6.70	4.80	3.90	3.40	2.70	2.40
2	7.40	6.60	5.40	4.70	4.10	3.70	3.40	3.00	2.80
3	12.70	9.60	6.90	5.50	4.20	3.30	2.80	2.40	2.20
4	7.60	6.60	5.40	4.70	4.00	3.60	3.10	2.90	2.60
5	9.80	8.80	7.20	6.20	5.00	4.10	3.70	3.20	2.90
6	7.00	6.50	5.60	5.20	4.60	4.20	3.80	3.50	3.30
7	9.20	7.80	6.40	5.40	4.50	3.80	3.30	2.90	2.60
8	6.60	6.10	5.20	4.80	4.20	3.80	3.50	3.20	2.90
9	19.20	15.70	11.30	9.30	7.10	5.70	4.80	4.20	3.80
10	11.00	9.80	7.90	7.20	6.20	5.50	5.00	4.60	4.30
11	16.00	12.90	9.00	7.60	5.70	4.70	3.90	3.40	3.10
12	9.70	8.30	6.90	6.10	5.40	4.70	4.30	3.90	3.60
13	13.80	11.80	9.70	8.30	7.10	6.00	5.40	4.70	4.30
14	9.60	8.80	7.70	7.30	6.50	6.10	5.60	5.20	4.80
15	11.90	10.50	8.40	7.50	6.20	5.20	4.70	4.20	3.80
16	8.60	7.70	6.90	6.40	6.10	5.30	4.90	4.50	4.20
17	17.09	13.71	9.02	7.36	5.37	4.06	3.28	2.70	2.39
18	6.31	5.83	4.75	4.63	4.19	3.96	3.82	3.59	3.44
19	9.20	8.40	7.00	6.40	5.50	4.90	4.40	4.00	3.60
20	7.70	6.70	5.60	4.90	4.20	3.70	3.30	3.00	2.80
21	12.49	10.01	7.51	6.34	5.04	4.08	3.57	3.26	2.93
22	8.16	8.15	6.91	6.46	5.61	5.13	4.66	4.45	4.06
23	6.96	6.21	4.82	4.14	3.53	3.08	2.69	2.44	2.22
24	13.40	12.00	9.30	8.70	7.60	6.60	5.90	5.30	5.00
25	10.17	8.89	7.14	5.72	4.96	4.36	4.05	3.53	3.66
26	10.00	9.00	7.00	6.40	5.40	4.60	4.20	3.80	3.40
27	10.00	8.90	7.40	6.60	5.60	4.90	4.40	4.00	3.70

Before discussing the significance of the different model terms, the reliability of the different models from a statistical point of view must be checked. The determination coefficient (R^2) and the prediction coefficient (Q^2) were thus determined for each response (Table 18). R^2 describes the fraction of variation of the response explained by the model and Q^2 describes the fraction of variation of the response that can be predicted by the model. When the 27 experiments are considered, the determination coefficient is high: depending on the response (Yi), R^2 varies from 96.9 to 99.2% (Table 18), indicating that around 1 to 3% of the total variation is not explained by the model. Moreover, the heat flux value is well predicted by the model because the coefficient of prediction (Q^2) ranges from 82.3 to 96.4% (Table 18). Thus, the models are reliable and the different model terms can then be determined. Their values are listed in Table 19.

From Table 19, it can be observed that, considering each response separately, order of magnitude of quadratic (β_{ii}) and interaction (β_{ij}) terms is generally much smaller than that of the linear coefficients (importance of the model coefficients is always considered in absolute terms). Thus, the discussion is only focused on β_i terms.

Whatever the response Y_i, the β_2 term is from 2.5 to 5 times smaller than the highest β_i value (*i.e.* β_1 for Y_1 and Y_2; and β_4 for the other responses), in absolute terms. It means that the measured heat flux is little affected by the radiant source area covered by the insulating material. Thus, it was decided not to obstruct the heat source (*i.e.* U_2=0) and so, to use the full surface of the panel. It also corresponds to the conditions used in the large-scale test.

Table 18: Statistical coefficients (R^2 and Q^2) (%) associated to the different responses.

	Y_1	Y_2	Y_3	Y_4	Y_5	Y_6	Y_7	Y_8	Y_9
R^2	98.6	98.4	96.9	96.9	97.6	98.1	98.8	98.9	99.2
Q^2	91.8	91.0	82.3	85.7	89.0	91.5	94.0	95.9	96.4

Table 19: Linear, quadratic and interactions coefficients* of the model determined with Modde7.0

Coefficients	Y_1	Y_2	Y_3	Y_4	Y_5	Y_6	Y_7	Y_8	Y_9
β_0	*10.06*	*8.93*	*7.18*	*6.24*	*5.32*	*4.62*	*4.22*	*3.78*	*3.59*
β_1	**-2.51**	**-1.82**	**-1.04**	**-0.65**	-0.24	0	0.11	0.20	0.23
β_2	-0.50	-0.55	-0.45	-0.41	-0.32	-0.3	-0.28	-0.24	-0.22
β_3	**-1.22**	-0.68	-0.22	-0.02	0.16	0.23	0.27	0.28	0.26
β_4	**1.62**	**1.41**	**1.09**	**1.07**	**0.96**	**0.83**	**0.75**	**0.69**	**0.66**
β_{11}	0.53	0.28	0.01	-0.01	-0.10	-0.13	-0.14	-0.15	-0.16
β_{22}	-0.29	-0.28	-0.13	-0.10	-0.08	-0.05	-0.07	-0.06	-0.09
β_{33}	0.18	0.11	0.10	0.09	0.04	0.02	0	0.03	-0.02
β_{44}	0.15	0.11	0.06	0.10	0.10	0.08	0.04	0.03	0.01
β_{12}	0.26	0.23	0.23	0.13	0.11	0.04	0.04	0.01	-0.01
β_{13}	**0.81**	0.52	0.23	0.17	0.04	0.03	-0.01	-0.02	-0.01
β_{14}	-0.33	-0.29	-0.11	-0.08	-0.02	-0.01	0.03	0.02	0.03
β_{23}	0.08	0.13	0.09	0.07	0.04	0.01	0.03	0.01	0
β_{24}	-0.36	-0.23	-0.17	-0.13	-0.12	-0.13	-0.09	-0.11	-0.09
β_{34}	-0.21	-0.19	-0.04	-0.04	0.02	0.04	0.06	0.04	0.04

*In bold: significant terms

Then, for responses from Y_5 to Y_9, β_4 value is much more important than that of the other β_i terms. Thus, for distances higher than 170mm, the heat flux value is mainly affected by a change in the propane flow rate (parameter X_4). Moreover, β_4 coefficients being positive, it means that an increase of the gas flow rate leads to an increase of the measured heat flux, which was expected. If the heat flux values of the entire set of experiments are considered for each response

(Table 17), it can be observed that, for Y_6 to Y_9 responses, they are all higher than the target range required by the standard. Regarding Y_5 response, only one measured heat flux is appropriate (3.53 for experiment 23), the others being too high. Moreover, for each response, the lowest heat flux is obtained when conditions corresponding to experiment 23 are applied (Table 20). For this experiment, the propane flow rate is set to its minimum value (200L/h). But, as the heat fluxes are too high, the propane flow rate has to be reduced. As a consequence, another optimization was considered with a gas flow rates ranging from 150 to 200 L/h (on our small-scale device, a 150L/h flow rate is the minimum value to have a stabilized propane flame). Considering Y_2 to Y_4 responses, order of magnitude of β_1 and β_4 terms is similar (Table 19). As β_4 term has been discussed previously, the adjustment of the heat flux value according to the ISO standard requirements has been done thanks to parameter X_1 for these three responses. β_1 coefficients are negative, meaning that an increase of the radiant source angle leads to a decrease of the measured heat flux, which was also expected. If experiment 23 (corresponding to the lowest gas flow rate and thus the best adapted conditions for this parameter) is considered, heat fluxes for Y_2 to Y_4 responses are much lower than the target range required by the ISO standard. To increase the heat flux value, the radiant source angle must be decreased compared to the one used in this experiment (*i.e.* 30°). Thus, in the next optimization step, the angle range will be set from 10 to 20°.

Table 20: Comparison of target range and minimum values of heat fluxes for Y5 to Y9 responses.

	Y_5	Y_6	Y_7	Y_8	Y_9
Target range of heat flux according to the ISO standard	3.3 to 3.7	2.3 to 2.7	1.6 to 2	1.2 to 1.6	0.9 to 1.3
Minimum heat flux value obtained considering the 27 experiments	3.53	3.08	2.69	2.44 / 2.4	2.22 / 2.2
Experiment number corresponding to the minimum heat flux value	23	23	23	23 / 3	23 / 3

Finally, for Y_1 response, three β_i terms are of importance: β_1, β_3 and β_4. β_{13} interaction is also significant but it is due to the importance of X_1 and X_3 parameters. X_1 and X_4 have been previously set. Thus, the discussion is now focused on X_3 as this parameter is only significant for Y_1 response. The negative sign of β_3 coefficient allows confirming that an increase of the distance between the radiant source and the test sample leads to a decrease of the measured heat flux. Experiments 21 and 22 correspond respectively to the lowest and highest distances for X_3 parameter (Table 16). In these conditions, the heat fluxes obtained for Y_1 response are largely

outside the target range (much higher and much lower for experiments 21 and 22 respectively). Thus, it has been decided to keep the experimental values corresponding to -1 and +1 coded values (*i.e.* 100 and 150 mm) for the next optimization step.

As the settings of the small-scale radiant panel device have to be determined so as to optimize simultaneously the nine responses, the optimizer function of Modde software was used, restricting the experimental range of each parameter according the previous conclusions: $10 \leq U1 \leq 20$; $U2=0$; $100 \leq U3 \leq 150$; $150 \leq U4 \leq 200$. The different solutions proposed by the optimizer to reach the heat flux target range required by the ISO standard for the nine distances show that:

- the optimal propane flow rate (X_4 parameter) must range between 160 and 170L/h
- the radiant source angle (X_1 parameter) lies mostly between 10 and 15°
- given the previous experimental ranges for X_1 and X_4, the distance (X_3 parameter) should vary between 100 and 130 mm to optimize Y_1 response

The tendencies given by the optimizer are based on the mathematical models associated to the different responses and only predicted values of heat flux are given. Thus, it is necessary to make experiments to precise the experimental conditions to use and thus to validate the experimental design approach. Using the new experimental range given by the optimizer, several experiments have been done and the conditions allowing to optimize the heat flux distribution on the small-scale device were determined as follows: a 10-degree angle, no obstruction of the radiant panel, a 110 mm distance and a 165 L/h propane flow rate. In these conditions, the heat flux obtained for the nine distances (Y_1 to Y_9) is given in Table 21. These values correspond to the average of 3 tests.

Considering the average heat flux values (Table 21), Y_1 is the only response that does not meet the ISO standard requirements. The target range is between 10.5 and 11.3kW/m² and the average heat flux value obtained with the small-scale device is 11.6kW/m². Thus, we have to note that experimental conditions are slightly stronger than in the large-scale test.

Table 21: Experimental conditions and heat fluxes obtained after optimization.

U1 (°)	U2 (%)	U3 (cm)	U4 (L/h)	Y_1	Y_2	Y_3	Y_4	Y_5	Y_6	Y_7	Y_8	Y_9
10	0	110	165	11.6 ±0.4	9.4 ±0.2	6.8 ±0.1	5.0 ±0.1	3.5 ±0.1	2.6 ±0.1	2.0 ±0.1	1.6 ±0.1	1.3 ±0.1

Artificial turf samples have then been tested with the small-scale device with those optimized parameters and results have been compared to those obtained with the large-scale test in order to study the correlation between both scale tests.

B. Fire properties: large-scale test VS small-scale test

Once the setting parameters of the small-scale test have been defined, it is necessary to determine whether the device can reliably discriminate the fire behaviour of different formulations. To this end, the various structures were tested on the large-scale and on the small-scale devices. The results, including the burnt length and the fire rating according to the Euroclass standard, are compared for both scales. Three specimens, cut in the production direction, and three others cut in the opposite direction have been tested per formulation. As the results showed that the direction had no impact on fire behaviour of artificial turf structures for both scales, only the results obtained for specimens cut in the production direction will be discussed.

1. Evaluation of artificial turf on the large-scale test

First of all, the fire behaviour of artificial turf structures has been evaluated on the standardized radiant panel apparatus at the University of Ghent (Belgium). For each type of infill material, three specimens have been tested and the results given in Table 22 correspond to the worse fire behaviour i.e. the longer distance (and thus the lower CHF) among the three specimens.

Table 22: Results obtained with the large-scale EN ISO 9239-1 test for five artificial turf structures.

Sample names / Parameters	S – SBR	S – EPDM	S – TPE	S – Cork	S – FR EPDM
Flame front position on extinction (mm)	1015	500	580	780	150
Percentage of burnt length (%)	100	49	57	77	15
Burning time (s)	1542	1800	1800	856	1062
CHF (kW/m²)	< 1.1	3.7	2.8	1.5	10.2
Class	E_{FL}	D_{FL}	E_{FL}	E_{FL}	B_{FL}
Smoke rate	s2	s1	s1	s1	s1

The worst behaviour in terms of flame spread and smoke emission is obtained in the case of S - SBR since 100% of the sample length is burnt before the end of the test (in less than 26 min) and the smoke rate is the only one with a s2 classification (data are higher than 750 %.min). S - TPE and S - Cork structures present intermediate flame spread behaviour as 57% and 77% of

the samples length burn respectively. However, after 30 minutes of test, S - TPE is still burning while a self-extinguishing behaviour is observed for S – Cork. In that case, the sample stops burning after about 14 minutes. The three previously mentioned structures are thus classified E_{FL} (Table 22). With a slightly lower flame spread, S - EPDM structure burns on half of its length after 30 min, leading to a D_{FL} rating. Finally, S – FR EPDM structure, containing the flame retarded infill, achieves the best performance in terms of flame propagation since the sample self-extinguishes after about 18 minutes of test with only 15% length burnt, resulting in a B_{FL} rating, the best classification with the EN ISO 9239-1 test.

2. Evaluation of artificial turf on the small – scale test

The fire behaviour of artificial turf structures has then been evaluated using the small-scale radiant panel test. Similarly to what was done on the large scale test, Table 23 gathers the results exhibiting the worse fire behaviour (lowest CHF) among the three structures tested for each formulation.

Table 23: Results obtained with the small-scale radiant panel test for five artificial turf structures.

Sample names / Parameters	S – SBR	S – EPDM	S – TPE	S – Cork	S – FR EPDM
Flame front position on extinction (mm)	338	180	220	150	70
Percentage of burnt length (%)	100	53	65	44	21
Burning time (s)	1625	938	1800	668	619
CHF (kW/m²)	< 1.3	3.2	2.3	4.3	9.4
Class	E_{FL}	D_{FL}	E_{FL}	D_{FL}	B_{FL}
Smoke rate	s2	s1	s1	s1	s1

The evaluation of the fire behaviour with the downscaled radiant panel test leads to the same rating as for the large-scale test considering the different structures, except for S-Cork. The worst behaviour in terms of flame spread is observed for S – SBR and S – TPE structures with a burnt length of 100% and 65 % respectively, leading to a E_{FL} rating. Moreover, the S – SBR structure releases the highest amount of smoke among the different structures and is the only one with a s2 classification as observed at large-scale test. S – cork and S – EPDM structures exhibit a better behaviour compared to the previous structures as 44% and 53% of the sample length is burnt respectively at the end of the test, corresponding to a D_{FL} rating. Finally, the S – FR EPDM structure reaches the best rating (B_{FL}) due to a very short burnt length (21 %).

3. Proof of concept: assessment of the radiant panel test downscaling reliability

The burnt lengths mentioned in Table 22 and Table 23 correspond to the position of the flame front at the end of the test, either after self-extinguishment or after a 30 minute test period. During both large-scale and small-scale tests, a phenomenon called "running flame" was observed for S-Cork and S-TPE turf structures. This phenomenon corresponds to a quick spread of the flame at the surface of the sample, burning only the top layer of the sample (no deep degradation). The flame moves along the whole sample length and rapidly goes back to the hotter end of the sample. Then, combustion continues over a certain distance until the end of the test. In order to explain this phenomenon, it is necessary to consider the results of **Chapter 1**. It was found that during MLC tests, for SBR-based and EPDM-based structures, the pile melted and remained at the surface of the samples, while for cork-based and TPE-based samples, the pile shrank, penetrating inside the infill layer and forming a mixture with it. As the running flame phenomenon is only visible for the cork-based and TPE-based structures, it could be reasonably supposed that the behaviour of the pile during the test affects the flame spread.

The assumption is that the flame 'runs' at the extreme surface of the sample due to the presence of PE fibres sticking out of the infill layer. Then, under the action of heat coming from the radiant source, the PE pile shrinks rapidly, going inside the infill layer. As the heat flux at the end of the sample (located at the opposite side of the radiant source) is low, the flame is smothered inside the infill layer, giving the impression that the flame goes back to the hotter end of the sample. However, beyond a critical heat flux value generated by the radiant source, the infill material also begins to burn and thus combustion is maintained. That is why the sample burns over a certain distance. Figure 15 illustrates the running flame phenomenon and the position of the flame front at extinction.

Furthermore, the 'running flame' phenomenon is visible at both scales. However, downscaling may have a further negative influence on the flame spread. For example, edge effects (neglected when samples are large enough) due to smaller sample size could appear [122], [123]. Moreover, the sample size influences the regime of flame spread leading to different spread rate [124]. Indeed, it was also shown that the width of the sample could affect the rate of flame spread at the radiant panel test up to 50% [125].

Depending on whether the running flame phenomenon is considered or not, the CHF value will be different. There are two possible approaches: either the entire burnt length is considered and the CHF corresponds to a E_{FL} rating; or the "running flame" spread is neglected and the position

of the flame front at extinction is considered. In the case of artificial turf structures, since the flame only burns the extreme surface of the sample, and as this phenomenon occurs very quickly and in a non-repeatable way (different behaviour between two samples of the same nature), it cannot be considered as representative of the real fire behaviour. Therefore, **it was decided to consider only the part of the sample that is really degraded in depth and thus, the running flame was not considered for the determination of the sample's rating.**
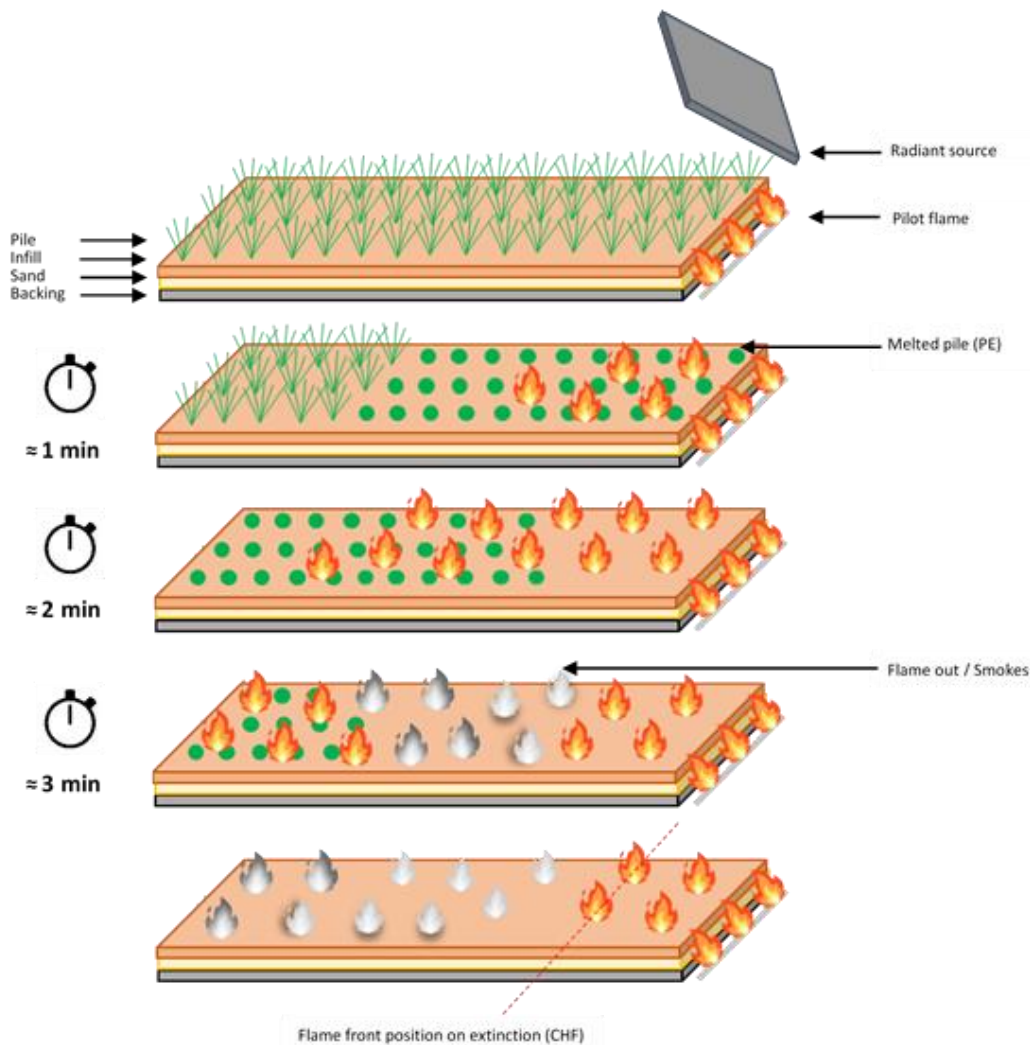
Figure 15: Illustration of the burning of turf samples at the radiant panel test as a function of time and representation of the flame front position (dotted line) at extinction

Secondly, Figure 16 (a) allows comparing the results obtained for both scales in terms of burnt length. As the difference ranges between 0 and 8% for S – SBR, S – EPDM, S – TPE and S – FR EPDM structures, the burnt length can be considered as similar between both scales. It is shown that S – SBR and S – TPE structures have the worst behaviour in terms of flame propagation, with a E_{FL} rating at both scales. On the contrary, the short burnt length of the S – FR EPDM structure leads to a B_{FL} rating. S – EPDM structure exhibits an intermediate behaviour with a D_{FL} rating. For S – Cork, the burnt length is longer at large scale as 77% of

the sample is burnt at the end of the test, compared to 44% at small scale. This result will be discussed in the second part of the study (Section C. 3. Discussion and conclusion, page 70). Thus, the EN ISO 9239-1 rating is different from one scale to another for S – Cork, i.e. E_{FL} rating and D_{FL} rating at large and small-scale respectively. On the contrary, the smoke rate classification for all turf structures is the same for both scales: S – SBR structure leads to a s2 classification while the other structures give a s1 one.
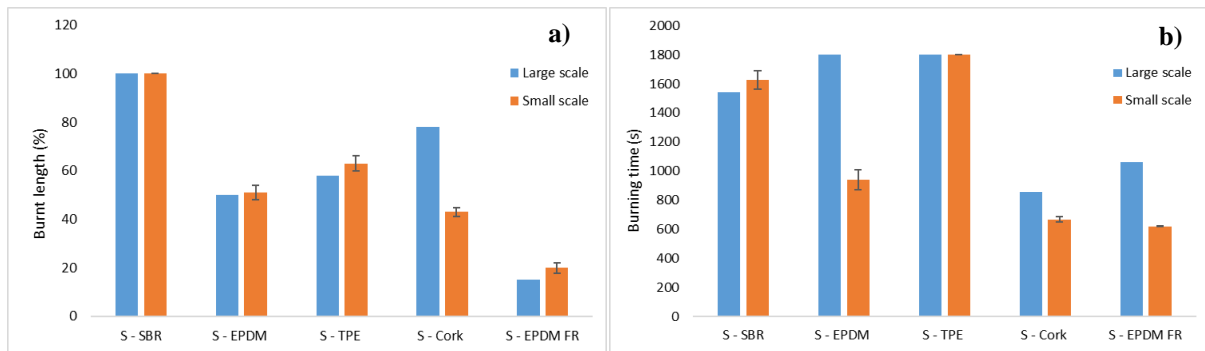
Figure 16: (a) Burnt length and (b) burning time of the different structures at large and small scales

On the other hand, the combustion times between the two scales are not necessarily correlated (Figure 16 (b)). Similar combustion times are obtained with S – SBR, S – TPE and S – Cork structures. For the S - EPDM structure, a self-extinguishing phenomenon can be observed after about 16 min with the small-scale test, whereas the sample still burns after 30 min of testing with the standardised apparatus. Finally, the S – FR EPDM structure exhibits a self-extinguishing character after around 10 min and 18 min of testing for the small-scale and large-scale tests respectively.

Thus, the fire performance differs greatly from one artificial turf structure to another. If the composition of the different structures is considered, only the nature and the thickness of the infill layer vary. In the case of the S - SBR structure, the infill layer thickness is relatively important (15 mm) and the highly flammable nature of SBR leads to a fast flame spread along the entire sample length, followed by a slow in-depth combustion and a large amount of smoke. For TPE and EPDM based structures, the infill layer thickness is lower (5 and 10 mm respectively) and TPE and EPDM granules are filled with calcium carbonate ($CaCO_3$) as mineral filler. So, the organic weight content is lower, leading to a different combustion behaviour i.e. lower flame spread, especially for the S - EPDM structure. The cork-based structure has a thick infill layer (15 mm). But as cork is naturally an excellent thermal insulator with a low heat transfer rate [91], the flame spread is lower than for the S – SBR structure and

the combustion time is smaller than with the other three non-flame retarded infills. Finally, the use of a flame retarded infill allows a significant improvement in the fire behaviour of the S – FR EPDM structure compared to the S - EPDM structure, reflected by a significant decrease in burnt length and burning time.

Except for S – Cork, the downscaling of the radiant panel test leads to a consistent assessment of the flame propagation and thus of the CHF value, as well as the smoke rate for samples subjected to a radiative heat flux distribution similar to that of the ISO standard.

4. Conclusion

To validate the downscaling, fire tests were performed on several artificial turf structures and results obtained at both scales were compared. The comparison of the results obtained on large- and small-scale tests is promising. Although for the cork-based structure significant differences in burnt length are noticeable leading to a different Euroclass rating, it was shown that for most infills, the CHF value and smoke rate classification were similar. The small-scale experimental device offers thus a promising method to predict the fire performance of floorings. Moreover, the results obtained with MLC cannot predict the behaviour of artificial turf structures at the radiant panel test: whereas better performances were obtained for S – Cork at the MLC test, the results obtained at the radiant panel test whatever the scale are less encouraging. If results obtained at the radiant panel for S – EPDM and S – FR EPDM structures are compared, it is shown that the fireproofing of the infill can sharply improve the fire behaviour of the whole structure. The fire retardancy of cork needs to be further investigated and this will be done in the next Chapter (**Chapter 3 PART III**). Before exposing those results, further experiments will be carried out using the radiant panel of S – Cork at various infill thicknesses to better understand the differences in results (burnt lengths and rating) between the two scales for the cork-based structure.

C. Evaluation of cork-based structures at the radiant panel test

This part thus focuses on the influence of the thickness of the cork layer on the fire behaviour of the overall structure on the radiant panel test. Three thicknesses of cork (10, 15 and 20 mm) were studied. Since the first part of the chapter showed that the radiant panel test at small scale did not provide the same results as those obtained at large scale for the 15 mm cork-based structure, the objective is to determine whether this difference is only due to the nature of the material (natural infill with a high degree of variability) or whether the thickness can also influence the results. It should also validate the optimal thickness that has to be used using cork

as infill as it was done with MLC test. Finally, in the discussion section, an attempt will be made to explain the differences in burnt length for cork-based structures depending on the scale or the infill thickness.

1. Evaluation of S – Cork at various infill thickness on the large-scale test

First of all, the fire behaviour of cork-based artificial turf structures filled with 10, 15 and 20 mm of infill has been evaluated on the standardized radiant panel apparatus at the University of Ghent (Belgium). For each infill thickness, three specimens have been tested and the results given in Table 24 correspond to the worse fire behaviour i.e. the longer distance (and thus the lower CHF) among the three specimens.

Table 24: Results obtained with the large scale EN ISO 9239-1 test for the three cork-based structures.

Parameters	Sample Infill thickness (mm)	S – Cork		
		10	**15**	**20**
Flame front position on extinction (mm)		650	780	610
Percentage of burnt length (%)		64	77	60
Burning time (s)		750	856	822
CHF (kW/m²)		2.2	1.5	2.5
Class		E_{FL}	E_{FL}	E_{FL}
Smokes rate		s1	s1	s1

In terms of flame propagation, the three structures have similar behaviour with a burnt length of 64%, 77% and 60% for the 10 mm, 15 mm and 20 mm structures respectively, resulting in a E_{FL} rating according to EN ISO 13501 with a s1 smoke emission rate. The burning times are also very close, i.e. 750 s, 856 s and 822 s for the three thicknesses. As previously discussed for the structure with 15 mm of cork, the running flame phenomenon was observed for the structures with 10 mm and 20 mm of cork. As mentioned before, this 'running flame' phenomenon was not considered to determine the CHF.

2. Evaluation of S – Cork at various infill thickness on the small-scale test

The fire behaviour of the three cork-based structures has been evaluated using the small-scale radiant panel test. Table 25 gathers the results obtained with the specimens exhibiting the worse fire behaviour (lowest CHF) among the three structures tested for each formulation.

Table 25: Results obtained with the small-scale radiant panel test for the three cork-based structures.

Parameters / Sample Infill thickness (mm)	S – Cork		
	10	15	20
Flame front position on extinction (mm)	338	150	190
Percentage of burnt length (%)	100	44	56
Burning time (s)	652	668	802
CHF (kW/m²)	<1.3	4.3	2.9
Class	E_{FL}	D_{FL}	E_{FL}
Smokes rate	s1	s1	s1

The worst behaviour in terms of flame spread is obtained with the 10 mm cork-based and 20 mm cork-based structures with burnt lengths of 100% and 56% respectively, leading to a E_{FL} rating. The structure with 15 mm of cork exhibits the best behaviour with a burnt length of 44%, leading to a D_{FL} rating. All the structures present a s1 smoke emission classification. For the three structures, the running flame phenomenon was noted without being considered.
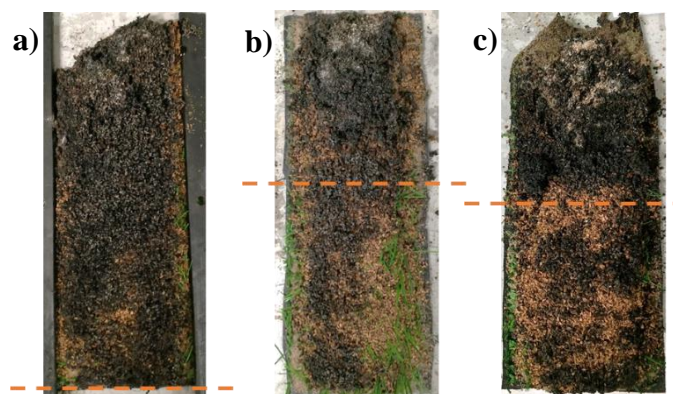
Figure 17: Residues of cork-based structures tested on the small-scale radiant panel test with a cork thickness of (a) 10 mm, (b) 15 mm and (c) 20 mm. Orange line: flame front position

Finally, the observation of the residues after testing in Figure 17 shows that, for the 10 mm cork structure, the backing at the zero point (contact with the pilot flame) is burnt over a length of

approximately 52 mm, i.e. 15% of the total length of the sample. For the other structures, the backing is completely preserved. Therefore, a thickness of 10 mm of cork seems insufficient to ensure good protection of the backing and similarly to what was observed with MLC tests, a minimum cork thickness of 15 mm must be used.

3. Discussion and conclusion

Comparing the results obtained at both scales for the 10 mm cork-based structures, much different burnt lengths are observed, i.e. 64% and 100% at large scale and small scale respectively, corresponding to a E_{FL} rating. After observation of the residues, it can be seen that the backing of the 10 mm structure has burnt at small scale. This can be explained by the fact that the test conditions are more critical at small scale (stronger first heat fluxes up to around 80mm, see Table 21) than at large scale. In addition, the burning of the backing may be responsible for a greater burnt length by providing an additional heat source leading to a stronger flame spread. Indeed, Benisek [76] already demonstrated that the flame spread properties are governed not only by the imposed heat flux but also by the heat release by the burning materials to its surroundings. Then, for the 20 mm cork-based structures, burnt lengths are similar, i.e. 60% and 56% at large scale and small scale respectively, also leading to a E_{FL} rating.

The main difference is observed for the 15 mm cork-based structures. At large scale, the sample has burnt on 77% of its length leading to a E_{FL} rating while at small scale, the burnt length is almost twice as short, i.e. 44%, leading to a D_{FL} rating. As a difference in rating is only observed for this thickness, the reliability of the small-scale radiant panel test can be considered as satisfactory. As cork is a natural compound that can vary in composition and structure, it can be assumed that the natural variability of cork can potentially influence the properties of cork and particularly its fire behaviour [96]. In addition, differences could be driven by infill thicknesses, infill distribution (infills may move), high variability of cork structure, shrinkage of the pile, etc [76]. Thus, antagonistic effects linked to the thickness of 15 mm and to the downscaling may disturb the fire behaviour of the 15 mm cork-based structure on the small-scale test (different heat dissipation, behaviour of the pile, etc). Benisek [75] highlighted that total pile weight and carpet thickness should not be excessive to allow effective heat dissipation from the pile and thus, ensuring short spread of flame. As low carpet thickness improves heat transfer, in the case of cork-based structures, it can be assumed that a cork thickness of 10 mm is too low leading to the burning of the backing but that 15 mm of cork seems to be an adequate

thickness for good heat dissipation at small scale, leading to a D_{FL} rating. Thus, determining an optimal thickness of infill in relation to the height of the pile, or changing the nature of the pile to prevent the shrinking, could help to better control and reduce flame spread.

IV. Conclusion of Chapter 2

As stated in **PART I**, one of the main drawbacks of the EN ISO 9239-1 radiant panel test is the amount of material needed to perform the fire tests, limiting the development of new materials. A 1/3 down-scaled version of the standardized test was thus developed and the experimental design methodology was implemented to replicate the radiative heat flux distribution required by the standard at reduced scale. To validate the downscaling, fire tests were performed on several artificial turf structures and results obtained at both scales were compared. It was shown that CHF value and smoke rate classification were similar for most structures. On the small-scale test, the behaviour of the 15 mm cork-based structure is different from the one observed at large scale (D_{FL} rating at small scale compared to E_{FL} rating at large scale). In order to better understand this difference, further experiments were carried out on structures containing 10 mm and 20 mm of cork. For these structures, the radiant panel test at reduced scale led to the same classification as the one obtained at large scale (E_{FL} rating). It was assumed that the variability of the properties of cork (natural compound with a high variability in structure and composition) could affect the fire behaviour of the overall structure and that the difference obtained for 15 mm can be explained by this variability. Since only one structure out of the seven tested was not correctly discriminated, it is assumed that the **small-scale test offers a reliable, fast and promising method to predict the fire performance of floorings.** These results also highlighted that, as demonstrated in Chapter 1, a thickness of 15 mm is a minimal value to ensure good protection of the backing. According to the EN 13501-1 standard, the CHF must be higher than 4.5 kW/m² for floorings to be used in closed areas, corresponding to a B_{FL} or C_{FL} rating. None of cork-based structures reaches the C_{FL} rating. Among the tested structures, only S – FR EPDM is suitable for indoor use (B_{FL} rating). Thus, the use of a flame retarded infill seems a promising way to improve the fire behaviour of artificial turf to allow indoor applications. The next chapter will thus concern the development of fireproofing methods for cork.

Key points & strategies of Chapter 2

Key points:

- ✓ Development of a 1/3 down-scaled EN ISO 9239-1 test allowing:
    - ➢ Cheaper testing
    - ➢ Reliable prediction of fire rating of floorings (Euroclass)
- ✓ According to the EN 13501-1 standard, only S – FR EPDM can be considered for indoor applications (B_{FL} rating)
- ✓ A minimum thickness of 15 mm cork is necessary to protect efficiently the backing and to provide adequate heat dissipation.

Strategies and objectives for the next chapter:

- ✓ Improving the fire behaviour of cork in order to enhance the overall fire behaviour of the cork-based structure to meet the fire safety regulation.
    - ➢ Review on the different approaches for cork modification
    - ➢ Development of an innovative fireproofing strategy
    - ➢ Characterization of the properties of the modified cork.

Chapter 3 - Cork: bulk modification by phosphorylation

In **Chapter 1** of **PART III**, MLC tests showed that the infill was the component with the greatest impact on the fire behaviour of the structure. Specifically, it was determined that cork is the infill with the best fire behaviour in terms of heat release rate. Moreover, Chapter 2 highlighted that the infill, being the top layer of the structure, protects efficiently the backing using a 15 mm cork thickness. But the cork-based structures are not adapted to indoor applications due to excessive flame spread. Moreover, the radiant panel tests carried out on the FR EPDM structure showed that fireproofing the infill can greatly improve the fire performance of the whole structure. Thus, the strategy developed in this chapter consists in improving the fire behaviour of cork using an eco-friendly method, without any toxic compound, in order to enhance the overall fire behaviour of the cork-based artificial turf structures to meet the fire safety regulation for indoor applications.

In a first part, an in-depth study of cork (origins, composition, etc.) is performed. The different approaches of natural-based products modification and more precisely bulk modifications are also reported. Then, the protocols selected from the literature are detailed in the 'Materials & Methods' section. In the 'Results and discussion' part, the method used to optimize the cork modification protocol is described. Upscaling of the system via a dimensional analysis is necessary to allow the modification of higher amounts of cork. Finally, modified cork is fully characterized in terms of efficiency of grafting and considering the functional properties.

I. Cork: a complex natural material

A. Cork cultivation

In the field of biology, "cork" represents the suberized tissue of periderms of some trees. It is mainly derived from the bark of cork oak, or Quercus L Suber, an evergreen oak so-called because of the thick cork bark at the surface of the trunk [92]. This tree is particularly well adapted to dry and hot climatic conditions and mainly grows in the western Mediterranean regions of south European Iberian Peninsula (Portugal and Spain) and in North Africa (Morocco, Algeria, Tunisia). Currently spread over more than 2 million hectares, the cultivation of cork oak is mainly oriented towards economic objectives, but it has also an ecological role through a contribution to the maintenance of biodiversity. Portugal and Spain are the largest cork producers in the world, as they supply 74% of the annual world cork production, representing approximately 370,000 tonnes.
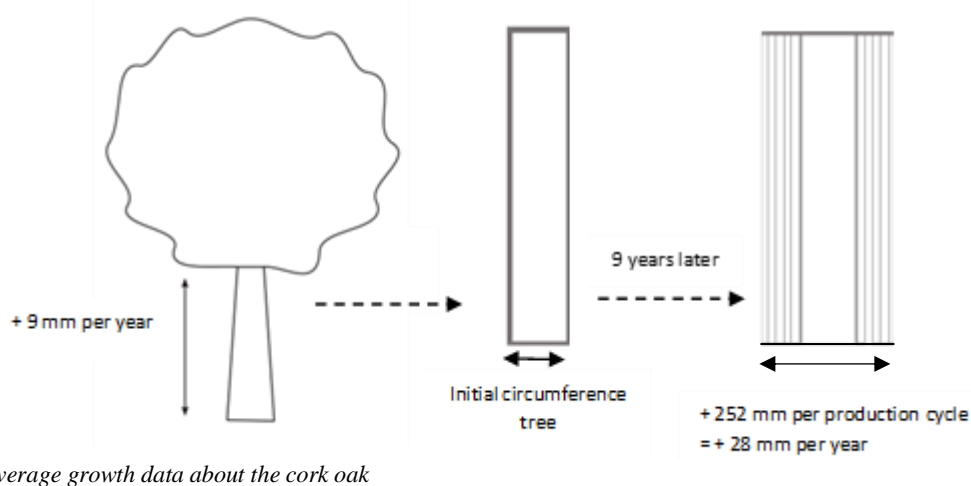
Figure 18: Average growth data about the cork oak

For its development and growth, cork has an intra-annual seasonality. Small in size as an oak tree (generally from 14 to 16 m high), the growth of cork oak is radial in three distinct phases with a main phase from May to August, corresponding to the largest increase in diameter (about 64% of the total annual growth) [126]. In addition, based on several studies on the quantification of the radial growth of cork oak [127]–[129], Pereira et al [92] determined that the average growth value was 9 mm per year, corresponding to an average annual perimeter increase of 28 mm, resulting in an increase in the cork oak circumference of 252 mm during a cork production cycle as shown in Figure 18. The first cork debarking, i.e. the first time the bark of a young tree is removed, is carried out when the tree is about 20-25 years old. Then, the complete production cycle of the cork oak is 9 years [127], [130]: this is the time required for the tree to produce

again a sufficiently thick and good quality bark, with the bark being renewed by natural regeneration, meaning that the bark is removed every 9 years. Moreover, the higher the number of production cycles, the smoother the cork becomes.

B. Cork composition

Cork plays a protective role for the tree and acts as a protective barrier between the living tissues of the tree and the potentially aggressive external environment. The ability to control gas transfer and water loss by limiting the exchange of molecules between the tree and its environment is also attributed to cork. The solid fraction of this material is small and gas is enclosed in small and closed cells. The chemical components are located in the faces and edges of the cells, forming a three-dimensional network of a solid matrix that surrounds the air-filled hollow cells. As most natural materials, the composition of cork can vary from one specie to another, depending on the place of growth (geographical area, climate, etc.), its age or other conditions [91], [92].

There are two main components of cork cells wall:

- The structural components, mainly suberin, lignins and polysaccharides (insoluble macromolecules (polymers)) whose presence considerably and structurally affects cork and its properties.
- The non-structural components, usually extractives (waxes, lipids and phenolic substances) and inorganic minerals constituting the ash after incineration, whose presence do not affect the cork structure.

To date, several authors [96], [131]–[133] described precisely the composition of cork. As shown in Table 26, it is supposed to be composed of about 40% suberin, 20% lignin, 20% polysaccharides (mainly cellulose and hemicellulose), 15% extractives and less than 1% ash.

Although the chemical composition of cork was widely studied since the end of the 18th century, first by Brugnatelli in 1787 and then, by Chevreul in 1807 [134] and 1815 [135], the exact composition of the constituents of cork, their arrangement and their biosynthesis are still under study. In order to better understand the properties of cork, the nature of the three main components, namely suberin, lignin and polysaccharides, is detailed below.

Table 26: Chemical composition of cork

Components (wt.%)	Virgin cork*			Reproduction cork					
	Caldas [136]	Pereira [137]	Gil [138]	Caldas [136]	Pereira [137]	Holloway [139]	Carvahlo [137]	Sen [140]	Jové [130]
Suberin	45	45	48	42	33.5	37	50	28.5	34.4 – 48.7
Lignin	27	21	21.5	29	26	14.8	19	28.1	14.6 – 25.3
Polysaccharides	12	13	16	12	25	/	13	16.5	7.1 – 15.8
Extractives	10	19	13	8.5	13	15.8	16	16.7	11.1 – 17.8
Ash	5	1.2	/	2.1	2.5	/	3	2.6	0.4 – 1.3
Others	/	0.8	7	/	/	/	/	/	/

*First cork extracted from a tree.

1. Suberin

Suberin, the main structural component of cork, is a family of macromolecular compounds, associated with membranes or plant layers, functioning as a sealing agent. Suberin especially provides waterproofing properties leading to the protection of the tree against its environment. Firstly identified by Chevreul in 1807 [134], then by Seoane and Ribas in 1951 [141] and studied by many other authors [142]–[144], suberin is mainly supposed to bring its properties to cork. As shown in Figure 19, this lipophilic macromolecule is a complex molecule considered as an aliphatic polyester, similar to a lipid biopolymer, built from poly-functional long-chain fatty acids (suberic acids) and glycerol, containing phenolic fragments such as lignins, associated and covalently linked to suberin [145]. However, although the monomeric composition of suberin is relatively well known, the molecular and supramolecular structures are still largely unknown. Therefore, suberin is composed of two domains: aliphatic and aromatic ones. The aliphatic domain is mainly responsible for the hydrophobicity and low permeability of cork to liquids and gases, as described in the works of Schönherr [146] and Riederer and Schreiber [147]. The aromatic domain is supposed to be closely related to the occurrence of lignin in the suberized cells. [92]
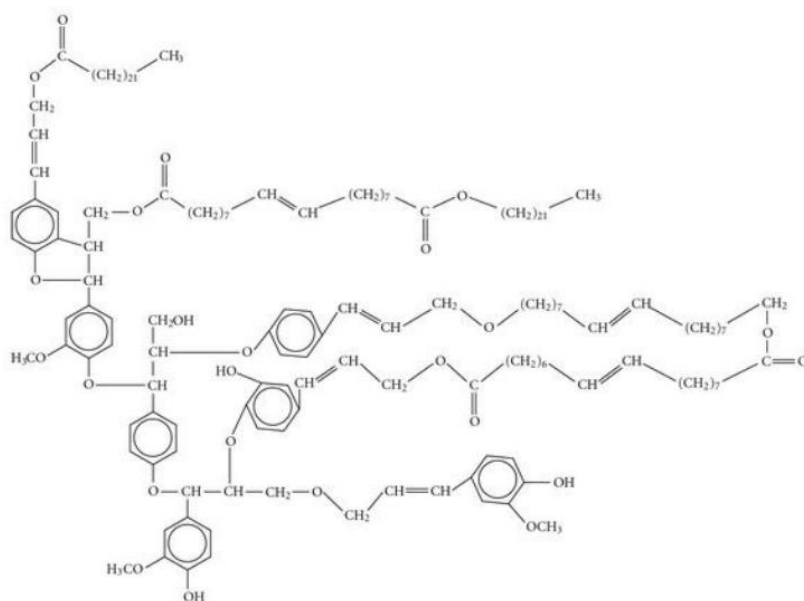
Figure 19: Suberin molecular structure [141]

2. Lignin

Lignin is one of the most abundant bio-polymers available on earth. In response to the growing trend for the use of materials from natural origin, lignin has emerged as an interesting alternative to bring antioxidant [148], surfactant [149], flame retardant properties [150], [151] or even as a source of chemicals. Lignin, a phenolic polymer of the parial matrix, composed of phenylpropene units [152], is a characteristic component of vascular tissues of plants and fibres. The lignification of walls occurs during the formation of the secondary wall, and proceeds gradually from the middle lamella to the secondary wall [153], [154]. It forms a kind of layer around the fibre, keeping the fibre hydrated and reducing its hydrophilicity [155]. Being a rigid and hard polymer with strong covalent bonds distributed in a three-dimensional network, lignin is mainly responsible for the stiffening of the cell wall and plays a very important supporting role. Mainly hydrophobic with low water absorption, the in-situ structure of lignin is, however, still unknown [92].

Lignin is actually a group of aromatic polymers, providing protection against microbial degradation to polysaccharides in the cell wall of trees and plants. Polymerization occurs through oxidative radicalization of the monolignols followed by combinatorial radical coupling [156]. Lignin, as shown in Figure 20 (A), is derived from the polymerization of three derived phenylpropane monomers, called monolignols: p-coumaryl, coniferyl and sinapyl alcohols. Linkage formation occurs randomly on each phenolic unit, leading to monomer units called p-hydroxyphenyl (H) from p-coumaryl alcohol, guaiacyl (G) from coniferyl alcohol and syringyl

units (S) from synapyl alcohol. Therefore, lignin is composed of the combination of these three monomers leading to a highly branched polyphenolic polymer with a three-dimensional structure [157], [158]. The nature of linkage and the proportion of each monolignol were investigated. At least 20 different linkages are present in common lignin, the most common are β-O-4, α-O-4, β-5, 5-5, 4-O-5, β-1 and β-β, as shown in Figure 20 (B) [159]–[161]. On this figure, the presence of several chemical groups, so-called phenylpropanoid units, such as aromatic and aliphatic hydroxyl, carboxylic, carbonyl and methoxy groups, is noticeable [158]. Lignin is the second most important structural component of cork since it represents approximately 20 wt.%. However, research on the chemical structure of lignin in suberised cells is rare. The isolation and characterization of lignins from cork was only carried out in 1996 by Marques et al [162]. Despite a difficult process due to a low yield of grounded cork lignin (about 2%), the composition of cork lignin was identified: G-type lignin containing 95% guaiacyl units (G), 2% 4-hydroxyphenyl units (H) and 3% syringyl units (S) with a 13.95% methoxy content (characteristic groups of lignins). The proportion of units with phenolic hydroxyl units is 27% and those with β-aryl ether bonds is 23%.
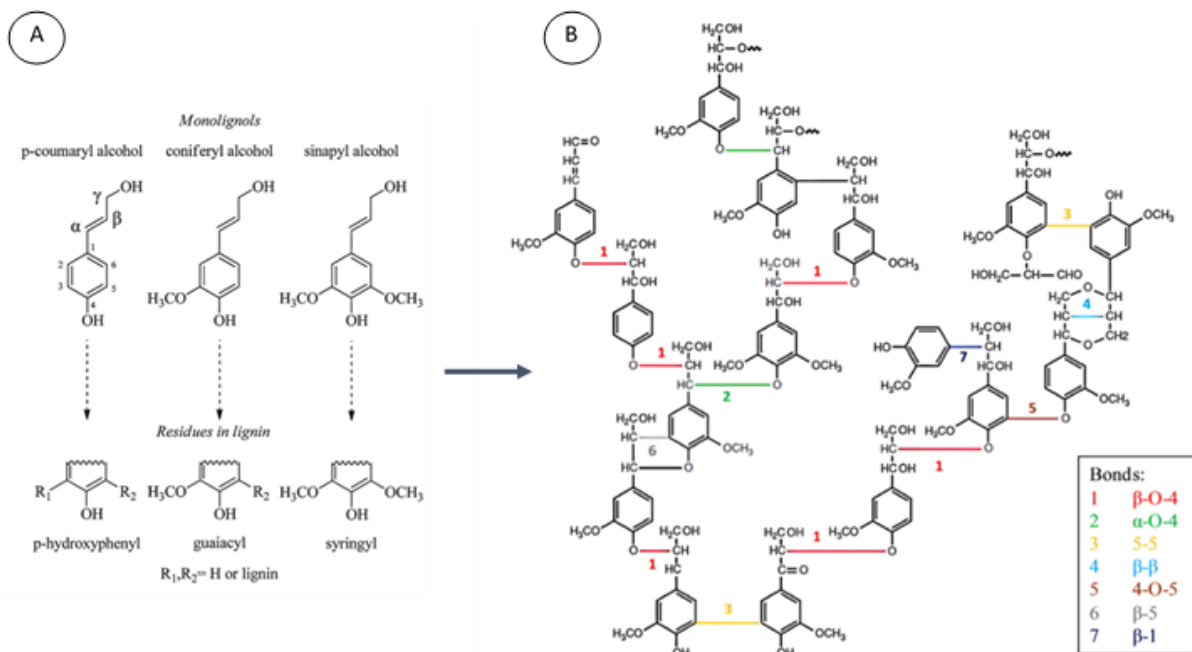
Figure 20: A) Three main lignin precursors (monolignols) and (B) the structure of lignin and its main linkages. From [152]

3. Polysaccharides

Polysaccharides are polymers so-called carbohydrates, such as cellulose, hemicellulose and pectins [131]. Polysaccharides are organic molecules composed of monosaccharides

(monomers) whose carbons carry an alcohol function (secondary or primary); aldehyde or ketone (carbonyl function); or an acid or amine function. As shown in Table 27, some authors were interested in the composition of cork monosaccharides, strongly influenced by various factors such as age of cork, variety of cork oak from which it is extracted or place of cultivation. The amount of polysaccharides in cork represents about 20 wt.%, glucose and xylose being the two main monosaccharides [92] corresponding to cellulose and hemicellulose polysaccharides respectively.

Table 27: Monosaccharides proportion in cork

Monosaccharides	Pereira		Asensio		Sen
(wt.%)	[132]	[131]	[163]	[164]	**[140]**
Glucose	50.6	46.1	68.8	63.9	47.2
Xylose	35	25.1	20.7	7.7	40.3
Galactose	3.6	7.3	1.83	17	3.6
Arabinose	7	18.0	5.52	3.1	6.6
Mannose	3.4	3.0	3.52	8.3	1.3
Rhamnose	/	0.5	/	/	1.0

Usually, as carbohydrates play an important structural role, cellulose and hemicellulose act as support elements for plants (cellulose) protection, recognition in the cell and reserve.

Pereira [132] and Conde et al [165] highlighted that cellulose of cork does not have the same importance as in other types of woods and barks as the structural role is rather played by suberin and hemicellulose. Although the cellulose content of cork is estimated at around 10 wt.% [132], its degree of polymerisation, crystallinity and orientation are not known [92]. In addition, in the specific case of cork, three xylan-based hemicelluloses were identified by Asensio et al [163], [164], [166], [167] namely 4-O-methylglucuronoxylan, arabino-4-O-methylglucuronoxylan and 4-O-methylglucurono-arabinogalactoglucoxylan.

Each type of hemicellulose has a different degree of branching, changing the supramolecular structure and the ability to create intermolecular hydrogen bonds. Some hemicelluloses have therefore an easier ability to bind to phenolic groups in the surrounding suberin or lignin [92].

C. Properties of cork

Chemical and biological inertia, insulation properties, water impermeability and, more recently, surface and dielectric properties are the main physical properties of cork directly related to its chemical composition and structure. Moreover, most of the incident sound waves are absorbed and transformed into thermal energy, which reduces reverberation [96], [138]. As shown in Figure 21, cork has a typical cellular structure. Individual closed cells are small hexagonal prisms stacked base to base and forming rows of cells, aligned parallel to each other in a compact and regular arrangement without intercellular voids. This structure is specific to cork but the size of the cells and the thickness of the walls can vary according to the species. The volume fraction of the solids is estimated at about 16 % [168] with a high gas content in the small cells.
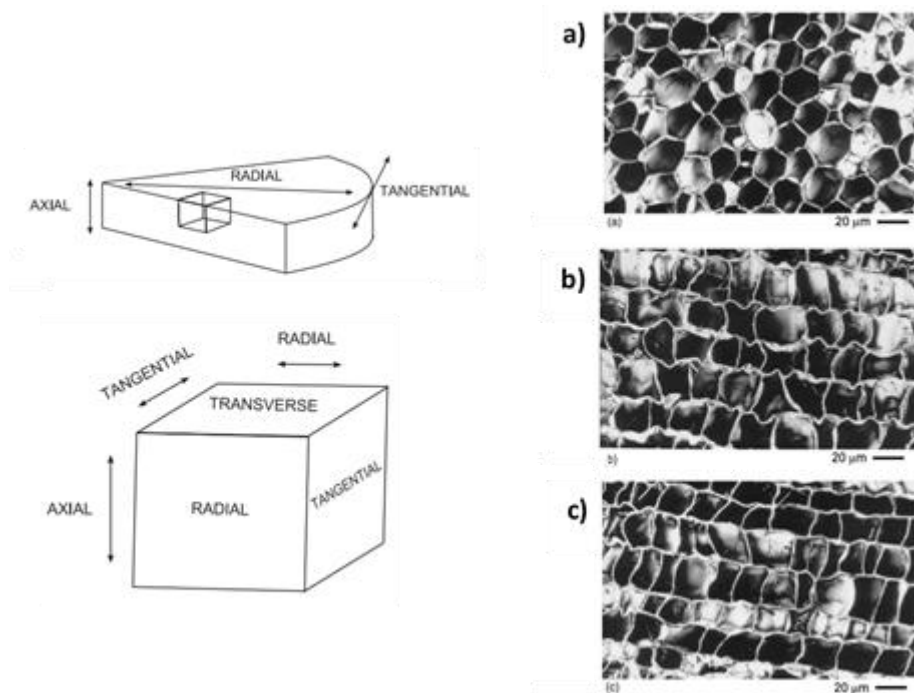
Figure 21: Scanning electron micrographs of sections of reproduction cork in (a) tangential, (b) radial and (c) transverse sections. Pictures extracted from [92]

This honeycomb structure obviously gives cork a low density. However, depending on the age of cork and the treatments applied, the density can vary from 120 to 240 kg/m² [96]. The factors influencing cork density are widely known, such as cell size, undulation of the cell wall and/or the volume fraction of lenticular channels (cavities), presented in Figure 22. Moreover, the more the cork is located at the outer side of the cork oak bark (outer bark), the thicker and the wavier the cork walls, the denser the cork is [169], [170]. On the contrary, a cork from the inner bark

is less dense. The low density of cork often appears as an advantage as, associated to the high porosity of cork, it provides excellent thermal insulating properties.
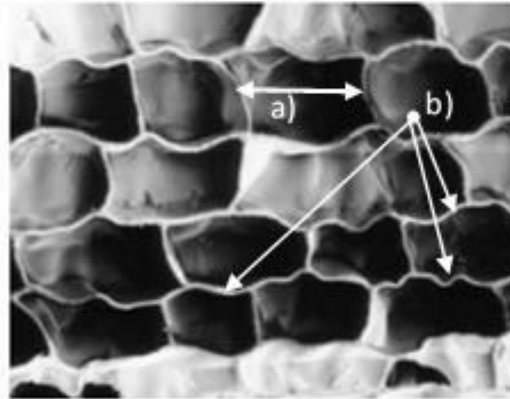
Figure 22: Structure of cork as observed by SEM in radial section with (a) the cell size, (b) the undulation of the cell wall and the cavities (volume fraction of lenticular channels). Picture extracted from [91]

In addition to these specific properties, cork has also remarkable mechanical properties as it possesses all the properties of flexible cellular materials. During compression, cork exhibits an elastic deformation, followed by a deformation caused by the progressive buckling of the cellular walls and finally, the crushing of the cellular walls. Furthermore, the Poisson's ratio is close to zero which prevents the material from suffering from excessive lateral expansion. The Young's modulus is quite high, especially in the radial direction, and can reach 13.2 MPa for a medium-calibre cork [131]. Rosa and Fortes [171] have shown that the Young's modulus in compression is lower than that in tension because tension increases the amplitude of the cell walls making them more rigid [138], [172]. Heating at medium temperature (100 - 150°C) for 24 hours increases its compressive strength due to the loss of water from the material [171]. When exposed to such temperatures for longer times, a decrease in compressive strength, probably related to thermomechanical degradation, occurs [173]. The authors also noted that when heated to 200°C and 300°C, the Young's modulus of cork was divided by 3 and 15 respectively. Other heat treatments can also influence the mechanical properties of cork [96]. Those results thus show that cork is sensitive to high temperatures and long exposure time to heat.

The properties of interest in our study concern the low heat transfer ability of cork due to its structural characteristics. Convection is avoided by the size of the cells and radiation is limited by absorption through the numerous walls [91], [174]. Thus, only conduction is important for heat transfer, the thermal conductivity of the walls being slightly higher than that of the gas in the cells [138]. In the event of fire, cork also has the advantage of being a low flammable

material and do not release any toxic compound. Even before being extracted, cork seems to bring fireproofing properties to oak tree trunks. In environments with high fire risks, such as savannah and sub-tropical biomes, trees have developed cork bark as an adaptation against fire because cork layer provides a considerable fire resistance [92], [175], [176]. However, although cork is increasingly used, the flame retardancy of cork has never been studied.

D. Applications of cork

Being a natural, biodegradable and renewable material with many specific properties as previously discussed, cork is used for various applications. The use of cork stoppers to seal wine bottles is the best know application of cork. Developed in the 7th century [138], [177], it is mainly based on the impermeability of cork to liquids and gases, due to its cellular structure and high suberin composition, as well as its high resilience and flexibility [96], [138]. Furthermore, the inert nature of cork is a considerable advantage for this application because cork does not release any product and does not alter the quality of the wine, unlike aluminium screw caps capable of releasing metal ions, or synthetic corks capable of transferring toxic compounds into the wine [178], [179].

However, the production of cork stoppers results in a large amount of waste, usually because the first debarkings provide a cork unsuitable for this application (too coarse). In that case, cork is granulated and used for other applications, such as:

- The processing of cork panels for sound and heat insulation [92], [144];
- The development of composites and in particular cork/rubber composites required in the automotive industry for seals or for oil containers;
- The manufacture of shoe soles; decorative panels and wall coverings [180], [181].

II. Cork modification

Thanks to various specific properties, such as a high energy absorption, low density, low thermal conductivity and excellent acoustic insulation properties, cork is the ideal material for various applications. However, cork must generally undergo physical or chemical modifications. The following section describes the various ways of modifying cork.

A. Cork processing methods

The most common cork modification consists in applying a water heat treatment, by immersion into boiling water. This heat treatment is used in the manufacturing process of cork stoppers or

panels. The objective of this treatment is to avoid giving a corky taste to the wine in the case of stopper application due to the natural oxidation of polyphenols. Cork is thus boiled for 1 hour into water to remove extractable compounds, to make it more flexible and to open the cells as much as possible. This dilatation causes the expansion of the gas inside the cells, leading to the reduction of the cork density [96], [170], by increasing its total volume by about 30 %, i.e. 10-15 % increase in the radial direction and 5-7 % in the axial and tangential directions [182], [183]. The volume of cork thus increases, it becomes smoother and the cell walls become more planar, as shown in Figure 23 [184]. After a few weeks of stabilization, cork stoppers are shaped in the stabilized cork plates, washed and finally disinfected [96]. For the manufacture of sound and heat insulation panels, cork granules are heated at high temperature (about 300°C) under pressure (40 kPa) [182], [185] inducing a thermo-chemical degradation of the cork cell wall with expansion of the cells and of the gas contained therein. The degradation by-products, mainly of the suberin [186], permit the cork granules to agglomerate to form a plate since these products act as a natural binder [171]. A stabilization phase takes place causing the cell walls to expand, of approximately 100 %. A light dark-coloured expanded cork sheet is finally obtained, due to the thermochemical degradation [182]. In the case of cork composites, cork can also be modified in order to improve its wettability or its adhesion to the polymer matrix. For example, cork surface can be treated with an alkaline solution, a silane or an appropriate compatibilizing agent to promote a chemical interaction between cork and the matrix. This treatment partially removes the hemicelluloses, the waxes, and the lignin present at the surface [187].
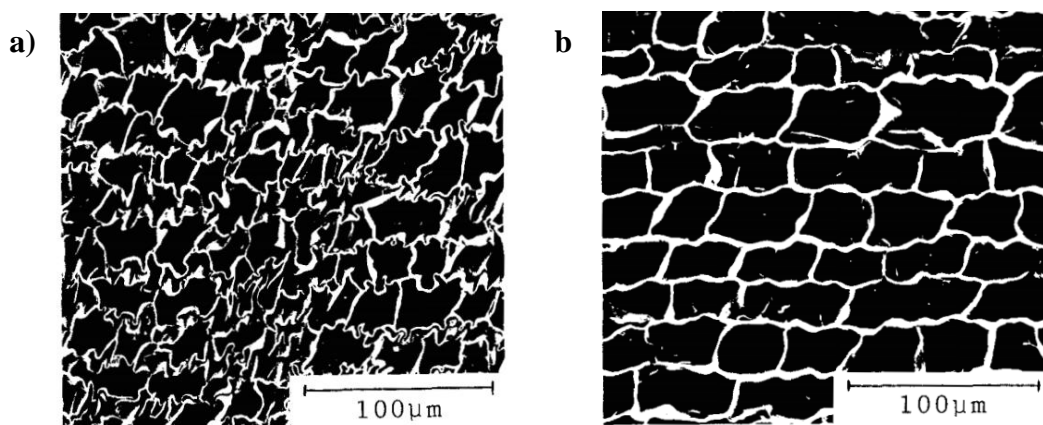
Figure 23: SEM pictures showing the effect of boiling water on the cellular structure of cork in transverse sections a) before and b) after boiling water treatment

B. Cork fireproofing methods

Even if some papers deal with the fire behaviour of cork-based composites [188], [189], no literature exists on the fire behaviour of cork neither in its natural form nor modified to improve its FR properties. However, the influence of cellulose, hemicellulose or lignin in other natural products is well documented. For example, it is reported that fire properties of natural fibres are mainly led by their cellulose and hemicellulose content: the higher the hemicellulose or cellulose content, the higher the flammability. The lignin content is also an important factor because the higher the lignin content, the higher the char formation during combustion [190]–[192].

Since no literature exists on the fire proofing methods applied to cork while lignin or cellulose (two components of cork) are well documented [193]–[195], it was decided to further study literature on natural compounds. It has to be noted that there is currently no work on the modification of suberin, the predominant component of cork. However, as suberin is mainly composed of suberic acid, chemical compound containing many hydroxyl groups, grafting can be considered.

III. Flame retardancy of natural products

A. Surface treatments

Surface treatments on natural compounds generally use laser, plasma or cold plasma technologies [196], [197]. However, in the case of cork, these techniques can hardly be used because the shape of cork granules does not allow a uniform treatment over the entire surface. For other natural compounds such as starch or cellulose, the layer-by-layer technique (LbL) can be considered. It consists in successive immersions of a substrate into positively charged solutions and then, into negatively charged solutions. An assembly is then formed between positive and negative species through different donor and acceptor interactions [198], hydrogen bonding [199], or covalent bond formation [200]. A flame retardant (FR) multi-layered film is deposited at the surface of the substrate and can exchange directly with the environment during combustion, limiting therefore the risks of modifying the intrinsic material properties [201]. The obtained coatings can be non-intumescent or intumescent. Despite the need for many layers, this technique is relatively environmentally friendly and permits to reach an efficient flame retardancy [202]. The materials submitted to this type of treatment are mainly natural fabrics (often cotton fabrics) [203], polymeric fabrics [204] and polyurethane (PU) foams [205].

The LbL technique could have been considered for cork granules because it is a porous material with a large specific surface area. However, considering our application, the use of a surface treatment presents a major risk of leaching and poor durability, leading to the release of chemicals in the environment as well as to a loss of fire properties over time. Therefore, bulk modification is recommended to have a better durability.

B. Bulk modifications

Considering lignin, the most common modifications reported in the literature are hydroxylation, alkylation, amination and nitration, carried out with the aim of improving specific properties such as adhesive or hydrophobic properties. In most cases, hydroxyl groups of lignin are functionalized [157]. The main modification processes to bring fire properties to lignin are:

- the derivatisation, i.e. the synthesis of a by-product from a precursor [206];
- the amination, consisting of the insertion of an amine into a molecule or at the surface of a material, mainly through a Mannich reaction [157], [207], [208], and;
- the phosphorylation, consisting of the phosphorus moieties grafting onto the hydroxyl groups [158], [209]. Phosphorylation of cellulose, one of the main polysaccharide present in cork, is also reported and permits to improve the fire properties of cellulose, exhibiting a lower THR at cone calorimeter test compared to virgin cellulose [210]. As phosphorylation of lignin and cellulose can lead to significant improvements in thermal stability and fire performance, and as suberin is a polymer with a cellulose-like structure containing hydroxyl groups, particular attention is paid to the phosphorylation method.

Phosphorylation allows grafting phosphorus moieties through covalent bonding onto the reactive -OH groups, usually located at chain ends of natural compounds. The aim of this process is to improve the fire behaviour and thermal stability of the compound. The reaction is an esterification of hydroxyl groups to graft phosphate, phosphite or phosphonic acid (including phosphonate) function onto the polymeric chain. The wise choice of solvents and phosphorylating agents (phosphorus precursors) is essential. The solvent diffuses inside the polymer and makes it swell permitting the reaction to occur. In order to have the best reaction conditions, the chosen solvent must allow the phosphorylating agent penetrating and diffusing efficiently into the material.

Some phosphorylation processes reported in the literature for natural products are detailed below and classified according to the phosphorus moieties.

1. Phosphorus pentoxide

Phosphorus pentoxide (P_2O_5) is the anhydrous form of phosphoric acid (H_3PO_4). Prieur et al [209] developed a simple lignin phosphorylation protocol that can be applied industrially. Lignin is dissolved into tetrahydrofuran (THF), followed by the addition of P_2O_5. After heating at 45°C for 8 h and precipitation, the mixture is cooled down and THF is evaporated using a rotatory evaporator. After filtration and rinsing, lignin is recovered and dried. Thermal characterizations are carried out. It was shown that the thermal stability of phosphorylated lignin is higher than the one of non-modified lignin, especially at high temperature. The authors proposed that phosphorous promotes dehydration and decarboxylation reactions leading to the formation of a thick carbonaceous residue and thus, to a stable structure at high temperature. When phosphorylated lignin is used at 30 wt.% addition rate in acrylonitrile butadiene styrene (ABS), the combustibility of the FR ABS proved to be significantly lower than that of virgin ABS with a decrease of 50 % in the pHRR at MLC test.

2. Phosphoric acid

Phosphoric acid can also be used as a precursor for the phosphorylation process and different protocols are reported.

2.a. Phosphoric acid combined with lithium chloride and urea

Lentsolo [211] studied the synthesis of phosphate cellulose fibres by using H_3PO_4 combined with lithium chloride (LiCl) and urea. First, the polymer to be phosphorylated is pre-treated and activated with LiCl. This allows the swelling of the polymer, increasing the diffusion of the phosphorus reagent inside the structure of the fibre and therefore the grafting of the phosphorus groups. In a second step, the pre-treated polymer is phosphorylated in a bath of H_3PO_4 and urea. The reaction is carried out under reflux for 3 hours followed by the filtration and drying of the product. The urea allows the H_3PO_4 penetrating more easily the polymer to increase the degree of esterification. Urea also buffers the action of phosphoric acid so that the polymer chains are not severely degraded. The phosphorus determination carried out by Inductively Coupled Plasma (ICP) showed a grafting rate of 24.3 %. This reaction route represents a good option in view of the simple reagents used and the efficiency of the reaction due to the pre-treatment.

2.b.   Phosphoric acid combined with phosphoric pentoxide

Granja et al [212] proposed to chemically modify the cellulose by phosphorylation in order to obtain a biocompatible material, able to promote bone regeneration. The cellulose powder is firstly dried under vacuum in the presence of P_2O_5 before being immersed in hexanol, the reaction solvent, in order to make the sample swell. The phosphorylation reaction is carried out stirring a suspension of cellulose (4 g) in hexanol (29 mL). Then, a mixture composed of P_2O_5 (50 g), triethyl phosphate (Et_3PO_4) (37 mL) and H_3PO_4 (42 mL) is progressively added. The complete mixture is stirred at 35°C for 72 h and then filtered. The phosphorylated cellulose is thoroughly rinsed with hexanol and ethanol and finally with water to remove the ungrafted extra H_3PO_4. A washing with deionised water and ethanol is then carried out for at least 24 h using a soxhlet extractor. The obtained gel is finally freeze-dried. After analyses, the degree of substitution is close to 3, making this method a versatile and interesting route to phosphorylate cellulose.

3. Phosphate salts

Phosphorylation of cellulose fibres with phosphate salts in a water/urea solvent mixture is one of the simplest processes to carry out [213]. The method involves mixing cellulose with phosphate salts and urea at room temperature for 30 min. The suspensions are then filtered, dried and cured at 150°C for 1 h in an oven. The fibres are then immersed in water, dispersed and washed several times with cold water and then with boiling water. It was shown that the reaction takes place mainly in the amorphous zones of cellulose but the degree of substitution is quite low (0.5). The phosphate salts that can be used to phosphorylate cellulose are monobasic ammonium phosphate ($NH_4H_2PO_4$), dibasic ammonium phosphate ((NH_4)$_2HPO_4$), monobasic lithium phosphate (LiH_2PO_4), monobasic sodium phosphate (NaH_2PO_4) or dibasic sodium phosphate (Na_2HPO_4). Urea is used to increase the swelling of fibres as well as to avoid the degradation of cellulose during the curing stage.

4. Phosphorus oxychlorides

Yu et al [214] synthetized a phosphorus-nitrogen lignin (PN lignin) using a method consisting firstly in grafting hydroxymethyl groups onto lignin to obtain hydroxymethylated lignin (lignin-OH). Lignin is firstly purified by dissolution in a basic aqueous solution, is then precipitated in an acid solution and washed. In a second step, imidazole and triethylamine are dissolved in dimethylformamide (DMF). The solution is heated and phosphorus oxychloride ($POCl_3$) is

added as well as the lignin-OH. At the end of the reaction, the solution is poured into methanol for precipitation. The resulting precipitate is washed 3 times with methanol and dried at 80°C. Analysis of the phosphorylated lignin shows high phosphorus and nitrogen contents, 8.1 wt.% and 7.2 wt.% respectively.

5. Phosphonamide

N-hydroxymethyl-3-dimethylphosphonopropionamide (HDPP) can be used for the phosphorylation of cellulosic materials. Following this approach, Gaan et al [215] studied the phosphorylation of cotton fibres by mixing them directly with HDPP in aqueous solution. The fibres are then dried at 80°C and stored at 21°C and 65 % relative humidity for 24 h. An increase in the final residue from 5.4% to 40.4% with only 2% of HDPP is observed at 500°C thanks to TGA analyses. It was shown that HDPP easily decomposes into acid intermediates oxidizing into phosphoric acid structures. It catalyses the dehydration of cellulose, and leads to the formation of a protective carbonaceous layer at the surface of the material, allowing to stop the combustion more rapidly.

6. Phosphonic acid

Hajj et al [216] propose a protocol for the phosphorylation of natural fibres with various phosphonic acids, particularly vinyl phosphonic acid (VPA). Fibres are mixed in a flask containing a 9:1 ethanol/water ratio and VPA or other biphosphonic acids (C6, C8 or C10). The mixture is heated under reflux for 2 h. At the end of the treatment, the solution is filtered. The fibres are washed three times for 1 min with ethanol to remove ungrafted molecules and then dried at room temperature. Analyses show that phosphorylation is less effective for VPA (0.1 % grafted phosphorus) than for other phosphonic acids (up to 1.4 % phosphorus grafted with C6 acids).

C. Selection of methods for cork phosphorylation

This review thus demonstrates that phosphorylation is a widespread method for the modification of natural biopolymers (in particular cellulose and lignin). It offers a wide range of processes and precursors that can be adapted to different needs. In the case of cork phosphorylation, the choice of precursors and processes was mainly based on the grafting efficiency, taking also into account the toxicity of compounds, the objective being to optimize the phosphorus content grafted onto cork.

Considering the toxicity of compounds, Table 28 gathers the properties and the hazards of phosphorus moieties mentioned before. The protocol mixing H_3PO_4, LiCl and urea was not selected because LiCl is a toxic compound [217]. The protocol with DMF and $POCl_3$ was also rejected for a similar reason (high toxicity of the phosphorus precursor [218]). The use of HDPP is also avoided because of the irritant character of phosphonamide and also because the protocol can hardly be industrialized due to the availability of compounds. Finally, the VPA-based protocol was discarded because the phosphorus grafting efficiency is too low. Therefore, three protocols were selected in a first investigation step. The first concerns the use of P_2O_5 and THF [209]. Despite the use of a carcinogenic, mutagenic and reprotoxic (CMR) solvent, MLC fire properties of phosphorylated lignin were significantly improved as well as the amount of carbonaceous residue, which is the purpose of this study. Moreover, if some efficiency is demonstrated, the protocol can be further improved, proposing an alternative solvent with less toxic properties. The method combining H_3PO_4, hexanol and P_2O_5 [212] is worth considering for the phosphorylation of cork because it allows a high degree of substitution to be achieved. Finally, the protocol using $H_2PO_4NH_4$ is also chosen because of its simplicity and speed of implementation without any toxic compound. These three protocols were therefore considered for the phosphorylation of cork in order to improve the fire behaviour. Preliminary experiments have been carried out and the most promising protocol has been selected for optimization and scale-up.

Table 28: Properties and hazards of considered phosphorus moieties

Phosphorus moieties	Properties	Hazards
H_3PO_4	Strong acid as aqueous solutions, colourless viscous liquid	Cause severe burns
$POCl_3$	colourless to light yellow liquid, strong smell. Reacts with water or air humidity: release of toxic and corrosive fumes. Soluble in many solvents.	Harmful by inhalation or ingestion, causes severe burns
P_2O_5	Anhydride of H_3PO_4: crystallised, colourless, highly deliquescent, very soluble in water and ethanol, extremely hygroscopic	Cause severe burns
$H_2PO_4NH_4$	White crystals or white powder, highly deliquescent, soluble in many solvents.	No hazard statement
HDPP	Colourless to light yellow liquid, formaldehyde smell	Cause allergic skin reaction, harmful by inhalation, CMR product

IV. Materials and Methods

A. Phosphorylation processes adapted to cork modification

The three protocols described hereafter are directly derived from literature and have sometimes been adapted for the modification of cork. The experimental conditions correspond to those initially defined for the first part of the study, in order to select the most promising protocol for the phosphorylation of cork. In a second step, the selected protocol will be further optimized (section V. B. Optimization of the phosphorylation protocol, page 100).

1. Tetrahydrofuran and phosphorus pentoxide protocol

On the basis of Prieur et al protocol [209], cork granules were dried at 90°C for at least 24 h in an oven. 12 g of cork and 130 mL of THF were introduced into a 125 mL round-bottom flask, and the mixture was stirred with a magnetic bar. After a few minutes of stirring at room temperature, 2 g of P_2O_5 were incorporated gradually. Then, the reaction took place for 8 hours under reflux with strong agitation to allow homogenisation. The mixture was left to cool overnight at room temperature and THF was then evaporated using a rotary evaporator. The modified cork was recovered and abundantly rinsed with deionized water, filtered under vacuum on a Büchner until the filtrate reaches a neutral pH. A last hot rinse was carried out using a soxhlet extractor for 4 h in order to remove the ungrafted excess P_2O_5. The phosphorylated cork is finally dried for 24 h in an oven at 90°C.

The cork phosphorylated with this method is further called "THF/P_2O_5 cork".

2. Phosphoric acid combined with phosphorus pentoxide protocol

Based on the article of Granja et al [212], the protocol has undergone some modifications to be adapted to the phosphorylation of cork. First of all, cork granules are dried at 90°C for at least 24 h in an oven. 12 g of cork are introduced into a round-bottom two-neck flask. Separately, 50 ml of ethanol (EtOH), as the reaction solvent, 50 ml of triethyl phosphate (Et_3PO_4), as a catalyst, and 50 ml of phosphoric acid (H_3PO_4), as the phosphorylating agent, are mixed under magnetic stirring. Once the mixture is homogeneous, 1.33 g of P_2O_5 is added, acting as a hygroscopic compound, absorbing the water released during the reaction of H_3PO_4 with the hydroxyl groups, to form again phosphoric acid, thus providing an additional source of phosphorus for the grafting reaction. When the mixture is perfectly homogeneous, it is poured onto cork. The mixture is then stirred at medium speed (1120 rpm) so that no vortex is created and each cork granule is carried away by the agitation, without being pressed against the walls of the flask.

The phosphorylation reaction is maintained for 72 hours under stirring at 35°C, controlling the temperature. At the end of the reaction, the mixture is filtered under vacuum on a Büchner and abundantly rinsed with ethanol and deionized water until the filtrate reaches a neutral pH. Cork is then thoroughly rinsed with hot deionized water for 24 h using a soxhlet extractor. Finally, the phosphorylated cork obtained is dried for 24 hours in an oven at 90°C.

The cork phosphorylated with this method is further called "H_3PO_4 cork".

3. Phosphate salts protocol

The protocol of Rol et al [213] was just slightly modified for the phosphorylation of cork. Firstly, cork granules are dried at 90°C for at least 24 h in an oven. 0.8 g of cork are placed in an Erlenmeyer flask with 0.31 g of urea and 0.14 g of monobasic phosphate salt ($H_2PO_4NH_4$). The mixture is placed under magnetic stirring for 1 h at room temperature. After reaction, cork granules are filtered and abundantly rinsed with deionized water under vacuum on a Büchner filter. Finally, the phosphorylated cork was dried for 24 h in an oven at 90°C.

The cork phosphorylated with this method is further called "P-salt cork".

B. Yield of reaction

The yield of reaction is one of the parameters used for the selection and optimization of the cork phosphorylation method. Thus, the yield of reaction (Y) corresponds to the quantity of P-Cork obtained compared to the quantity of initial cork. It is calculated with Equation 5 and it is expressed as a percentage:

Equation 5:
$$Y = \frac{Q_{P-cork}}{Q_{Cork}} \times 100$$

With Q_{P-cork} the amount of cork obtained after the phosphorylation process and Q_{Cork} the amount of initial cork, i.e 12 g in the present case.

C. Phosphorus content determination by Inductively Coupled Plasma

Inductively Coupled Plasma coupled with Atomic Emission Spectrometry (ICP-AES) is an analytical technique for measuring the content of an inorganic element in a sample. This technique is applicable to all types of elemental chemicals including phosphorus. Firstly, the solid sample, in powder form, is mineralised, i.e. put in solution using a mixture of strong acids. The preparation is then vaporised in argon plasma and placed at very high temperatures. These

thermal excitations lead to ionisation and separation of elements, allowing the detection and quantification of each element by measuring the wavelengths emitted by ions.

This characterization was carried out by an external company, CREALINS (member of Groupe 6NAPSE), on virgin cork powder and on phosphorylated cork powder (optimal formulation) before and after combustion (MLC testing). The phosphorus content is given as a percentage by weight (%.wt) and indicates the amount of phosphorus present in the sample.

D. Microscopy

1. Electron Probe Micro Analysis

Electron probe micro analysis (EPMA) is a non-destructive in-situ analysis device that allows a qualitative analysis of the elements present in a material and permits to obtain mappings of elements. The surface of the sample is exposed to an electron beam, emitting X-rays in return, themselves reflected on a crystal of variable orientation. The electron microprobe thus analyses the X-ray emission produced by the interaction between the incident electrons and the elements of the material.

Mapping of the chemical elements in the cross-section of cork materials was carried out. Before analysis, the samples were embedded into a slow-curing epoxy resin. After 48h at room temperature, the samples were polished (down to 0.25 µm) with silicon carbide discs (ESCIL, Chassieu, France), and then metallised with carbon with a Bal-Tec SCD005 sputtering machine (Bal-Tec, Los Angeles, California, USA). Cross-sectional backscattered electron (BSE) images and X-ray mappings were performed at 15 KV, 40 nA using an EPMA Camera SX100 (Cameca, Gennevilliers, France).

2. Scanning electron microscopy

Scanning electron microscope (SEM) observations were carried out with a JEOL JSM 7800F LV (JEOL ltd, Tokyo, Japan), in order to observe the surface of cork materials. The aim was to analyse the cork surface and the shape or size of its cavities. Samples were prepared following the same procedure as the one used for EPMA.

V. Results and discussions

A. Choice of the phosphorylation protocol: preliminary characterizations

Three phosphorylation protocols were selected leading to the production of three different phosphorylated corks (P-corks) namely "THF/P_2O_5 cork", "H_3PO_4 cork" and "P-salt cork". The aim of this section is to identify the most promising and relevant protocol for the phosphorylation of cork granules. The quality of grafting (through EPMA), the presence of signals characteristic of phosphorus compounds (thanks to infrared spectroscopy) and the improvement in thermal stability (characterized by TGA) are the three criteria that will be considered for the selection of the phosphorylation protocol.

1. Characterization of P-corks

1.a. Mapping of the ^{31}P phosphorus element by EPMA

Mappings of the ^{31}P phosphorus element were performed using EPMA to assess the distribution of phosphorus in virgin and P-cork samples (Figure 24). At the right side of images, a colour scale from 0 (black) to 23 (red) is used to highlight the intensity of the phosphorus element: the closer from the red colour, the stronger the presence of the phosphorus element. To allow qualitative comparisons, the scale is the same for the three protocols and for the virgin cork.
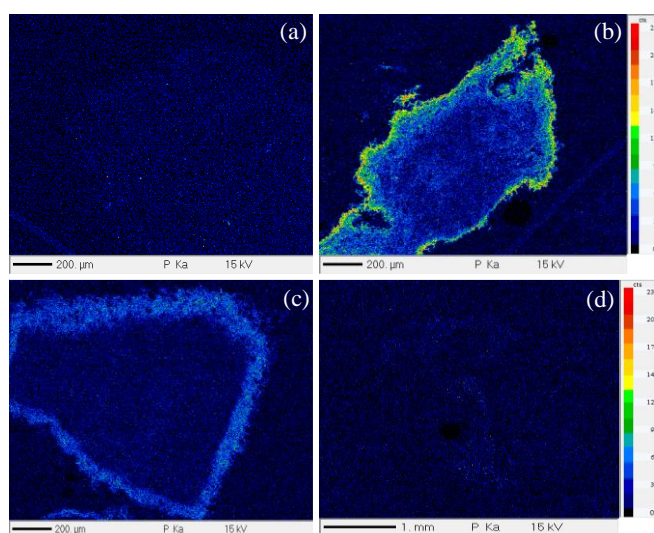
Figure 24: EPMA mapping of (a) virgin cork, (b) THF/P_2O_5 cork, (c) H_3PO_4 cork and (d) P-salt cork

The mapping obtained for the virgin cork (Figure 24 (a)) is almost completely black, confirming that the amount of phosphorus in virgin cork is very low. A similar signal is observed for P-salt cork (Figure 24 (d)), showing that the grafting with this method is not efficient. Then, looking

at THF/P_2O_5 cork and H_3PO_4 cork, the mappings (Figure 24 (b) and Figure 24 (c)) show that phosphorus is present in thin layers on the cork granules as well as partially inside the granule (signal of lower intensity). The grafting seems to be homogeneous. A rather high amount of phosphorus is observed for the phosphorylation reaction that used THF and P_2O_5.

The next step is to determine the nature of the phosphorus elements highlighted by the EPMA.

1.b. Infrared spectroscopy analysis

Infrared spectroscopy (IR) analysis was carried out for two purposes: (1) to identify the signals corresponding to cork and its components and, (2) to identify the signals due to the phosphorylation reaction and the nature of phosphorus bonds.
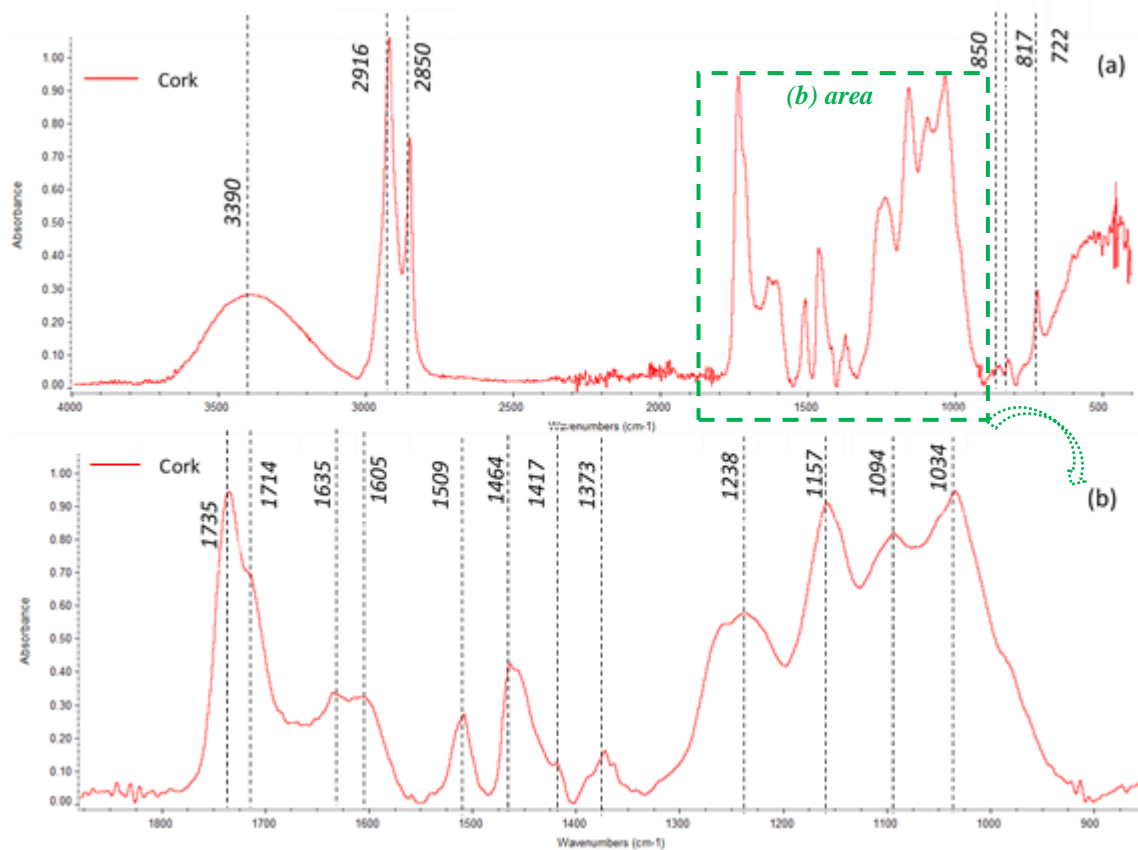
Figure 25: Cork FTIR spectrum of virgin cork (a) 4000 – 500 cm^{-1} (entire spectrum) and (b) focus on the 1800 – 900 cm^{-1} range

First, the virgin cork sample was characterized. Some databases give the different wavenumbers corresponding to cork FTIR signals and their assignment [219]–[221]. However, due to the complex structure of cork, some signals are difficult to identify accurately, especially because of the risk of overlapping. Figure 25 shows FTIR ATR spectrum of cork and results are in

94

agreement with literature data. The assignment of the main bands is summarised in Table 29. Cork exhibits numerous signals mainly attributable to suberin and lignin as well as a broad band centred around 3390 cm^{-1} corresponding to hydroxyl groups of suberin, lignin, polysaccharides (including cellulose and hemicellulose) and water [222]. Being a natural material, the amount of lignin in natural cork can vary from 19 % to 24 % and the amount of suberin can vary from 30 % to 50 %. It can have an influence on the proportion of the signals.

Table 29: Assignment of the infrared peaks observed in the spectrum of cork (consistent with [219])

Wavenumber $\tilde{\nu}$ (cm^{-1})	Assignment	Cork components
3350	ν O-H	Suberin, lignin, polysaccharides and adsorbed water
2924	ν_{as} CH2	Suberin alkyl chains
2853	ν_{as} CH2	Suberin alkyl chains
1739	ν C=O	Suberin ester groups
1714	ν C=O	Lignin
1635	ν C=C	Suberin aliphatic groups
1606	ν C=C	Suberin and lignin aliphatic groups
1509	ν C-C	Lignin aromatic rings (fingerprint)
1457	δs CH2	Suberin aliphatic groups (fingerprint)
1420	δs (O) CH3	Lignin
1364	δs CH3	Suberin (fingerprint)
1236	ν CO	Suberin (fingerprint)
1161	ν_{as} COC	Suberin (fingerprint)
1094	δ CH	Polysaccharides
1039	δ CO	Polysaccharides
852	τ CH (oop)	Suberin
818	ρ CH3	Suberin/lignin
723	τ CH (oop)	Suberin

Figure 26 compares the FTIR spectra of virgin cork and P-corks. All the spectra were normalized with respect to the aliphatic carbon band (ν_{as} CH2, at 2850 cm^{-1}) to allow the observation of changes in the relative intensities of peaks and to highlight the potential variation of chemical components' proportion in cork after the phosphorylation reaction. Other differences in signals intensity are also observed and should be due to the natural variability of cork. However, the most important differences, shown in Figure 26 (b), are attributed to the phosphorylation reaction. Table 30 reports the assignments of the peaks observed for P-corks.

The broad band, centred around 3400 cm^{-1} (ν O-H, suberin, lignin and adsorbed water), is more intense for P-corks. This result was not expected since phosphorylation should occur on the –OH bands of virgin cork. It can be assumed that during the phosphorylation reaction, extractives and polysaccharides can be degraded and extracted from the material leading to a significant decrease of –OH groups.
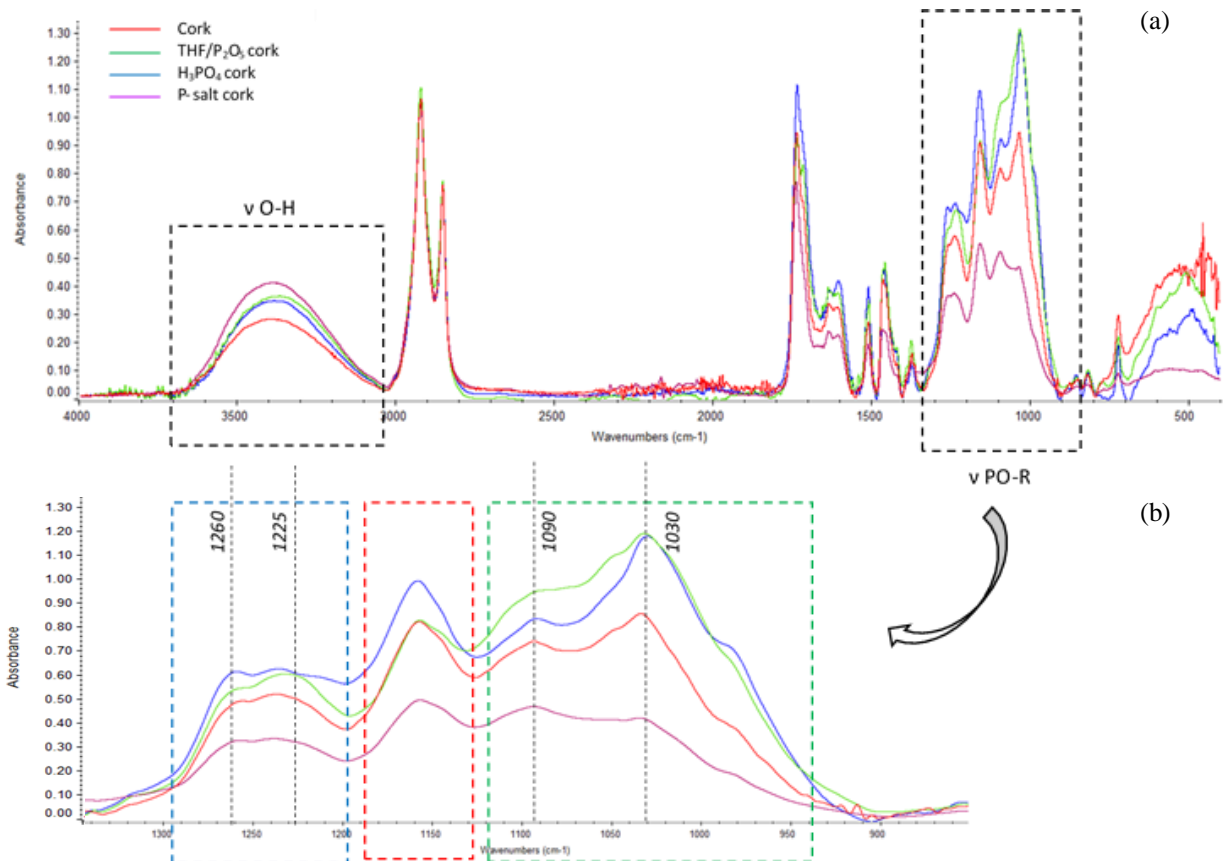
Figure 26: (a) FTIR spectra of virgin cork and P-corks and (b) focus on the grafting area corresponding to phosphorus moities

In the 900 to 1300 cm^{-1} range (Figure 26 (b)), the increase in intensity for some peaks can be attributed to the phosphorylation reaction (Table 30) and more precisely to the presence of phosphorus bonds, confirming EPMA results. In the 950 to 1120 cm^{-1} range (green frame), two bands (centred around 1030 cm^{-1} and 1090 cm^{-1}) can be related to the presence of PO-R bonds of phosphate groups, corresponding to $\nu_{as}PO_4$ et $\nu_s PO_3$ respectively. It has to be mentioned that virgin cork spectrum exhibits peaks at 1039 cm^{-1} and 1094 cm^{-1} (Table 29) overlapping those bands. However, since peaks intensity of P-corks is higher (except for P-salt cork), it could be reasonably concluded that PO-R bonds are formed. The broad band between 1130 cm^{-1} and 1200 cm^{-1} (red frame) can also be attributed to phosphate bonds, corresponding to the

elongation of the PO-C bond in the presence of phosphate (PO_4). As previously discussed, virgin cork presents a peak at 1160 cm^{-1} assigned to suberin but the higher intensity of the peak of H$_3$PO$_4$ cork could support the phosphorylation reaction. Finally, in the blue frame, the two bands correspond to two types of bonds: aromatic ethers, that could be formed during the phosphorylation reaction (ν CO, 1220-1260 cm^{-1}) and phosphonate bonds (ν PO-R, 1230-1260 cm^{-1}).

Table 30: Band assignment related to phosphorylation reaction

Wavenumber $\tilde{\nu}$ (cm^{-1})	Assignment	Phosphorus bonds
1220-1260	ν CO	Aromatic ethers (formed during phosphorylation reaction)
1230-1260	ν PO-R	Presence of phosphonate (ν $P(O)(OR)_3$)
1100-1200	ν PO-R	Elongation of the PO-C bond in the presence of phosphate (PO_4)
1030-1090	ν PO-R	PO-R bonds of phosphate groups ($\nu_{as}PO_4$ et $\nu_s PO_3$ respectively)

If the three P-Corks are compared, two main behaviours can be observed: one for both THF/P$_2$O$_5$ cork and H$_3$PO$_4$ cork and, the second one for P-salt cork. In the first case, the peak intensities at 1030 cm^{-1}, 1090 cm^{-1}, 1225 cm^{-1} and 1260 cm^{-1} increase significantly whereas for the band centred around 1150 cm^{-1} (red frame), the two P-corks behave differently: the intensity of the peak is equivalent for virgin cork and THF/P$_2$O$_5$ cork, while it is much higher for H$_3$PO$_4$ cork. In the second case, for P-salt cork, the different bands between 900 and 1300 cm^{-1} are much less intense than those of the other two P-corks but also less intense than those of virgin cork. Thus, the treatment applied to P-salt cork seems to modify the structural composition of cork and in that case, phosphorylation could not be confirmed.

1.c. Thermal stability

Finally, thermogravimetric analyses (TGA) were carried out to compare the thermal stability of P-corks with that of virgin cork as a function of temperature as well as the charring ability. TGA curves and DTG curves are shown in Figure 27 (a) and Figure 27 (b) respectively, for virgin and modified corks. The corresponding data are given in Table 31.

Firstly, the onset of thermal decomposition of cork (that is to say the temperature corresponding to 2 % of mass loss (T$_{2\%}$)) occurs at 220 °C and the temperature of maximum degradation is about 430 °C (Figure 27). The residual solid mass fraction is around 18.5 % for virgin cork at the final temperature of degradation (800°C). These data are consistent with those reported in the literature [223], [224]. It has to be noted that cork being a complex and natural material

composed of several biopolymers, its degradation rate depends on its composition and thus on the proportion of the different components that can vary from one cork to another. The thermal degradation of cork components is reported in the literature. Pyrolysis of hemicelluloses and cellulose occurs over short temperature ranges of 220-315°C and 315-400°C respectively [225]. Suberin is known to be a temperature resistant component and degrades over a longer temperature range of 230-490°C [226]. Finally, lignins are even more resistant to thermal degradation and degrade progressively over a wide temperature range from 160 to 900°C [225]. As lignin is a charring material [209], it leads to a final residue (ash) significantly higher than that of cellulose, hemicellulose or suberin.
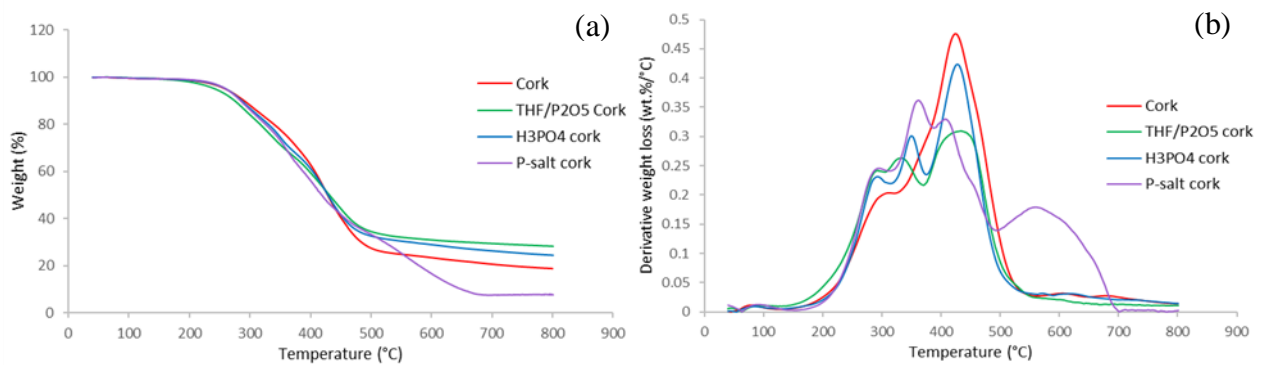
Figure 27: (a) TGA curves and (b) DTG curves for virgin cork and the three phosphorylated corks

Table 31: Thermogravimetric data for the virgin cork and the three phosphorylated corks

	$T_{2\%}$ (°C)	T_{MAX} (°C)	Residue at 600°C (%)	Residue at 800°C (%)
Cork	220	429	23.2	18.5
THF/P$_2$O$_5$ cork	200	421	31	28.3
H$_3$PO$_4$ cork	225	422	29	24.5
P-salt cork	229	368	16.8	7.8

Thermal decomposition begins at approximately the same temperature for H_3PO_4 cork and P-salt cork (225°C and 229°C respectively) as for virgin cork. On the contrary, the onset of degradation occurs at lower temperature for THF/P_2O_5 cork. Once the degradation has started, THF/P_2O_5 cork and H_3PO_4 cork exhibit similar behaviour with 3 steps of degradation occurring at the same temperature ranges and with similar T_{MAX} (421 °C and 422 °C respectively, slightly lower than the value observed for virgin cork). Phosphorylation usually results in a slight decrease in thermal stability since it usually catalyses the dehydration reaction [158], [227]. This trend is also observed for the two P-corks up to around 350°C. Then, from 350 °C, the mass loss of THF/P_2O_5 cork and H_3PO_4 cork is lower than that of virgin cork, leading to an increase in stability at high temperature. This result is confirmed by the significant increase in

the residual mass at 800°C: from 18.5 % for virgin cork to 28.3 % and 24.5 % for THF/P_2O_5 cork and H_3PO_4 cork respectively. If P-salt cork is considered, the maximum temperature of degradation is much lower ($T_{MAX} = 368$°C) compared to the other three corks. Moreover, the weight loss is almost always higher than for virgin cork over the whole temperature range, except between 380 and 500°C. P-salt is also the unique material exhibiting four steps of degradation compared to three steps of degradation for the other three corks (Figure 27 (b)). This additional step of degradation between 500 and 700 °C leads to a significant decrease in thermal stability at high temperatures, giving a very low amount of final residue at 800°C (7.8%), much lower than that of virgin cork (18.5%). A loss of thermal stability compared to virgin cork is therefore highlighted, showing that the phosphorus has not been grafted onto P-salt cork. This result is in good agreement with EPMA and FTIR data. It is assumed that the high residue obtained for virgin cork is attributed to the presence of aromatic structures, mainly found in lignin and suberin, condensing with increasing temperature and giving fairly stable structures. Since the difference is mainly observed at high temperature, it could be suspected that the reaction conditions carried out on P-salt mainly affect the aromatic structures of the cork (degradation or solubilisation of such part of cork) leading to a structure less stable at high temperatures and degrading more easily (hence the lower final residue). However, further experiments are required to confirm this hypothesis.

2. Discussion and conclusion

Considering the three characterization methods (EPMA, FTIR and TGA), the results obtained for P-salt cork are completely different from those of the other two P-corks. Firstly, the phosphorus element is almost not visible on the EPMA mapping, showing that the amount of phosphorus is really small, comparable to that of virgin cork. Then, the IR analysis showed a significant decrease in the intensity of the characteristic cork peaks: the signals at 1030 cm^{-1}, 1090 cm^{-1} corresponding to the -CH and -CO of the polysaccharides respectively; the area from 1220 to 1260 cm^{-1} corresponding to the CO bonds of suberin (Table 29). It can thus be concluded that the phosphorylation protocol used to obtain P-salt cork leads to the modification of cork composition in particular in the aromatics structures (lignin and suberin content) as suggested by TGA data. It could be assumed that urea, used in this protocol to limit the degradation of the material during the reaction, does not provide sufficient protection to prevent the degradation of cork. The characterizations performed on the P-salt cork did not allow evidencing the phosphorus grafting and even showed a decrease in the thermal stability of cork.

Thus, the protocol using phosphate salts in a water/urea mixture solvent will not be further considered in this study.

The other two P-corks, THF/P_2O_5 cork and H_3PO_4 cork, show similar behaviour. First, EPMA phosphorus mapping of both P-Corks reveals the presence of phosphorus mainly located at the surface of granules in a thin and relatively homogeneous layer. Phosphorus is also observed in the bulk of granules but in lower amounts. Infrared spectroscopy confirmed the presence of phosphorus since an increase in intensity of bands corresponding to phosphorus bonds, mainly in the form of PO-R in phosphates, is observed. Thus, it is confirmed that phosphorus moieties are grafted and the phosphorylation reaction actually happened. Finally, the thermal stability of P-cork was investigated using TGA and improved thermal stability and higher charring capacity of THF/P_2O_5 cork and H_3PO_4 cork are confirmed through a significant increase in residual mass at 800°C: increase of + 34 % and + 21 % respectively compared to virgin cork. It can be assumed that the presence of phosphorus increases the formation of char through interactions occurring in the condensed phase but this assumption has to be confirmed by additional characterizations.

Those results demonstrate that the protocols used to obtain both THF/P_2O_5 cork and H_3PO_4 cork are suitable for the phosphorylation of cork, leading to close results in terms of grafting and thermal stability. However, in the GRASS project, the use of solvents or additives harmful for people and for the environment should be avoided. As THF is a CMR solvent, requiring a lot of precautions for handling, the phosphorylation protocol used to obtain H_3PO_4 cork is selected for further investigations, even if this method is more time consuming. The following section aims to further optimize the selected phosphorylation protocol and the modified cork will be simply called "P-cork".

B. Optimization of the phosphorylation protocol

The experimental phosphorylation protocol is based on that of Granja et al [212] and consists in carrying out the reaction with EtOH, Et_3PO_4, H_3PO_4 and P_2O_5. The aim of this section is to optimize the protocol by determining the experimental conditions allowing to obtain the highest amount of grafted phosphorus and the highest amount of residue at 600°C.

1. Design of experiments: theoretical part

To optimize the phosphorylation reaction, a similar approach (i.e the advantageous use of experimental design methodology) as the one used to optimize the settings of the small-scale radiant panel test was followed. Six experimental parameters have been varied: (1) P_2O_5 mass;

(2) H_3PO_4 volume; (3) Et_3PO_4 volume, (4) EtOH volume; (5) reaction time; and (6) reaction temperature. The amount of cork is set at 12 g as it allows an optimal filling of the reaction flask.

A Plackett-Burman experimental design consisting of 8 experiments was implemented. Experiments were conducted randomly to provide protection against the extraneous factors, able to affect the measured response. Adapted from literature data, the experimental values associated to the coded levels of the different variables are given in Table 32.

Table 32: Coded and real values of experimental parameters used in the design of experiments

Coded variables	Parameters	Levels	
		-1	**+1**
X_1	U_1: P_2O_5 mass (g)	1.3	3
X_2	U_2: H_3PO_4 volume (mL)	40	60
X_3	U_3: Et_3PO_4 volume (mL)	40	60
X_4	U_4: EtOH volume (mL)	40	60
X_5	U_5 : Time reaction (h)	24	72
X_6	U_6: Temperature (°C)	25	45

Experimental conditions (U_i) associated to the coded values (X_i) applied for the 8 experiments are shown in Table 33.

Table 33: Experimental conditions (Ui) associated to the coded values (Xi) applied for the 8 experiments

Exp	X1	X2	X3	X4	X5	X6	U1 (g)	U2 (mL)	U3 (mL)	U4 (mL)	U5 (h)	U6 (°C)
P-cork 1	1	1	-1	-1	1	-1	3	60	40	40	72	25
P-cork 2	-1	1	-1	1	-1	1	1.3	60	40	60	24	45
P-cork 3	-1	1	1	1	1	-1	1.3	60	60	60	72	25
P-cork 4	1	-1	1	1	-1	-1	3	40	60	60	24	25
P-cork 5	1	1	1	-1	-1	1	3	60	60	40	24	45
P-cork 6	1	-1	-1	1	1	1	3	40	40	60	72	45
P-cork 7	-1	-1	1	-1	1	1	1.3	40	60	40	72	45
P-cork 8	-1	-1	-1	-1	-1	-1	1.3	40	40	40	24	25

For each experiment, P-cork was characterized. The aim is to enhance the thermal stability of cork and in particular to improve the charring. The choice of optimal conditions will thus be made considering two main criteria: the quantity of residue obtained after heat treatment at 600°C in a furnace and the reaction yield. The intensity of characteristic bands of phosphorus moieties measured by infrared spectroscopy and the amount of phosphorus, thanks to EPMA, were also determined although only qualitative results are obtained.

2. Characterization of P-corks

2.a. Carbonization rates at 600°C

The charring ability was evaluated by heating the P-corks from room temperature to 600°C in a furnace (HTT= 600°C) and then determining the amount of final residue. The final carbonization rates obtained for the eight P-corks compared to virgin cork are given in Table 34.

Table 34: Carbonization rates obtained after HTT=600°C and reaction yields of the 8 P-corks

	Virgin cork	P-cork 1	P-cork 2	P-cork 3	P-cork 4	P-cork 5	P-cork 6	P-cork 7	P-cork 8
Carbonaceous residue at 600°C (%)	1.0 ± 0.4	3.7 ± 0.5	6.1 ± 0.5	6.0 ± 0.7	3.8 ± 0.6	6.2 ± 1.5	11.7 ± 1.9	1.3 ± 0.7	1.5 ± 0.8
Yield of the reaction (%)*	/	90	89	91	92	86	85	86	92

*No standard deviation values as only one formulation was produced per protocol

The experimental conditions used for P-cork 6 allow increasing the carbonization rate up to 12 % of the initial cork mass, compared to 1 % of residual mass (ash) for virgin cork. Quite high and intermediate carbonization rates of around 6 % are obtained for P-cork 2, P-cork 3 and P-cork 5. Then, rates slightly lower than 4% are observed for P-cork 1 and P-cork 4, while P-cork 7 and P-cork 8 have carbonization rates barely better than that of virgin cork. Thus, a significant variability in the carbonization rate is observed according to the phosphorylation conditions.

2.b. Yield of reaction

The reaction yields for the different P-corks are given in Table 34. The highest yields (between 89 and 92%) are obtained for P-cork 1, P-cork 2, P-cork 3, P-cork 4 and P-cork 8. The remaining P-corks (i.e. P-cork 5, P-cork 6 and P-cork 7) exhibit the lowest yields (around 85 %).

2.c. Mapping of the phosphorus element by EPMA

The mappings of the phosphorus element for the eight P-corks are shown in Figure 28. Since cork is a natural material, the grafting may be different from one granule to another. Several P-cork granules from the same experiment were mapped to provide a representative image of the whole sample.

P-cork 4, P-cork 5 and P-cork 8 seem to be very little modified, as a low signal can be seen at the surface of cork granules. P-cork 1, P-cork 2, P-cork 3 and P-cork 7 show thin and uniform modification around the granules and partially inside. The highest phosphorus content is

observed for P-cork 6 as a thick and uniform phosphorus signal is observed around granules as well as in the centre. A small granule also appears almost entirely red, corresponding to a very high amount of phosphorus. Several analyses were carried out to confirm that this result is representative of the whole modified material. Therefore, EPMA mappings suggest that experimental conditions corresponding to experiment 6 are the most adapted to obtain an efficient grafting but it has to be confirmed by infrared spectroscopy analyses.
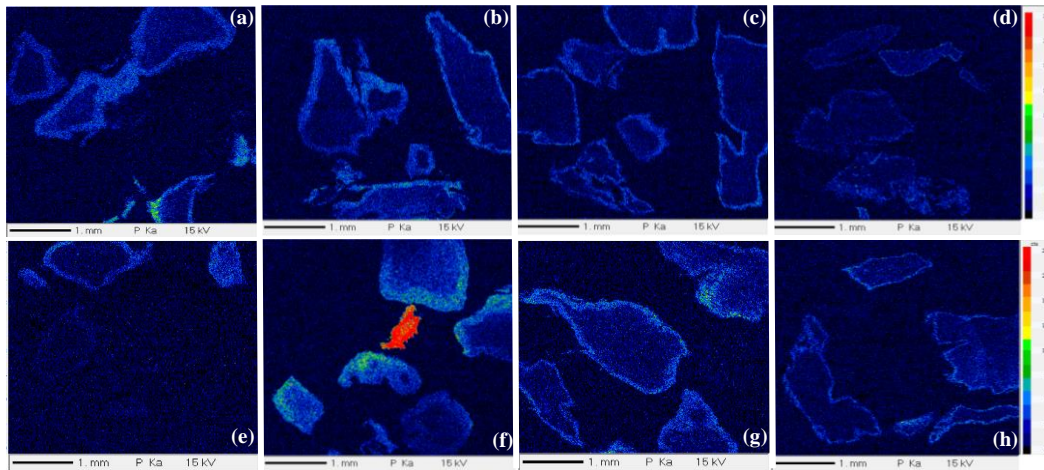
Figure 28: EPMA mapping of (a) P-cork 1, (b) P-cork 2, (c) P-cork 3, (d) P-cork 4, (e) P-cork 5, (f) P-cork 6, (g) P-cork 7 and (h) P-cork 8

2.d.   Infrared spectroscopy

As phosphorylation conditions influence the phosphorus content, infrared spectroscopy was performed on the eight P-corks and results are given in Figure 29. Table 30 **(page 97)** previously presented the main bands related to phosphorus bonds.
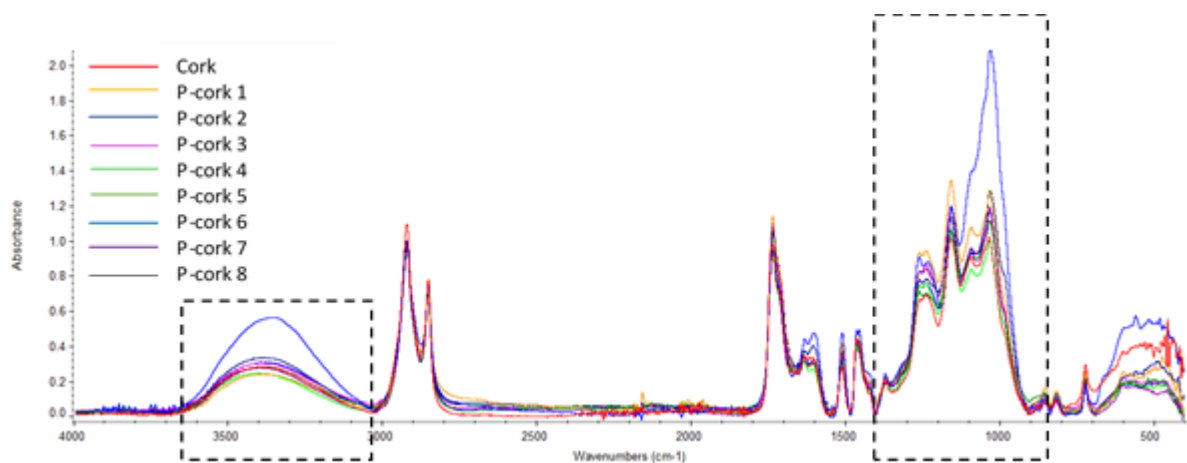
Figure 29: FTIR spectra of virgin cork and P-corks obtained for the 8 experiments of the design of experiments

As mentioned previously, the spectra in Figure 29 are normalized with respect to the strongest aliphatic carbon band (ν_{as} CH$_2$, at 2850 cm^{-1}). Two ranges of wavenumbers have to be considered to validate the efficiency of the phosphorylation protocol: the 3600-3000 cm^{-1} range corresponding to hydroxyl groups and the 1400-900 cm^{-1} range for the phosphorus-based structures. For the latter range, the difficulty in the analysis of the peaks is that, as previously shown, the experimental conditions of the phosphorylation reaction can modify the cork structure and the corresponding signals are in the same wavenumbers range as those of the phosphorus bonds. Infrared data have thus to be considered in conjunction with the other characterization results.

Among the eight P-corks, P-cork 2 (dark blue curve) exhibits a significantly stronger signal for the large band centred around 3400 cm^{-1} (ν OH, suberin, lignin and adsorbed water) and for the bands characteristic of the presence of PO-R bonds of phosphate groups at 1030 cm^{-1} and 1090 cm^{-1}. Moreover, the bands corresponding to the presence of phosphonates bonds (ν PO-R, 1230-1260 cm^{-1}) and of phosphate groups (between 1100 and 1200 cm^{-1}) have higher intensity than bands of virgin cork (red curve), confirming phosphorous grafting. Although P-cork 1 seems slightly more grafted (bands at 1150 and 1230 cm^{-1} on the yellow curve) and P-cork 4 slightly less (band at 1090 cm^{-1} on the light green curve), the spectra of the other P-corks are all relatively close to each other in terms of intensity and therefore, phosphorus grafting seems comparable.

3. Discussion and first screening of experimental conditions

As the reaction yields are rather comparable for the 8 P-corks (from 85 to 92%), this criterion can hardly be used to determine the optimal experimental conditions. Furthermore, the data obtained from IR spectroscopy analyses are not, or hardly, quantitative and the phosphorus content determined using EPMA is a qualitative information. Thus, the carbonization rate was mainly considered to determine the experimental conditions of the phosphorylation process. Results obtained with the other characterization techniques will support the argumentation to validate the selected experimental conditions. Finally, information about the cork behaviour during phosphorylation and about the visual aspect of the material after phosphorylation will be provided to refine the conclusions.

Firstly, it appears that the two P-corks with the highest yield, i.e. P-cork 4 and P-cork 8 (92 %), are also those presenting a low carbonization rate (3 % and 1 % respectively), as well as low phosphorus content as observed by EPMA, in particular for P-cork 4. Thus, the conditions used to synthetize these two corks will not be further considered. The P-cork giving the lowest yield

(P-cork 6) shows the highest carbonization rate (12 %) and potentially the highest phosphorus content. After the reaction, the surface aspect of cork is degraded and the granule size is reduced. During the rinsing step, the filtrate recovered (liquid part) was particularly thick and full of cork dust. The same phenomenon occurred when P-cork 7 was rinsed. For both P-corks, a synthesis time of 72 h and a temperature of 45 °C were used. It is assumed that the combination of these two conditions is too severe and leads to the degradation of cork. Finally, P-cork 2, P-cork 3 and P-cork 5 show an interesting carbonization rate (around 6 %). However, P-cork 5 exhibits a low EPMA signal. Thus, experimental conditions used for P-cork 2 and P-cork 3 allow obtaining the best compromise: intermediate carbonization rate (around 6 %), good grafting (EPMA) and similar reaction yields (around 90%). But P-cork 2 shows a particularly intense IR signal in the grafting zone of phosphorus compounds. Moreover, the reaction time to obtain P-Cork 2 is 24 h compared to 72 h for P-Cork 3, leading to significant time savings. It can be concluded that experiment 2 leads to the best compromise: a fairly high carbonization rate (6 %) and intermediate phosphorus content and yield. Thus, after the first optimization step, the selected phosphorylation conditions correspond to experiment 2 of the experimental design (Table 33) and are as follows: $m_{cork\ granules} = 12$ g, $V_{EtOH} = V_{H_3PO_4} = 60$ mL, $V_{Et_3PO_4} = 40$ mL and $m_{P_2O_5} = 1.3$ g. The mixture was kept at 45 °C for 24 h.

A much higher carbonization rate was obtained for P-cork 6 compared to P-cork 2 (11.7% vs. 6.1% respectively). Even if the experimental conditions corresponding to experiment 6 were not selected because of the strong degradation of cork, this result could suggest that a carbonization rate higher than 6% can be achieved.

Thus, additional experiments were carried out varying P_2O_5 mass and Et_3PO_4 volume. Characterizations performed on these P-corks gave a carbonization rate around 3%, confirming that experimental conditions used for the production of 'P-cork 2' correspond to the optimized phosphorylation conditions. Moreover, this additional study allowed confirming the repeatability of P-cork 2 synthesis, validating the proposed protocol.

C. Upscaling of the phosphorylation system

The experimental conditions of the phosphorylation protocol have been optimized and allow the grafting of 12 g of cork. The final aim is to determine if artificial turf structures containing the phosphorylated cork can be used for indoor applications, reaching a C_{FL} rating at the radiant panel test. Even if a small-scale radiant panel test has been developed, a full characterization of the FR properties of turf structures still requires large amounts of cork, approximately 250 g for

a 15 mm cork layer thickness and considering three replicates for MLC and radiant panel tests. Thus, upscaling of the phosphorylation protocol to produce larger amounts of P-cork is necessary. To determine the experimental conditions to be used at larger scale, dimensional analysis (DA) was implemented. The two main criteria considered for the application of the DA approach are the reaction yield and the carbonization rate as they give quantitative results and as they are the most relevant for the intended application.

1. Dimensional analysis modelling

Dimensional analysis (DA) consists of listing and gathering the input and output variables of a system, in order to reveal the factors that have the greatest impact on the studied system. DA provides a synthetic representation of the system data to determine the optimal operating points or correlations that can be used for upscaling [228]. In DA, the input variables are defined as dimensionless numbers and they are kept constant from one scale to another. Modelling by DA thus means establishing correlations, called process relationships, involving dimensionless numbers, also called pi numbers or internal measurements. These dimensionless numbers describe the cause-and-effect relationships between the operating conditions, i.e. the physical input and output variables of the system under study (the flask for the phosphorylation reaction). The transformation of physical variables into dimensionless numbers is associated with a reduction in the number of measurements describing the evolution of the system.

From these dimensionless numbers, an extrapolation of the system is possible. Extrapolation is based on the principle of similarity whereby the ratios of one or more parameters, geometric or operational, are the same at both scales. Five similarities can be considered [229], [230]:

- – Geometric similarity, related to the ratios of geometric dimensions.
- – Dynamic similarity, related to the ratios of forces.
- – Kinematic similarity, related to the ratios of speeds at corresponding points.
- – Chemical similarity, related to concentrations.
- – Thermal similarity, related to temperatures.

DA modelling is generally divided into 12 main steps:

- a. Listing the independent physical variables.
- b. Writing the dimensional matrix.
- c. Selecting the repeated physical variables (basis) in the dimensional matrix.
- d. Identifying the residual matrix and the central matrix.

e. Linearizing the central matrix and obtaining the modified residual matrix.

f. Determining the dimensionless numbers from the modified residual matrix.

g. Rearranging the dimensionless numbers.

h. Identifying the system configuration, the process relationship and the monomial form.

i. Designing the experimental programme, identifying the operating points.

j. Analysing the process relationship.

k. Using the process relationship (reverse engineering process).

l. Analysing the operating points leading to extrapolation.

In the present case, as steps 8 to 12 require the development of a substantial and time-consuming experimental work programme, only the first 7 steps were fully carried out.

1.a. Listing the independent physical variables

The system used for cork phosphorylation reaction consists of a stirred tank reactor (reaction medium stirred by magnetic agitation). The power number P, or Newton number, is generally considered to be the target variable in such a system since it is a dimensionless number used in fluid mechanics and process engineering to characterize the conditions of a mechanical mixture for a liquid.
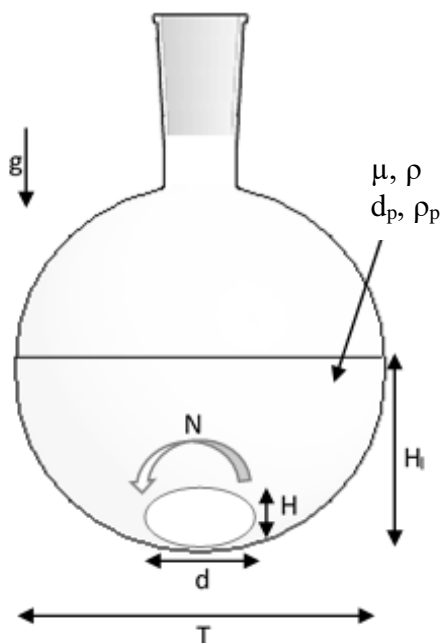
Boundary conditions:

- d: length of the magnetic stirrer (mm)
- T: diameter of the flask (mm)
- H: height of the magnetic stirrer (mm)
- H_l: height of liquid in the flask (mm)
- g: gravity (m/s²)

Materials characteristics:

- µ: viscosity (Newtonian) (Pa s)
- ρ: density of the liquid (g/cm^3)
- d_p: diameter of cork particles (mm)
- ρ_p: density of cork particles (g/cm^3)

Process parameter:

- N: rotation speed of the magnetic stirrer (rpm)

Figure 30: Studied system and associated physical variables

The physical variables that can influence the power number can be the characteristics of materials, the process parameters (influencing the distribution of cork particles in the medium) and the boundary conditions (defining the flow domain). Figure 30 shows the studied system with the associated independent physical variables impacting the power number.

1.b. Writing the dimensional matrix

From the list of the physical variables (Figure 30), it is possible to write the corresponding dimensional matrix [D], establishing the dimensions of the variables according to the fundamental units of the International System (SI). The dimensional matrix [D] is given in Table 35. The first column (in green) represents the fundamental units adequate to describe the system, i.e mass (M), length (L) and time (T). The second column (in blue) is dedicated to the target variable under consideration, here the power number (P). It is expressed using the three fundamental units [M. L^2. T^{-3}]. Finally, the other columns of the matrix represent each independent physical variable of the system with the corresponding fundamental units.

Table 35: Dimensional matrix [D]

	P	μ	ρ	ρ_p	N	d	d_p	H	H_l	T	g
M	1	1	1	1	0	0	0	0	0	0	0
L	2	-1	-3	-3	0	1	1	1	1	1	1
T	-3	-1	0	0	-1	0	0	0	0	0	-2

1.c. Selecting the repeated physical variables (basis) in the dimensional matrix

The dimensionless numbers characterising the process are determined from the dimensional matrix [D]. Among the physical variables of the matrix, three of them are selected to represent a set of repeated physical variables constituting "the basis".

Here, the variables ρ, N and d were chosen as repeated variables because:

- d (length of the magnetic stirrer) can influence the mixing of particles.
- ρ (density of the medium) can influence the grafting quality.
- N (stirrer rotation speed) can influence particle mixing and grafting quality.
- These three variables are dimensionally independent.

1.d. Identifying the residual matrix and the central matrix

The repeated variables constituting the basis are then placed in the last 3 columns of the dimensional matrix [D] (in orange) and constitute the central matrix [C]. The remaining physical variables are called non-repeated physical variables and represent the residual matrix [R]. Table *36* shows the [C] and [R] matrices within the [D] matrix.

Table 36: Central matrix [C] and residual matrix [R]

	P	μ	ρ_p	d_p	H	H_l	T	g	ρ	N	d
M	1	1	1	0	0	0	0	0	1	0	0
L	2	-1	-3	1	1	1	1	1	-3	0	1
T	-3	-1	0	0	0	0	0	-2	0	-1	0

Residual matrix   Central matrix

1.e. Linearizing the central matrix and obtaining the modified residual matrix

To make the dimensionless numbers appear, the fundamental units of the dimensional matrix [D] must be changed. The central matrix [C] must be transformed into the identity matrix [I] whose diagonal contains only coefficients equal to 1, the remaining coefficients being equal to zero. Thus, the transformation of the central matrix into the identity matrix allows the change of basis, from the (M, L, T) basis to the (ρ, N, d) basis.

During this transformation, the residual matrix [R] is modified and becomes the linearized residual matrix [R_m] (in pink in Table 37). The [R_m] matrix is obtained according to Equation 6:

Equation 6: $$[R_m] = [C]^{-1} \times [R]$$

With [C]$^{-1}$ the inverse matrix of [C]. This operation is equivalent to the application of the Gauss pivot method so that the central matrix [C] becomes the identity matrix [I] (in orange in Table 37).

Table 37: Identity matrix [I] and linearized residual matrix [Rm] within the dimensional matrix [D]

	P	μ	ρ_p	d_p	H	H_l	T	g	ρ	N	d
M	1	1	1	0	0	0	0	0	1	0	0
-T	3	1	0	0	0	0	0	2	0	1	0
L +3M	5	2	0	1	1	1	1	1	0	0	1

Linearized residual matrix   Identity matrix

1.f.   Determining the dimensionless numbers from the modified residual matrix

From matrix [I], the dimensionless numbers, or π-numbers, characterising the physical phenomenon related to the system can be written. Based on the coefficients in the columns of the linearized residual matrix [R_m] (in pink in Table 37), each dimensionless number consists of a fraction with the non-repeated variable (for instance P for π_1) in the numerator and the repeated variables (for instance ρ, N, d for π_1) raised to the exponents specified in the [R_m] matrix (respectively 1, 3 and 5 for π_1) in the denominator as shown in Table 38.

Table 38: Dimensionless numbers characteristic of the phosphorylation protocol

	π_1	π_2	π_3	π_4	π_5	π_6	π_7	π_8
π numbers	$\dfrac{P}{\rho N^3 d^5}$	$\dfrac{\mu}{\rho N d^2}$	$\dfrac{\rho_p}{\rho}$	$\dfrac{d_p}{d}$	$\dfrac{H}{d}$	$\dfrac{Hl}{d}$	$\dfrac{T}{d}$	$\dfrac{g}{dN^2}$

The dimensionless numbers equation is defined by applying the π theorem, also called Vaschy-Buckingham theorem [231], [232], leading to Equation 7:

Equation 7:

$$\pi_{target} = \frac{P}{\rho N^3 d^5} = F_1 (\pi_2, \pi_3, \pi_4, \pi_5, \pi_6, \pi_7, \pi_8) = F_1 \left(\frac{\mu}{\rho N d^2}, \frac{\rho_p}{\rho}, \frac{d_p}{d}, \frac{H}{d}, \frac{Hl}{d}, \frac{T}{d}, \frac{g}{dN^2} \right)$$

with F_1 the process relation adapted to the system.

Therefore, during the upscaling process, the dimensionless numbers (Table 38) must be kept constant. Moreover, to obtain maximum similarity between scales, the temperature (T) and the ratio between the solid volume (cork) and the liquid volume (mixture) (so-called $\pi_9 = \frac{V_{SOL}}{V_{LIQ}}$) must also remain constant.

1.g.   Rearranging the dimensionless numbers

Equation 7 can be revised so that known dimensionless numbers (e.g. Reynolds numbers (Re), Froude numbers (Fr) or Galileo numbers (Ga)) can replace some of the dimensionless numbers of the process relation. This is done by raising dimensionless numbers to certain powers. In the case of cork phosphorylation, the Reynolds number (allowing to characterize a flow) and the Froude number (often used when studying agitation in a reactor) can be incorporated as dimensionless numbers in the process relation.

Equation 8 shows the relationship between π_2 and the Reynolds number and Equation 9 the relationship between π_8 and the Froude number.

Equation 8:
$$(\pi_2)^{-1} = \left(\frac{\mu}{\rho N d^2}\right)^{-1} = \frac{\rho N d^2}{\mu} = Re$$

Equation 9:
$$(\pi_8)^{-1} = \left(\frac{g}{d N^2}\right)^{-1} = \frac{N^2 g}{d} = Fr$$

Finally, the rearranged system is described by Equation 10.

Equation 10:
$$\pi_{target} = \frac{P}{\rho N^3 d^5} = F_2 \left(Re, \pi_3, \pi_4, \pi_5, \pi_6, \pi_7, Fr\right)$$

with F_2 the process relation adapted to the rearranged system.

It has to be mentioned that the dimensional analysis does not give the mathematical form of the process relation (correlating the dimensionless numbers to the π-target number). But experimentation allows approaching the mathematical expression of the process relation and provides information on the impact of each internal measure (Re and Fr) on the target variable (P). However, as such experimental work is generally very time-consuming, the process relations F_1 and F_2 were not approximated, the objective of this part being to obtain enough P-cork for its characterization. However, this approach should be achieved in the case of an industrial production of P-cork. When easily applicable, the adaptation of dimensionless numbers from one scale to another was achieved.

2. Optimal large-scale formulation

The dimensionless variables were distributed among the five similarities defined previously (section V. C. Upscaling of the phosphorylation system, p.105). First, the dimensionless numbers π_4, π_5, π_6 and π_7 belong to the geometric similarities, while π_1, π_2 and π_8 belong to the dynamic and kinematic similarities. Finally, the chemical similarities include π_3 and π_9. Temperature is the only thermal similarity.

To transpose the system to a larger scale, the small-scale dimensionless numbers corresponding to the variables of the system must be defined first. In order to preserve these dimensionless numbers, it is necessary to take geometric similarities as a starting point because geometric variables are the easiest to set. Thus, the equipment used for the phosphorylation protocol (flask, stirrer, etc.) has to be adapted to get similar π_4, π_5, π_6, π_7 and π_8 numbers at large scale. For this purpose, the corresponding geometric variables, namely d, H, H_l, T and N must be adapted. The volume of the flask was set at 2 L because this is the maximum size available to adapt the

protocol at laboratory scale and only 4 batches are necessary to obtain the required amount of P-cork for the fire tests. The dimensions of the flask being standard, the diameter T is 166 mm. The magnetic stirrer selected to stir properly the mixture in the 2 L flask has also standard dimensions: the length d and height H are 50 and 20 mm respectively. Thus, H, d and T variables have been fixed at large scale. Then, the height of the liquid in the flask (H$_l$) is adapted so that the $\frac{Hl}{d}$ ratio is similar from one scale to another, the variable d being constrained by the stirrer size. Once the variable H$_l$ is known at large scale, the volume of cork granules is adapted to the volume of the mixture so that the $\frac{Vsol}{Vliq}$ ratio is the same as the one used at small scale.

Considering these experimental conditions, the amount of phosphorylated cork per experiment increases from 12 g at small scale to 80 g at large scale, representing a solid volume of about 100 mL and about 667 mL respectively. Finally, the rotation speed N is adjusted to keep the same Froude number (π_8) between both scales (agitation visually identical). The stirring rate of the medium is thus fixed at 1120 rpm and 520 rpm (i.e. 1.8 m/s and 1.4 m/s) at small and large scales respectively. On the other hand, ρ_p, ρ and d$_p$ variables do not change from one scale to another because they are specific to the materials, as well as the g variable related to the gravity force. Table 39, gathers the values of the independent variables of the system for both scales. Variables P and µ are not mentioned as they cannot be known without a thorough experimental work.

Table 39: Independent variables of the system at small and large scales

Independent variables	ρ$_p$ (g/cm³)	ρ (g/cm³)	d (mm)	d$_p$ (mm)	H (mm)	T (mm)	H$_l$ (mm)	N (rpm)	g (m/s²)	V$_{sol}$ (mL)	V$_{liq}$ (mL)
Small scale	0.4	1.2	30	2	12	85	60	1120	9.81	100	163
Large scale	0.4	1.2	50	2	20	166	105	520	9.81	667	1073

Table 40 gives the values of the dimensionless numbers, at both scales. As the dimensionless numbers $\pi 1$ and $\pi 2$ corresponding to the dynamic and kinematic similarities are linked to P and µ, it could not be known whether they are preserved during upscaling.

Table 40: Dimensionless numbers of the system at small and large scales

π-numbers	π_1 $\frac{P}{\rho N^3 d^5}$	π_2 $\frac{\rho N d^2}{\mu}$	π_3 $\frac{\rho_p}{\rho}$	π_4 $\frac{d_p}{d}$	π_5 $\frac{H}{d}$	π_6 $\frac{Hl}{d}$	π_7 $\frac{T}{d}$	π_8 $\frac{dN^2}{g}$	π_9 $\frac{V_{sol}}{V_{liq}}$
Small scale	/	/	$^1/_3$	0.07	0.4	2	3	10x10^{-3}	0.6
Large scale	/	/	$^1/_3$	0.04	0.4	2	3	10x10^{-3}	0.6
Statement*	U	U	P	D	P	P	P	P	P

*U: Unknown; P: Preserved; D: Different.

Thanks to Table 40, it can be seen that the majority of ratios are preserved from one scale to another. The dimensionless number π_4 is different between both scales and it would be necessary to check if the d_p variable has an influence on the quality of grafting (specific surface). However, the size of cork particles cannot be modified in the GRASS project since it will have an influence on the damping properties of the infill and thus of the turf structure. π_1 and π_2 numbers are unknown. Finally, temperature is considered to be isothermal because of the rapid heating rate of the system. As a conclusion, after applying the basic principles of DA to be as close as possible to the initial experimental conditions (small scale), the phosphorylation conditions selected for large-scale synthesis are: $m_{cork\ granules} = 80$ g, $V_{EtOH} = V_{H_3PO_4} = 400$ mL, $V_{Et_3PO_4} = 270$ mL and $m_{P_2O_5} = 8.8$ g. The reaction was performed at 45 °C for 24 h.

3. Characterizations

Large-scale phosphorylated cork (called 'LS P-cork') processed with the previously defined experimental conditions was then fully characterized: the reaction yield and the carbonization rate obtained after heat treatment at 600°C were determined. Yield assessment will allow evaluating the degradation of cork during the phosphorylation process and the determination of the residual mass will allow evaluating the thermal stability. These two characterization methods are used in a first approach to determine in a fast way if the results are comparable to those of the small-scale phosphorylated cork (called 'P-cork'). Then, if upscaling is validated, additional characterizations of LS P-cork will be performed.

3.a. Reaction yield

The reaction yields obtained for 'P-cork' and 'LS P-cork' are 89 % and 87 % respectively. The values being comparable, it means that upscaling did not change the reaction yield.

3.b. Carbonization rates of LS P-cork

The thermal stability of LS P-cork was evaluated by determining the amount of final residue after heat treatment from 0 to 600°C in a furnace (HTT= 600°C). The carbonization rates at 600°C obtained for corks phosphorylated at both scales were compared to that of virgin cork and are given in Table 41.

Table 41: Carbonization rates obtained for virgin cork, 'P-cork' and 'LS P-cork' at HTT=600°C

	Virgin cork	P-cork	LS P-cork
Carbonaceous residue at 600°C (%)	1.0 ± 0.4	6.1 ± 0.5	9.4 ± 1.5

As mentioned previously, P-cork has a much higher residual mass at 600°C than virgin cork: 6.1 % vs 1% respectively. LS P-cork shows a carbonization rate increase of more than 8 % compared to virgin cork, and also a significant increase (+ 50 %) compared to the small-scale P-cork. The standard deviation is also higher, around 1.5 % for LS P-cork compared to 0.5% for P-cork, showing that the large-scale process leads to a less homogeneous grafting than the small-scale process.

3.c. Discussion

DA approach allowed determining the optimal experimental conditions for the phosphorylation of cork at large scale, without modifying the properties of P-cork. The first characterizations of LS P-cork confirm that the large-scale protocol is slightly aggressive (little degradation during reaction) and leads to a reaction yield equivalent to that obtained at small scale. A significant increase in the carbonization rate is noted. The value increases from around 6 % for P-cork to around 9 % for LS P-cork. This could be due to a higher phosphorus content. It could be assumed that the diameter of cork particles (d_p) and thus the specific surface of granules is responsible for this increase. π_1 and π_2 numbers, relative to the dynamic and kinematic similarities, can also influence the quality of grafting by influencing the reaction kinetics but these parameters were not determined. In order to validate those assumptions, experiments should have been done using granules of lower diameter at small-scale and π_1 and π_2 numbers should have been determined. Finally, a larger standard deviation is obtained in the case of LS P-cork (1.5 % compared to 0.4 % for P-cork), demonstrating that the homogeneity of P-cork grafting is lower at larger scale. This could be reasonably explained by the fact that cork is a natural product and thus the inhomogeneity of this material should be higher considering larger volume.

Thanks to DA, promising results are obtained but additional experiments must be carried out to study the repeatability of the large-scale protocol and thus to validate the experimental conditions used.

4. Large scale formulation checking and conclusions

The last step of the upscaling approach consisted in checking the repeatability of the phosphorylation reaction. Two new large-scale formulations were carried out using the same experimental conditions as for 'LS P-cork'. The characterizations performed on these modified corks confirmed the previous results in terms of reaction yield and carbonization rate.

As a conclusion, large-scale experimental conditions determined thanks to DA allow leading to an average reaction yield of 88 %, similar to that obtained for P-cork at small scale (89 %), and to a carbonization rate of 9.3 % (average of the 3 repetitions), much higher than that obtained at small scale (6.1 %), highlighting an improvement in thermal stability. Thus, a large-scale P-cork with characteristics equivalent or superior to those obtained for P-cork at small scale is obtained. Upscaling through DA can therefore be validated.

A large volume production programme was launched using these experimental conditions to synthesize enough P-cork to determine the fire properties of the modified infill and of the whole artificial turf structure. However, before performing the fire tests, LS P-cork must be fully characterized both in terms of grafting quality and functional properties. This step is crucial to validate the proposed flame retardant approach applied to the turf structure.

D. Full characterization of LS P-cork

Several experimental techniques were used to characterize LS P-cork. First, EPMA, IR and ^{31}P NMR analyses were carried out to validate the chemical structure of the modified cork. In a second part, the study of some cork properties, required for the intended application is performed. It includes DVS (dynamic vapour sorption) and study of the stability in water. The FR properties of the materials will be detailed in the last chapter of the manuscript (**Chapter 4**).

1. Chemical characterization of LS P-cork

Since the repeatability of the phosphorylation protocol is validated, the following characterizations are carried out on LS P-cork and compared to those of virgin cork.

1.a. Microscopic analysis

Figure 31 shows the EPMA mappings of virgin cork and of LS P-cork to visually assess the quality of grafting and the location of the phosphorus element.
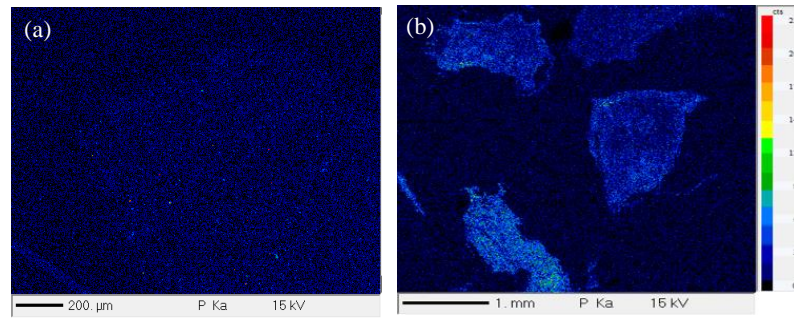
Figure 31: EPMA mapping of (a) virgin cork and (b) LS P-cork

Phosphorus can be observed inside the LS P-cork granules (Figure 31 (b)) and the phosphorus distribution is rather uniform throughout the entire thickness of granules. The granule at the bottom left appears to contain a higher amount of phosphorus compared to the other ones. It confirms that the variability of cork, due to its natural origin, can affect the phosphorus content on cork granules and this characteristic can also justify the previous assumption about the higher standard deviation observed at large scale.

The cork structure may also be damaged by the phosphorylation reaction due to the processing conditions. SEM images of cork granules were recorded before and after modification. Figure 32 (a) and (b) show the surface of a virgin cork granule and of a LS P-cork granule respectively.
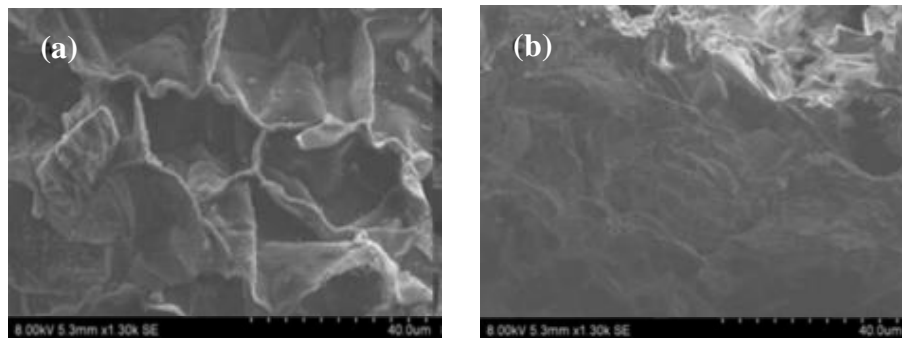
Figure 32: SEM pictures of the (a) cork surface and of the (b) LS P-cork surface

Small hexagonal cavities connected to each other can be seen at the surface of virgin cork granules. This specific structure corresponds to the one reported in the literature [92]. On the contrary, LS P-cork has a rather flat surface and the cavities are no longer visible. Thus, the surface of the infill material appears to be significantly damaged by the phosphorylation process. As cork cavities allow providing many properties [138], [168], it can be assumed that alteration of LS P-cork structure leads to a change in properties and in particular in the thermal insulative properties of cork.

1.b. Infrared spectroscopy analysis

Infrared spectroscopic analysis was also carried out and the spectra of virgin cork and LS P-cork are shown in Figure 33. The spectra were normalized with respect to the strongest suberin band (ν_{as}COC at 1160 cm^{-1}). The signal intensities of LS P-cork , at 2924 cm^{-1}, 1739 cm^{-1} and 1464 cm^{-1} ((b), (c) and (d) frames) decrease compared to the suberin fingerprint at 1160 cm^{-1} while those at 3500 cm^{-1}, 1090 cm^{-1} and 1040 cm^{-1} increase (see Table 29 for the wavelength correspondence). These results are consistent with literature data [219]−[221], confirming that the chemical components' proportion of cork varied during the phosphorylation reaction (probably due to the extraction in hot ethanol). The same trends have already been observed by some authors who studied the influence on cork of hot extraction in water [184], [223].
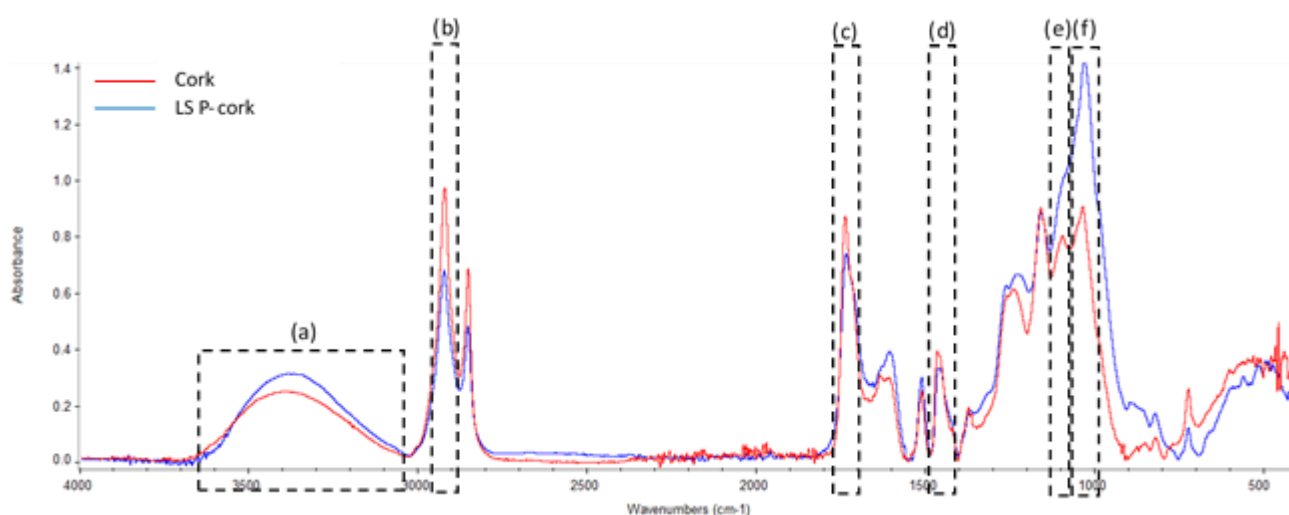
Figure 33: FTIR spectra of virgin cork and LS P-cork with focus on signals at (a) 3500 cm^{-1}, (b) 2924 cm^{-1}, (c) 1739 cm^{-1}, (d) 1464 cm^{-1}, (e) 1090 cm^{-1} and (f) 1040 cm^{-1}

However, as the band at 1160 cm^{-1} is impacted by grafting (grafting zone of PO-R bonds), the spectra of virgin cork and LS P-cork were then normalized with respect to the strongest aliphatic carbon band (ν_{as} CH$_2$, at 2850 cm^{-1}) as shown in Figure 34 (A).

The intensity of peaks generally assigned to PO-R bonds of phosphate groups (1030 cm^{-1} and 1090 cm^{-1} (see Table 30)) is much higher for LS P-cork ((c) and (d)-frames), showing that such phosphorus bonds were created during phosphorylation. Moreover, the band between 1130 cm^{-1} and 1200 cm^{-1} ((b)-black frame) and the peaks centred at 1230 cm^{-1} and 1260 cm^{-1} ((a)-black frame) are more intense, confirming the presence of phosphate and phosphonate respectively.
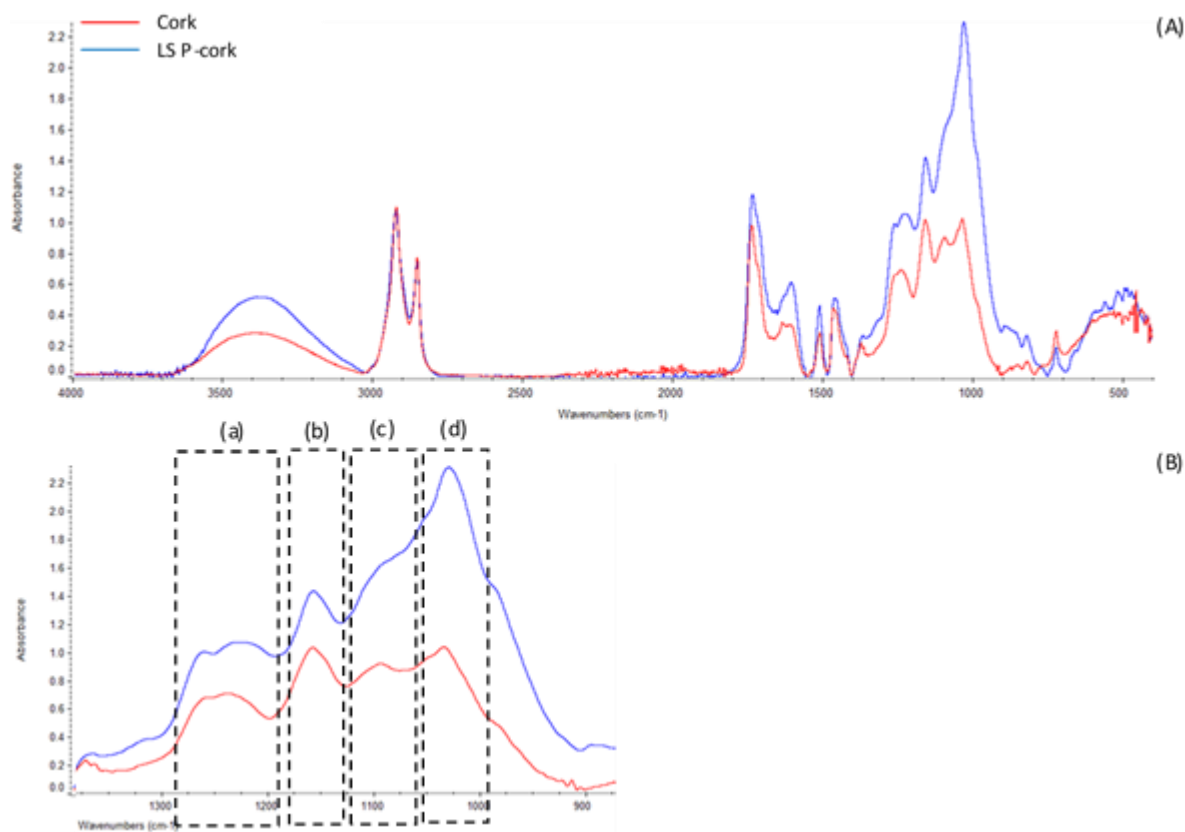
Figure 34: (A) FTIR spectra of virgin cork and LS P-cork and (B) focus on signals at (a) 1230 – 1260 cm^{-1}, (b) 1100 – 1200 cm^{-1}, (c) 1090 cm^{-1} and (d) 1030 cm^{-1}

1.c. Nuclear magnetic resonance spectroscopy analysis

As cork is not soluble in an organic solvent, and as the latter may degrade cork, liquid NMR (more accurate) could not be performed. Therefore, solid state ^{13}C and ^{31}P NMR analyses were carried out on virgin cork and LS P-Cork in order to evaluate the influence of the phosphorylation reaction on the cork structure. Figure 35 and Figure 36 show the spectra of virgin cork and LS P-cork, assignments of peaks being reported in Table 42 and in Table 43. Virgin cork and LS P-Cork (red and blue curves respectively) exhibit the expected signals corresponding mainly to carbohydrate carbons, suberin and lignin. These spectra are consistent with those mentioned in the literature [233], [234]. Both corks show the same chemical shifts (ppm). The signals in the 25 - 33 ppm area, corresponding to the presence of the methylene carbons of suberin, do not have the same intensity. In fact, two strong signals centred at 33 ppm and 30 ppm are visible for virgin cork, whereas the signal at 25 ppm is low. On the contrary, for P-cork, only the signal centred at 30 ppm is intense, the other two at 33 ppm and 25 ppm being much lower. These results demonstrate that the phosphorylation reaction modifies the structure of suberin.
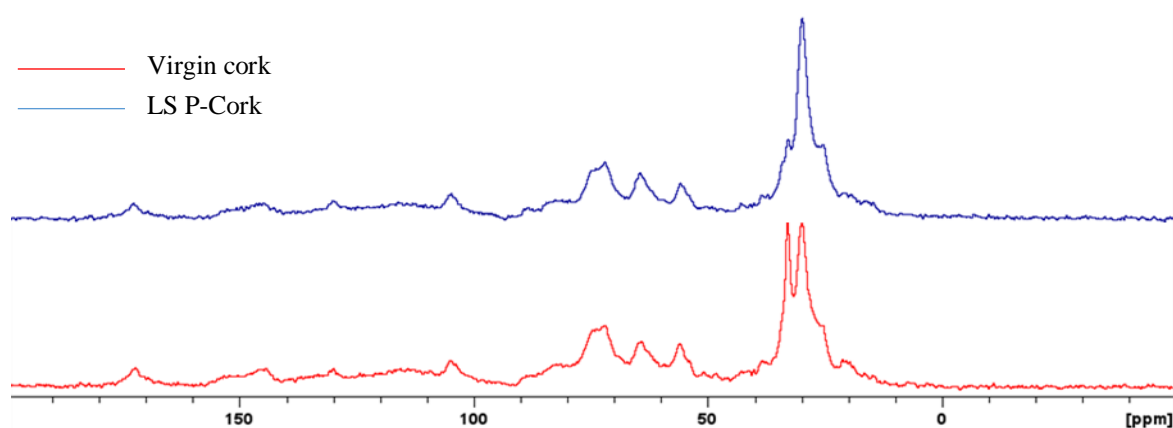
Figure 35: Solid state ^{13}C NMR spectra of virgin cork and LS P-cork

Table 42: Chemical shift assignment of 13C SS NMR peaks of cork [233], [234]

Peak (ppm)	Assignation
21	Ester groups of hemicelluloses
25 – 50	Waxes
25 – 33	Methylene carbons of suberin
56	Methoxy groups of suberin, lignin and hemicelluloses
65 – 105	Carbohydrate carbons (hemicellulose and cellulose)
110 – 155	Lignin aromatic carbons
172	Suberin ester groups
110 – 160	Lignin and polyphenols

Considering ^{31}P NMR, while a low signal at -1 ppm can be observed for virgin cork, that may be assigned to orthophosphates or phosphate monoesters naturally present in cork, the LS P-cork spectrum exhibits two peaks: the first one at -1 ppm and the second one centred at 16 ppm. The latter corresponds to phosphonate structures and was not expected considering the oxidation degree of the phosphorus moieties used in the reaction. It will be further discussed in this section.
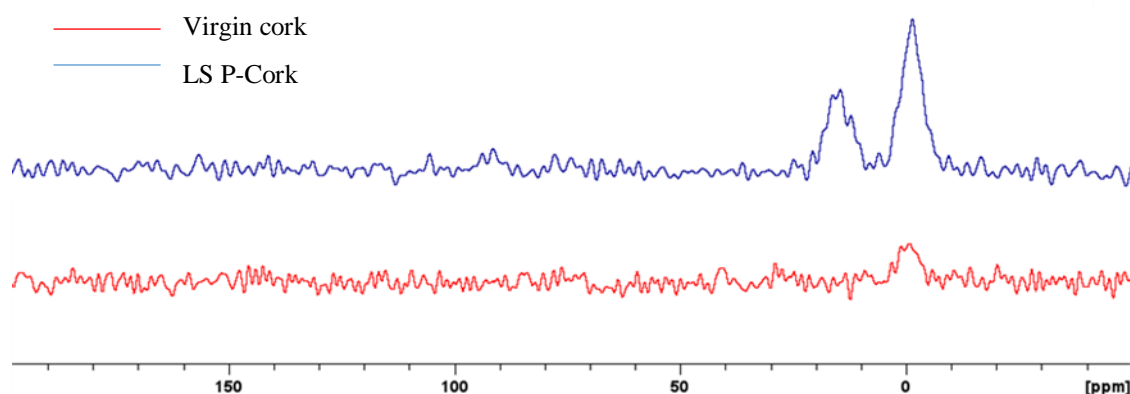
Figure 36: Solid state ^{31}P NMR spectra of virgin cork and LS P-cork

119

Table 43: Chemical shift assignment of common phosphorus functional groups. [235], [236]

Peak (ppm)	Assignation
15 – 30	Phosphonate
10 – 0	Phosphate monoester
5 – 0	Orthophosphate
0	Phosphoric acid
0 – (-5)	Phosphate diester
(-5) – (-10)	Pyrophosphate
(-15) – (-30)	Polyphosphate

1.d.   Phosphorus content

The aim is to determine the amount of phosphorus grafted during the phosphorylation reaction. The amount of phosphorus in LS P-cork was measured by ICP-AES and was compared to that in virgin cork.

The phosphorus contents are very low, i.e. 0.03 % and 0.21 % for virgin cork and LS P-cork respectively. However, the amount of phosphorus in LS P-cork is seven times higher than in virgin cork, demonstrating that the phosphorylation process was efficient. Moreover, the efficiency of phosphorus to favour carbonization of cork was previously shown.

1.e.   Discussion

Chemical characterizations led to two main conclusions: (1) the phosphorylation reaction modified the structure of cork (mainly suberin) and (2) the phosphorylation reaction occurred efficiently, leading to the structural and chemical modification of cork.

After the phosphorylation step, the phosphorus amount measured using ICP is 7 times higher for LS P-cork than for virgin cork (i.e. 0.21 % compared to 0.03 % respectively), showing a significant phosphorus grafting during the reaction. Moreover, thanks to EPMA mappings, an large increase in the phosphorus content was evidenced after upscaling, leading to a rather uniform grafting up to the core of LS P-cork. The fact that phosphorus is grafted inside the granules, and in greater quantities, can presumably be related to the improvement in the carbonization rate of LS P-cork compared to P-cork. The high standard deviation in the residual mass can be explained by the natural character of cork, leading to a variable grafting from one granule to another.

FTIR as well as NMR analyses evidenced the presence of phosphorus compounds in the form of phosphate and also phosphonate, confirming the occurrence of phosphorus compounds grafting. However, as previously mentioned, the presence of phosphonate was not expected as to obtain phosphonates, a reduction reaction must occur to reduce phosphates (oxidation degree +V) into phosphonates (degree +III). To obtain this kind of reaction, a reducing medium, generally basic, is necessary while phosphorylation occurs in an acidic medium since phosphoric acid is used. We may find an explanation of such results in the work of Khavryuchenko et al [237] that propose the transformation of phosphoric esters into phosphonates through Michaelis-Arbuzov-type reaction happened. The main difference for the carbonization of H_3PO_4-impregnated PhF-resin and the neat resin was attributed to the behaviour of phosphorus containing fragments. In the very early steps of the first stage of carbonization (CP#1−3), phosphoric esters are formed due to the reaction of terminal P=O of H_3PO_4 with unsaturated carbon atoms, exposed after the elimination of water molecules. Furthermore (CP#4−5), upon stepwise dehydratation of −O−P(OH)$_3$ the di- and triesters of phosphoric acid (−O−PO(OH)−O− and O=P(−O−R)$_3$, respectively) arise (structure I shown in Figure 37). At this point (CP#6), unsaturated radical centring carbons appear in the vicinity of O=P(−O−)$_3$ groups (structure II shown in Figure 37) leading to the spontaneous transfer of phosphoric oxygen to the unsaturated carbon by radical mechanism and the formation of three-coordinated P^{3+} in P(−O−R)$_3$ groups (structure III shown in Figure 37); i.e. reduction of P^{5+} by unsaturated carbon atom occurs. Because of steric strain in the carbonizing backbone and flexibility of polymer chain, allowing easy change of conformation, an internal rearrangement may occur, resulting in the formation of spatially neighbouring quinoid structure and of a phosphonate group (structure IV shown in Figure 37). These series of elementary acts can be considered to be a Michaelis−Arbuzov-type reaction, leading to the formation of strong C−P bonds. Upon dehydration, no spontaneous reaction was observed because of the significant distance between three-coordinated phosphorus and unsaturated (radical) C atoms. This also proves that the steric factor plays an important role in the formation of phosphonates upon carbonization, preventing the spreading of the polymer chain and thus making reacting centres closer.

This type of reaction can be considered for the phosphorylation of cork with H_3PO_4 and more particularly, for suberin. Indeed, the presence of unsaturations in the suberin structure (Figure 37) allows the radical transfer reaction explained previously, leading to the internal rearrangement of the structure and thus, to the transition from II to III structures (Figure 37).
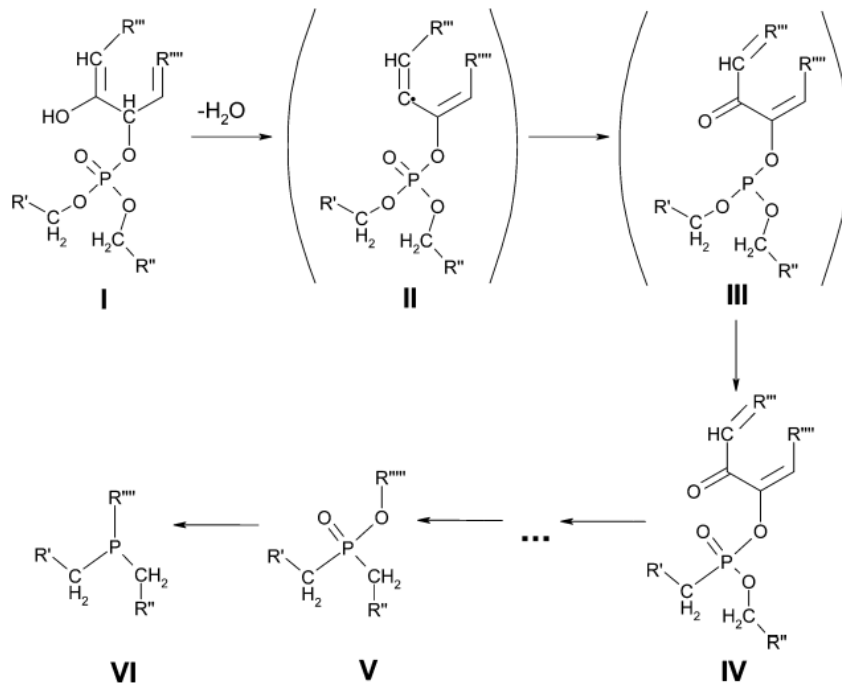
Figure 37: Simplified scheme of Michaelis-Arbuzov-type reaction. Extracted from [237]

On the contrary, this type of reaction cannot be considered for the lignin part of the cork structure, due to its lack of flexibility (too rigid structure), preventing rearrangement. In the following section, some other properties required for infill to be used in artificial turf structures for sports applications, such as low water absorption and stability to leaching, are discussed.

2. Evaluation of the other properties of cork

Artificial turf structures are intended both for indoor and outdoor applications. In the second case, cork granules must be resistant to external aggressions, particularly to bad weather such as rain. Thus, in order to evaluate the impact of water on the behaviour of LS P-cork granules, water absorption and ageing analyses were carried out.

2.a. Dynamic vapor sorption analysis

Dynamic vapour sorption experiments were carried out on virgin cork and on LS P-cork granules to assess the influence of the phosphorylation reaction on water absorption. Figure 38 shows the sorption-desorption cycles reflecting moisture content evolution as a function of relative humidity for the both materials.
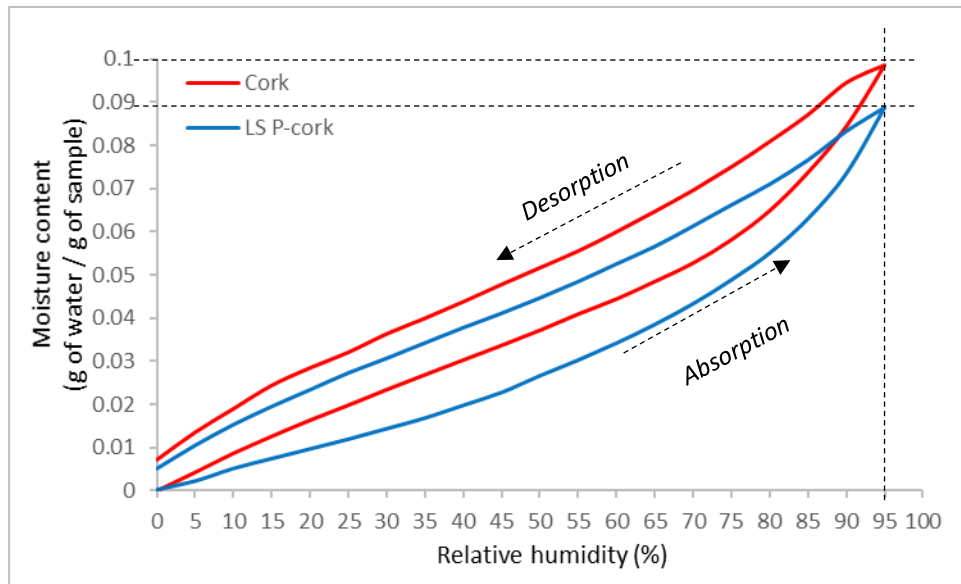
Figure 38: Sorption-desorption cycles of virgin cork and LS P-cork

Firstly, it is observed that at the end of the desorption cycle, none of the two curves come back to the value at 0% relative humidity (RH), demonstrating that corks never completely desorb. Virgin cork (red curve) absorbs slightly more water than LS P-cork, reaching a moisture content of 0.1 g of water per gram of sample (gow/gos) at 95 % RH, whereas LS P-cork (blue curve) is less sensitive to water with a moisture content below 0.09 gow/gos at 95% RH.

Contrary to phosphonates, phosphates are known to increase the hydrophilicity of a material. Taylor et al [238] and Li et al [239] demonstrated that the use of phosphonates led to the development of more moisture-stable materials. As the moisture content is lower for LS P-cork than for virgin cork, it can be assumed that phosphonates have a greater influence on the hydrophilicity of LS P-cork than phosphate bonds and lead to an increase in moisture stability.

2.b. Ageing in water

The stability of LS P-cork in water was evaluated by means of a leaching study and the results were compared to those of virgin cork. The evolution of the pH value of the medium was determined over thirty days (D +30) after the start of the experiment. Figure 39 shows the evolution of pH values over 30 days (i.e. 720h).

The pH value measured for virgin cork after 30 days is slightly lower than the initial value, but the two values can be considered as equivalent taking into account the uncertainty of measurement. This inaccuracy also explains the random variations in the pH value over time, between 7.9 and 7.4 for virgin cork. For LS P-cork, a significant acidification of the medium is observed, since the pH value decreases from 7.9 to 5.9 after 30 days.
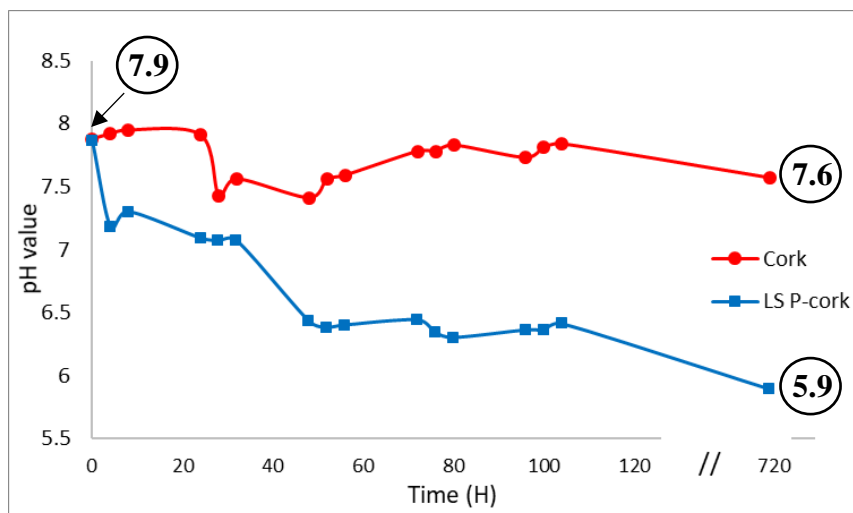
Figure 39: Evolution of water pH for virgin cork and LS P-cork over the 720h of ageing

As the pH value for LS P-cork decreases from 2 units while a stable pH is observed for virgin cork, the stability in water of the phosphorylated cork is not high enough. This phenomenon is probably due to the leaching of phosphorus compounds, and more precisely to the hydrolysis of P-O bonds of phosphate ester. Indeed, studies from the literature already highlighted the low resistance to hydrolysis of phosphate groups [239], whereas phosphonate groups show a better resistance [238], [240].

Since this leaching could affect the carbonization rate, the carbonization rates of 'aged cork' and 'aged LS P-cork' were determined and compared to those of virgin cork and LS P-cork. The thermal stability of virgin cork and of LS P-cork after ageing was evaluated after heat treatment at 600°C (HTT= 600°C). The final carbonization rates obtained for virgin cork and LS P-cork before and after ageing are given in Table 44. The carbonization rate of LS P-cork after ageing decreases significantly compared to LS P-cork (66 % reduction), confirming that the probable leaching of phosphorus compounds leads to a decrease in the thermal stability.

Table 44: Carbonization rate obtained for virgin cork, aged cork, LS P-cork and aged LS P-cork after HTT=600°C

	Virgin cork	Aged cork	LS P-cork	Aged LS P-cork
Carbonaceous residue at 600°C (%)	1.0 ± 0.4	0.9 ± 0.5	9.4 ± 1.5	3.2 ± 0.7

2.c.   Conclusion

The study revealed that water has a strong impact on the phosphorylated cork. Indeed, while LS P-cork absorbs less water than virgin cork, the phosphorylation process leads to a strong decrease of cork stability after 30 days into water. The carbonization rate of phosphorylated

cork at 600°C was also significantly reduced, from 9.4% to 3.2%, after ageing in water. It can be supposed that phosphorus compounds are released into water, leading to a much lower thermal stability of phosphorylated cork after ageing. Further investigations are needed to obtain a modified cork that can be used in artificial turf structures intended for outdoor applications.

VI.   Conclusion of Chapter 3

In this chapter, three phosphorylation protocols were investigated. The phosphorylation protocol using EtOH, H_3PO_4, Et_3PO_4 and P_2O_5 was chosen because a good compromise was achieved in terms of grafting (EPMA and FTIR-ATR), thermal stability and impact on the environment (use of lower toxicity compounds). Experimental conditions used for the small-scale phosphorylation reaction were optimized and the selected conditions led to the formation a thin and uniform layer of phosphorus mainly around cork granules. The carbonization rate of P-cork was about 6.1 %.

Then, upscaling of the protocol was performed in order to produce larger amounts of phosphorylated cork per experiment. Dimensional analysis was used to determine the experimental conditions allowing to transpose the phosphorylation protocol from small-scale to large-scale. The majority of the dimensionless numbers were preserved, although some remained unknown. Despite the lack of information on the kinetics and dynamics of the reaction, further improvements of the phosphorylation protocol could probably be proposed to obtain better grafting level. The large-scale phosphorylation protocol allowed the production of a phosphorylated cork with even better properties than those obtained at small scale. Indeed, a residual mass of about 9 % after treatment at 600°C was obtained, higher than that at small scale, highlighting an improvement in charring. The reliability of the process was also assessed. Finally, LS P-cork was fully characterized. It was shown that phosphorylation results in the formation of phosphate and phosphonate structures. However, the study of the ageing of LS P-cork in water demonstrated that the phosphorylation treatment was not fully durable although water sorption was decreased.

The next chapter is dedicated to the fire properties of artificial turf structures containing the modified cork, using MLC and the small-scale radiant panel test. Characterizations will be performed to elucidate the mechanisms of action of modified cork during combustion.

Key points & strategies of Chapter 3

Key points:

- ✓ A phosphorylation protocol was developed.
- ✓ The optimal experimental conditions at large scale (upscaling) were determined through dimensional analysis.

- ✓ Phosphorylated cork with improved properties was obtained:
    - o Carbonization rate of about 9 % after heat treatment (HTT = 600°C)
    - o Uniform grafting of phosphorus
    - o Decrease of water sorption properties
    - o Presence of bonds characteristic of phosphates and phosphonates
    - o 7-fold increase of the phosphorus content

- ✓ Phosphorylation has also some drawbacks:
    - o Extraction of structural compounds
    - o Degradation of cork structure
    - o Poor stability in water: indoor applications should be favoured

Objectives for the next chapter:

- ✓ Investigation of the fire behaviour of LS P-cork and of LS P-cork-based turf structures with MLC and small-scale radiant panel tests.
- ✓ In-depth analysis of the mechanism of action of phosphorylated cork.

Chapter 4 - Thermal degradation and fire behaviour of phosphorylated cork

The objective of **Chapter 3** was to develop a bulk modified cork (LS P-cork) that will be further incorporated in the turf structure to improve the fire properties. The large-scale phosphorylation protocol of cork was previously validated: a uniform phosphorus grafting through the cork granules thickness was observed and the presence of phosphate and phosphonate groups was evidenced. Moreover, an increased carbonization rate was obtained, showing an improvement of the thermal stability that can potentially affect positively the fire properties of cork. Using MLC test, the use of LS P-cork is expected to reduce the amount of heat released compared to virgin cork. But the main objective is to achieve a low burnt length at the radiant panel test, i.e. a critical heat flux (CHF) higher than 4.5 kW/m², to allow the use of the artificial turf structure for indoor applications. The assessment of the fire properties of LS P-cork is first necessary to determine if the phosphorylation of cork leads to a fire-retardant effect and allows meeting the requirements of the European standard.

As a consequence, the first part of **Chapter 4** is devoted to the evaluation of the fire behaviour of LS P-cork using MLC and the small-scale radiant panel test developed in **Chapter 2**: the modified cork will be first tested alone and then incorporated into the whole artificial turf structure. In a second part, characterizations are performed to study the impact of temperature on the behaviour of cork and phosphorylated cork, to better explain the fire properties obtained and to understand the role of the cork infill during the fire tests. The thermal properties of LS P-cork were first studied using TGA. Then, both virgin cork and LS P-cork were heat treated at characteristic temperatures and ^{13}C NMR and ^{31}P NMR analyses were performed on the collected residues. The phosphorus content in both virgin and phosphorylated residue obtained at 600°C was also determined. Finally, the last part of this chapter is intended to propose a mechanism of action of phosphorylated cork inside the artificial turf structure during the fire test.

I.   Fire behaviour of LS P-cork

The aim of this part is to evaluate the fire behaviour of LS P-cork, tested alone and then integrated into the whole turf structure, and results will be compared to those obtained with the virgin cork. The fire properties are first investigated using MLC test. Moreover, during the tests with the LS P-cork based artificial turf structure, thermocouples (TC) are used to determine the temperature distribution inside the sample and thus to assess the protection brought by the LS P-cork layer to the turf structure. Finally, the flame spread of LS P-cork based artificial turf structure will be investigated using the small-scale radiant panel test.

The infill layer thickness has been set at 15 mm as it was previously shown that this thickness is optimum to protect efficiently the backing (**Chapter 1**).

A. Fire behaviour of phosphorylated cork

MLC curves giving the HRR evolution versus time for both cork materials are shown in Figure 40 and the corresponding data are given in Table 45.
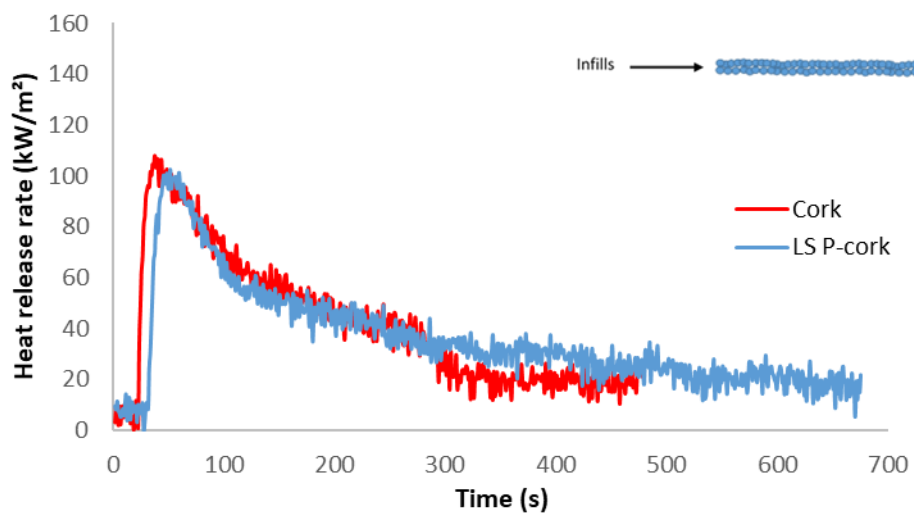
Figure 40: Heat release rate curves of cork and LS P-cork

Table 45: Mass Loss Calorimeter results of cork and LS P-cork.

Infills	Thickness (mm)	TTi (s)	pHRR (kW/m²)	THR (MJ/m²)	TOF (s)
Virgin cork	15	19 ± 3	108 ± 1	20 ± 1	284 ± 4
LS P-cork	15	28 ± 2	102 ± 9	21 ± 1	676 ± 56

Firstly, the main difference between cork and LS P-cork concerns the TTi. The amount of energy required to ignite the LS P-cork layer is more significant, leading to an increase of around 9 s of the ignition time compared to virgin cork. A difference can be visually observed on the burning behaviour of the cork. Indeed, contrary to virgin cork, when LS P-cork is exposed to the MLC radiative heat flux, granules strongly blacken and carbonize at the surface. On the other hand, the presence of phosphonate groups in LS P-cork has been evidenced using ^{31}P NMR in **Chapter 3**. As phosphonate groups generally act in the gas phase, it can be assumed that this increase in TTi can be attributed to a gas phase phenomenon. No gas phase analysis has been performed in this study and therefore this hypothesis cannot be demonstrated. However, the mechanisms of actions of phosphorus flame retardants, in gas and condensed phase, will be further discussed in the last section of this chapter (Section III. Mechanisms of action of P-cork, page 141).

Then, virgin cork and phosphorylated cork infills show similar curves with close heat release rates leading to similar pHRR values of 108 kW/m² and 102 kW/m² respectively. The THR value is also equivalent for the both corks, i.e. 20 MJ/m² and 21 MJ/m² for virgin cork and LS P-cork respectively. Moreover, in the case of virgin cork, the curve rapidly decreases from around 280 s leading to a relatively short TOF (284 s) while for LS P-cork a longer TOF is observed. This longer TOF can be directly related to a deeper degradation in the cork thickness as observation of the residues after testing shows that cork burns rather superficially (approximately on a 5mm depth) whereas LS P-cork leads to a completely carbonized residue. **Moreover**, LS P-cork has a greater charring behaviour: the granules are held together and form a dense, solid and cohesive layer, whereas virgin cork decomposes into ashes.

B. Fire behaviour of phosphorylated cork in the whole artificial turf structure

The fire behaviour of LS P-cork based artificial turf structure, called S – P-cork structure, was evaluated. First, fire properties of the structure were investigated with MLC test. Additional experiments were performed to determine the protective behaviour of LS P-cork (thermal insulation and protective properties of the modified cork) using thermocouples (TC). Then, the flame spread of the S - P-cork was evaluated using the small-scale radiant panel test. All the results were compared to those of the virgin cork-based structure (results presented in **Chapter 1** and **Chapter 2**).

1. Assessment of the fire behaviour of cork-based and LS P-cork-based structures using MLC test

The fire behaviour of the cork-based structure and of the LS P-cork based structure, called S – Cork and S – P-cork respectively, has been determined. HRR curves are shown in Figure 41 and the corresponding data are given in Table 46.
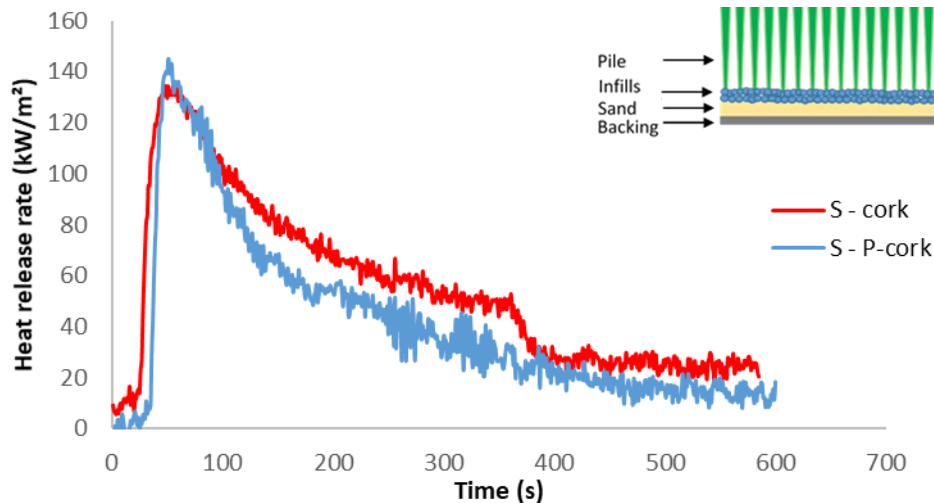
Figure 41: Heat release rate curves of the complete structures with virgin cork and LS P-cork as infill materials

Table 46: Mass Loss Calorimeter results of the complete structures with virgin cork and LS P-cork as infill materials.

Structures	Infill thickness (mm)	TTI (s)	pHRR (kW/m²)	THR (MJ/m²)	TFO (s)
S – Cork	15	22 ± 1	143 ± 6	34 ± 1	272 ± 22
S – P-cork	15	34 ± 4	145 ± 6	27 ± 1	376 ± 18

As observed for the infill alone, the ignition time of the S – P-cork is higher (+ 12 s) than that of S-Cork. As discussed in the previous section, this delay can be attributed to the action of phosphonates in the gas phase. Then, the maximum heat release rate values (pHRR) are similar, i.e. 143 kW/m² and 145 kW/m² for S – Cork and S – P-cork structures respectively. Moreover, when the fire behaviour of LS P-cork alone is compared to that of the S – P-cork structure, a significant increase in pHRR is observed (pHRR is around 105 kW/m² for the infill and around 145 kW/m² for the whole structure). The same phenomenon was previously observed for the cork-based structure (**Chapter 1**) and was attributed to the combustion of PE fibres. Then, while it was equivalent for the two corks tested alone, the total heat release value (THR) of the S – P-cork structure is 21% lower than the THR value of the S – Cork structure that can be attributed

to a decrease in the amount of burnt material. Finally, the TFO of the S – P-cork is quite longer than that of S – Cork (376 s vs. 272 s respectively).

Observation of the residues after testing (Figure 42) reveals that all the LS P-cork is degraded inside the turf structure: granules have strongly carbonized, forming a dense and thick infill, confirming the enhanced charring phenomenon previously observed for LS P-cork alone. On the contrary, a thin layer of cork is preserved above the sand layer in the case of the S – Cork structure.
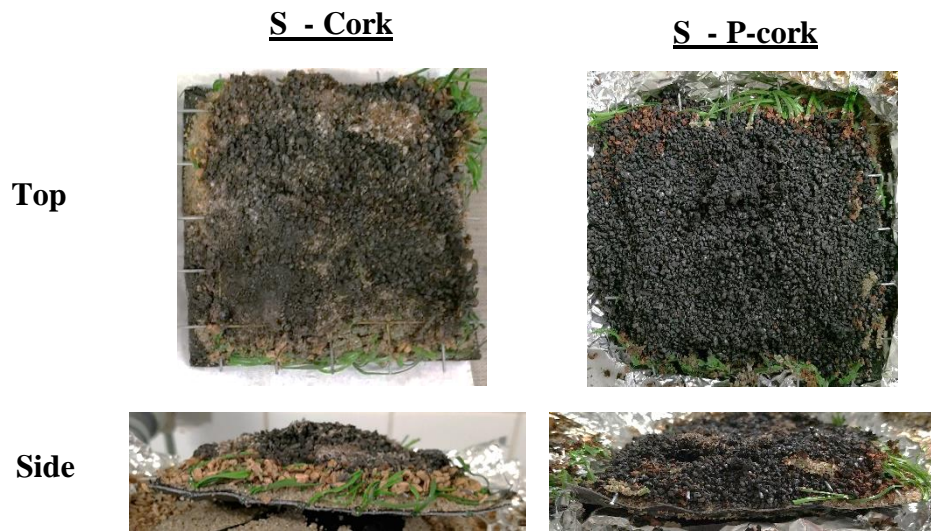
S - Cork   **S - P-cork**

Figure 42: Top view and side view pictures of cork-based structure and S – P-cork structure after fire tests

Samples have been weighed before and after MLC testing: the S – Cork structure loses 38 % of its mass after combustion against a loss of only 30 % for the S – P-cork structure. It is assumed that phosphorylated cork granules only degrade at the surface, resulting in a lower amount of burnt cork. Charring allows saving more material, also leading to a decrease in THR as previously shown. Moreover, charring is supposed to decrease the burning rate of the material: the carbon layer formed at the surface of cork slows down the flame spread but does not prevent the material from burning in the depth, as already highlighted by Atreya et al [241] for charring materials, explaining the longer burning time of phosphorylated cork.

2. Protective behaviour of the phosphorylated cork

The charring ability of LS P-cork was previously demonstrated and the protective behaviour was assumed to be due to the phosphorylation according to visual observation of the residue at the end of MLC test. To confirm the protective character brought by the phosphorylated cork layer to the turf structure, six thermocouples were placed between the backing and the sand layer (Figure 5, page 24) to measure the temperature distribution inside the sample over the

entire surface during MLC tests. Similar experiments were previously done and the results discussed for virgin cork (**Chapter 1**). The curves giving the temperature evolution for the six thermocouples are shown in Figure 43 (the data obtained for virgin cork (S-cork) are added for comparison) and the corresponding temperature values obtained after 70, 200 and 600 s of experiment with TC 1, 2 and 4 are given in Table 47.

.
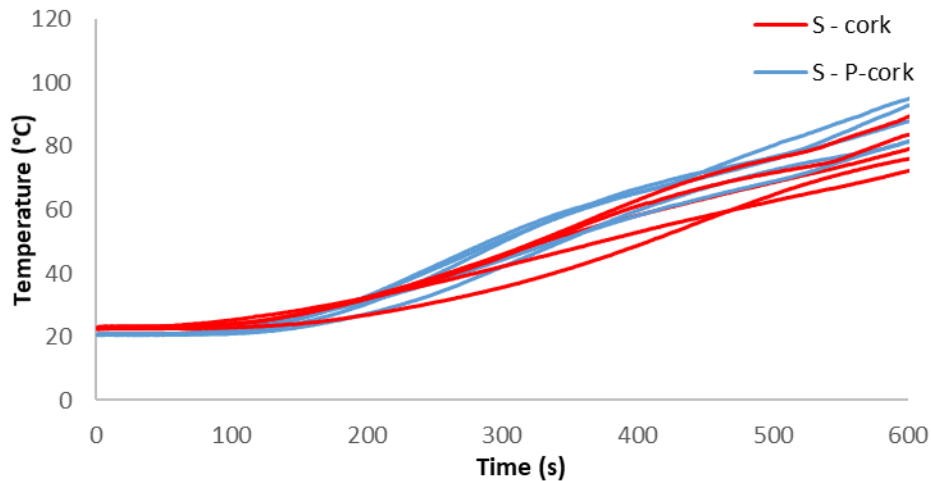
Figure 43: Temperature evolution of the six thermocouples for virgin cork and S – P-cork turf structures

Table 47: Maximum temperatures (°C) of thermocouples 1, 2 and 4 for both virgin cork and S – P-cork structures after 70, 200 and 600 s of testing.

Infill \ Time (s)	Thermocouple 1 (TC1)			Thermocouple 2 (TC2)			Thermocouple 4 (TC4)		
	70	200	600	70	200	600	70	200	600
Cork	23	31	82	33	52	93	23	27	76
LS P-cork	21	32	79	24	50	90	21	27	82

As shown in Figure 43, curves of S-Cork and S – P-cork structures are relatively close. Furthermore, the recorded values for LS P-cork are similar to those of cork considering a given thermocouple (TC1, TC2 or TC4) and a given test time (70, 200 or 600 s). Thus, the heat flow spread through the sample is equivalent for both corks whatever the temperature. Moreover, the increase in temperature between 70 and 600 s is small (a maximum of 60°C for TC 2), confirming that a thickness of 15 mm of cork provides sufficient protection to the backing. The benefits of using phosphorylated cork are low considering MLC testing.

3. Fire behaviour of LS P-cork based structure on the small-scale radiant panel test

To complete the characterization of the FR properties of LS P-cork, the fire behaviour of the S – P-cork structure has been evaluated on the small-scale radiant panel test previously developed. Results were compared to those of S – Cork structure. Table 48 gathers the results obtained for the specimens exhibiting the worse fire behaviour, i.e. the longer distance and thus, the lowest CHF, among the three specimens tested for each turf structure (S-cork and S – P-cork).

Table 48: Results obtained with the small-scale EN ISO 9239-1 test for both cork-based artificial turf structures.

Parameters	Sample S – Cork	S – P-cork
Flame front position on extinction (mm)	150	100
Percentage of burnt length (%)	44	30
Burning time (s)	668	623
CHF (kW/m²)	4.3	7.0
Class	D_{FL}	C_{FL}
Smokes rate	S1	S1

First, the 'running flame' phenomenon, visible during the previous tests on cork-based and TPE-based structures (**Chapter 2**), is also noticeable in the case of the S – P-cork structure. Indeed, the flame propagates very quickly at the extreme surface and along the entire length of the sample in less than 3 min. Then, the flame front goes back towards the hotter end and then the sample continues to burn over a certain distance (100 mm for the S – P-cork structure). The part before the orange line on the pictures of the samples collected after the tests (**Figure 44 (b)**) is deeply degraded. In **Chapter 2**, in the case of cork-based structure, this 'running flame' phenomenon was neglected because the flame only burnt the extreme surface of the sample and this effect was considered to be non-representative of the real fire behaviour. The same approach was adopted for the phosphorylated cork samples (degraded part in **Figure 44 (a)**), leading to the values given in Table 48. Thus, the best behaviour in terms of flame spread is obtained with the S – P-cork structure since only 30 % of the sample length is burnt in a short time (slightly more than 10 min), leading to a C_{FL} rating. These results show that cork phosphorylation permits to significantly reduce the burnt length of the structure (33 % decrease

compared to S–cork structure). The improvement of the fire properties allows reaching a C_{FL} rating and to meet the EN ISO 13501-1 regulation for indoor applications.
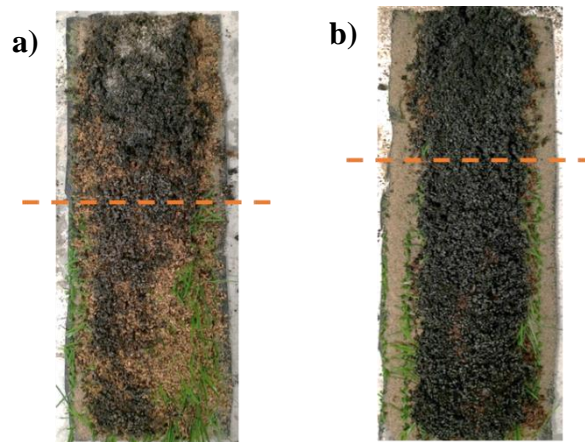
Figure 44: Residues after small-scale radiant panel tests of (a) cork-based structure and of (b) S – P-cork structure. Orange line: flame front position

C. Conclusion

The FR properties of phosphorylated cork, alone and inside the turf structure, were thus evaluated using MLC and small-scale radiant panel tests. MLC results show that no significant improvement in the fire behaviour of LS P-cork alone is observed compared to virgin cork alone but **a slight increase in TTi and a decrease in THR** is observed for the S – P-cork structure compared to S – Cork. Moreover, investigation with thermocouples highlighted that heat spreads relatively evenly through the sample, as for each measurement time, comparable temperature values are recorded by the three TC. Thus, as the heat flow through the cork thickness is similar between the two cork-based structures, phosphorylation does not seem to change the thermal protective behaviour and conductivity of cork. Thus, considering MLC testing, phosphorylation does not significantly change the thermal characteristics of cork [91], [92] nor its combustion behaviour. It **is assumed that the charring phenomenon compensates the alteration of the chemical and structural properties of cork shown in Chapter 3, leading to comparable results at MLC test.** On the other hand, **a significant decrease in the burnt length at the small-scale radiant panel test was observed, leading to a lower CHF and therefore a better rating (C_{FL} compared to D_{FL}). Phosphorylation thus permits to meet the Euroclass requirements, allowing the use of such turf structures for sports applications to be considered**.

Thus, as improved fire properties are obtained with the small-scale radiant panel test, it is necessary to understand the behaviour of phosphorylated cork during the combustion process. The purpose of the next part of this chapter is to further characterize the modified cork when subjected to high temperatures.

II. Influence of temperature on the properties of LS P-cork

The aim of this section is to evaluate the behaviour of LS P-cork as a function of temperature in order to better understand the role played by LS P-cork during the fire tests. Characterizations such as TGA or solid-state NMR were carried out to provide further information on the degradation process of phosphorylated cork when heated up.

A. Thermogravimetric analyses of cork and LS P-cork

TGA was carried out to determine the evolution of mass loss of LS P-cork compared to that of virgin cork and thus the degradation of cork materials as a function of temperature. TGA curves giving the evolution of weight versus time and the DTG curves for both virgin and phosphorylated corks are shown in Figure 27 (a) and Figure 27 (b) respectively. The corresponding data are given in Table 49.
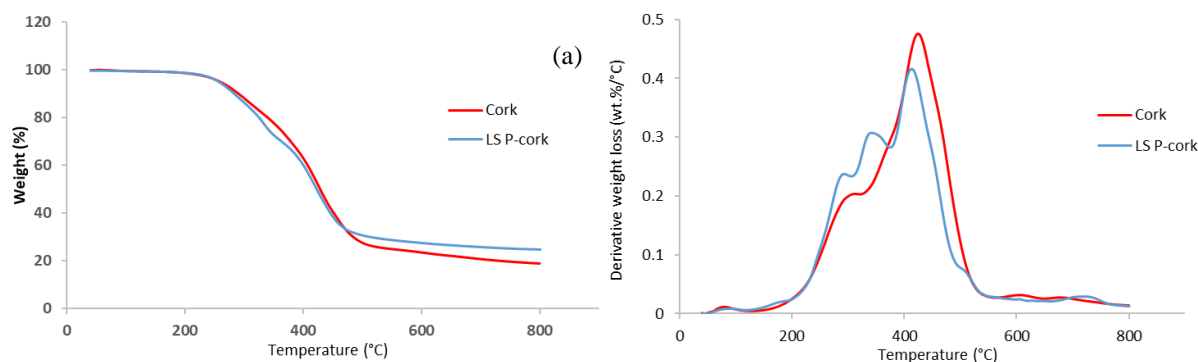
Figure 45: (a) TGA curves and (b) DTG curves of virgin cork and LS P-cork

Table 49: TGA data for virgin cork and LS P-cork.

	$T_{2\%}$ (°C)	T_{MAX} (°C)	Residue at 600°C (%)	Residue at 800°C (%)
Virgin cork	220	429	23.2	18.5
LS P-cork	224	420	27.4	24.7

As previously described (Chapter 3, Section V. A. 1.c. Thermal stability, page 97), the onset of decomposition temperature of virgin cork occurs at 220 °C ($T_{2\%}$) and the maximum degradation

temperature is around 430°C (T_{MAX} = 429°C) (Figure 27 (a)). The residual solid mass fraction is around 18.5 % at 800°C. For LS P-cork, the onset temperature of decomposition shows a similar trend ($T_{2\%}$ = 224 °C) and the maximum degradation temperature is also close to that of virgin cork (T_{MAX} = 420°C). However, LS P-cork shows a lower mass loss from 400°C and the final residual mass fraction obtained at 800°C is 34% higher (24.7% vs 18.5% for virgin cork). The DTG curves (Figure 27 (b)) allow seeing that decomposition occurs differently for virgin cork and LS P-cork. Two decomposition steps can be observed for virgin cork with maximum decomposition rates around 300°C and 430°C respectively. Those degradation steps were previously described and assigned: the first step can be attributed to hemicelluloses degradation (temperature range 220-315°C [225]) and the second step, with a broad degradation area, corresponds to suberin and lignin degradation (230-490°C and 160-900°C respectively [225], [226]). On the contrary, for LS P-cork, three decomposition steps can be observed, with maximum decomposition rates around 300°C, 330°C and 420°C respectively. Thus, an additional degradation step is noticeable for LS P-cork compared to virgin cork. Without determination of the degradation products, this additional peak can hardly be assigned. However, since the maximum temperatures of the first and third steps of LS P-cork are similar to the maximum temperatures of the two degradation steps of virgin cork, it could be assumed that the second peak of LS P-cork can be due to the degradation of the phosphorus structure. This assumption is plausible since literature reports the degradation of phosphate ester in the same temperature range [242]. As an example, in a work carried out by Delobel [243], the evolution of the char in an intumescent system containing ammonium pyrophosphate is analysed. Solid state ^{13}C NMR spectra revealed the presence of aromatic structures around 340 °C related to the decomposition of phosphate ester.

In order to confirm this hypothesis and to better understand the degradation mechanism of LS P-cork, thermal treatments were carried out at various temperatures and the obtained residues were characterized using ^{13}C and ^{31}P NMR. The results are discussed in the next section.

B. Solid state nuclear magnetic resonance spectroscopy of cork and LS P-cork

Virgin cork and LS P-cork samples were submitted to a heat treatment at different temperatures, *i.e.* HTT = 200°C, 300°C, 400°C, 500°C and 600°C, in a furnace. The residual masses of cork and LS P-cork (%) as a function of temperature (HTT) are given in Table 50. In addition to a lower final residual mass for virgin cork compared to LS P-cork (i.e. 1 % compared to 9.4 %),

the residual masses obtained at intermediate temperatures are also systematically higher for the modified cork. On the other hand, the standard deviations of the modified cork are greater, this was also noted in **Chapter 3** (Section V. C. 3.b. Carbonization rates of LS P-cork, page 114) concerning the standard deviation of the carbonaceous residue of the LS P-cork at 600°C and was attributed to a quite low homogeneous grafting of phosphorous during phosphorylation reaction.

Table 50: The residual masses of cork and LS P-cork as a function of temperature (HTT).

	HTT					
	Room temperature	200°C	300°C	400°C	500°C	600°C
Cork	0.139*	94.2	91.4	64	19.4	1
	± 0.02	± 1.2 %	± 1 %	± 1 %	± 0.7 %	± 0.4 %
LS P-cork	0.163*	96.3	93.3	68.7	34.4	9.4
	± 0.02	± 1.3 %	± 1 %	± 1.2 %	± 1.3 %	± 1.5 %

*Initial mass (g)

Solid state ^{13}C NMR and ^{31}P NMR spectroscopies were carried out on heat treated corks in order to study the evolution of the structure as a function of temperature.

1. Characterization of cork and LS P-cork versus temperature using solid-state ^{13}C NMR

Figure 46 (a) and (b) show the ^{13}C NMR spectra of both heat-treated cork and heat-treated LS P-cork respectively. The assignments of signals are given in Table 42.
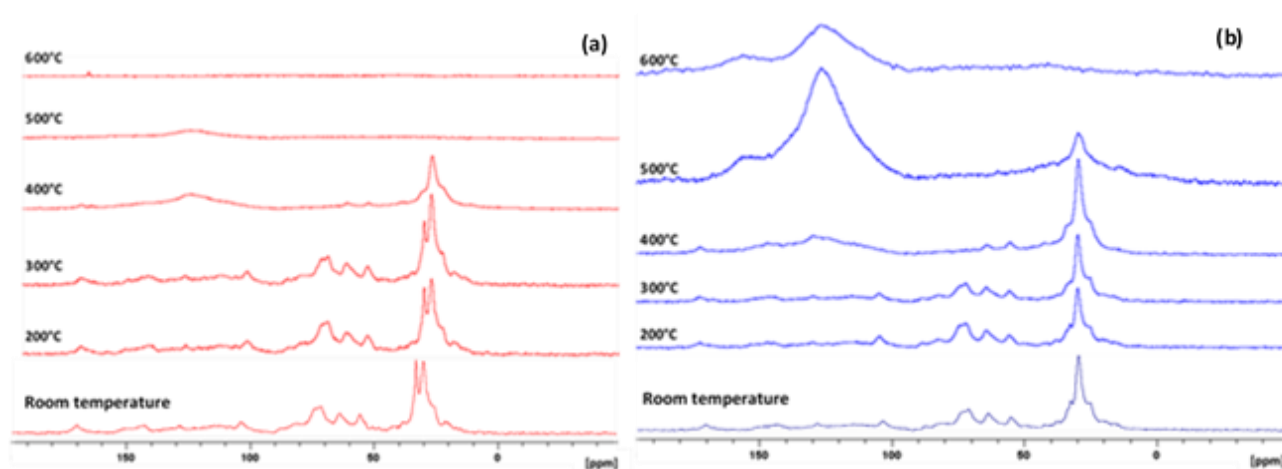
Figure 46: Solid state ^{13}C NMR spectra of (a) virgin cork and (b) LS P-cork at room temperature and after HTT = 200°C, 300°C, 400°C, 500°C and 600°C

At 200°C and 300°C, the spectra of virgin cork and LS P-cork are similar as the ones observed at room temperature [233], [234]. Then from 400°C, the increase in temperature leads to the degradation of cork and LS P-cork structures. Degradation of the carbohydrate structures (25-33 ppm and 65-105 ppm), as well as parts of lignin and suberin (56 ppm and 172 ppm respectively) is progressively observed. It should be mentioned that the degradation of phosphorylated cork is less pronounced as the intensity of the peaks decreases less rapidly for LS P-cork than for virgin cork, indicating a better stability of the modified cork at these temperatures. Indeed, up to 500°C, part of the aliphatic carbons (25-33 ppm) of LS P-cork is preserved while they are no longer observed at 500°C in the virgin cork. On the other hand, a large peak centred at 130 ppm appears for both corks, corresponding to aromatic carbons, highlighting the aromatisation phenomenon. This signal is significantly more intense for LS P-cork compared to virgin cork when temperature increases (at 500 and 600°C). This result demonstrates that a charring phenomenon is favoured in the case of phosphorylated cork, leading to the formation of a thermally stable residue. The assumption previously proposed regarding the decomposition of phosphate esters is therefore verified and observations are consistent with TGA results. Furthermore, the shoulder at 160 ppm, visible from 500°C on the LS P-cork spectra, represents the start of oxidation of the residue due to oxidative conditions. The intensity of this shoulder is low thanks to the action of phosphorus, known to limit the oxidation of aromatic structures [244]. Finally, at 600°C, the virgin cork structure is completely degraded as there is no signal on the spectrum. On the contrary, the peaks at 130 ppm and 160 ppm are still visible on the LS P-cork spectrum, showing the presence of aromatic species.

Table 51: Chemical shift assignment of ^{13}C SS NMR peaks of cork [233], [234].

Peak (ppm)	Assignation
21	Ester groups of hemicelluloses
25 – 50	Waxes
25 – 33	Methylene carbons of suberin
56	Methoxy groups of suberin, lignin and hemicelluloses
65 – 105	Carbohydrate carbons (hemicellulose and cellulose)
110 – 155	Lignin aromatic carbons
172	Suberin ester groups
110 – 160	Lignin and polyphenols

2. Characterization of cork and LS P-cork versus temperature using solid-state ^{31}P NMR

Solid state ^{31}P NMR spectra of cork, heat treated at 600°C, and of LS P-cork, heat treated at HTT = 200°C, 300°C, 400°C, 500°C and 600°C, are presented in Figure 47 and Figure 48 respectively. For virgin cork, the spectra for HTT = 200°C, 300°C, 400°C and 500°C are not given since no signal is visible at these temperatures.

Table 52 shows the assignments of peaks corresponding to the common phosphorus functional groups.
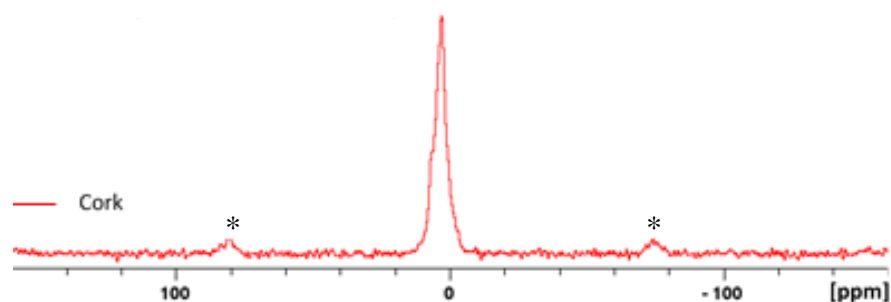
Figure 47: Solid state ^{31}P NMR spectra of cork after HTT = 600°C. spinning side band*

Table 52: Chemical shift assignment of common phosphorus functional groups. [235], [236].

Peak (ppm)	Assignation
15 – 30	Phosphonate
10 – 0	Phosphate monoester
5 – 0	Orthophosphate
0	Phosphoric acid
0 – (-5)	Phosphate diester
(-5) – (-10)	Pyrophosphate
(-15) – (-30)	Polyphosphate

The spectrum of the virgin cork residue at 600°C shows an intense peak centred around 3 ppm, indicating the presence of phosphate bonds. At this temperature, only ashes remain and it can be assumed that the amount of phosphorus increases due the concentration of minerals into the very low residue, since only the mineral part is not degraded at 600°C. Finally, as the rotation speed was set at 12.5 kHz, the peaks around 80 ppm and -75 ppm (indicated by asterisks in Figure 47) are attributed to the spinning side bands of the signal observed at 3 ppm.

139

In the case of LS P-cork, the spectrum at 200°C is similar to that obtained at room temperature, demonstrating that at this temperature the modified cork has not yet started to degrade (Figure 48). Two peaks are observed and correspond to the presence of phosphoric acid or orthophosphates linked to aliphatic carbons (band centred at -1 ppm) and to the presence of phosphonates (band at 15 ppm). After a 300°C thermal treatment, the same species are observed but the intensity of the two peaks is reversed compared to the first two spectra: the peak corresponding to phosphonates is more intense than that of orthophosphates. At 400°C and 500°C, the signals are no longer clearly defined: the band assigned to phosphonate gradually disappears whereas the one corresponding to phosphate progressively broadens towards negative ppm values (from 0 to -30 ppm). Thus, **from 400°C, a condensation phenomenon of the phosphorous structure is evidenced.** Then, at 600°C, a large band containing three peaks is observed. The peak around 0 ppm is attributed to phosphoric acid or orthophosphate linked to aliphatic structures, the one at around -9 ppm to pyrophosphates or orthophosphates linked to aromatic carbons and finally, at -25 ppm, the peak is due to the formation of polyphosphates. Thus, **the condensation phenomenon increases as the temperature rises since the stabilisation of the system is evidenced at high temperature, i.e. from 600°C**. This phenomenon is usually observed in the case of intumescent structures [245]–[249].
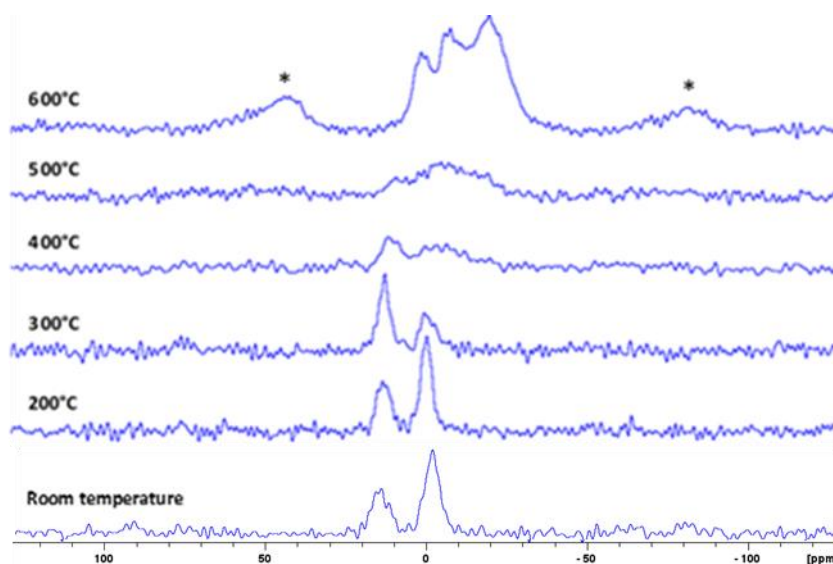
Figure 48: Solid state ^{31}P NMR spectra of LS P-cork at room temperature and after HTT = 200°C, 300°C, 400°C, 500°C and 600°C

C. Phosphorus content of cork and LS P-cork at 600°C

To complete the NMR characterizations of cork and LS P-cork versus temperature, the phosphorus content was determined for the residue collected at 600°C. The aim is to determine the amount of phosphorus in both degraded corks in order to assess the evolution of the

phosphorus content according to temperature. The amount of phosphorus into heat-treated corks at 600°C was determined by ICP-AES and compared to the amount into cork and LS P-cork at room temperature. Results are given in Table 53.

Table 53: Phosphorus content of the both heat-treated cork and LS P-cork at room temperature and at 600°C.

	Phosphorus amount (%)	
	At room temperature	At 600°C
Cork	0.03	0.10
LS P-cork	0.21	0.77

At 600°C, the amount of phosphorus in LS P-cork is almost eight times higher than the one in virgin cork. Moreover, higher phosphorus amounts are obtained after degradation for both cork and LS P-cork, being more than 3 times higher at 600°C than at room temperature. It shows that the phosphorylation process was efficient to increase the stability of cork at high temperature. It also demonstrates that phosphorus participates to the aromatisation of the structure and favour it. Thus, these results are consistent with ^{31}P NMR results showing the condensation phenomenon of the phosphorus system at high temperature.

D. Conclusion

TGA, ^{13}C and ^{31}P NMR analyses were carried out to have information on the degradation of phosphorylated cork as a function of temperature. It was mainly show that even if the characteristic temperatures of degradation of cork are only slightly affected by the phosphorylation reaction, the mechanism of degradation differs. An aromatisation process was demonstrated (Figure 48), leading to the formation of a solid residue at high temperature (condensation of the system). This significant charring phenomenon is due to phosphorylation and leads to a better thermal stability at high temperatures. These results were confirmed by the higher amount of phosphorus in the residue of phosphorylated cork at 600°C (Table 53).

The next section is intended to describe the mechanisms of action involved during LS P-cork degradation based on the mechanisms of action of phosphorus flame retardants reported in the literature.

III. Mechanisms of action of P-cork

The mechanisms of action describe all the mechanisms occurring during the combustion of a material. The aim of this section is to explain the mechanisms of action involved during the

combustion of phosphorylated cork. Results obtained from TGA and NMR analyses will be combined with the results of the fire tests (MLC and radiant panel) to propose a mechanism of action for the phosphorylated cork.

A. Modes of action of phosphorus flame retardants – State of the art

In a first step, a review of the modes of action of phosphorus flame retardants is performed. As briefly presented in **PART I** (Table 3, page 15), phosphorus FRs can act in the gas phase and/or in the condensed phase.

1. Action in the condensed phase

In the condensed phase, phosphorus compounds act mainly <u>physically</u> by promoting the carbonization of the material leading to the formation of a protective phosphorus-carbon layer providing flame protection for the part of the material underneath the carbonized layer (referred as the underlayer), and by providing thermal insulation and reduction of heat and mass transfer to the underlayer.

The char layer must have certain characteristics in order to effectively protect the material: high cohesion, low porosity and sufficient thickness are necessary to achieve a positive effect on the fire behaviour of the material [33]. Moreover, the carbonized layer is mainly composed of carbon in the form of aromatic compounds, and of other heteroatoms such as oxygen, nitrogen and phosphorus [250]. The relative proportions vary depending, among other things, on the chemical composition of the polymer and of the flame retardant, on the decomposition temperature and the atmosphere. A general chemical mechanism for the formation of the carbonized layer is reported in the literature. It is generally accepted that during decomposition, the phosphorus in the FR is transformed into phosphoric acid and then into polyphosphoric acid. The first dehydroxylation step leads to the formation of unsaturated carbon structures, transformed into polyaromatic structures by a Diels-Alder cyclisation reaction [242], [251], [252] shown in Figure 49.

Figure 49: Cyclisation reaction Diels-Alder. Extracted from [242]

On the other hand, molecules such as orthophosphoric and pyrophosphoric acids are transformed into metaphosphoric acid $(O)P(O)(OH)$ and its polymers $(PO_3H)_n$. The pyrophosphate and polyphosphate anions created during decomposition can then participate in the formation of a carbon structure (char) [69].

2. Action in the gas phase

During the decomposition of the material, free radicals (notably $H°$ and $OH°$) are formed and generate exothermic reactions that help to keep the flame active. However, the mechanisms involving gas phase flame retardants are generally radical mechanisms. The molecules of phosphorus-containing FRs decompose leading to the formation of phosphorus-based radicals ($PO°$, $HPO°$, $HPO_2°$) that could trap the free radicals $H°$ and $OH°$ and decrease the energy of the combustion reaction. These reaction lead to the formation of inactive chemical compounds such as water that can dilute the reaction medium or smother the flame [33]. The main free radical reactions occurring in the gas phase for phosphorus-based compounds are presented from Equation 11 to Equation 16 [51].

Equation 11	$$PO° + H° \rightarrow HPO$$
Equation 12	$$PO° + OH° \rightarrow HPO_2$$
Equation 13	$$HPO + H° \rightarrow H_2 + PO°$$
Equation 14	$$OH° + H_2 + PO° \rightarrow H_2O + HPO$$
Equation 15	$$HPO_2° + H° \rightarrow H_2O + PO$$
Equation 16	$$HPO_2° + H° \rightarrow H_2 + PO_2$$
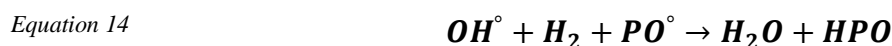
3. Mode of action in both phases

It should be noted that depending on the degree of oxidation of phosphorus, activity in the condensed phase or in the gas phase is favoured: the higher the degree of oxidation, the more favoured the condensed phase mechanism and inversely [253], [254]. Thus, phosphates (+V) mainly act in the condensed phase, while phosphonates (+III) tend to act in the gas phase. Figure 50 illustrates and summarises the action of phosphorus flame retardants in the gas and condensed phases and the associated physical effects.
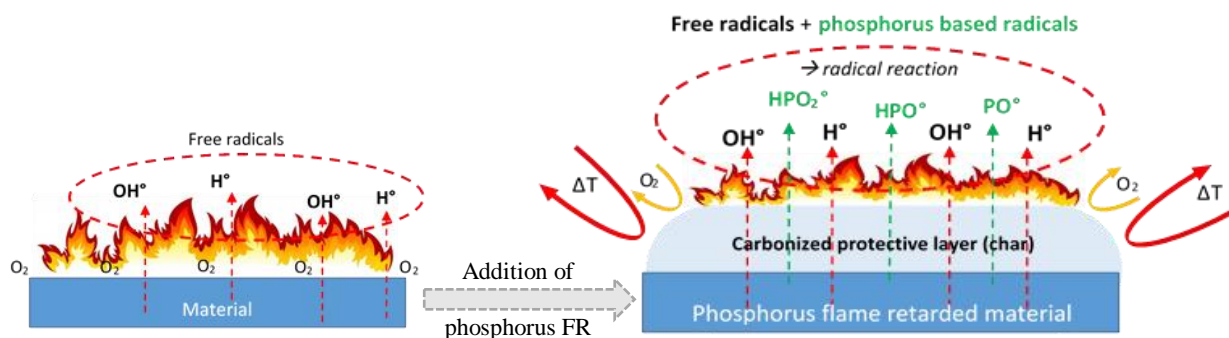
Figure 50: Action of phosphorus flame retardants in the gas and condensed phases

B. Mechanisms of action of phosphorus in phosphorylated cork

Firstly, MLC tests of phosphorylated cork and phosphorylated cork-based artificial turf structures show an increase in TTi is visible, i.e. + 9 s and + 12 s respectively compared to virgin cork and S – cork. This delay in ignition time has previously been attributed to a gas phase phenomenon. Indeed, as explained in the previously literature review, it can also be assumed that the phosphorus-based radicals released by phosphorylated cork (PO°, HPO°, HPO2°) trap the highly reactive radicals resulting from the combustion of the material (OH° and H°), leading to the modification of the degradation mechanisms, in particular via the dilution of gases in the environment. Additional time is then required to reach the critical temperature required for ignition. As the gas phase has not been studied, this hypothesis cannot be verified. Then, after ignition, the material degrades strongly. Cork granules highly blacken and start to char: a thick phospho-carbonaceous layer, protecting the underlayer from the flame, gradually appears and spreads to all cork granules. As explained in the previous section, this layer limits heat transfers by providing an insulating action to the underlayer and gas transfer is also limited between the flame and the released gases. Considering the standard deviations, the presence of phosphorus compounds in the cork structure do not seem to have any effect on the pHRR, the values being similar between the virgin and the fireproofed structure and between virgin cork and LS P-cork. Although the presence of the protective barrier (char) created in the condensed phase is supposed to modify the thermal transfers, the study of the temperatures recorded at the backing surface for the turf structures proves that the heat spreads in an equivalent way whatever the cork used. It can therefore be concluded that no positive impact of using phosphorylated cork in the turf structure is demonstrated in the condensed phase. The 21% decrease in THR for S - P-cork compared to S – Cork is assumed to be attributed to the radical action in the gas phase of phosphorylated cork limiting the energy

transfer to the material and thus the decomposition of the whole structure. Finally, although charring reduces the burning rate of the infill [241], the presence of phosphorus does not positively impact the burning times. In the case of the radiant panel test, the same phenomenon take place. The condensed phase action promotes the formation of a thick carbonized layer limiting heat and mass transfer and thus limiting flame spread (i.e. 33% reduction in the burnt length for S - P-cork compared to S - Cork). It can be assumed that gas phase action also takes place and allows the trapping of free radicals, thus leading to a slower rate of flame spread. However, no characterization has been carried out to validate this assumption.

Secondly, thermal characterizations were carried out. ^{31}P NMR analyses highlight the presence of phosphonate groups from room temperature up to 400°C. The radical action in the gas phase, previously assumed, would thus be facilitated at the beginning of the combustion by the presence of these species of lower oxidation degree (influence on the TTi for example as previously supposed). Then, at higher temperature, the action in the condensed phase seems to be favoured with the progressive appearance of new species considered to be more thermally stable than phosphate ester, namely phosphoric acid, pyrophosphates or orthophosphate linked to aromatic structures as well as polyphosphates (at 0 ppm, -9 ppm and -25 ppm respectively). The ^{13}C NMR study show an aromatisation of the material when the temperature increases that can be linked to the progressive blackening of cork granules observed during the fire tests. Thus, from 400 °C, the condensation of the system is highlighted. Moreover, only phosphate groups or derivatives are still present in the thermally stable residue, promoting further action in the condensed phase (+V degree of oxidation). These results are consistent with those obtained with TGA, showing a lower mass loss for LS P-cork from 400°C (formation of the protective layer in the condensed phase, evidenced with ^{31}P NMR by the peak at 130 ppm showing the beginning of the aromatization) but leading to a higher amount of residue at 800°C. Finally, the amount of phosphorus detected in LS P-cork at 600°C is more than 3 times higher than at room temperature. It is assumed that the condensation of the phosphorus system in the condensed phase, evidenced with ^{31}P NMR, leads to a significant increase in the amount of phosphorus in the fireproofed heat-treated cork.

IV.   Conclusion of Chapter 4

In this chapter, the fire behaviour of LS P-cork based structure was evaluated. Slight improvements in the fire behaviour in terms of TTi and THR were found using MLC test compared to the S – Cork structure. For the small-scale EN ISO 9239-1 test, a fast flame spread at the surface of the sample is observed. However, as this surface flame spread (running flame

phenomenon) had not been considered in the case of virgin cork-based structures (**Chapter 2**), only the severely degraded part of LS P-cork based structure was considered. In this case, only 30 % of the length of the structure was burnt, thus achieving a C_{FL} rating. Considering the results of **Chapter 3** regarding the ageing in water of phosphorylated cork, it can be concluded that phosphorylated cork-based artificial turf structures should be suitable for indoor use and comply with the European fire safety regulation [10]. Testing the S – P-cork structures on the large-scale EN ISO 9239-1 test appears now to be crucial to confirm the C_{FL} rating.

Thermal characterizations with TGA and ^{13}C and ^{31}P NMR analyses highlighted that cork degrades more quickly than phosphorylated cork from 400°C and has a lower thermal stability, especially because LS P-cork shows an improvement in the charring phenomenon leading to a significantly higher residual mass at high temperature.

Based on those results, mechanisms of action for LS P-cork have been proposed. Despite the absence of characterizations in the gas phase, it can be reasonably assumed that phosphorus compounds used for the fireproofing of cork generate a radical action in the gas phase, leading to the trapping of free radicals, to the dilution of gases in the environment and to the modification of degradation mechanisms. The action in the condensed phase is also clearly visible since a thick and dense carbonized layer gradually appears at the surface of cork granules as the temperature increases. This protective layer also leads to limit heat and mass transfers.

Key points of Chapter 4

✓ Phosphorylation led to an increased charring phenomenon leading to a significantly higher residual mass at high temperature

✓ At MLC test:
  ➢ Slight improvements in terms of TTi and THR for S – P-cork structure are observed compared to the S – Cork structure.
  ➢ Equivalent insulating properties between both corks are demonstrated.

✓ At the small-scale EN ISO 9239-1 test:
  ➢ A running flame phenomenon is observed for both corks
  ➢ LS P-cork based structure shows better performances
    ▪ 30% of burnt length compared to 44% for virgin cork
    ▪ C_{FL} rating is achieved
    ▪ Should be suitable for indoor uses

✓ Mechanisms of action of LS P-cork:
  ➢ In the gas phase: radical action with the:
    ▪ Trapping of free radicals
    ▪ Dilution of gases in the environment
    ▪ Modification of the degradation mechanisms.
  ➢ In the condensed phase:
    ▪ Condensation of the phosphorus system
    ▪ Thick and dense phospho-carbonaceous layer leading to changes in heat and mass transfers and to a thermally stable residue.

PART IV - General conclusion and outlook

The aim of this PhD work was to improve the fire behaviour of artificial turf structures intended for sports applications using innovative, environmentally and health friendly processes to ensure fire safety for users. Artificial turf is considered as a flooring material whose fire behaviour must comply with the EN ISO 13501-1 European standard for building products. In this Euroclass system, the EN ISO 9239-1 radiant panel test has to be performed. This fire test allows determining the critical heat flux (CHF), corresponding to the furthest extent of flame spread, of horizontally-mounted flooring systems exposed to a flaming ignition source within a test chamber. The specimen is exposed to a defined heat flux mapping and the progress of the flame front along the specimen length is recorded for a maximum of 30 min. The smoke development during the test is also measured. Finally, from the CHF, a rating is defined. The targeted specification in the GRASS project corresponds to **a C_{FL} rating and a smoke rate lower than 750 %.min (s1 rate) to allow indoor use of the structures**. In order to follow an eco-responsible approach, the use of toxic flame retardants was banned and halogen-free as well as nanoparticle-free additives were considered. Moreover, as ECHA is currently debating on the prohibition of the use of micro-plastics for this kind of application, the use of natural infill was favoured over traditional petroleum-based infills.

One of the major obstacles to the development of artificial turf structures for indoor use is the lack of information on its fire behaviour. As very little literature is available on the subject, the first step of this PhD work was to study the fire behaviour of artificial turf structures using the MLC test, considering first each component separately and then the whole structure. Results showed that the infill layer had the greatest impact on the overall fire behaviour of the structure and the infill material allowing to obtain the lowest heat release rate and the shortest burning time was cork. Moreover, cork is the only infill material of natural origin and the only bio-degradable one among all those tested (i.e. SBR, EPDM and TPE), thus allowing an eco-friendlier approach. Finally, as the use of micro-plastics should be banned in the near future, cork was selected as the most relevant infill to achieve the objectives of this work. Additional experiments performed on the MLC test allowed determining that a 15 mm cork layer thickness was optimal to avoid the degradation of the backing and to limit heat transfer during combustion.

MLC was used as a first approach to study the fire properties of turf structures because this bench-scale test allows collecting a lot of information on the behaviour of materials during combustion. However, the fire regulation relative to floor coverings requires that artificial turf structures be tested according to the standardised EN ISO 9239-1 test. But the radiant panel test involves the use of large amounts of material (sample size (1050 ± 5) mm $\times$ (230 ± 5) mm), thus hindering the development of new fire-retardant turf structures. To overcome this drawback, the radiant panel test was reproduced on a small scale, i.e. a $^1/_3$ reduction. The experimental design methodology was implemented to transpose the heat flux mapping of the standard radiant panel test to the small-scale test. Then, fire properties of artificial turf structures were evaluated on the developed bench-scale device and the results were compared to those obtained at large scale (tests carried out by one of the GRASS partners, the University of Ghent). During the tests, a "running flame" phenomenon was observed at the surface of some samples but was not considered to determine the classification of the samples as it was not representative of the real fire behaviour. The same CHF were observed for most structures between the two scales: the SBR-based, EPDM-based and TPE-based structures had an E_{FL} rating and the FR EPDM-based structure had a B_{FL} rating at both scales. Finally, the 15 mm cork-based structure exhibited a better rating at small scale, i.e. a D_{FL} rating against a E_{FL} rating at large scale. Further tests were therefore carried out on 10 mm and 20 mm cork-based structures in order to better understand the reason for this difference. For these other two thicknesses, the same CHF and thus the same rating as observed at large scale were obtained (E_{FL}). It can therefore be assumed that the difference in classification with 15 mm of cork is due to the nature of the infill material itself, the variability of cork properties (natural compound with a high variability in structure and composition) being able to affect the fire behaviour of the overall structure. As a result of these tests, the reproduction of the radiant panel test at reduced scale was validated and further used in the study.

By gathering the results obtained with the two fire tests, it appeared that the infill is the component with the greatest impact on the overall fire performance of the structure and **the use of a flame-retardant infill is essential to improve the fire performance of artificial turf structures to reach at least a C_{FL} classification.** The fireproofing of cork granules was considered to improve the fire behaviour of the infill and therefore of the whole structure. First, an in-depth literature survey was carried out on cork (origin, composition, processing, etc.) and on the fireproofing methods used to flame retard natural materials such as cellulose or lignin. A fireproofing strategy was then defined: bulk modification of cork granules by means of phosphorylation, a method consisting of functionalizing the free hydroxyl (-OH groups) present

in the cork structure with phosphorus compounds. Since this approach is reported as efficient to improve the carbonization phenomenon of systems, a protective behaviour of the modified cork should be expected during combustion. **The phosphorylation of cork granules has never been reported in the literature, making this work innovative.** Three phosphorylation protocols were developed and adapted to the fireproofing of cork. Modified corks were characterized in terms of grafting efficiency and yield, leading to the selection of the protocol that uses phosphoric acid, triethyl phosphate, phosphorus pentoxide as phosphorus source, and ethanol as solvent. Extensive work was carried out to optimize the phosphorylation conditions and dimensional analysis was then implemented to upscale the reaction. A large amount of modified cork was obtained, allowing the characterization after large-scale phosphorylation: it was shown that higher grafting rate (50% increase in the carbonization rate) and similar yield than those obtained at small scale were obtained. The upscaling procedure was therefore validated and the phosphorylation reaction was extensively carried out in order to obtain the required amount of phosphorylated cork allowing the MLC and small-scale radiant panel tests to be performed.

Finally, the fire behaviour of phosphorylated cork was evaluated using MLC test and that of the phosphorylated cork-based structure was evaluated using both MLC and small-scale radiant panel tests. When used alone, phosphorylated cork did not lead to any improvement since the heat release rate was similar to the one obtained for virgin cork. When added in the whole turf structure, slight improvements are achieved in terms of TTi and THR compared to the virgin cork-based structure. Thus, **in terms of heat release rate, the benefits of phosphorylated cork are small.** However, the use of phosphorylated cork in the turf structure leads to a significant reduction in the flame spread at the small-scale radiant panel test, i.e. only 30% of burnt length for the modified cork-based structure compared to 44% with virgin cork, thus leading to a lower CHF and a better classification of the fireproofed structure (C_{FL} against D_{FL}). Thus, **cork phosphorylation allows a significant improvement of the fire properties of artificial turf, and thus the use of the fireproofed structure for indoor applications can be considered.**

Finally, the mechanisms of action of phosphorylated cork were studied in order to better understand what happens during combustion. More precisely, the influence of temperature on the properties of phosphorylated cork was analysed using TGA and solid-state NMR. Even if no gas-phase analysis has been carried out, it was assumed that phosphorus radicals were formed during the first phase of combustion (before 400°C, promoted by the presence of phosphonate groups), leading to a trapping action through radical mechanisms in the gas phase.

On the other hand, analyses also revealed a condensation of the phosphorus system at high temperature, leading to changes in heat and mass transfers and to a lower mass loss than for virgin cork. It was thus also possible to demonstrate that a dense, solid and thermally stable phospho-carbonaceous residue was formed. A protective behaviour through the formation of a condensed structure could thus be suspected and is promoted by the presence of phosphate groups appearing in higher proportion in the second phase of the combustion of modified cork. This was confirmed by observation of the materials collected after the fire tests (char layer at the surface of samples after testing).

At the end of this work, **several perspectives** appear. Firstly, it seems essential to test phosphorylated cork-based artificial turf structures on the large-scale EN ISO 9239-1 radiant panel in order to confirm the results. To perform these tests, much higher amounts of phosphorylated cork are required and larger scale production is thus needed, using very large reactors. The first dimensional analysis carried out in this work will be helpful to further upscale the process. On the other hand, analysing the gases evolved during fire tests (or at least during thermal degradation of the materials) would make it possible to confirm the assumptions previously made on the mechanisms of action of phosphorylated cork in the gas phase. Finally, the pile can contribute to the propagation of fire or, on the contrary, can play a "barrier" role, for instance through the formation of an intumescent layer if it is fireproofed. To be used into the pile, the flame-retardant additives should be environmentally and health friendly. In addition, in order to allow polyethylene (PE) fibres composing the pile to be spun, additives have to meet a certain number of criteria, in particular: a thermal stability higher than the processing temperature of PE, i.e. above 200°C (extrusion temperature of LLDPE); a good compatibility with PE without modifying its properties; a low filler content, i.e. a maximum of 10wt.%; and, ideally, an ability to reduce the toxicity of gases and smokes during combustion. Thus, the use of a fire-retarded pile could improve the fire behaviour of the whole turf structure. Finally, the combination of a FR cork infill and a FR pile into the same artificial turf structure could lead to further improvements of the fire properties.

To conclude, this PhD work covered a variety of subjects and areas: **fire characterizations, reproduction of a fire test device at small-scale and innovative synthesis of fire-retardant phosphorylated cork.** The researches carried out have allowed a better understanding of the fire behaviour of artificial turf structures and have allowed developing a FR cork-based artificial turf meeting the fire regulations for indoor use (C_{FL} rating and s1 smoke rate, according to the EN ISO 13550-1 standard). Although this result still needs to be confirmed by testing on the large-scale radiant panel test and although the mechanisms of action should be further

investigated, **the development of this new fireproof artificial turf structure is a major step forward for both the artificial turf industry and the safety of users.**

References

[1] P. Dierkens and A. Fiolet, 'Artificial turf', US20080187689A1, Aug. 07, 2008 Accessed: Apr. 30, 2020. [Online]. Available: https://patents.google.com/patent/US20080187689A1/en?oq=US20080187689A1

[2] R. S. Reddick, 'Filler for artificial turf system', US20150044395A1, Feb. 12, 2015 Accessed: Apr. 16, 2020. [Online]. Available: https://patents.google.com/patent/US20150044395A1/en

[3] R. J. Seaton, 'Artificial turf system', US6491991B2, Dec. 10, 2002 Accessed: Apr. 16, 2020. [Online]. Available: https://patents.google.com/patent/US6491991B2/en

[4] J. C. Benedyk, 'Artificial turf-like product of thermoplastic polymers', US4356220A, Oct. 26, 1982 Accessed: Apr. 16, 2020. [Online]. Available: https://patents.google.com/patent/US4356220A/en

[5] Y. Ishikawa, 'Artificial turf, pile yarn for artificial turf and process and spinneret for producing pile yarn', US005462778A, Oct. 31, 1995

[6] A. Paturel, M. Casetta, S. Rambour, L. Janus, and S. Duquesne, 'Comprehensive study of the fire behaviour of artificial turf - improved and sustainable solutions', *Fire and Materials*, UNDER REVIEW 2021.

[7] 'Twin Lakes playground engulfed in flames', *Juneau Empire*, Apr. 25, 2017. https://www.juneauempire.com/news/twin-lakes-playground-engulfed-in-flames/ (accessed Jul. 30, 2021).

[8] avec AFP, 'Marseille. Un gigantesque incendie en cours dans un entrepôt de garde-meuble', *Ouest-France.fr*, Oct. 06, 2020. https://www.ouest-france.fr/provence-alpes-cote-dazur/marseille-13000/marseille-un-gigantesque-incendie-est-en-cours-dans-un-entrepot-de-garde-meuble-7003690 (accessed Jul. 30, 2021).

[9] SF Parks, *Synthetic Turf Fires - (artificial soccer / football sports fields) sbr crumb*. Accessed: Jul. 30, 2021. [Online Video]. Available: https://www.youtube.com/watch?v=YEFKHuWLgx4&ab_channel=SFParks

[10] 'EN-ISO 13501 – 1: 2010. Fire classification of building products and building elements - Part 1: Classification on the basis of tests of reaction to fire.', 2010, Accessed: Apr. 09, 2021. [Online]. Available: https://www.iso.org/

[11] 'EN-ISO 9239: 2010. Reaction to fire tests for floorings. Part 1: Determination of the burning behaviour using a radiant heat source.', 2010, Accessed: Apr. 09, 2021. [Online]. Available: https://www.iso.org/

[12] 'EN - ISO 11925 - 2: 2020. Reaction to fire tests - Ignitability of products subjected to direct impingement of flame - Part 2: Single-flame source test', *ISO*, 2020, Accessed: Feb. 11, 2021. [Online]. Available: https://www.iso.org/

[13] J. Rodgers, 'Fire resistant artificial turf', US8986807B2, Mar. 24, 2015 Accessed: Apr. 16, 2020. [Online]. Available: https://patents.google.com/patent/US8986807B2/en

[14] S. Lehner, M. Jovic, M. Lienhard, R. Hufenus, and S. Gaan, 'Improving flame retardancy of DOPO-PEPA for polyethylene applications using various thermal stabilizers.', Jul. 2019.

[15] H. Cheng, Y. Hu, and M. Reinhard, 'Environmental and Health Impacts of Artificial Turf: A Review', *Environ. Sci. Technol.*, vol. 48, no. 4, pp. 2114–2129, Feb. 2014, doi: 10.1021/es4044193.

[16] B. Bocca, G. Forte, F. Petrucci, S. Costantini, and P. Izzo, 'Metals contained and leached from rubber granulates used in synthetic turf areas', *Science of the total environment*, vol. 407, no. 7, pp. 2183–2190, 2009.

[17] 'SO.CA.MONT - Société Caoutchoutière de Montaigut-SA', *http://www.socamont.fr*.

[18] 'Avient | Specialty Polymer Formulations'. https://www.avient.com/ (accessed May 06, 2021).

[19] 'SIST-TP CEN/TR 17519:2020 - Surfaces for sports areas - Synthetic turf sports facilities - Guidance on how to minimize infill dispersion into the environment', *iTeh Standards Store*. https://standards.iteh.ai/catalog/standards/sist/78fb251f-346f-40cf-847f-fd98c7f3203e/sist-tp-cen-tr-17519-2020 (accessed Apr. 09, 2021).

[20] 'Astro Turf - The Inventor and Leader of the Synthetic Turf Market.', *https://www.astroturf.com*.

[21] 'RoyalGrass. Why spread sand on artificial grass?' http://www.royalgrass.com/artificial-grass-sand (accessed Mar. 18, 2020).

[22] 'Idée Gazon - Spécialiste gazon synthétique', *Idée Gazon*. https://www.ideegazon.fr/ (accessed Aug. 18, 2021).

[23] 'FieldTurf – a TARKETT sports company : a world leader in artificial turf', *https://fieldturf.com*.

[24] E. G. Xu *et al.*, 'Artificial turf infill associated with systematic toxicity in an amniote vertebrate', *PNAS*, vol. 116, no. 50, pp. 25156–25161, Dec. 2019, doi: 10.1073/pnas.1909886116.

[25] K. Schneider, A. Bierwisch, and E. Kaiser, 'ERASSTRI - European risk assessment study on synthetic turf rubber infill – Part 3: Exposure and risk characterisation', *Science of The Total Environment*, p. 137721, Mar. 2020, doi: 10.1016/j.scitotenv.2020.137721.

[26] R. Massey, L. Pollard, M. Jacobs, J. Onasch, and H. Harari, 'Artificial Turf Infill: A Comparative Assessment of Chemical Contents', *New Solut*, vol. 30, no. 1, pp. 10–26, May 2020, doi: 10.1177/1048291120906206.

[27] 'The European Synthetic Turf Organisation', *https://www.theesto.com/wp-content/uploads/2017/06/2016-crumb-rubber-infill-FAQs-FR.pdf*.

[28] P. Wang, X. Legrand, and D. Soulat, 'Three-Dimentional Textile Preform Using Advanced Textile Technologies for Composite Manufacturing', 2017. doi: 10.5772/intechopen.68175.

[29] 'Tufting Machine for Manufacturing Carpets'. https://www.baneclene.com/Professionals/Content.aspx?xps=NTY0 (accessed Sep. 05, 2021).

[30] Comité Européen de normalisation, 'PN-EN-ISO 15330-1. Sols sportifs - Surfaces en gazon synthétique et surfaces en textile aiguilleté principalement destinées à l'usage en extérieur Partie 1: Spécifications relatives aux surfaces en gazon.', 2013.

[31] J. Sánchez-Sánchez, P. Haxaire, J. Garcia Unanue, J. Felipe, A. Gallardo, and L. Gallardo, 'Determination of mechanical properties of artificial turf football pitches according to structural components', *Journal of sports engineering and technology*, 2017, Accessed: Apr. 16, 2020. [Online]. Available: https://journals.sagepub.com/doi/abs/10.1177/1754337117717803

[32] R. Hufenus, 'Design and Characterization of a Bicomponent Melt-Spun Fiber Optimized for Artificial Turf Applications', 2013. Accessed: Apr. 16, 2020. [Online]. Available: https://onlinelibrary.wiley.com/doi/full/10.1002/mame.201200088?casa_token=S53cyP8B_18A AAAA%3AMWqpouQ6RGfKO_BX6y0lZH9QR50R-OCAG0hHHmBr0gRxzy3TLDRke7VxPyo4yPal9cOumfMjqxSgLY7o

[33] C. VAGNER, M. COCHEZ, H. VAHABI, and M. FERRIOL, 'Chimie de la combustion des polymères et ignifugation', *Ref : TIP100WEB - 'Plastiques et composites'*, Jul. 2016, Accessed: Mar. 17, 2021. [Online]. Available: https://www.techniques-ingenieur.fr/base-documentaire/materiaux-th11/adjuvants-des-plastiques-42138210/chimie-de-la-combustion-des-polymeres-et-ignifugation-af6049/

[34] C. Vovelle and J.-L. Delfau, 'Combustion des plastiques', *Ref : TIP100WEB - 'Plastiques et composites'*, Jul. 1997, Accessed: Mar. 17, 2021. [Online]. Available: https://www.techniques-ingenieur.fr/base-documentaire/materiaux-th11/proprietes-generales-des-plastiques-42152210/combustion-des-plastiques-am3170/

[35] T. R. Hull and B. K. Kandola, 'Polymers and Fire', in *Fire Retardancy of Polymers*, 2008, pp. 1–14. doi: 10.1039/9781847559210-00001.

[36] J. J. Lentini, 'Chapter 2 - The Chemistry and Physics of Combustion', in *Scientific Protocols for Fire Investigation, Protocols*, 2012, pp. 50–58. Accessed: Mar. 17, 2021. [Online]. Available: https://dokumen.pub/scientific-protocols-for-fire-investigation-third-edition-3rd-ed-9781138037014-9781138037021-9781315178097-113803701x-9781351712378-1351712373.html

[37] S. Boryniec and W. Przygocki, 'Polymer Combustion Processes. 3. Flame Retardants for Polymeric Materials', *Progress in Rubber and Plastics Technology*, vol. 17, no. 2, pp. 127–148, May 2001, doi: 10.1177/147776060101700204.

[38] T. Kashiwagi, 'Polymer combustion and flammability—Role of the condensed phase', *Symposium (International) on Combustion*, vol. 25, no. 1, pp. 1423–1437, Jan. 1994, doi: 10.1016/S0082-0784(06)80786-1.

[39] Y. Wang, I. Burgess, F. Wald, and M. Gillie, 'Chapter 5 - Material Properties', in *Performance-Based Fire Engineering of Structures*, CRC Press, 2012, pp. 132–140.

[40] M. Lackner, Á. Palotás, and F. Winter, *Handbook of Combustion: From Basics to Applications*. John Wiley & Sons, 2013.

[41] A. B. Morgan and J. W. Gilman, 'An overview of flame retardancy of polymeric materials: application, technology, and future directions', *Fire and Materials*, vol. 37, no. 4, pp. 259–279, 2013, doi: https://doi.org/10.1002/fam.2128.

[42] S. Bourbigot, R. Delobel, and S. Duquesne, 'Fire behavior of composites', *Tech. ing., Plast. compos*, vol. AM6, no. AM5330, p. AM5330.1-AM5330.12, 2006.

[43] S. T. Lazar, T. J. Kolibaba, and J. C. Grunlan, 'Flame-retardant surface treatments', *Nature Reviews Materials*, vol. 5, no. 4, Art. no. 4, Apr. 2020, doi: 10.1038/s41578-019-0164-6.

[44] J. Brossas, 'Retardateurs de flammes', *Techniques de l'ingénieur. Plastiques et composites.*, 1999, Accessed: May 12, 2020. [Online]. Available: https://www.techniques-ingenieur.fr/base-documentaire/archives-th12/archives-plastiques-et-composites-tiaam/archive-1/retardateurs-de-flammes-am3237/

[45] C. D. Blasi and C. Branca, 'Mathematical model for the nonsteady decomposition of intumescent coatings', *AIChE Journal*, vol. 47, no. 10, pp. 2359–2370, 2001, doi: 10.1002/aic.690471020.

[46] I. S. Reshetnikov, A. V. Antonov, and N. A. Khalturinskii, 'Mathematical description of combustion of intumescent polymer systems', *Combust Explos Shock Waves*, vol. 33, no. 6, pp. 669–684, Nov. 1997, doi: 10.1007/BF02671799.

[47] N. K. Jha, A. C. Misra, and P. Bajaj, 'Flame-Retardant Additives for Polypropylene', *Journal of Macromolecular Science, Part C*, vol. 24, no. 1, pp. 69–116, Jan. 1984, doi: 10.1080/07366578408069971.

[48] S. Shaw, 'Halogenated Flame Retardants: Do the Fire Safety Benefits Justify the Risks?', *Reviews on Environmental Health*, vol. 25, no. 4, Jan. 2010, doi: 10.1515/REVEH.2010.25.4.261.

[49] M. Alaee, P. Arias, A. Sjödin, and Å. Bergman, 'An overview of commercially used brominated flame retardants, their applications, their use patterns in different countries/regions and possible modes of release', *Environment International*, vol. 29, no. 6, pp. 683–689, Sep. 2003, doi: 10.1016/S0160-4120(03)00121-1.

[50] P. A. Cusack, M. S. Heer, and A. W. Monk, 'Zinc hydroxystannate as an alternative synergist to antimony trioxide in polyester resins containing halogenated flame retardants', *Polymer Degradation and Stability*, vol. 58, no. 1, pp. 229–237, Jan. 1997, doi: 10.1016/S0141-3910(97)00055-4.

[51] C. Negrell and R. Menard, 'Retardateurs de Flammes Phosphorés commerciaux pour les polymères', *Techniques de l'Ingenieur*, vol. TIB138DUO, p. af6044, Jul. 2016.

[52] K. A. Salmeia, S. Gaan, and G. Malucelli, 'Recent Advances for Flame Retardancy of Textiles Based on Phosphorus Chemistry', *Polymers*, vol. 8, no. 9, Art. no. 9, Sep. 2016, doi: 10.3390/polym8090319.

[53] S. Wendels, T. Chavez, M. Bonnet, K. A. Salmeia, and S. Gaan, 'Recent Developments in Organophosphorus Flame Retardants Containing P-C Bond and Their Applications', *Materials*, vol. 10, no. 7, Art. no. 7, Jul. 2017, doi: 10.3390/ma10070784.

[54] K. A. Salmeia and S. Gaan, 'An overview of some recent advances in DOPO-derivatives: Chemistry and flame retardant applications', *Polymer Degradation and Stability*, vol. 113, pp. 119–134, Mar. 2015, doi: 10.1016/j.polymdegradstab.2014.12.014.

[55] H. Horacek and R. Grabner, 'Advantages of flame retardants based on nitrogen compounds', *Polymer Degradation and Stability*, vol. 54, no. 2, pp. 205–215, Nov. 1996, doi: 10.1016/S0141-3910(96)00045-6.

[56] X.-P. Hu, W.-Y. Li, and Y.-Z. Wang, 'Synthesis and characterization of a novel nitrogen-containing flame retardant', *Journal of Applied Polymer Science*, vol. 94, no. 4, pp. 1556–1561, 2004, doi: https://doi.org/10.1002/app.20792.

[57] M. Klatt, 'Nitrogen-Based Flame Retardants', in *Non-Halogenated Flame Retardant Handbook*, John Wiley & Sons, Ltd, 2014, pp. 143–168. doi: 10.1002/9781118939239.ch4.

[58] X. Zhang, Q. Shen, X. Zhang, H. Pan, and Y. Lu, 'Graphene oxide-filled multilayer coating to improve flame-retardant and smoke suppression properties of flexible polyurethane foam', *J Mater Sci*, vol. 51, no. 23, pp. 10361–10374, Dec. 2016, doi: 10.1007/s10853-016-0247-3.

[59] H. Pan, Y. Lu, L. Song, X. Zhang, and Y. Hu, 'Construction of layer-by-layer coating based on graphene oxide/β-FeOOH nanorods and its synergistic effect on improving flame retardancy of flexible polyurethane foam', *Composites Science and Technology*, vol. 129, pp. 116–122, Jun. 2016, doi: 10.1016/j.compscitech.2016.04.018.

[60] S.-H. Chiu and W.-K. Wang, 'The dynamic flammability and toxicity of magnesium hydroxide filled intumescent fire retardant polypropylene', *Journal of Applied Polymer Science*, vol. 67, no. 6, pp. 989–995, 1998, doi: https://doi.org/10.1002/(SICI)1097-4628(19980207)67:6<989::AID-APP4>3.0.CO;2-I.

[61] H. Pan, Y. Pan, W. Wang, L. Song, Y. Hu, and K. M. Liew, 'Synergistic Effect of Layer-by-Layer Assembled Thin Films Based on Clay and Carbon Nanotubes To Reduce the Flammability of Flexible Polyurethane Foam', *Ind. Eng. Chem. Res.*, vol. 53, no. 37, pp. 14315–14321, Sep. 2014, doi: 10.1021/ie502215p.

[62] J. W. Gilman, 'Flammability and thermal stability studies of polymer layered-silicate (clay) nanocomposites', *Applied Clay Science*, vol. 15, no. 1, pp. 31–49, Sep. 1999, doi: 10.1016/S0169-1317(99)00019-8.

[63] Y.-C. Li *et al.*, 'Flame Retardant Behavior of Polyelectrolyte−Clay Thin Film Assemblies on Cotton Fabric', *ACS Nano*, vol. 4, no. 6, pp. 3325–3337, Jun. 2010, doi: 10.1021/nn100467e.

[64] R. Horrocks, B. K. Kandola, G. Smart, S. Nazaré, and D. Marney, 'Polypropylene fibers containing dispersed clays having improved fire performance. Part II: characterization of fibers and fabrics from PP–nanoclay blends - Smart - 2008 - Polymers for Advanced Technologies - Wiley Online Library', *Polymers for Advanced Technologies*, vol. 19, no. 6, pp. 658–670.

[65] S. Gaan, G. Sun, K. Hutches, and M. H. Engelhard, 'Effect of nitrogen additives on flame retardant action of tributyl phosphate: Phosphorus–nitrogen synergism', *Polymer Degradation and Stability*, vol. 93, no. 1, pp. 99–108, Jan. 2008, doi: 10.1016/j.polymdegradstab.2007.10.013.

[66] J. Wagner, P. Deglmann, S. Fuchs, M. Ciesielski, C. A. Fleckenstein, and M. Döring, 'A flame retardant synergism of organic disulfides and phosphorous compounds', *Polymer Degradation and Stability*, vol. 129, pp. 63–76, Jul. 2016, doi: 10.1016/j.polymdegradstab.2016.03.023.

[67] K. Xie, A. Gao, and Y. Zhang, 'Flame retardant finishing of cotton fabric based on synergistic compounds containing boron and nitrogen', *Carbohydrate Polymers*, vol. 98, no. 1, pp. 706–710, Oct. 2013, doi: 10.1016/j.carbpol.2013.06.014.

[68] G. Camino, L. Costa, and M. P. Luda di Cortemiglia, 'Overview of fire retardant mechanisms', *Polymer Degradation and Stability*, vol. 33, no. 2, pp. 131–154, Jan. 1991, doi: 10.1016/0141-3910(91)90014-I.

[69] L. Ferry and J.-M. Lopez-Cuesta, 'Retardateurs de flammes RF des matériaux polymères', in *Techniques de l'Ingénieur - Matériaux - Plastiques et composites - Adjuvants des plastiques*, 2016, p. Réf : AM3237 v2. Accessed: Mar. 17, 2021. [Online]. Available: https://hal.archives-ouvertes.fr/hal-02949175

[70] A. B. Morgan and A. Z. Worku, 'Flame Retardants: Overview', in *Kirk-Othmer Encyclopedia of Chemical Technology*, American Cancer Society, 2015, pp. 1–28. doi: 10.1002/0471238961.1522051807011414.a01.pub3.

[71] J. Green, 'Mechanisms for Flame Retardancy and Smoke suppression -A Review', *Journal of Fire Sciences*, vol. 14, no. 6, pp. 426–442, Nov. 1996, doi: 10.1177/073490419601400602.

[72] 'European Chemical Agency (ECHA). Substances restricted under REACH.' https://echa.europa.eu/substances-restricted-under-reach (accessed Mar. 18, 2020).

[73] M. Day, T. Suprunchuk, and D. M. Wiles, 'A Systematic Study of the Effects of Individual Constructional Components on the Flammability Characteristics of a Carpet', *Textile Research Journal*, vol. 49, no. 2, pp. 88–93, Feb. 1979, doi: 10.1177/004051757904900206.

[74] M. M. Hirschler and R. A. Poletti, 'Latex Backcoatings on Polypropylene Carpets: Fire Performance Testing', *Journal of Coated Fabrics*, vol. 19, no. 2, pp. 94–111, Oct. 1989, doi: 10.1177/152808378901900204.

[75] L. Benisek, 'Burning Behavior of Carpets: The Advantages of Wool and Flame-Resistant Wool', *Textile Research Journal*, 1975, Accessed: Apr. 17, 2020. [Online]. Available: https://journals.sagepub.com/

[76] L. Benisek, M. J. Palin, and R. Woollin, 'Fair and Realistic Flammability Tests for Carpets', *Journal of Fire Sciences*, vol. 6, no. 1, pp. 25–41, Jan. 1988, doi: 10.1177/073490418800600102.

[77] J. Diswat, L. Hes, and K. Bal, 'Thermal resistance of cut pile hand tufted carpet and its prediction', *Textile Research Journal*, vol. 1, 2016, Accessed: Apr. 17, 2020. [Online]. Available: https://journals.sagepub.com/doi/abs/10.1177/0040517515612356

[78] W. D. Timmons, 'Fireproofing coating method and product', US2395922A, Mar. 05, 1946 Accessed: Apr. 20, 2021. [Online]. Available: https://patents.google.com/patent/US2395922A/en

[79] R. Crowley, 'Flame-retardant carpet and method of preparing same', US3825464A, Jul. 23, 1974 Accessed: Apr. 20, 2021. [Online]. Available: https://patents.google.com/patent/US3825464A/en

[80] P. S. Minhas and B. Sukornick, 'Flame-retardant carpet and composition for preparing the same', US4061810A, Dec. 06, 1977 Accessed: Apr. 20, 2021. [Online]. Available: https://patents.google.com/patent/US4061810A/en

[81] D. Maples, G. Danker, and D. Campanella, 'Low smoke, low toxicity carpet', US6284343B1, Sep. 04, 2001 Accessed: Apr. 20, 2021. [Online]. Available: https://patents.google.com/patent/US6284343B1/en

[82] W. Kelkheim and M. Rieber, 'Fire-proofing of polyester fibers', US3708328A, Jan. 02, 1973 Accessed: Apr. 20, 2021. [Online]. Available: https://patents.google.com/patent/US3708328/en

[83] J. G. Helmstetter, 'Fireproofing of wood, cellulosic, and fabric containing products', US5453119A, Sep. 26, 1995 Accessed: Apr. 20, 2021. [Online]. Available: https://patents.google.com/patent/US5453119A/en

[84] N. Erdem, A. A. Cireli, and U. H. Erdogan, 'Flame retardancy behaviors and structural properties of polypropylene/nano-SiO2 composite textile filaments', *Journal of Applied Polymer Science*, vol. 111, no. 4, pp. 2085–2091, 2009, doi: 10.1002/app.29052.

[85] E. J. Blanchard, E. E. Graves, and P. A. Salame, 'Flame Resistant Cotton/Polyester Carpet Materials', *Journal of Fire Sciences*, vol. 18, no. 2, pp. 151–164, Mar. 2000, doi: 10.1177/073490410001800205.

[86] B. Kukfisz, 'The degree of flammability for an artificial grass surface system', *E3S Web Conf.*, vol. 45, p. 38, 2018, doi: 10.1051/e3sconf/20184500038.

[87] 'EN-ISO 13927. Plastics simple heat release test using a conical radiant heater and a thermopile detector. International Organization for Standardization. Geneva Switzerland', 2001.

[88] 'EN ISO 5660- 1: Reaction-to-fire tests — Heat release, smoke production and mass loss rate — Part 1: Heat release rate (cone calorimeter method)', 2002. https://www.iso.org/obp/ui/#iso:std:iso:5660:-1:ed-2:v1:en (accessed Mar. 24, 2021).

[89] V. Babrauskas, 'The Cone Calorimeter', in *SFPE Handbook of Fire Protection Engineering*, M. J. Hurley, D. Gottuk, J. R. Hall, K. Harada, E. Kuligowski, M. Puchovsky, J. Torero, J. M. Watts, and C. Wieczorek, Eds. New York, NY: Springer, 2016, pp. 952–980. doi: 10.1007/978-1-4939-2565-0_28.

[90] B. Schartel and T. R. Hull, 'Development of fire-retarded materials—Interpretation of cone calorimeter data', *Fire and Materials*, vol. 31, no. 5, pp. 327–354, 2007, doi: https://doi.org/10.1002/fam.949.

[91] H. Pereira, 'The Rationale behind Cork Properties: A Review of Structure and Chemistry', *BioResources*, vol. 10, no. 3, Art. no. 3, Jul. 2015, doi: 10.15376/biores.10.3.Pereira.

[92] H. Pereira, *Cork: Biology, Production and Uses*. Elsevier, 2011.

[93] J. Park *et al.*, 'Styrene-Based Elastomer Composites with Functionalized Graphene Oxide and Silica Nanofiber Fillers: Mechanical and Thermal Conductivity Properties', *Nanomaterials*, vol. 10, no. 9, Art. no. 9, Sep. 2020, doi: 10.3390/nano10091682.

[94] K. George, S. Mohanty, M. Biswal, and S. K. Nayak, 'Thermal insulation behaviour of Ethylene propylene diene monomer rubber/kevlar fiber based hybrid composites containing Nanosilica for solid rocket motor insulation', *Journal of Applied Polymer Science*, vol. 138, no. 9, p. 49934, 2021, doi: https://doi.org/10.1002/app.49934.

[95] M. Nikolaeva and T. Kärki, 'Influence of mineral fillers on the fire retardant properties of wood-polypropylene composites', *Fire and Materials*, vol. 37, no. 8, pp. 612–620, 2013, doi: 10.1002/fam.2160.

[96] S. P. Silva, M. A. Sabino, E. M. Fernandes, V. M. Correlo, L. F. Boesel, and R. L. Reis, 'Cork: properties, capabilities and applications', *International Materials Reviews*, vol. 50, no. 6, pp. 345–365, Dec. 2005, doi: 10.1179/174328005X41168.

[97] D. Hohenwarter, H. Mattausch, C. Fischer, M. Berger, and B. Haar, 'Analysis of the fire behavior of polymers (Pp, pa 6 and pe-ld) and their improvement using various flame retardants', *Materials*, vol. 13, no. 24, pp. 1–22, 2020, doi: 10.3390/ma13245756.

[98] M. Xiao, D. Liang, and H. Shen, 'Research on Flame Retardancy and Combustion Characteristics of PE and PE-MH-NC Cable Materials', *Procedia Engineering*, vol. 135, pp. 243–247, Jan. 2016, doi: 10.1016/j.proeng.2016.01.119.

[99] G. P. Bernardes, N. da R. Luiz, R. M. C. Santana, and M. M. de C. Forte, 'Rheological behavior and morphological and interfacial properties of PLA/TPE blends', *Journal of Applied Polymer Science*, vol. 136, no. 38, p. 47962, 2019, doi: https://doi.org/10.1002/app.47962.

[100] J. Abenojar, A. Barbosa, J. Del Real, L. F. M. Silva, and M. Martínez Casanova, 'Effect of surface treatments on natural cork: Surface energy, adhesion, and acoustic insulation', *Wood Science and Technology*, Nov. 2013, doi: 10.1007/s00226-013-0599-7.

[101] A. Ansarifar, G. Critchlow, R. Guo, R. Ellis, S. Kirtley, and B. Seymour, 'Effect of Rubber Chemicals on the Surface Free Energy of NR and NR–SBR Rubber Blends', *Journal of Rubber Research*, vol. 10, pp. 148–160, Sep. 2007.

[102] J. V. da Maia *et al.*, 'Influence of gas and treatment time on the surface modification of EPDM rubber treated at afterglow microwave plasmas', *Applied Surface Science*, vol. 285, pp. 918–926, Nov. 2013, doi: 10.1016/j.apsusc.2013.09.013.

[103] M. Lindner, N. Rodler, M. Jesdinszki, M. Schmid, and S. Sängerlaub, 'Surface energy of corona treated PP, PE and PET films, its alteration as function of storage time and the effect of various corona dosages on their bond strength after lamination', *Journal of Applied Polymer Science*, vol. 135, no. 11, p. 45842, 2018, doi: https://doi.org/10.1002/app.45842.

[104] R. M. Novais, L. Senff, J. Carvalheiras, M. P. Seabra, R. C. Pullar, and J. A. Labrincha, 'Sustainable and efficient cork - inorganic polymer composites: An innovative and eco-friendly approach to produce ultra-lightweight and low thermal conductivity materials', *Cement and Concrete Composites*, vol. 97, pp. 107–117, Mar. 2019, doi: 10.1016/j.cemconcomp.2018.12.024.

[105] B. Girardin, D. Flammier, and G. Auguin, 'Numerical simulation of EN 50399 standard test – Calibration and validation of a numerical virtual test', *J. Phys.: Conf. Ser.*, vol. 1107, p. 032025, Nov. 2018, doi: 10.1088/1742-6596/1107/3/032025.

[106] D. E. Sikoutris, D. E. Vlachos, V. Kostopoulos, S. Jagger, and S. Ledin, 'Fire burnthrough response of CFRP aerostructures. Numerical investigation and experimental verification', *Applied Composite Materials*, vol. 19, no. 2, pp. 141–159, 2012.

[107] P. Van Hees, T. Hertzberg, and A. Steen Hansen, 'Development of a Screening Method for the SBI and Room Corner using the Cone Calorimeter - Nordtest project 1479-00', SP Swedish National Testing and Research Institute, ISBN 91-7848-904-0, 2002.

[108] A. Dexters, R. Leisted, R. Van Coile, S. Welch, and G. Jomaas, 'Testing for knowledge: maximising information obtained from fire tests by using machine learning techniques', Interflam 2019.

[109] P. Benner, D. C. Sorensen, and V. Mehrmann, 'Preface. In: Dimension Reduction of Large-Scale Systems', in *Proceedings of a Workshop held in Oberwolfach, Germany*, 2003.

[110] B. Girardin, G. Fontaine, S. Duquesne, and S. Bourbigot, 'Fire tests at reduced scale as powerful tool to fasten the development of flame-retarded material: Application to cables', *Journal of Fire Sciences*, vol. 34, no. 3, pp. 240–264, May 2016, doi: 10.1177/0734904116642618.

[111] E. Gallo, W. Stöcklein, P. Klack, and B. Schartel, 'Assessing the reaction to fire of cables by a new bench-scale method', *Fire and Materials*, vol. 41, no. 6, pp. 768–778, 2017, doi: 10.1002/fam.2417.

[112] S. Bourbigot, P. Bachelet, F. Samyn, M. Jimenez, and S. Duquesne, 'Intumescence as method for providing fire resistance to structural composites: application to poly(ethylene terephtalate) foam sandwich–structured composite', *Composite Interfaces*, vol. 20, no. 4, pp. 269–277, Jun. 2013, doi: 10.1080/15685543.2013.793586.

[113] S. Bourbigot, J. Sarazin, P. Bachelet, F. Samyn, M. Jimenez, and S. Duquesne, 'Scale reduction: How to play with fire?', San Francisco, United States, Feb. 2017.

[114] J. Axelsson and P. V. Hees, 'New data for sandwich panels on the correlation between the SBI test method and the room corner reference scenario', *Fire and Materials*, vol. 29, no. 1, pp. 53–59, 2005, doi: https://doi.org/10.1002/fam.879.

[115] R. Mierlo and B. Sette, 'The Single Burning Item (SBI) Test Method - A Decade of Development and Plans for the Near Future', *Heron*, vol. 50, pp. 191–208, Jan. 2005.

[116] 'EN 13823:2010 - Reaction to fire tests for building products - Building products excluding floorings exposed to the thermal attack by a single burning item', *iTeh Standards Store*, Accessed: Apr. 28, 2021. [Online]. Available: https://standards.iteh.ai/catalog/standards/cen/751eff61-51ce-42df-a894-c74914ac2c4b/en-13823-2010

[117] N. A. McARTHUR and C. B. Jolliffe, 'Development of a demountable fire test corridor for assessment of floor coverings', *Fire Safety Science*, vol. 5, pp. 1273–1284, 1997.

[118] F. C. W. Fung, M. R. Suchomel, and P. L. Oglesby, 'The NBS Program on Corridor Fires', *Fire Journal*, vol. 61, no. 3, pp. 41–48, 1973.

[119] W. J. Christian and T. E. Waterman, 'Fire behavior of interior finish materials', *Fire Technology*, vol. 6, no. 3, pp. 165–178, 1970.

[120] J. H. McGuire, 'The spread of fire in corridors', *Fire Technology*, vol. 4, no. 2, pp. 103–108, 1968.

[121] J. Quintiere and C. Huggett, 'An evaluation of flame spread test methods for floor covering materials', *Special Publication*, vol. 41, no. 1, pp. 59–89, 1974.

[122] Z. Han, A. Fina, G. Malucelli, and G. Camino, 'Testing fire protective properties of intumescent coatings by in-line temperature measurements on a cone calorimeter', *Progress in Organic Coatings*, vol. 69, no. 4, pp. 475–480, 2010, doi: 10.1016/j.porgcoat.2010.09.001.

[123] S. J. Ritchie, K. D. Steckler, A. Hamins, T. G. Cleary, J. C. Yang, and T. Kashiwagi, 'The Effect Of Sample Size On The Heat Release Rate Of Charring Materials', *Fire Safety Science*, vol. 5, pp. 177–188, 1997.

[124] Y. Zhang, J. Ji, X. Huang, and J. Sun, 'Effects of sample width on flame spread over horizontal charring solid surfaces on a plateau', *Chin. Sci. Bull.*, vol. 56, no. 9, pp. 919–924, Mar. 2011, doi: 10.1007/s11434-011-4386-2.

[125] G. E. Settle, 'Assessment of draft ISO radiant panel spread-of-flame test', *Fire and Materials*, vol. 3, no. 3, pp. 171–181, 1979, doi: https://doi.org/10.1002/fam.810030310.

[126] A. Costa, H. Pereira, and Â. Oliveira, 'Influence of climate on the seasonality of radial growth of cork oak during a cork production cycle', *Ann. For. Sci.*, vol. 59, no. 4, pp. 429–437, May 2002, doi: 10.1051/forest:2002017.

[127] A. Costa, H. Pereira, and A. Oliveira, 'Variability of radial growth in cork oak adult trees under cork production', *Forest Ecology and Management*, vol. 175, no. 1, pp. 239–246, Mar. 2003, doi: 10.1016/S0378-1127(02)00145-7.

[128] G. Oliveira, M. A. Martins-Loução, and O. Correia, 'The relative importance of cork harvesting and climate for stem radial growth of Quercus suber L.', *Ann. For. Sci.*, vol. 59, no. 4, pp. 439–443, May 2002, doi: 10.1051/forest:2002018.

[129] C. Fialho, F. Lopes, and H. Pereira, 'The effect of cork removal on the radial growth and phenology of young cork oak trees', *Forest Ecology and Management*, vol. 141, no. 3, pp. 251–258, Feb. 2001, doi: 10.1016/S0378-1127(00)00333-9.

[130] P. Jové, À. Olivella, and L. Cano, 'Study of the variability in chemical composition of bark layers of quercus suber l. From different production areas', *BioResources*, vol. 6, no. 2, Art. no. 2, Apr. 2011.

[131] H. Pereira, 'Variability of the Chemical Composition of Cork', *BioResources*, vol. 8, no. 2, Art. no. 2, Mar. 2013.

[132] H. Pereira, 'Chemical composition and variability of cork from Quercus suber L.', *Wood Sci.Technol.*, vol. 22, no. 3, pp. 211–218, Sep. 1988, doi: 10.1007/BF00386015.

[133] N. Cordeiro, M. N. Belgacem, A. J. D. Silvestre, C. Pascoal Neto, and A. Gandini, 'Cork suberin as a new source of chemicals.: 1. Isolation and chemical characterization of its composition', *International Journal of Biological Macromolecules*, vol. 22, no. 2, pp. 71–80, Apr. 1998, doi: 10.1016/S0141-8130(97)00090-1.

[134] M. Chevreul, 'De l'action de l'acide nitrique sur le liège.', *Annales de Chimie*, vol. 92, pp. 323–333, 1807.

[135] M. Chevreul, 'Mémoire sur le moyen d'analyser plusieures matières végétales et le liège en particulier.', *Annales de Chimie*, vol. 96, pp. 141–189, 1815.

[136] M. Caldas, J. Ferreira, and M. Borges, 'About the chemical characterization of cork in the several stages of industrial processing.', *Boletim do Instituto dos Produtos Florestais*, 1985.

[137] H. Pereira, 'Studies on the chemical composition of virgin and reproduction cork of Quercus suber L.', *Anais do Instituto Superior de Agronomia, Vol. 40, p. 17*, 1982, Accessed: May 20, 2020. [Online]. Available: https://www.repository.utl.pt/handle/10400.5/17165

[138] L. Gil, 'Gil L. Cork: Production, Technology and Application. INETI Lisboa, 1998.', 1998.

[139] P. J. Holloway, 'The suberin composition of the cork layers from some ribes species', *Chemistry and Physics of Lipids*, vol. 9, no. 2, pp. 171–179, Oct. 1972, doi: 10.1016/0009-3084(72)90012-6.

[140] A. Şen, I. Miranda, S. Santos, J. Graça, and H. Pereira, 'The chemical composition of cork and phloem in the rhytidome of Quercus cerris bark', *Industrial Crops and Products*, vol. 31, no. 2, pp. 417–422, Mar. 2010, doi: 10.1016/j.indcrop.2010.01.002.

[141] E. Seoane and I. Ribas, 'Seoane E et al. Sobre la quimica del chorcho VII. Los acidos floionico y floionolico.', *Anales de la Real Sociedad Española de Física y Química*, 1951.

[142] W. Jensen and P. Rinne, 'Comparison of the chemical compositions of suberins from Betula verrucosa and Quercus suber.', *Paper Timber*, 1954.

[143] A. Guillemonat, 'Sur la constitution chimique du liège. 4e mémoire. Structure de la phellocryséine.', *Bulletin de la société chimique de France*, 1962.

[144] L. Duhamel, 'Les études sur les produits cireux du liège: les hydroxyacides en C18.', *Bulletin de la société chimique de France*, 1964.

[145] J. Graça, 'Suberin: the biopolyester at the frontier of plants', *Front. Chem.*, vol. 3, 2015, doi: 10.3389/fchem.2015.00062.

[146] J. Schönherr, 'Resistance of Plant Surfaces to Water Loss: Transport Properties of Cutin, Suberin and Associated Lipids', in *Physiological Plant Ecology II: Water Relations and Carbon Assimilation*, O. L. Lange, P. S. Nobel, C. B. Osmond, and H. Ziegler, Eds. Berlin, Heidelberg: Springer, 1982, pp. 153–179. doi: 10.1007/978-3-642-68150-9_7.

[147] M. Riederer and L. Schreiber, 'Protecting against water loss: analysis of the barrier properties of plant cuticles', *J Exp Bot*, vol. 52, no. 363, pp. 2023–2032, Oct. 2001, doi: 10.1093/jexbot/52.363.2023.

[148] A. Naseem, S. Tabasum, K. M. Zia, M. Zuber, M. Ali, and A. Noreen, 'Lignin-derivatives based polymers, blends and composites: A review', *International journal of biological macromolecules*, vol. 93, pp. 296–313, 2016.

[149] X. Du, J. Li, and M. E. Lindström, 'Modification of industrial softwood kraft lignin using Mannich reaction with and without phenolation pretreatment', *Industrial Crops and Products*, vol. 52, pp. 729–735, 2014.

[150] A. De Chirico, M. Armanini, P. Chini, G. Cioccolo, F. Provasoli, and G. Audisio, 'Flame retardants for polypropylene based on lignin', *Polymer Degradation and Stability*, vol. 79, no. 1, pp. 139–145, Jan. 2003, doi: 10.1016/S0141-3910(02)00266-5.

[151] Y. Yu *et al.*, 'Functionalized lignin by grafting phosphorus-nitrogen improves the thermal stability and flame retardancy of polypropylene', *Polymer Degradation and Stability*, vol. 97, no. 4, pp. 541–546, Apr. 2012, doi: 10.1016/j.polymdegradstab.2012.01.020.

[152] A. Voxeur, Y. Wang, and R. Sibout, 'Lignification: different mechanisms for a versatile polymer', *Current Opinion in Plant Biology*, vol. 23, pp. 83–90, Feb. 2015, doi: 10.1016/j.pbi.2014.11.006.

[153] B. E. Pallesen, 'The quality of combine-harvested fibre flax for industrials purposes depends on the degree of retting', *Industrial crops and products*, vol. 5, no. 1, pp. 65–78, 1996.

[154] D. Reis and J. Roland, 'Mise en évidence de l'organisation de parois des cellules végétales en croissance par extractions ménagées des polysaccharides associées à la cytochimie ultrastructurale', *Journal of microscopie*, 1974.

[155] A. Day *et al.*, 'Caffeoyl-coenzyme A 3-O-methyltransferase enzyme activity, protein and transcript accumulation in flax (Linum usitatissimum) stem during development', *Physiologia Plantarum*, vol. 113, no. 2, pp. 275–284, 2001, doi: 10.1034/j.1399-3054.2001.1130216.x.

[156] R. Frederik, K. Morreel, J. Ralph, W. Boerjan, and R. M. H. Merks, 'Modeling Lignin Polymerization. I. Simulation Model of Dehydrogenation Polymers', *Plant Physiology*, vol. 153, no. 3, pp. 1332–1344, Jul. 2010, doi: 10.1104/pp.110.154468.

[157] S. Laurichesse and L. Avérous, 'Chemical modification of lignins: Towards biobased polymers', *Progress in Polymer Science*, vol. 39, no. 7, pp. 1266–1290, Jul. 2014, doi: 10.1016/j.progpolymsci.2013.11.004.

[158] B. Prieur, 'Modified lignin as flame retardant for polymeric materials', These de doctorat, Lille 1, 2016. Accessed: May 20, 2020. [Online]. Available: https://www.theses.fr/2016LIL10083

[159] E. Sjostrom, *Wood Chemistry: Fundamentals and Applications*. Gulf Professional Publishing, 1993.

[160] R. W. Whetten, J. J. MacKay, and R. R. Sederoff, 'Recent Advances in Understanding Lignin Biosynthesis', *Annual Review of Plant Physiology and Plant Molecular Biology*, vol. 49, no. 1, pp. 585–609, 1998, doi: 10.1146/annurev.arplant.49.1.585.

[161] E. Windeisen and G. Wegener, 'Lignin as Building Unit for Polymers', in *Polymer Science: A Comprehensive Reference*, Elsevier, 2012, pp. 255–265. doi: 10.1016/B978-0-444-53349-4.00263-6.

[162] A. V. Marques, H. Pereira, D. Meier, and O. Faix, 'Isolation and Characterization of a Guaiacyl Lignin from Saponified Cork of Quercus suber L.', *Holzforschung*, vol. 50, no. 5, pp. 393–400, Jan. 1996, doi: 10.1515/hfsg.1996.50.5.393.

[163] A. Asensio, 'Structural studies of the hemicellulose A from the cork of Quercus suber', *Carbohydrate Research*, vol. 161, no. 1, pp. 167–170, Mar. 1987, doi: 10.1016/0008-6215(87)84017-X.

[164] A. Asensio, 'Structural studies of a hemicellulose B fraction from the cork of Quercus suber', *Carbohydrate Research*, vol. 165, no. 1, pp. 134–138, Jul. 1987, doi: 10.1016/0008-6215(87)80088-5.

[165] E. Conde, E. Cadahía, M. C. Garcia-Vallejo, and J. R. Gonźalez-Adrados, 'Chemical Characterization of Reproduction Cork from Spanish Quercus Suber', *Journal of Wood Chemistry and Technology*, vol. 18, no. 4, pp. 447–469, Nov. 1998, doi: 10.1080/02773819809349592.

[166] A. Asensio, 'Polysaccharides from the cork of Quercus suber. II. Hemicellulose.', *Journal of Natural Products*, vol. 51, pp. 488–491, 1988.

[167] A. Asensio, 'Structural studies of a hemicellulose B fraction (B-2) from the cork of Quercus suber', *Can. J. Chem.*, vol. 66, no. 3, pp. 449–453, Mar. 1988, doi: 10.1139/v88-078.

[168] I. Miranda, J. Gominho, and H. Pereira, 'Cellular structure and chemical composition of cork from the Chinese cork oak (Quercus variabilis)', *Journal of wood science*, vol. 59, no. 1, pp. 1–9, 2013.

[169] A. M. A. Pintor *et al.*, 'Use of cork powder and granules for the adsorption of pollutants: A review', *Water Research*, vol. 46, no. 10, pp. 3152–3166, Jun. 2012, doi: 10.1016/j.watres.2012.03.048.

[170] L. J. Gibson, M. F. Ashby, and B. A. Harley, *Cellular Materials in Nature and Medicine*. Cambridge University Press, 2010.

[171] M. E. Rosa and M. A. Fortes, 'Temperature-induced alterations of the structure and mechanical properties of cork', *Materials Science and Engineering*, vol. 100, pp. 69–78, Apr. 1988, doi: 10.1016/0025-5416(88)90240-6.

[172] E. Conde, M. C. García-Vallejo, and E. Cadahía, 'Waxes composition of reproduction cork from Quercus suber and its variability throughout the industrial processing', *Wood Science and Technology*, vol. 33, no. 3, pp. 229–244, Jun. 1999, doi: 10.1007/s002260050112.

[173] M. E. Rosa and H. Pereira, 'The Effect of Long Term Treatment at 100°C–150°C on Structure, Chemical Composition and Compression Behaviour of Cork', *Holzforschung*, vol. 48, no. 3, pp. 226–232, Jan. 1994, doi: 10.1515/hfsg.1994.48.3.226.

[174] L. J. Gibson and M. F. Ashby, *Cellular Solids: Structure and Properties*. Cambridge University Press, 1999.

[175] V. de L. Dantas and J. G. Pausas, 'The lanky and the corky: fire-escape strategies in savanna woody species', *Journal of Ecology*, vol. 101, no. 5, pp. 1265–1272, 2013, doi: 10.1111/1365-2745.12118.

[176] J. R. Molina, C. Prades, Á. Lora, and F. Rodríguez y Silva, 'Quercus suber cork as a keystone trait for fire response: A flammability analysis using bench and field scales', *Forest Ecology and Management*, vol. 429, pp. 384–393, Dec. 2018, doi: 10.1016/j.foreco.2018.07.041.

[177] L. J. Gibson, K. E. Easterling, and M. F. Ashby, 'The structure and mechanics of cork', *Proceedings of the Royal Society of London. A. Mathematical and Physical Sciences*, vol. 377, no. 1769, pp. 99–117, Jun. 1981, doi: 10.1098/rspa.1981.0117.

[178] A. Silva, M. Lambri, and M. D. De Faveri, 'Evaluation of the performances of synthetic and cork stoppers up to 24 months post-bottling', *European Food Research and Technology*, vol. 216, no. 6, pp. 529–534, 2003.

[179] A. Mas, J. Puig, N. Lladoa, and F. Zamora, 'Sealing and storage position effects on wine evolution', *Journal of food science*, vol. 67, no. 4, pp. 1374–1378, 2002.

[180] M. Takayuki, T. Nobuhiro, K. Akio, and S. Minoru, 'Water pressure resisting sound insulator', JP9198050, Japan Patent Office, 1997

[181] H. Akita, 'Gasket material layer including cork, fibers, rubber, and a rubber chemical', US Patent 5615897, United States Department of Commerce: Patent and Trademark Office, Arlington, VA, Apr. 01, 1997

[182] H. Pereira and E. Ferreira, 'Scanning electron microscopy observations of insulation cork agglomerates', *Materials Science and Engineering: A*, vol. 111, pp. 217–225, 1989.

[183] F. Cumbre, F. Lopes, and H. Pereira, 'The effect of water boiling on annual ring width and porosity of cork.', *Wood and Fiber Science*, vol. 32, no. 1, pp. 125–133, 2000.

[184] M. E. Rosa, H. Pereira, and M. A. Fortes, 'Effects of Hot Water Treatment on the Structure and Properties of Cork', *Wood and Fiber Science*, vol. 22, no. 2, Art. no. 2, Jun. 2007.

[185] A. P. M. Baptista and M. do Carmo Vaz, 'Comparative wear testing of flooring materials', *Wear*, vol. 162, pp. 990–995, 1993.

[186] C. Amen-Chen, H. Pakdel, and C. Roy, 'Production of monomeric phenols by thermochemical conversion of biomass: a review', *Bioresource technology*, vol. 79, no. 3, pp. 277–299, 2001.

[187] D. S. Varma, M. Varma, and I. K. Varma, 'Coir Fibers: Part I: Effect of Physical and Chemical Treatments on Properties', *Textile Research Journal*, vol. 54, no. 12, pp. 827–832, Dec. 1984, doi: 10.1177/004051758405401206.

[188] R. Ferreira, D. Pereira, A. Gago, and J. Proença, 'Experimental characterisation of cork agglomerate core sandwich panels for wall assemblies in buildings', *Journal of Building Engineering*, vol. 5, pp. 194–210, Mar. 2016, doi: 10.1016/j.jobe.2016.01.003.

[189] M. Rahm and P. Blomqvist, 'Fire testing on cork–furan/glass fibre sandwich panel for marine application. FIRE-RESIST project.', SP Technical Research Institute of Sweden, 2015.

[190] D. B. Dittenber and H. V. S. GangaRao, 'Critical review of recent publications on use of natural composites in infrastructure', *Composites Part A: Applied Science and Manufacturing*, vol. 43, no. 8, pp. 1419–1429, Aug. 2012, doi: 10.1016/j.compositesa.2011.11.019.

[191] N. P. G. Suardana, M. S. Ku, and J. K. Lim, 'Effects of diammonium phosphate on the flammability and mechanical properties of bio-composites', *Materials & Design*, vol. 32, no. 4, pp. 1990–1999, Apr. 2011, doi: 10.1016/j.matdes.2010.11.069.

[192] M. Jawaid, M. Thariq, and N. Saba, *Durability and Life Prediction in Biocomposites, Fibre-Reinforced Composites and Hybrid Composites*. Woodhead Publishing, 2018.

[193] O. Grexa and H. Lübke, 'Flammability parameters of wood tested on a cone calorimeter', *Polymer Degradation and Stability*, vol. 74, no. 3, pp. 427–432, Jan. 2001, doi: 10.1016/S0141-3910(01)00181-1.

[194] O. Grexa, F. Poutch, D. Manikova, H. Martvonova, and A. Bartekova, 'Intumescence in fire retardancy of lignocellulosic panels', *Polymer Degradation and Stability*, vol. 82, no. 2, pp. 373–377, Jan. 2003, doi: 10.1016/S0141-3910(03)00215-5.

[195] J. Lazko, N. Landercy, F. Laoutid, L. Dangreau, M. H. Huguet, and O. Talon, 'Flame retardant treatments of insulating agro-materials from flax short fibres', *Polymer Degradation and Stability*, vol. 98, no. 5, pp. 1043–1051, May 2013, doi: 10.1016/j.polymdegradstab.2013.02.002.

[196] S. Lazare, I. Elaboudi, M. Castillejo, and A. Sionkowska, 'Model properties relevant to laser ablation of moderately absorbing polymers', *Appl. Phys. A*, vol. 101, no. 1, pp. 215–224, Oct. 2010, doi: 10.1007/s00339-010-5754-5.

[197] A. Grill, *Cold plasma in materials fabrication*, vol. 151. IEEE Press, New York, 1994.

[198] Y. Shimazaki, M. Mitsuishi, S. Ito, and M. Yamamoto, 'Preparation of the layer-by-layer deposited ultrathin film based on the charge-transfer interaction', *Langmuir*, vol. 13, no. 6, pp. 1385–1387, 1997.

[199] W. B. Stockton and M. F. Rubner, 'Molecular-level processing of conjugated polymers. 4. Layer-by-layer manipulation of polyaniline via hydrogen-bonding interactions', *Macromolecules*, vol. 30, no. 9, pp. 2717–2725, 1997.

[200] M. Fang, D. M. Kaschak, A. C. Sutorik, and T. E. Mallouk, 'A "mix and match" ionic- covalent strategy for self-assembly of inorganic multilayer films', *Journal of the American Chemical Society*, vol. 119, no. 50, pp. 12184–12191, 1997.

[201] X. Qiu, Z. Li, X. Li, and Z. Zhang, 'Flame retardant coatings prepared using layer by layer assembly: a review', *Chemical Engineering Journal*, vol. 334, pp. 108–122, 2018.

[202] G. Malucelli, 'Layer-by-Layer nanostructured assemblies for the fire protection of fabrics', *Materials Letters*, vol. 166, pp. 339–342, 2016.

[203] H. Pan, W. Wang, Y. Pan, L. Song, Y. Hu, and K. M. Liew, 'Formation of self-extinguishing flame retardant biobased coating on cotton fabrics via Layer-by-Layer assembly of chitin derivatives', *Carbohydrate polymers*, vol. 115, pp. 516–524, 2015.

[204] Y. Fang, X. Liu, and X. Tao, 'Intumescent flame retardant and anti-dripping of PET fabrics through layer-by-layer assembly of chitosan and ammonium polyphosphate', *Progress in Organic Coatings*, vol. 134, pp. 162–168, 2019.

[205] F. Carosio and J. Alongi, 'Influence of layer by layer coatings containing octapropylammonium polyhedral oligomeric silsesquioxane and ammonium polyphosphate on the thermal stability and flammability of acrylic fabrics', *Journal of Analytical and Applied Pyrolysis*, vol. 119, pp. 114–123, May 2016, doi: 10.1016/j.jaap.2016.03.010.

[206] L. Costes *et al.*, 'Phosphorus and nitrogen derivatization as efficient route for improvement of lignin flame retardant action in PLA', *European Polymer Journal*, vol. 84, pp. 652–667, 2016.

[207] Y. Matsushita, M. Imai, T. Tamura, and K. Fukushima, 'Preparation and evaluation of a dispersant for gypsum paste from acid hydrolysis lignin', *Journal of applied polymer science*, vol. 98, no. 6, pp. 2508–2513, 2005.

[208] R. Zhang, X. Xiao, Q. Tai, H. Huang, and Y. Hu, 'Modification of lignin and its application as char agent in intumescent flame-retardant poly(lactic acid)', *Polymer Engineering and Science*, vol. 52, no. 12, pp. 2620–2626, 2012, doi: 10.1002/pen.23214.

[209] B. Prieur *et al.*, 'Phosphorylation of lignin: characterization and investigation of the thermal decomposition', *RSC Adv.*, vol. 7, no. 27, pp. 16866–16877, Mar. 2017, doi: 10.1039/C7RA00295E.

[210] F. Niu, N. Wu, J. Yu, and X. Ma, 'Gelation, flame retardancy, and physical properties of phosphorylated microcrystalline cellulose aerogels', *Carbohydrate polymers*, vol. 242, p. 116422, 2020.

[211] G. C. Lentsolo Yalli, 'Synthèse et utilisation de fibres cellulosiques phosphatées pour la valorisation de la fibre végétale dans l'amélioration des propriétés de surface du papier et la fabrication de matériaux ignifuges', PhD Thesis, Université du Québec à Trois-Rivières, 2013.

[212] P. L. Granja, L. Pouységu, M. Pétraud, B. D. Jéso, C. Baquey, and M. A. Barbosa, 'Cellulose phosphates as biomaterials. I. Synthesis and characterization of highly phosphorylated cellulose gels', *Journal of Applied Polymer Science*, vol. 82, no. 13, pp. 3341–3353, 2001, doi: https://doi.org/10.1002/app.2193.

[213] F. Rol *et al.*, 'Cellulose phosphorylation comparison and analysis of phosphorate position on cellulose fibers', *Carbohydrate polymers*, vol. 229, p. 115294, 2020.

[214] Y. Yu *et al.*, 'Functionalized lignin by grafting phosphorus-nitrogen improves the thermal stability and flame retardancy of polypropylene', *Polymer degradation and stability*, vol. 97, no. 4, pp. 541–546, 2012.

[215] S. Gaan and G. Sun, 'Effect of phosphorus and nitrogen on flame retardant cellulose: a study of phosphorus compounds', *Journal of Analytical and Applied Pyrolysis*, vol. 78, no. 2, pp. 371–377, 2007.

[216] R. Hajj *et al.*, 'Influence of lignocellulosic substrate and phosphorus flame retardant type on grafting yield and flame retardancy', *Reactive and Functional Polymers*, vol. 153, 2020, doi: 10.1016/j.reactfunctpolym.2020.104612.

[217] 'Lithium et composés (FT 183). Généralités - Fiche toxicologique - INRS'. https://www.inrs.fr/publications/bdd/fichetox/fiche.html?refINRS=FICHETOX_183 (accessed Aug. 13, 2021).

[218] 'Trichlorure de phosphoryle (FT 108). Généralités - Fiche toxicologique - INRS'. https://www.inrs.fr/publications/bdd/fichetox/fiche.html?refINRS=FICHETOX_108 (accessed Aug. 13, 2021).

[219] A. R. Garcia, L. F. Lopes, R. B. de Barros, and L. M. Ilharco, 'The problem of 2, 4, 6-trichloroanisole in cork planks studied by attenuated total reflection infrared spectroscopy: Proof of concept', *Journal of agricultural and food chemistry*, vol. 63, no. 1, pp. 128–135, 2015.

[220] C. Ortega-Fernández, J. R. González-Adrados, M. C. García-Vallejo, R. Calvo-Haro, and M. J. Cáceres-Esteban, 'Characterization of surface treatments of cork stoppers by FTIR-ATR', *Journal of agricultural and food chemistry*, vol. 54, no. 14, pp. 4932–4936, 2006.

[221] G. González-Gaitano and M. A. C. Ferrer, 'Definition of QC Parameters for the Practical Use of FTIR-ATR Spectroscopy in the Analysis of Surface Treatment of Cork Stoppers', *Journal of Wood Chemistry and Technology*, vol. 33, no. 3, pp. 217–233, Jul. 2013, doi: 10.1080/02773813.2013.779715.

[222] M. À. Olivella, I. Fernández, L. Cano, P. Jové, and A. Oliveras, 'Role of chemical components of cork on sorption of aqueous polycyclic aromatic hydrocarbons', 2013.

[223] A. Şen, J. Van den Bulcke, N. Defoirdt, J. Van Acker, and H. Pereira, 'Thermal behaviour of cork and cork components', *Thermochimica Acta*, vol. 582, pp. 94–100, Apr. 2014, doi: 10.1016/j.tca.2014.03.007.

[224] M. EMILIA ROSA and M. A. Fortes, 'Thermogravimetric analysis of cork', *Journal of materials science letters*, vol. 7, no. 10, pp. 1064–1065, 1988.

[225] H. Yang, R. Yan, H. Chen, D. H. Lee, and C. Zheng, 'Characteristics of hemicellulose, cellulose and lignin pyrolysis', *Fuel*, vol. 86, no. 12–13, pp. 1781–1788, 2007.

[226] W. Shangguan, Z. Chen, J. Zhao, and X. Song, 'Thermogravimetric analysis of cork and cork components from Quercus variabilis', *Wood science and technology*, vol. 52, no. 1, pp. 181–192, 2018.

[227] A. Awal and M. Sain, 'Spectroscopic studies and evaluation of thermorheological properties of softwood and hardwood lignin', *Journal of Applied Polymer Science*, vol. 122, no. 2, pp. 956–963, 2011, doi: 10.1002/app.34211.

[228] J. Villermaux, 'Génie de la réaction chimique, conception et fonctionnement des réacteurs, chapitre 8', *TEC & DOC Lavoisier, 2e édition revue et augmentée édition*, vol. 21, pp. 326–334, 1993.

[229] J. Romain, D. Guillaume, L. Karine, and D. Fabrice, *Modélisation en génie des procédés par analyse dimensionnelle*. Lavoisier, 2014.

[230] G. Delaplace, K. Loubière, F. Ducept, and R. Jeantet, *Dimensional Analysis of Food Processes*. Elsevier, 2015.

[231] E. Buckingham, 'On physically similar systems; illustrations of the use of dimensional equations', *Physical review*, vol. 4, no. 4, p. 345, 1914.

[232] A. A. Sonin, 'A generalization of the Π-theorem and dimensional analysis', *Proc Natl Acad Sci U S A*, vol. 101, no. 23, pp. 8525–8526, Jun. 2004, doi: 10.1073/pnas.0402931101.

[233] M. H. Lopes, C. P. Neto, A. S. Barros, D. Rutledge, I. Delgadillo, and A. M. Gil, 'Quantitation of aliphatic suberin in Quercus suber L. cork by FTIR spectroscopy and solid-state 13C-NMR spectroscopy', *Biopolymers*, vol. 57, no. 6, pp. 344–351, 2000, doi: https://doi.org/10.1002/1097-0282(2000)57:6<344::AID-BIP40>3.0.CO;2-#.

[234] M. H. Lopes, A. S. Barros, C. P. Neto, D. Rutledge, I. Delgadillo, and A. M. Gil, 'Variability of cork from Portuguese Quercus suber studied by solid-state 13C-NMR and FTIR spectroscopies', *Biopolymers*, vol. 62, no. 5, pp. 268–277, 2001, doi: https://doi.org/10.1002/bip.1022.

[235] P. Sannigrahi and E. Ingall, 'Polyphosphates as a source of enhanced P fluxes in marine sediments overlain by anoxic waters: Evidence from 31P NMR', *Geochemical Transactions*, vol. 6, Jun. 2005, doi: 10.1186/1467-4866-6-52.

[236] B. Cade-Menun, J. Navaratnam, and M. Walbridge, 'Characterizing Dissolved and Particulate Phosphorus in Water with 31 P Nuclear Magnetic Resonance Spectroscopy', *Environmental science & technology*, vol. 40, pp. 7874–80, Jan. 2007, doi: 10.1021/es061843e.

[237] V. D. Khavryuchenko and O. V. Khavryuchenko, 'Quantum Chemical Simulation of Phenol-Formaldehyde Resin Carbonization in the Presence of Phosphoric Acid: Computational Evidence

of Michaelis–Arbuzov-Type Reaction', *J. Phys. Chem. C*, vol. 117, no. 15, pp. 7628–7635, Apr. 2013, doi: 10.1021/jp4000736.

[238] J. M. Taylor, R. Vaidhyanathan, S. S. Iremonger, and G. K. Shimizu, 'Enhancing water stability of metal–organic frameworks via phosphonate monoester linkers', *Journal of the American Chemical Society*, vol. 134, no. 35, pp. 14338–14340, 2012.

[239] Y. Li, H. Zheng, M. Xu, B. Li, and T. Lai, 'Synthesis of a novel phosphonate flame retardant and its application in epoxy resins', *Journal of Applied Polymer Science*, vol. 132, no. 45, 2015.

[240] X.-L. Huang and J.-Z. Zhang, 'Phosphorus sorption on marine carbonate sediment: phosphonate as model organic compounds', *Chemosphere*, vol. 85, no. 8, pp. 1227–1232, 2011.

[241] A. Atreya and H. R. Baum, 'A model of opposed-flow flame spread over charring materials', *Proceedings of the Combustion Institute*, vol. 29, no. 1, pp. 227–236, Jan. 2002, doi: 10.1016/S1540-7489(02)80031-1.

[242] R. Menard, 'Synthèse de retardateurs de flamme phosphorés biosourcés pour résines epoxy.', PhD Thesis, Ecole Nationale Supérieure de Chimie de Montpellier, 2015.

[243] R. Delobel, M. Le Bras, N. Ouassou, and R. Descressain, 'Fire retardance of polypropylene by diammonium pyrophosphate-pentaerythritol: Spectroscopic characterization of the protective coatings', *Polymer Degradation and Stability*, vol. 30, no. 1, pp. 41–56, Jan. 1990, doi: 10.1016/0141-3910(90)90116-O.

[244] D. W. McKee, C. L. Spiro, and E. J. Lamby, 'The inhibition of graphite oxidation by phosphorus additives', *Carbon*, vol. 22, no. 3, pp. 285–290, Jan. 1984, doi: 10.1016/0008-6223(84)90172-6.

[245] T. Mariappan, 'Recent developments of intumescent fire protection coatings for structural steel: A review', *Journal of fire sciences*, vol. 34, no. 2, pp. 120–163, 2016.

[246] J. Alongi, Z. Han, and S. Bourbigot, 'Intumescence: Tradition versus novelty. A comprehensive review', *Progress in Polymer Science*, vol. 51, pp. 28–73, 2015.

[247] X. H. Dai, Y.-C. Wang, and C. G. Bailey, 'Effects of partial fire protection on temperature developments in steel joints protected by intumescent coating', *Fire Safety Journal*, vol. 44, no. 3, pp. 376–386, 2009.

[248] K. P. Nørgaard, K. Dam-Johansen, P. Català, and S. Kiil, 'Investigation of char strength and expansion properties of an intumescent coating exposed to rapid heating rates', *Progress in Organic Coatings*, vol. 76, no. 12, pp. 1851–1857, 2013.

[249] R. G. Puri and A. S. Khanna, 'Intumescent coatings: A review on recent progress', *Journal of Coatings Technology and Research*, vol. 14, no. 1, pp. 1–20, 2017.

[250] S. Levchik, 'Introduction to flame retardancy and polymer flammability', in *Flame Retardant Polymer Nanocomposites*, John Wiley & Sons, 2007.

[251] J. W. Lyons, 'Mechanisms of fire retardation with phosphorus compounds: Some speculation', *J. Fire Flammability*, vol. 1, no. 302311, p. 85, 1970.

[252] R. R. Hindersinn, G. Witschard, W. C. Kuryla, and A. J. Papa, 'The importance of intumescence and char in polymer fire retardance', *Flame retardancy of polymeric materials*, vol. 4, pp. 1–107, 1978.

[253] T. Mariappan, Y. Zhou, J. Hao, and C. A. Wilkie, 'Influence of oxidation state of phosphorus on the thermal and flammability of polyurea and epoxy resin', *European polymer journal*, vol. 49, no. 10, pp. 3171–3180, 2013.

[254] U. Braun *et al.*, 'Influence of the oxidation state of phosphorus on the decomposition and fire behaviour of flame-retarded epoxy resin composites', *Polymer*, vol. 47, no. 26, pp. 8495–8508, 2006.

PhD communications

Internal written and oral communications within GRASS project:

- 10 technical meetings with project members
- 6 meetings with the project's support committee
- Writing of a bibliographic report
- Writing of 5 half-yearly reports
- Writing of 4 deliverables

Presentations at conferences / congresses:

3 national poster presentations without proceedings:

- <u>Angeline Paturel</u>, Sophie Duquesne, Mathilde Casetta, Ludovic Janus, Olivier Talon, Nicolas Martin, Stijn Rambour, Johanna Louwagie, Geert De Clercq. Gazons aRtificiels Anti-feu Sûrs et durableS. Journées des Jeunes Chercheurs UGéPE_Nord de France-GEPROC, 20-21 Novembre 2018, Villeneuve d'Ascq, France.
- <u>Angeline Paturel</u>, Sophie Duquesne, Mathilde Casetta, Ludovic Janus, Olivier Talon, Nicolas Martin, Stijn Rambour, Johanna Louwagie, Geert De Clercq. Comportement au feu de gazons synthétiques à différentes échelles. GDR Feux, 6-7 Juin 2019, Marseille, France.
- <u>Angeline Paturel</u>, Sophie Duquesne, Mathilde Casetta, Ludovic Janus, Olivier Talon, Nicolas Martin, Stijn Rambour, Geert De Clercq. Study of the fire behavior of artificial turf – Role of cork as a performance layer. GDR Feux, 13-14 Février 2020, Lille, France.

1 international poster presentations without proceedings:

- <u>Angeline Paturel</u>, Sophie Duquesne, Mathilde Casetta, Ludovic Janus, Olivier Talon, Nicolas Martin, Stijn Rambour, Johanna Louwagie, Geert De Clercq. Relations structures / propriétés et comportement au feu de gazons artificiels. Journées des Jeunes Chercheurs UGéPE_Nord de France-GEPROC, 7 Novembre 2019, Mons, Belgique.

1 national oral communication without proceedings:

- <u>A Paturel</u>, Casetta M, Janus L, Duquesne S. Amélioration du comportement au feu du liège par phosphorylation - Application au gazon artificiel. 29èmes journées du GDR Feux, 1-2 Juillet 2021 (à distance).

2 international oral communications without proceedings:

- <u>A Paturel</u>, Casetta M, Janus L, Duquesne S. Improvement of the flame retardancy of cork by phosphorylation - Application to artificial turf structures. IFATCC 2020: Textile &Chemistry [R]evolution, 27-29th April 2021, Roubaix (à distance).
- <u>Duquesne S</u>, Paturel A, Casetta M. Understanding of the fire behaviour of artificial grass - new approaches. FRPM21, 29th August – 1st September, Budapest, Hungary.

1 international oral communication with proceedings:

- <u>Casetta M</u>, Paturel A, Duquesne S, Janus L, Talon O, Martin N, Rambour S, Louwagie J, De Clercq G. Contribution of infill materials to the fire behavior of artificial grass. AUTEX2019 – 19th World Textile Conference on Textiles at the Crossroads, 11-15th June 2019, Ghent, Belgium

Written communications through peer-reviewed scientific articles:

- <u>Paturel A</u>, Casetta M, Rambour S, Janus L, Duquesne S. Comprehensive study of the fire behaviour of artificial turf - improved and sustainable solutions. Fire and Materials, May 2021 – **Under Review.**
- <u>Paturel A</u>, Casetta M, Rambour S, Janus L, Duquesne S. ISO 9239-1 RADIANT PANEL TEST at reduced scale: application to artificial turf structures. Journal of Fire Sciences, July 2021 – **Under Review**.

List of figures

List of tables

With $[C]^{-1}$ the inverse matrix of [C]. This operation is equivalent to the application of the Gauss pivot method so that the central matrix [C] becomes the identity matrix [I] (in orange in Table 37).

Résumé

Le gazon artificiel utilisé pour le sport est un revêtement de sol généralement composé d'un support tufté, de brins en polyoléfine, d'une couche de sable et d'un matériau de remplissage (souvent en polymère synthétique, parfois d'origine naturelle comme le liège). Même si le gazon artificiel présente un risque d'incendie important en raison de sa teneur élevée en matière organique, son comportement au feu a rarement été étudié. D'autre part, les structures de gazon artificiel sont de plus en plus utilisées en intérieur ou dans des espaces fermés. Dans ce cas, la réglementation incendie en vigueur est la norme européenne EN ISO 13501-1 pour les matériaux de construction. Dans ce système Euroclass, le panneau radiant (norme EN ISO 9239-1) est le principal test permettant d'évaluer le comportement au feu des revêtements de sol. Un classement C_{FL} avec un taux de fumée inférieur à 750 %/min est requis pour une utilisation en intérieur. Cependant, très peu de structures de gazon artificiel répondent à ces exigences. Dans ce cadre, l'objectif de cette thèse est triple ; il s'agira d'une part (i) de mieux comprendre le comportement au feu de ces structures complexes, d'autre part (ii) de développer une méthodologie d'étude afin, in fine (iii) de développer des structures aux propriétés feu améliorées.

Afin de répondre au premier objectif, des essais au calorimètre à perte de masse ont été réalisés sur plusieurs structures de gazon artificiel et ont mis en évidence l'impact majeur du matériau de remplissage qui contribue majoritairement à la chaleur dégagée durant la combustion. Parmi les quatre matériaux de remplissage testés, le liège présente le meilleur comportement avec une quantité de chaleur libérée plus faible et un temps de combustion plus court. La performance au feu des structures a ensuite été évaluée en utilisant le test au panneau radiant EN ISO 9239-1. De grandes quantités de matière étant nécessaires à la réalisation des tests à échelle réelle, un plan d'expériences a été mis en œuvre pour permettre la transposition du test à petite échelle. La performance au feu des structures de gazon artificiel a ensuite été évaluée aux deux échelles et les résultats obtenus ont été comparés, conduisant à la validation du test à échelle réduite et de la méthodologie d'essai. Enfin, la réalisation d'une structure ignifugée plus performante a été envisagée, en utilisant un remplissage à base de liège modifié. Une recherche bibliographique importante a d'abord été effectuée sur le liège et sur la manière d'ignifuger les composés naturels plus généralement car l'ignifugation du liège n'a jamais été décrite auparavant. La phosphorylation est la méthode de modification en masse choisie afin d'améliorer le comportement au feu du liège. Elle consiste à fonctionnaliser les groupes hydroxyles du liège avec des retardateurs de flamme phosphorés. Le protocole de phosphorylation a d'abord été développé puis optimisé. Enfin, le comportement au feu du liège modifié, seul et intégré à la structure de gazon, a été évalué au calorimètre à perte de masse et au panneau radiant à petite échelle. Diverses caractérisations ont également été réalisées afin de mieux comprendre le comportement du liège modifié, notamment lors de la combustion, et de déterminer les mécanismes d'action impliqués. Ce travail a permis de conclure que l'utilisation d'un remplissage en liège phosphorylé dans une structure de gazon artificiel permet d'obtenir une amélioration notable des propriétés feu au panneau radiant à échelle réduite et ainsi a priori, d'atteindre les exigences de la norme Européenne pour une utilisation en intérieur. La nécessité d'utiliser un remplissage ignifugé dans les structures de gazon artificiel pour améliorer leur comportement au feu a été clairement mise en évidence.

Mots clefs : Gazon artificiel ; Panneau radiant EN ISO 9239-1 ; Plan d'expériences ; Ignifugation ; Phosphorylation ; Changement d'échelle

Abstract

Artificial turf for sports applications is a floor covering generally composed of a tufted backing, a polymeric pile, a sand layer and an infill material (often petroleum-based polymer, sometimes of natural origin such as cork). Even if artificial turf presents a significant fire hazard due to its high organic content, its fire behaviour has rarely been studied. Moreover, artificial turf structures are increasingly used in closed areas. In this case, the current fire regulation is the EN ISO 13501-1 European standard for building materials. In this Euroclass system, the EN ISO 9239-1 radiant panel test is the main test for assessing the fire behaviour of flooring products. A C_{FL} rating is required for indoor use and the smoke rate must be lower than 750 %/min (s1). However, only few structures meet these requirements. In this context, the PhD work has three objectives: (i) to better understand the fire behaviour of such complex structures, (ii) to develop a new testing method to allow fast screening of new formulations and (iii) to develop new artificial turf structures with improved fire-retardant performances.

First, in order to better understand the fire behaviour of the structures, investigations with the Mass Loss Calorimeter test on several artificial turf structures were carried out and highlighted the major impact of the infill material. Infills represent the main contributor to the heat release during combustion. Among the four different tested materials, cork shows the best performance with the lowest heat release rate and the shortest combustion time. The fire performance of the turf structures has then been assessed using the EN ISO 9239-1 radiant panel test. As large amounts of material are needed to perform the test, an experimental design methodology was implemented to allow the test to be transposed on a small-scale. The fire performance of artificial turf structures was evaluated at both scales and the results were compared leading to the validation of the downscaling method. Based on those results, the use of a flame retarded cork-based infill was considered. An important literature review was carried out on cork and on the different fireproofing methods for natural compounds, as the fireproofing of cork has never been reported previously. Phosphorylation, a method of bulk modification, has been selected to improve the fire behaviour of cork. This method consists of functionalizing the hydroxyl groups of cork with phosphorus-containing fire retardants. The phosphorylation protocol was first developed and then optimized. The fire behaviour of modified cork, alone and integrated into the turf structure, was evaluated using the Mass Loss Calorimeter test and the small-scale radiant panel test confirming the benefits of the proposed approach. Various characterizations were also performed to demonstrate the efficiency of the phosphorylation protocol, to better understand the behaviour of modified cork, especially during combustion, and to define the involved mechanisms of action. It was concluded that phosphorylation of cork resulted in a significant improvement of the fire properties of artificial turf at the small-scale radiant panel test according to the European standard, allowing to reach the requirements for indoor use. The need to use a fire-retarded infill in artificial turf structures to improve their fire behaviour was clearly evidenced.